Cronfa
Swansea University's Research Repository

Optimisation of solar thermally driven building cooling and heating system

Enock Ankamah Ebbah

A thesis submitted in partial fulfilment of the requirements of Swansea University for the Degree of Doctor of Engineering in Materials, Modelling and Manufacturing

Swansea University
Prifysgol Abertawe

College of Engineering

Swansea University

2024

Copyright: The Author, Enock Ankamah Ebbah, 2024

Abstract

Buildings account for about 30% of global final energy and 28% of total energy sector emissions. Applying solar heat for cooling could reach 1.5 EJ per year, accounting for nearly 17% of energy use for cooling in 2050. Almost half the worldwide building energy demand is for space and water heating. Solar thermally driven diffusion absorption cooling and heating systems present the opportunity to sustainably meet the growing building cooling and heating energy demand. This research describes how improving a building's thermal envelope design and adopting solar heat capture technology can reduce a building's heating and cooling energy demand. TRNSYS simulation software has been used to determine the cooling and heating demand of a thermally efficient (TE) building in four climatically varying locations in India, Tunisia, Russia, and the UK. The building design criteria varied, including the thermal characteristics of the building envelope material and the use of a solar heat capture device fitted to a diffusion absorption cooling system. The results show that the TE building has less combined heating and cooling loads than that constructed using local building regulations for the four climatic locations, except in India, where insulative properties lead to a requirement for additional cooling. A solar-driven diffusion absorption cooling system, modelled with the EES modelling tool and compared with experimental data, could reduce the TE building cooling energy consumption by 70% for India and Tunisia climatic locations and TE building heat energy demand by up to 28% for Russia and the UK climatic zones. The economic analysis demonstrates that while energetically compelling, local fuel costs mean the energy and CO_2 impacts are not immediately translated to short-term financial benefits. The solar collector and storage design indicates that the mass flow rate, collector area, and buffer tank volume influence the cooling engine's generator temperature. Also, the solar collector achieves the optimum 190-205 °C temperatures with up to 10 kg/hr mass flow rates. Using a small buffer store of 2 litres/ m^2 of solar collector area, the solar fraction was between 40-65 %. On the other hand, a cold energy storage design, with tank sizes between 120-500 litres, provides adequate cooling energy throughout the year, with a latent heat medium (eutectic water-salt solution) storing more than three times the energy and less heat loss than sensible heat storage (ethylene glycol and water mixture). The discounted payback times for Tunis, New Delhi, Volgograd, and Swansea are 12.7, 6.8, 0.8, and 2.1 years, respectively, compared with residential air source heat pumps, reported to have paybacks between 3 – 15 years.

Declarations

This work has not previously been accepted in substance for any degree and is not being concurrently submitted in candidature for any degree.

Signed 

Date: 18/05/2024

This thesis is the result of my own investigations, except where otherwise stated. Other sources are acknowledged by footnotes giving explicit references. A bibliography is appended.

Signed 

Date: 18/05/2024

I hereby give my consent for my work, if relevant and accepted, to be available for photocopying and for inter-library loans after expiry of a bar on access approved by the University.

Signed 

Date: 18/05/2024

The University's ethical procedures have been followed and, where appropriate, that ethical approval has been granted.

Signed 

Date: 18/05/2024

Acknowledgements

I would like to thank my academic supervisors, Dr. Eifion Jewell and Dr. Jonothan Elvins, for their advice, encouragement, and help during various stages of this research project. I am thankful to Mr. Michael Reid and Dr. Robert Edwards of Solar Polar Limited for collaborating on this research project, sponsoring it, and for their insights into the practical application of this research.

I want to express my gratitude to all the staff in the M2A team who have been very supportive during my time at Swansea University. Also, I would like to thank the technical enquiries team at the TRNSYS and EES modelling software companies for their assistance during enquiries for further clarifications of their software technical manual.

I want to express my appreciation to my family for their love, support and patience throughout my research study.

Supporting Peer Reviewed Work

Conference presentations relating to this research study are listed below.

Conference Presentation

1. Enock Ebbah, Modelling solar-powered diffusion absorption machines to meet building cooling and heating demand, World Energy Storage Conference (WESC), hosted by the University of Birmingham, 13 October 2022.

2. Enock Ebbah, Modelling solar-powered diffusion absorption machines to meet building cooling and heating demand, Engineering a Future Wales PhD Conference, Techniquest, Cardiff, 15 November 2022.

Table of Contents

List of Figures

List of Tables

Abbreviations

AC	Air conditioners
ACC	Absorption cooling cycle
ACH	Air exchange rate
AHU	Air handling unit
ANN	Artificial neural network
ASHP	Air-source heat pump
ASHRAE	American Society of Heating, Refrigerating and Air-Conditioning Engineers
BEM	Building energy management
BIM	Building information modelling
°C	Degree celsius
CFC	Chlorofluorocarbons
CHP	Combined heat and power
CIBSE	Chartered Institution of Building Services Engineers
CO_2	Carbon dioxide
CO2e	Carbon dioxide equivalent
COP	Coefficient of performance
CPC	Compound parabolic concentrators
CTF	Conduction transfer function
DACC	Diffusion absorption cooling cycle
DACS	Diffusion absorption cooling system
DLL	Dynamic link library
DX	Direct expansion
EATEP	Energy Assessment Tool of Energy Projects
EES	Engineering Equation Solver
EJ	exajoule [1 J x 10^{18}]
EU	European Union
GDP	Gross domestic product
GHE	Gas heat exchanger
GSHP	Ground-source heat pump
GWP	Global warming potential
H_2	Hydrogen
H_20	Water
HCFC	Hydro-chlorofluorocarbons
HFC	Hydrofluorocarbons
HP	Heat pump
HPWH	Heat pump water heaters
HVAC	Heating, ventilation, and air conditioning
HX	Heat exchanger
IEA	International Energy Agency
KW	Kilowatt
LHS	Latent heat storage

LiBr	Lithium bromide
LPG	Liquified petrol gas
NH3	Ammonia
NZEB	NetZero Energy Building
ODP	ozone depletion potential
PCM	Phase change material
PTAC	Packaged Terminal Air Conditioning
PV	Photovoltaic
PV/T	Photovoltaic/thermal collectors
RoTF	Room transfer functions
SATF	Space air transfer function
SHE	Solution heat exchanger
SHS	Sensible heat storage
TE	Thermally efficient
TFM	Transfer Function Method
TMY	Typical meteorological year
TRNBuild	TRNSYS building tool
TRNSYS	Transient Energy Simulation System
TWV	Three-way valve
UK	United Kingdom
USA	United States of America
USD	United States dollars
VAV	Variable Air Volume
VCC	Vapour compression cycle
VRF	Variable Refrigerant Flow
VRV	Variable Refrigerant Volume
W	Watt
WSHP	Water-source heat pump
XCPC	External compound parabolic concentrating

Chapter 1 : Introduction

1.1 Introduction

In 2021, buildings accounted for 30% of global final energy consumption and 27% of total energy sector emissions. The International Energy Agency (IEA) reports the energy use in buildings increased from 115 EJ in 2010 to almost 135 EJ in 2021, with electricity accounting for about 35% of building energy use. Despite the progressive shift from fossil fuels to other options, fossil fuel constitutes at least 35% of total buildings' energy [1].

About half of the worldwide energy demand for buildings was used for space and water heating in 2021 [2]. Building space cooling is the fastest-growing end-use in buildings, and the energy used to cool buildings has doubled since 2000 [1,3]. The leading equipment used to maintain building temperature, air conditioners (AC) and electric fans, account for about 20% of the total electricity consumed in buildings worldwide [4]. Also, building space cooling energy is projected to triple by 2050 to 6000 TWh/year globally, equating to installing ten new air conditioning equipment each second for the next 30 years [5]. Thus, the high use of heating and cooling equipment over the next three decades will drive up global electricity and carbon emissions.

Under the current climate and socioeconomic conditions, about 2-4 billion people will need cooling in residential building spaces to avoid health risks from deadly heatwaves [6,7]. Also, in Europe, it was estimated to cost between € 22-89 million per year to generate additional electricity for cooling purposes and compensate for the climate change impact. Globally, it is estimated that a 1 K average ambient temperature increase could result in cooling energy consumption costing $ 75.1 billion [8,9]. High temperatures recorded within building spaces and heatwaves increase mortality and morbidity rates, severe discomfort, and adverse health effects for low-income families, where the indoor temperature could exceed 35 °C [10-12]. Besides, the increased ambient temperature-induced climate change, poor building design, and lack of access to mechanical cooling systems have forced more than one billion people worldwide to dwell in uncomfortable indoor temperatures [13,14].

The demand for air-conditioning is growing faster because of increasing wealth in sunbelt countries, a record increase in high temperatures and associated discomfort in summer months, population growth, and a reduction in unit costs [15-18]. Most homes in hot climates have yet to purchase their first air-conditioning equipment. In India, for example, the annual sales of room air conditioning equipment are growing at around 20% annually [19], while in China, the adoption of air conditioning equipment in urban households has increased from 1% in 1990 to almost 100% in 2010 [20]. Besides, about 2/3 of the world’s households could own air-conditioning equipment by 2050 [5]. Moreover, summertime

overheating occurs in many temperate regions with rare air-conditioning usage in domestic buildings, e.g., the northern USA, the UK, France, Germany, and New Zealand [21,22].

Most countries use conventional cooling systems, e.g., heat pumps, based on the vapour compression cycle (VCC) to deliver building space cooling [23,24]. Among the carbon dioxide equivalent (CO_2-eq.) emissions of conventional cooling systems, AC equipment energy consumption accounts for more than 70%, followed by refrigerant leakages of fluorinated gases (F-gases) such as Chlorofluorocarbons (CFCs), Hydro-chlorofluorocarbons (HCFCs) and Hydrofluorocarbons (HFCs) [25-28]. The solar-powered diffusion absorption system (DACS) uses ammonia refrigerant, which has less environmental impact than F-gases. Ammonia has no ozone depletion potential (ODP) and lower global warming potential (GWP). However, it has toxicity and corrosion issues which need mitigation with strict safety standards and adequate training [29,30].

To achieve NetZero by 2050, building energy consumption must drop by 25%, and fossil fuel use must decrease by more than 40% to today's levels [1]. Additionally, for new buildings and 20% of the existing building stock to achieve the NetZero milestones by 2030, the building envelopes must be thermally efficient to reduce thermal energy consumption [1].

The absorption cooling cycle (ACC) differs from VCC in using a thermally driven generator instead of the VCC's mechanically driven compressor [31]. The most common working pairs for absorption cooling systems are water-lithium-bromide and ammonia-water [32,33]. This diffusion absorption cooling cycle uses ammonia-water working pairs with hydrogen as the auxiliary gas.

Solar air-conditioning is an alternative to conventional cooling systems to meet rising cooling and heating demands and reduce building carbon emissions [34,37]. Solar cooling is attractive because the demand for daytime cooling typically matches the availability of sunshine. Energy storage is generally implemented to meet night-time cooling demand and compensate for the intermittency of the solar heat source. For heat-driven cooling applications, solar thermal collectors generate heat to drive thermal chillers to deliver cooling for building thermal comfort [36,38,39]. A solar-powered DACS uses a solar heat source to minimise the pressure on electricity grids and produces fewer operational carbon emissions than heat from fossil fuels [5,13].

1.2 Basic layout, Solar Polar cooling system principles and current markets.

This section presents an overview and description of the science of a diffusion absorption cooling cycle (DACC) used by Solar Polar Limited. The source of information is from published literature on DACC systems. Thus, there may be differences in what Solar Polar limited supply. Solar Polar Limited's objective is to convert the DACC system currently used for refrigeration into building air-conditioning applications. Thus, variations in cooling

applications are highlighted where possible. Firstly, a description of the DACC layout and principles is presented. Secondly, the current markets are described.

1.2.1 Basic layout and principles of the Solar Polar system

A basic layout of the DACC cycle is shown in Figure 3 [40]. The DACC was invented and patented by Von Platen and Munters [41]. It uses ammonia-water-hydrogen as a working fluid, where ammonia is the refrigerant, water is the absorbent, and hydrogen gas is an auxiliary gas. Ammonia (refrigerant) transports energy from a low-temperature source to a high-temperature sink. At the same time, water (absorbent) absorbs the ammonia (refrigerant) at low partial pressure to release it at high pressure [42]. The hydrogen (auxiliary gas) provides pressure equalisation throughout the thermodynamic cycle [43].

The DACC system has eight main components: absorber, solution heat exchanger, generator bubble pump, rectifier, condenser, evaporator, gas heat exchanger, and solar thermal collector [40]. Two circulating loops pass through the absorber. The absorber has a sub-component known as a reservoir, which resides at the bottom of the absorber. The location of the reservoir is such that a refrigerant-rich solution, consisting of ammonia and water, flows from it to the bottom section of the generator via a solution heat exchanger (SHE). The solution heat exchanger absorbs heat from warm, weak ammonia-water solution returning from the outer space of the generator to the absorber [40,44].

The generator houses a bubble pump, where refrigerant-rich solution from the absorber is heated to produce refrigerant vapour (ammonia). The shape of the generator allows ammonia vapour bubbles to separate from the ammonia-water solution and subsequently flow towards the rectifier. The rectifier ensures that any remaining water in ammonia vapour is removed so that ammonia vapour flows to the condenser. The condenser rejects heat from ammonia vapour so that ammonia vapour is condensed to ammonia liquid before it flows to the evaporator. Heat is absorbed from a conditioned space into the evaporator to achieve the desired cooling effect. The gas heat exchanger (GHE), positioned between the evaporator and absorber, extracts heat from hydrogen and ammonia gas from the absorber and moves it towards the evaporator. A solar thermal collector converts light from the sun into useful heat energy to power the generator. The DACC system can be thermally driven by energy sources such as waste heat or solar thermal energy [40,43-46].

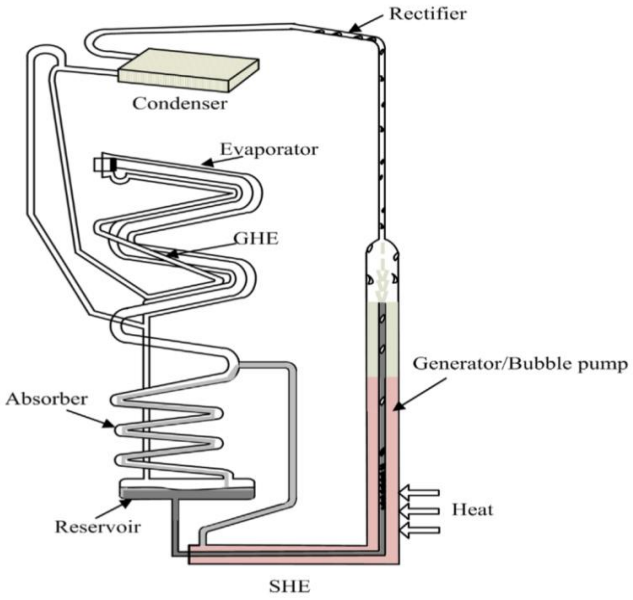

Figure 1.1 Diffusion Absorption Cooling Cycle (DACC) diagram [40].

The performance of the solar-powered DACC system is measured as a ratio of the heat removed by the evaporator to the heat supplied to the generator by the solar collector. Commercial DACC cooling systems typically require temperatures of 150–200 °C to achieve refrigeration [16]. Thus, solar collectors that can generate 150–200 °C temperatures have been the focus of solar-powered DACC research studies. Recent investigations of refrigerant-absorbent pairs other than ammonia-water aim to reduce generation temperatures, e.g., R22-dimethylacetamide [47] and ammonia-lithium nitrate [48]. Lower generation temperatures allowed low-temperature flat plate and evacuated tube solar collectors to be studied. Rattner et al. [49] reviewed passively operated DACC systems and showed that 125–200 °C generator temperatures are required to deliver a cooling coefficient of performance (COP) below 0.2. Also, Zohar et al. [47] predicted 135–150 °C generator temperatures for R22-dimethylacetamide and R32-dimethylacetamide working fluid pairs.

1.2.2 Solar Polar's current market

Solar Polar's solar-powered DACS is currently used to refrigerate vaccines (med box) and food crops (crop box) in remote and off-grid locations worldwide with high solar radiation levels, such as in Africa, Middle Eastern countries and South America. Solar Polar's med box and crop box have been successful because they have few electrical parts, low running costs, and low maintenance requirements. Their modular construction capability makes them adaptable to different needs [50].

Solar Polar aims to diversify into the building air-conditioning sector using the existing solar-powered DACS as a viable alternative to mainstream air-conditioning systems. Solar Polar Limited would like to apply solar-powered DACS to cool and heat buildings for human thermal comfort. The fundamental challenges of switching Solar Polar's existing DACS refrigerator to building cooling include solar energy design, building integration and a route to market entry.

1.3 Research aim and objectives.

This research aims to use modelling to design a solar-powered diffusion absorption cooling and heating system to meet building cooling and heating demands for a standard building. This research uses a solar-powered diffusion absorption cooling and heating system to meet building cooling and heating demands. The study quantifies the heat source from solar thermal collectors as well as the cost and avoided carbon emissions. The design maximises solar capture and storage to reduce the need for backup energy to meet building thermal loads. For the building heating needs, the energy from the solar collector is used to meet the heating load. On the other hand, for the building cooling load, the solar fraction for the solar collector is evaluated with and without a hot store and cold store so that an economic analysis and environmental impact assessment are performed on the optimised operating system with the highest solar fraction. Although the average COP of the diffusion absorption cooling machine is 0.2 [51], the significance of the solar-powered DACS is revealed when the economic and environmental assessment is completed, along with the energetic analysis [36,52].

TRNSYS modelling software is used to model the solar collector and storage system and to simulate the cooling and heating demand for a building. Additionally, the Engineering Equation Solver (EES) software is used to complete the thermodynamic modelling of the solar-powered DACS and compare it with experimental data. The experiments were previously conducted by Solar Polar Ltd and Imperial College, London, and the experimental results in published literature by Najjaran et al. [51] have been shared with this author to complete this research.

This research has the following objectives:

Objectives:

1. Review the design parameters and operational characteristics of the solar-powered diffusion absorption cooling and heating system to assess equipment technical capabilities and requirements for cooling and heating buildings (Chapters 1-3, 6).

2. Develop simulation and appropriate models to calculate the cooling and heating loads for a residential building in appropriate selected climatic locations (Chapters 3, 4).
3. Evaluate and calculate the sizing of external compound parabolic concentrating (XCPC) solar collectors that meet the thermal energy requirements for solar-powered diffusion absorption cooling and heating systems (Chapters 3, 5 - 8).
4. Evaluate the physical and technical requirements and capabilities of implementing thermal energy storage systems in the solar-powered diffusion absorption cooling and heating system (Chapters 5 - 9).
5. Calculate the auxiliary energy consumption and complete an economic analysis of the solar-powered diffusion absorption cooling and heating system (Chapters 8-10).
6. Design a standard building with a thermally efficient envelope, i.e., low thermal transmittance (U-value) with thermal characteristics meeting or contributing to achieving the NetZero milestones for 2030 (new buildings) and 2050 (all buildings) (Chapters 3, 4).
7. Calculate and analyse the environmental carbon impact of the solar-powered diffusion absorption cooling and heating system and assess how that fits with the NetZero milestones to 2030 (new buildings) and 2050 (all buildings) (Chapter 10).
8. Examine and recommend solutions for integrating the solar-powered diffusion absorption cooling and heating system with buildings (Chapters 8,9).

1.4 Outline of the Thesis

This thesis comprises twelve Chapters and Appendices. The current Chapter presents the introduction of the thesis, the research aim and objectives, the basic layout of Solar Polar's solar-powered DACS system, and the structure of the thesis.

Chapter Two is a literature review on cooling and heating systems, solar energy capture, building integration requirements, and building use considerations.

Chapter Three explains the methodology applied for this research based on modelling using TRNSYS and EES software. This Chapter describes the modelling theories implemented, the strategy used, the performance parameters investigated, and the justification of assumptions. Also, it details the source of the experimental data and how it was used in the research.

Chapter Four presents the results of the modelling and simulation of building energy demand for a standard building as well as a local building for case study locations in Swansea (United Kingdom), New Delhi (India), Volgograd (Russia), and Tunis (Tunisia) cities. The Chapter describes the strategy employed and the building design specification and presents results for the thermal energy performance for both a standard building and a local building.

Chapter Five presents the solar thermal energy production and storage results from the XCPC solar collector design.

Chapter Six presents the cooling engine performance by describing how the cooling engine is modelled and presents the modelling results with EES software. Then, a comparison is made between the modelling and experimental results, explaining how the experimental results will be used going forward. The Chapter describes how the cooling engine will be integrated with the building.

Chapter Seven explains how the cooling engine cools a standard New Delhi and Volgograd building. The Chapter begins with the rationale for the design approach to maximise solar energy capture. Then, the results are presented for a sensitivity analysis based on the mass flow rate in the solar collector, the solar collector's area, and the thermal energy storage volume.

Chapter Eight presents the results of the solar energy capture and storage capabilities and how auxiliary energy may be used to meet the lag between demand and supply. The Chapter also discusses the thermodynamic and practical implications of hot thermal storage.

Chapter Nine evaluates cold energy storage as an alternative to the hot storage analysis previously presented in Chapters 7 and 8. The Chapter discusses the design logic applied, the cold storage capacity and the cold store energy loss.

Chapter Ten presents the economic evaluation and the environmental impact assessment of the solar-powered DACS system using cold energy storage for the building cooling loads and direct solar thermal power for building heating.

Chapter Eleven discusses the main findings of this research and the impact of the results on current applications and future opportunities. The discussion also includes possible design improvements and practical ways to proceed with future works.

Chapter Twelve presents the conclusion and recommends further improvement for future work.

1.4.1 Overall methodology of how all chapters is connected to achieve the objectives.

Chapter One presents the thesis introduction and Research Objectives. Chapter Two (literature review) synthesises existing knowledge on solar thermal energy capture, building cooling and heating energy systems, building thermal energy performance and use considerations, and applying thermodynamic modelling techniques. This comprehensive review establishes the theoretical basis for the subsequent Chapters and to achieve the first Research Objective. Chapter Three describes the research methodology based on the TRNSYS and EES modelling theories, the strategy used, the performance parameters investigated, and the justification of assumptions providing the basis for achieving the first, second, third and sixth Research Objectives.

Chapter Four describes the strategy employed and the building design specification and presents results for the thermal energy performance for both a standard building and a local building, ensuring that the second and sixth Research Objectives are achieved. Chapter Five discusses the XCPC solar collector design, thermal energy production and storage results used to achieve the third and fourth Research Objectives. The cooling engine performance discussed in Chapter Six allows the thermal energy requirements for the solar-powered diffusion absorption cooling and heating systems to achieve the first, third, and fourth Research Objectives. The sensitivity study in Chapter Seven is based on the mass flow rate in the solar collector, the solar collector's area, and the thermal energy storage volume, which contribute to achieving the third and fourth Research Objectives. Solar energy capture and storage capabilities and the quantification of backup energy contribute to achieving the third and eighth Research Objectives.

The assessment of cold energy storage (Chapter 9) as an alternative to hot thermal energy storage completes achieving the fourth, fifth, and eighth Research Objectives. In Chapter Ten, the economic and environmental assessment based on solar-powered DACS is completed, achieving the fifth and seventh Research Objectives.

Chapter 2 : Literature review

2.1 Introduction

This literature review covers the main topics of solar energy capture, building cooling and heating systems, building thermal performance, building use considerations, and the thermodynamic modelling techniques applied to study building thermal energy systems. The review on solar energy capture introduces the available energy in solar radiation and the types of solar thermal collectors and storage materials used in building cooling and heating systems. The study of building cooling and heating systems presents the performance features of equipment used to deliver thermal comfort, the device options, and the thermodynamics of solar absorption cooling systems. The review of building thermal performance describes the mechanisms of heat gain and loss within and through the building thermal envelope and how the building heat balance is used to calculate the thermal load. Afterwards, several building thermodynamic modelling tools are presented on how they are used to calculate thermal loads and design solar thermally powered cooling and heating systems.

2.2 Solar Energy capture

The sun is a sphere of intensely hot gaseous matter with a diameter of 1.39×10^9 m and has an effective blackbody temperature of 5777 K. The energy produced at the sun's core must be transferred out to the surface and radiated to space. The radiation in the sun's core is in the x-ray and gamma-ray parts of the spectrum, and the radiation's wavelengths increase as the temperature reduces at larger sun radial distances [53].

The solar constant is the amount of solar energy per unit time received on a unit area of the surface perpendicular to the sun's rays, and its value is approximately 1367 watts per square meter (W/m^2). The solar constant is used in solar energy applications to determine the maximum amount of solar energy that can be received at the top of the Earth's atmosphere at a given location. However, the amount of solar energy available on the earth's surface at a given site is lower due to atmospheric absorption, scattering, time of day, season, latitude, and cloud cover [53,54].

Total solar radiation is the amount of solar energy that reaches the earth's surface, and it is related to the solar constant and the angle at which the sun's rays hit the earth's surface. Total solar radiation, often called global radiation, is the sum of the beam and the diffused solar radiation on a surface. The beam solar radiation is the solar radiation received from the sun

without being scattered by the atmosphere. In contrast, diffuse solar radiation is the solar radiation received from the sun after its direction has been changed by scattering by the atmosphere [53,54].

The solar collector is the main component that captures solar energy and converts it into thermal energy to drive solar thermally powered cooling and heating systems [37,54,55]. The main solar collector types are described in this section.

2.2.1 Solar thermal collectors

A solar thermal collector converts solar radiation into thermal energy and transfers the heat through a fluid in the collector for intended uses [53,54,56]. In buildings, the heat collected can be used for space heating, hot water service, space conditioning equipment, and many other applications [57]. Many solar thermal collectors are available on the market, and they can be categorised into two major systems: non-concentrating or stationary and concentrating. Besides, there are hybrid systems that combine photovoltaic and thermal collector features called photovoltaic/thermal (PV/T) collectors [58,59].

A non-concentrating collector has the same area for absorbing solar radiation. In contrast, a concentrating solar collector uses reflective surfaces to focus solar radiation to a smaller receiving area to increase radiation flux [54,60]. Non-concentrating solar collectors are primarily used in residential and commercial building spaces and for hot water heating applications. Concentrating solar collectors are suitable for high-temperature applications in solar power plants [54,60]. The heat transfer fluids typically used in solar collectors include water, air, oil, glycol water, and molten salts. Non-concentrating solar collectors used in residential building heating applications include flat plate collectors, unglazed collectors, evacuated tube collectors, and solar air collectors [54]. Moreover, according to Evangelisti et al. [60] the solar collectors used for space heating and cooling applications include flat plate collectors, evacuated tube collectors, and compound parabolic collectors.

2.2.1.1 Flat-plate collectors using liquid

The flat plate collector is the most common low-temperature collector, and its components include a cover, absorber plate, headers, insulation, casing, and heat removal tubes and fins [54,60]. The absorber plate is typically made of metal or polymer material to absorb incident solar radiation. The absorbed solar energy heats up a fluid flowing through tubes or channels in the flat plate. The cover is a glazing material able to transmit the radiation to the absorber.

The casing encapsulates the insulation at the back and sides to reduce collector heat losses. The indicative operating temperature range is 30-80 °C [54].

2.2.1.2 Evacuated tube solar collectors

Evacuated tube solar collectors consist of glass tubes, each containing an absorber plate and a pipe through which flows a heat transfer fluid [54,60]. The space between the glass tube and the absorber plate is evacuated free of air to reduce heat losses from the collector. Sunlight is transmitted via the glass tube to the absorber plate, which heats up. The captured heat is transferred from the absorber plate to fluid inside the pipe attached to the absorber plate. The tubes are connected to a horizontal tank where the heated water is transported for intended use. The typical operating temperature range is 50-200 °C [54].

Three fundamental types of evacuated tube collectors are water-in-glass, U-type, and heat-pipe type, Figure 2.1, [60,61]. The water-in-glass type has glass tubes, each filled with a small amount of water, to be heated by the sun's rays. The heated water by the solar radiation drives the heated water by natural convection into the horizontal tank. Cold water from the tank substitutes the warmer water. In the U-type design, the absorber plate is bent into a U-shape so that the fluid flows through the entire tube length twice compared to once in the water-in-glass type. Also, the U-type consists of two glass tubes with evacuated space in between to improve thermal efficiency [60-63]. The heat-pipe type is equipped with a heat-pipe system to recover heat from the absorber to the horizontal tank instead of having fluid flowing through pipes in the absorber plate. With the heat-pipe mechanism, heated fluid in the heat pipe vaporises and rises to the top of the pipe, where it condenses to release heat to a sink such as the horizontal tank [62,63].

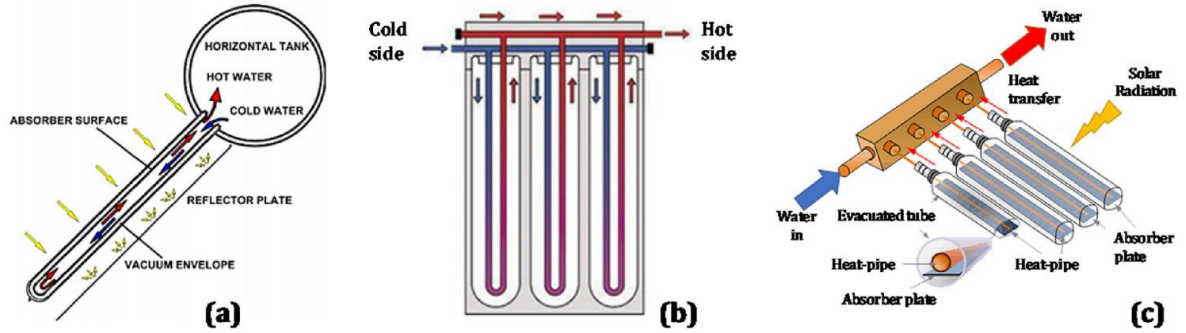

Figure 2.1: Representations of (a) a water-in-glass collector, (b) a U-type collector, and (c) a heat pipe collector taken from ([60]).

2.2.1.3 Compound parabolic concentrating (CPC) collector

Compound parabolic concentrators (CPC) apply reflectors to focus the sun's rays onto an absorber, thereby increasing the amount of heat capture, Figure 2.2 [64,65]. CPC can accept incoming radiation over a wide range of angles and uses multiple internal reflections to focus any radiation entering the aperture or acceptance angle onto the absorber surface at the bottom of the collector. The absorber configuration can be flat, bifacial, wedge, or cylindrical. The reflector is made of curved surfaces, each with a parabolic shape. CPCs have a concentration ratio between 1 and 5 and an operating temperature range of 60 to 240 °C [54].

Two major CPC design types are symmetrical and asymmetrical. The absorbers of the symmetrical type include flat, bifacial, or wedge, and they can be a straight channel or multichannel. In contrast, the asymmetrical type can be combined with a reverse or upside-down absorber plate configuration so that the CPC's concentrator directs radiation on the underside of the absorber plate. In the asymmetrical design, convective heat losses from the absorber are reduced because the upper plate side is well insulated [54,64].

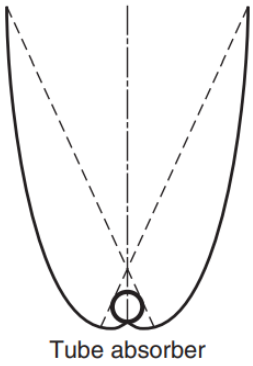

Figure 2.2: Showing a compound parabolic concentrator (CPC) with a tube absorber [54].

2.2.1.4 External concentrating compound parabolic concentrator (XCPC)

An external concentrating parabolic concentrator (XCPC) solar collector comprises glass evacuated tubes, manifolds of copper head pipes, copper u-tube and aluminium heat spreading fins, CPC reflector, aluminium frame, and insulation, Figure 2.3 [66,67]. The non-imaging reflector concentrates incoming radiation over wide acceptance angles onto the absorber of the evacuated tube. An XCPC can have two orientations: East/West (EW) and North/South (NS). For the EW orientation, the optics are designed so that the horizontally positioned absorber can accept seasonal sing ($\delta = \pm 23.5°$) of the sun's rays. In contrast, NS collectors receive light based on the sun's daily motion, thus needing large acceptance angles ($\theta = \pm 60°$) to deliver

significant operation hours [67]. The heat source temperature for the generator of the DACC cycle operates in the range of 135-230 °C [51,68].

The copper U-tubes serve as the liquid channel inside the collector. The channel structure has less circulating mass and low heat capacity, which enables the solar collector to reach higher temperatures in less time. The CPC reflector is fixed parallel to and underneath the evacuated tube's axis. During operation, beam and diffuse sun rays can be reflected onto the absorber material in the evacuated tube. The number of evacuated tubes is usually reduced, and insulation materials are used to minimise heat loss from the solar collector [65].

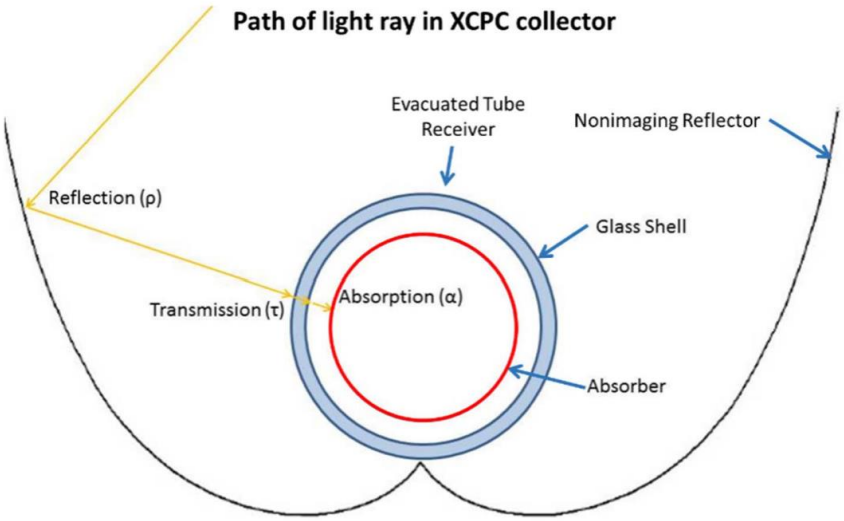

Figure 2.3: An XCPC solar collector showing a light ray (taken from [67]).

2.2.2 Thermal energy storage materials for solar energy applications

The availability of solar energy requires storing solar energy captured for future use at night or low solar radiation [53,54]. The performance of thermal energy storage systems fundamentally depends on the properties of the selected storage materials [53,69]. There are different types of energy storage solutions, and for solar energy systems, Alva et al. [69] categorised thermal energy storage materials and systems into sensible heat storage, latent heat storage, composite and microencapsulated phase change materials, and thermochemical heat storage systems. The thermophysical properties of thermal energy storage materials include specific heat, melting point, density, latent heat of fusion, thermal conductivity, thermal and chemical stability, volume change, toxicity, flammability, corrosivity, and vapour pressure [53,69,70].

2.2.2.1 Sensible heat storage materials

Sensible heat thermal energy storage materials in their specific heat capacity and the amount of heat stored is proportional to the density, volume, specific heat and variation of storage material temperature. Some examples of sensible heat storage materials include liquid mediums such as water, mineral oil, molten salts, liquid metals and alloys and solid mediums such as rocks, concrete, sand, and bricks [69,71]. Water is one of the best thermal storage materials for building space heating and hot water applications because it has high specific heat, low cost, non-toxic, and easy availability. However, it has drawbacks like high corrosiveness and vapour pressure [53,69]. Other liquid medium materials, such as mineral oil and molten salts, can deliver high-temperature heat transfer fluids. However, low thermal conductivity and volume changes make them less preferable to water. Solid storage materials are cheap, have no vapour pressure issue, and are readily available. However, these materials may need additional fluid to transport energy from one location to another effectively, reducing the system's efficiency [53,69,71].

2.2.2.2 Latent heat storage materials

Latent heat storage materials are also known as phase change materials (PCM) because they absorb heat as latent heat of fusion during melting [70]. A phase change occurs during heat absorption at near-constant temperature. A fundamental requirement for using PCMs as storage materials is their melting point should coincide with the operating temperature range of the thermal energy system. The melting process must occur with minimal subcooling, and the temperature of the storage medium remains constant during the discharge process [70,71]. Additionally, there is minimal temperature change between the storing and releasing heat, and the material’s latent heat of fusion is typically large compared to the specific heat. The significant difference gives PCM the advantage of high energy storage density, thus having a smaller storage volume and associated energy losses than sensible energy storage systems. Examples include organics (e.g., paraffin, esters, glycols, fatty acids, alcohols), inorganics (e.g., salt hydrates, metals and metal alloys, salts), and eutectics [70,72].

Organic PCMs have low melting points and thermal conductivity; thus, they are restricted to low temperatures and need higher surface areas during operation. Inorganic PCMs remain stable over many operating cycles; however, they are prone to phase segregation and sub-cooling and melt incongruently. Eutectics comprise two or more components, e.g., organic-organic, organic-inorganic, and inorganic-inorganic, that typically melt and freeze congruently

with no chance of separating components with a definitive melting/freezing point [69,72-74]. Composite PCMs are so-called when PCMs are dispersed with high thermal conductive materials, e.g., carbon and graphite, to improve their thermal conductivity. Moreover, some PCMs may be coated by microcapsules of various shapes and sizes to increase their contact surface area and mechanical stability. Nonetheless, microencapsulation is an expensive process requiring specialised techniques [69,70].

2.2.2.3 Thermochemical heat storage materials

The thermochemical heat storage system uses a reversible chemical reaction, so the reaction enthalpy equals the stored heat. During the charging process, a forward endothermic reaction absorbs thermal energy to dissociate a chemical reactant into products. During discharging, the reactants undergo a backward exothermic reaction to release heat. Both reaction products can be stored at a working or ambient temperature [75]. Thermochemical heat storage systems, though still at the laboratory stage, typically have higher energy density than sensible and latent heat storage systems. Besides, thermochemical energy storage has low heat loss and insulation requirements; thus, it has fewer limitations on storage duration [69,75].

2.3 Cooling systems

2.3.1 Global demand and markets for cooling systems

The International Energy Agency (IEA) research suggests that building energy consumption is growing faster [76]; however, there is limited consistent information on the pattern of energy usage on a regional basis and historical trends [77]. Refrigeration and air-conditioning systems consume around 30% of worldwide energy consumption [78]. Fifteen per cent of global electricity is used for cooling purposes, 45% of which is consumed by air-conditioning systems for domestic and commercial buildings [39].

The air conditioning industry is a business sector with huge market potential for further development and expansion. Well over 100 million units of vapour compression cooling machines were sold worldwide in 2014 [79,80]. The penetration of air conditioning is very high in developed countries like the United States of America and Japan; nonetheless, the worldwide average diffusion of mechanical cooling remains low to allow further expansion of the cooling market [79]. In Greece, for example, during 1990-2000, the number of air-conditioning units sold rose from 76,000 to more than 200,000 units [81]. For a predominantly cold-climate country like Canada, the overall power demand for space cooling doubled from

1990 to 2008 [82]. In Jordan, the market for air conditioning systems is projected to double by 2030 compared to 2015 [81]. About 60% of Australian residential homes have at least one air conditioner installed [83]. The European Union (EU) consumes about 40 % of its total energy for building energy usage, constituting 20% of total CO_2 emissions [81].

Several factors continue to drive the future growth and penetration of air conditioning systems worldwide. These factors include local climate conditions, global and local warming, an increase in the earth's population, growth of the local income and gross domestic product (GDP), electricity and equipment prices, efficiency, and energy performance of the equipment [13,79]. In Europe, the costs of additional electricity required for cooling due to global and local warming by 2050 is predicted to be between 22-89 billion euros per year, while the corresponding investment costs to purchase new air conditioners are projected to be close to 8 and 20 billion by 2050 and 2100 respectively. India is one of the leading countries in the developing world with high air conditioning sales due to significant improvements in economic and business conditions [79,81].

Regarding market shares, the Split systems have the highest market share, with total sales close to 74.5 billion USD. Also, Variable Refrigerant Flow (VRF) systems presented significant growth, reaching a total market value of 9.7 billion US dollars. Packaged Terminal Air Conditioning (PTAC), indoor packaged, and windows air conditioning systems have a lower market share [13,79]. For the residential sector, North American countries have the highest average energy intensity for cooling with 8,1 kWh/m^2/y, followed by Latin American countries, 8 kWh/m^2/y, the Middle East and Northern Africa zone, 4 kWh/m^2/y, Pacific Asia (3 kWh/m^2/y), and the Western European Countries, (2.2 kWh/m^2/y) [84]. Likewise, for the cooling of commercial buildings, the Middle East and Northern African zone have the highest energy intensity for cooling (42 kWh/m^2/y), followed by Latin American countries (38 kWh/m^2/y), North America (34 kWh/m^2/y), and Pacific Asian countries, (33 kWh/m^2/y) and Europe (10 kWh/m^2/y) [85]. The differences in energy intensity for cooling suggest that there is a potential to penetrate AC equipment to deliver building thermal comfort requirements [13,79].

2.3.2 Types of air conditioning (cooling) systems

Air conditioning may be defined as providing and maintaining a desirable internal environment temperature regardless of the external building conditions. A comfortable, healthy air supply often requires cool air, humidity regulation, air movement, and dust and odour removal [86].

The demand for building air conditioning primarily depends on the building design parameters (e.g., the building form and shape) and the air-conditioning system design itself (e.g., plant efficiency, method of distribution network, efficiency of prime movers). The desired atmospheric condition for cooling comfort applications usually aims for 22-24 degrees Celsius, relative humidity of about 40-60 per cent, air movement up to 0.25 meters per second, and a high degree of air purity [86,87].

Different climates, latitudes and seasons dictate the various treatments required for building comfort cooling [87]. Likewise, choosing the type of air-conditioning for a building depends on the climate, age of the building, individual preferences of the building owner, project budget, and the architectural design of the building [88]. Countries in warm climates require comfort cooling for building occupants. However, in predominantly cold weather countries with warm summers, e.g., the United Kingdom and Germany, many circumstances in the design and use of the building may lead to the need for comfort cooling [87]. The following section describes the different types of building cooling systems, Figure 2.4. It starts with a definition and description of passive cooling, and then the different active building cooling system types are presented.

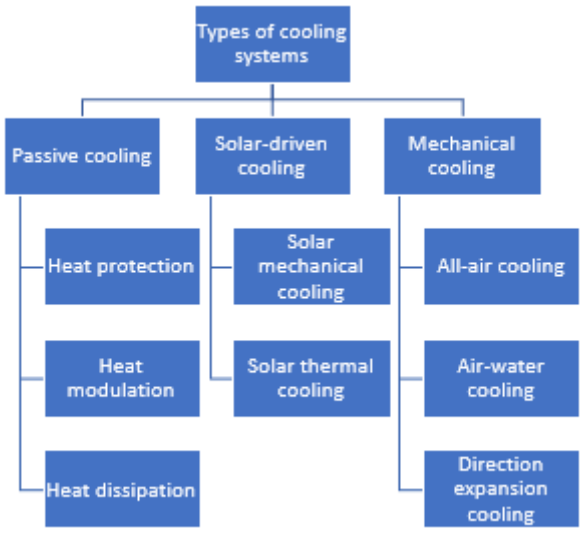

Figure 2.4: Types of cooling systems

2.3.2.1 Passive cooling techniques

Using active air-conditioning equipment to deliver thermal comfort in buildings poses issues associated with global warming and the depletion of the ozone layer. As a result, passive cooling strategies are explored to reduce building cooling loads, support the environmental

ecosystem, and deliver satisfactory human thermal comfort [13,17]. Bhamare et al. [89] define passive cooling as the application of several techniques that use cooling sinks such as building fabric, air, water, night sky, etc., to mitigate a rise in building internal temperature due to a variety of heat sources such as solar heat gain, internal building heat gain from appliances and lighting, infiltration. Three fundamental passive cooling strategies include heat protection, heat modulation and heat dissipation techniques [17,89,90].

2.3.2.1.1 Heat protection

In this passive cooling technique, the main objective is to protect the building from direct solar heat gains. Protecting from solar heat gain includes landscaping, water surfaces, active vegetation, and shading of the building's external surfaces [17]. The sources of building heat gains are either from the exterior building environment or heat sources from the internal building compartments. External heat gains are mainly from direct solar radiation and infiltration from ambient air temperature, while internal heat gains come from appliances, lighting, cooling, etc. [89,90].

Protection from external heat sources is achieved by improving microclimatic conditions or controlling direct solar heat. By enhancing a building’s microclimatic condition, landscaping, green vegetation, or water surfaces vary the atmospheric conditions around the building. Thus, landscaping and strategically planted vegetation or water surface are employed as effective ways of limiting the building’s solar heat gain and reducing the building's indoor temperature [89,90]. The building roof receives the most substantial solar radiation for the longest time compared to other building elements. As a result, water surfaces such as ponds can be installed on building roofs to reduce building heat gain [91,92]. Nonetheless, the lack of stable water is a limitation for implementing roof ponds on a large scale in buildings.

The solar heat control method is the reduction of transmitted solar radiation through the building’s thermal components. Transmission of solar radiation is controlled by reducing the intensity of transmitted solar radiation by applying windows or by diverting the incoming incident (beam or diffuse) solar radiation via solar shading devices. In buildings where the window covers 20-30 % of the building walls, as high as 45-60% of the cooling load originates from solar heat gain via the windows. Thus, sizing windows for daylighting performance and aesthetics must also consider the potential to cause overheating issues [93,94].

The solar shading technique is another solar control strategy that uses building extensions such as overhangs, horizontal louvres, or blind systems to reduce heat capture from the sun rays in

hot climatic zones or during summer months. Solar shading is strategically designed onto buildings to achieve a balanced solution of improved daylighting, visibility, and excess heat gain reduction [90,91]. Simulation studies by Krimtal et al. [95] suggest that effective shading design and strategic placement on buildings depend on design parameters such as climate, occupancy, and energy efficiency requirements. Shading techniques have been proven to potentially reduce cooling loads in countries such as the United States of America and Italy. However, solar shading's full potential is met when it is factored in the initial building design stage instead of retrofitting shading after building construction [95].

2.3.2.1.2 Heat modulation

In this passive cooling technique, the heat gain of a building is modulated by utilising the heat storage capacity of the building structure. In this method, the heat absorbed by the building's structural material (known as thermal mass) is stored and released later to remove heat from the building [89,90]. Thermal mass provides thermal inertia and stability and smoothens the heat fluctuations between outdoor and indoor conditions. Building thermal mass depends on many parameters, such as climatic conditions, building orientation, material properties, etc [90]. Building materials can be sensible heat storage material or latent heat storage material. Sensible heat storage materials usually have limited capacity compared to latent heat storage materials because latent heat storage materials (also called phase change materials) store and release heat during the phase change process at a nearly constant temperature [17,90].

In the daytime, the phase change material (PCM) absorbs latent heat from the opaque and glazed surface of the building while melting at a constant temperature. As a result, the temperature of the internal parts of the building is reduced or maintained at a stable temperature during the day compared to the absence of PCM [89]. To complete the process, the absorbed latent heat is rejected during night-time. The primary techniques for incorporating PCMs into building construction materials include vacuum impregnation, encapsulation, shape stabilisation, direct incorporation, and immersion [89]. Also, research by [91,96] shows that PCMs are usually integrated with various building compartments such as wallboards, ceilings, roofs, and windows. Shilei et al. [74] studied the effect of PCM integrated with gypsum boards. They found that during the summer, the PCM integrated board maintained the indoor temperature within the comfort range by absorbing 39.126 kJ/kg of heat before a total melting at 24 degrees Celsius. Jaalath et al. [97] studied the thermal effect of PCM integrated with building roofs for the weather conditions of Melbourne and Sydney and found there were

cooling load savings of up to 25% and 39%, respectively. Moreover, Goia et al. [98] compared the effects of traditional double glazing with PCM integrated with glazing and found increased comfort conditions when PCM glazing was used.

2.3.2.1.3 Heat dissipation

In the heat dissipation method, excess heat from a building is rejected to a suitable environmental heat sink at a lower temperature. The heat sink includes ambient air, water, and the sky. This process is possible because of the availability of an environmental heat sink and thermal linkage between the building and the heat sink. The heat dissipation method can achieve an instantaneous cooling effect, or coolth can be extracted at night-time and released during the daytime. Depending on the available heat sink, the heat dissipation technique can be grouped into convective, evaporative and radiative cooling [17,89].

In convective cooling, the unwanted heat in the building is rejected by the ambient air via natural ventilation. Natural ventilation can be driven by wind speed or the buoyancy effect of air due to air temperature difference between the internal and external compartments [99]. With the evaporative cooling technique, the large enthalpy of water evaporation is used to absorb heat from ambient air, thus resulting in reduced air temperature but increased air humidity[100]. With radiative cooling, heat is usually rejected from the surface of a building to a clear night sky [101,102]. Nwaigwee et al.'s [96] research showed that nocturnal radiative cooling can deliver a 14-48% reduction in cooling energy demand. However, material properties such as durability and water permeability limit the widescale adoption of the various heat dissipation techniques.

2.3.2.2 Solar cooling: renewable sources for building cooling

Solar cooling may be classified based on the energy input into two main groups: solar mechanical cooling and solar thermal cooling [34].

2.3.2.2.1 Solar mechanical cooling system

Solar mechanical cooling systems use a solar-powered prime mover to drive a conventional air-conditioning system. In these systems, solar photovoltaic panels are used to convert solar energy into electricity, which drives an electric motor of a vapour compression cooling system. Solar photovoltaic panels have low field efficiencies of about 10-15 %, resulting in low overall efficiencies of these solar mechanical systems [57,103].

2.3.2.2.2 Solar thermal cooling technologies

In solar thermal cooling systems, heat from the sun is absorbed by solar collectors and delivered to cooling machines to produce chilled water for refrigeration or building air-conditioning [104]. Solar thermal cooling technologies [15,105] are classified into three principal categories: (1) thermo-mechanical cooling, (2) open sorption cooling, and (3) desiccant cooling. Furthermore, thermo-mechanical cooling comprises two groups: solar ejector cooling and solar Rankine cooling. Moreover, open sorption cooling is grouped into two subdivisions: adsorption cooling and absorption cooling. All five thermal cooling technologies are described below.

2.3.2.2.2.1 *Thermo-mechanical cooling processes*

In the solar thermo-mechanical cooling method, heat from the sun drives compressor components of vapour compression and Rankine engines to produce a cooling effect [103]. The two subdivisions of thermo-mechanical cooling are described below. First, solar ejector cooling is presented, followed by the Rankine cycle.

2.3.2.2.2.1.1 *Solar ejector cooling cycle*

A solar ejector cooling cycle is fundamentally the same as a vapour compression cooling system, except that an ejector replaces the mechanical compressor. High-pressure vapour flowing through the nozzle of the ejector attains increased velocity such that the fluid pressure is lower than inside the evaporator. Consequently, flow is sucked into an ejector to mix with the primary flow towards a condenser. Ejector cooling systems have simple construction, are inexpensive and have low maintenance requirements [103,106]. Ejector cycles have low efficiencies, and their performance depends on geometrical parameters, operational conditions, and the type of working fluids [107].

2.3.2.2.2.1.2 *Solar Rankine cooling cycle*

In the solar Rankine cooling cycle, heat from the sun is harnessed to produce mechanical work and drive steam and organic Rankine cycles. Solar Rankine systems were proposed in the late 1970s during the oil crisis. However, this cooling system has not progressed further from the demonstration phases because they are not economically competitive [108]. Small-scale solar-powered organic Rankine cycle has high theoretical efficiencies with low working temperature [109]. The working fluid of an organic Rankine cycle must be selected carefully to meet building safety requirements. A study by Wali [109] suggests refrigerant type R-11 and

refrigerants consisting of fluoro inert compounds (e.g., fluorocarbon-75) comply with building safety requirements.

2.3.2.2.2.2 *Desiccant cooling process*

Desiccant cooling cycles are classified as open sorption cooling because sorbent is used to dehumidify the air. Desiccant systems use two main methods, known as sorption and desorption, to transfer moisture from one medium to another [15,104]. During the sorption process, variation in water vapour pressure of humid air and a desiccant causes moisture in the air to be transferred and absorbed into a desiccant material. In desorption, the increase in desiccant temperature causes absorbed moisture to be released to the airstream—the desiccant surface vapour pressure changes continuously to absorb moisture to complete the cycle [110]. Desiccant capacity and dew-point performance depend on desiccant characteristics, set-up temperature, and reactivation methods. In a solar-powered desiccant cooling system, solar thermal energy and a combination of direct and indirect evaporative stages are utilised to cool dry air [111].

2.3.2.2.2.3 *Adsorption cooling process*

Adsorption is bonding a fluid onto a solid surface [104]. When an adsorbent and liquid adsorbate (refrigerant) coexist in a closed vessel, the refrigerant migrates in vapour towards the adsorbent, so the refrigerant temperature reduces while the adsorbent temperature increases. The adsorption process is an exothermic reaction. Adsorption cooling cycle is designed to utilise this phenomenon [15]. The adsorption cooling cycle comprises two sorption chambers, an evaporator, and a condenser. The cooling effect is achieved in the evaporator, where the refrigerant vaporises under low pressure and temperature. Typical working pairs for adsorption cooling cycles include silica gel/water, activated carbon/methanol, and metal chloride/ammonia [105]. Depending on the driving heat temperature, adsorption cooling cycles usually achieve a COP between 0.3 and 0.7 [104,112]. Adsorption cooling cycles are attractive because they operate with environmentally friendly refrigerants, use low-temperature heat sources, and do not involve moving parts [105,112].

2.3.2.2.2.4 *Absorption cooling process*

The absorption cooling cycle is similar to the vapour compression cycle, except that the absorption cooling cycle replaces the compressor with a circuit loop consisting of a generator, an absorber, a liquid pump, an expansion valve, and a heat exchanger [113]. The absorption

cooling system is heat-driven with minimal work input from pumps, unlike the vapour compression cooling cycle, which utilises a mechanical vapour compressor [114]. The main components of an absorption cooling system are an absorber, generator, condenser, evaporator, solution pump, and expansion valves [42].

The absorption cooling cycle operates at two primary pressure levels: the absorber and evaporator operate at a low-pressure level. In contrast, the generator and condenser operate at a high-pressure level [115]. At the start of the cooling cycle, Figure 2.5, heat extracted from a conditioned space is transferred through a chilled water loop to an evaporator, causing the refrigerant to evaporate [15].

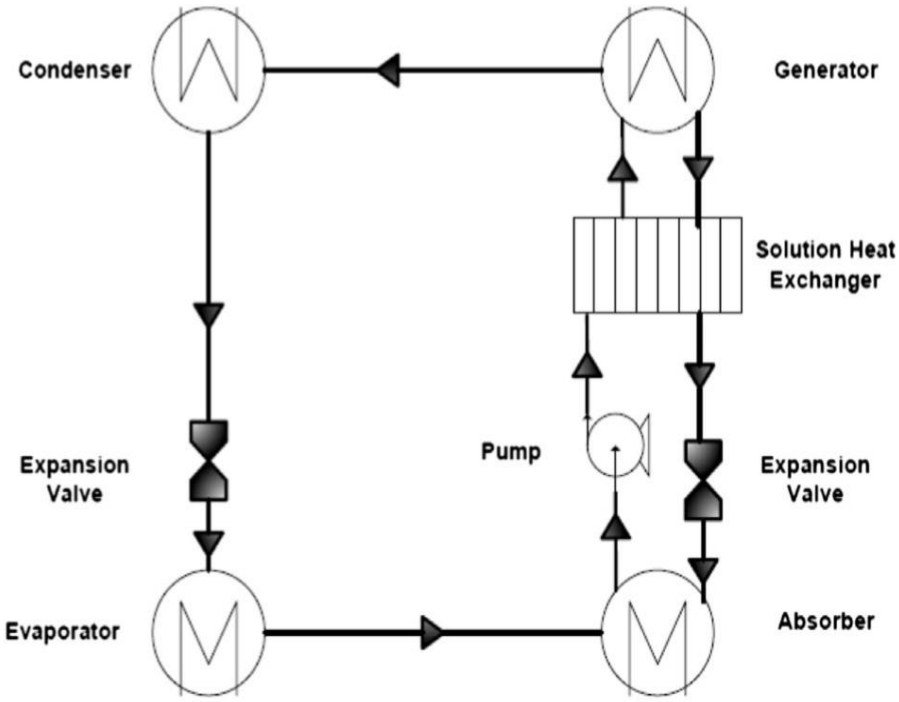

Figure 2.5: Schematic diagram of a single-stage absorption cooling cycle [15].

The low-pressure refrigerant vapour is transferred to the absorber, which is initially absorbed by a secondary fluid known as an absorbent to form a weak solution. A cooling water medium extracts the heat released from this process. The solution pump transfers the diluted refrigerant-absorbent solution to the generator, which is at a high-pressure level. In the generator, external heat input boils the refrigerant from the refrigerant-absorbent solution, leaving the concentrated absorbent in the solution. The strong solution returns to the absorber via a throttle valve. The regenerated refrigerant vapour flows to the condenser, where heat is rejected from the

refrigerant vapour to a cooling water loop. After this condensing process, the resultant high-pressure liquid flows through an expansion valve to the evaporator, thereby reducing the fluid pressure and temperature and completing the cooling cycle [15,111].

The "number of effects" can categorise the absorption cooling system, which is the number of times the heat source is recycled inside a chiller to produce a cooling effect [115]. Three common types or “number of effects” available on the market are single-stage, double-stage, and triple-stage effects. An additional generator delivers refrigerant vapour at a higher pressure level for double-stage effect chillers than a single-stage effect chiller. Meanwhile, triple-stage effect chillers use three generators to drive heat input three times to produce the highest pressure refrigerant vapour. Likewise, an absorption cooling system can be classified based on the working fluid pair [116,117].

For a more straightforward distinction of the different types of absorption cooling systems, the following review is grouped into two major working fluid pairs: water-lithium bromide and ammonia-water. Additionally, the section ends with a brief introduction of other working fluids for completeness.

2.3.2.2.2.4.1 *Absorption cooling using water-lithium bromide working pairs*

Water/lithium bromide (H_2O/LiBr) working pair uses water (H_2O) as refrigerant and lithium bromide (LiBr) as absorbent. Using water as refrigerant limits this type to cooling temperatures above 0 °C; thus, H_2O/LiBr working pairs are ideal for building air-conditioning [52,54]. An absorption cooling system that uses an H_2O/LiBr working pair has many advantages. In essence, it has a low maintenance cost, is non-toxic, has relatively higher COP, has low working pressure, and the absorbent is non-volatile [53,104,105]. Nonetheless, a significant challenge with using H_2O/LiBr solar absorption chillers is a two-phase H2O/LiBr solution mixture and LiBr crystals can coexist in equilibrium [113,118]. H_2O/LiBr absorption cooling systems have a typical generator operating temperature range of 70 – 90 °C. Thus, heat requirements can be delivered by non-concentrating types of solar collectors [104].

2.3.2.2.2.4.2 *Absorption cooling using ammonia-water working pairs*

Absorption cooling systems utilising ammonia/water (NH_3/H_20) working pair have a cooling cycle similar to the H_2O-LiBr absorption system. Nonetheless, their operational characteristics differ from H2O-LiBr systems because they use ammonia (NH_3) as refrigerant and water (H_2O) as absorbent [42]. Furthermore, in the NH_3/H_20 absorption cooling cycle, a rectifier separates

water vapour from NH_3 to prevent freezing and cooling performance degradation [110,119]. The freezing point of NH_3 is -77°C; as a result, NH_3/H_20 can be utilised for sub-zero temperature cooling applications. Thus, earlier cooling applications were predominantly used for refrigeration [120].

2.3.2.2.2.4.3 *Absorption systems using other working pairs*

The fluids discussed above have two working fluid pairs- H_2O/LiBr and NH_3/H_20. However, absorption cooling systems utilise three-component working fluids, i.e., refrigerant-absorber-auxiliary gas (e.g., ammonia-water-hydrogen). Here, the absorber and refrigerant behave the same as refrigerant-absorber pairs previously discussed, and the auxiliary gas provides pressure equalisation in the cooling system. Sun et al. [117] categorised absorption cooling working fluids into five series according to refrigerants using (1) NH_3, (2) H_2O, (3) alcohol, (4) halogenated hydrocarbon, and (5) other mediums. Recent research into working fluids aims to improve cooling cycle operation characteristics. However, most innovative working pairs are in the research and development phase.

2.3.2.3 Mechanical cooling

Central heating, ventilation, and air conditioning (HVAC) systems can be grouped into four functional subsystems: a source subsystem, a distribution subsystem, a delivery subsystem, and a control subsystem [87,121]. The source subsystem delivers the heating and cooling effect, including chillers, boilers, and cooling towers. The distribution system moves the heating or cooling effect from the source to the building space, including ductwork, fans, piping, and pumps. The control subsystem regulates equipment operation for comfort, safety, process, and energy efficiency. The delivery subsystem, also known as “terminal devices”, delivers the heating or cooling effect into the building spaces and includes fan coils, baseboard radiators, and diffusers [122].

For cooling systems, the delivery components are classified into three main groups: all-air, air-and-water, and all-water cooling systems. The following section describes an all-air cooling system, an air-and-water cooling system and an all-water cooling system [122,123].

2.3.2.3.1 All-air cooling systems

All-air cooling systems deliver sensible and latent cooling capacity via cold supply air into building-conditioned space. No chilled water or supplementary cooling is supplied to the

building space [87]. The following section describes the various all-air cooling systems available on the market.

2.3.2.3.1.1 *Single-zone system*

Single zone all air systems are employed in circumstances or designs where the load is either constant or varies uniformly in each building zone [87]. A single-zone system consists of an air handling unit, a cooling source, distribution ductwork and an appropriate terminal device installed in a single location, Figure 2.6. The temperature control in single-zone all-air systems is achieved by adjusting the supply air temperature at the central plant. A cooling system installed in a single zone has fewer components compared to multi-one installations; as a result, it has a simple design, and there are fewer associated capital and maintenance costs [87,124].

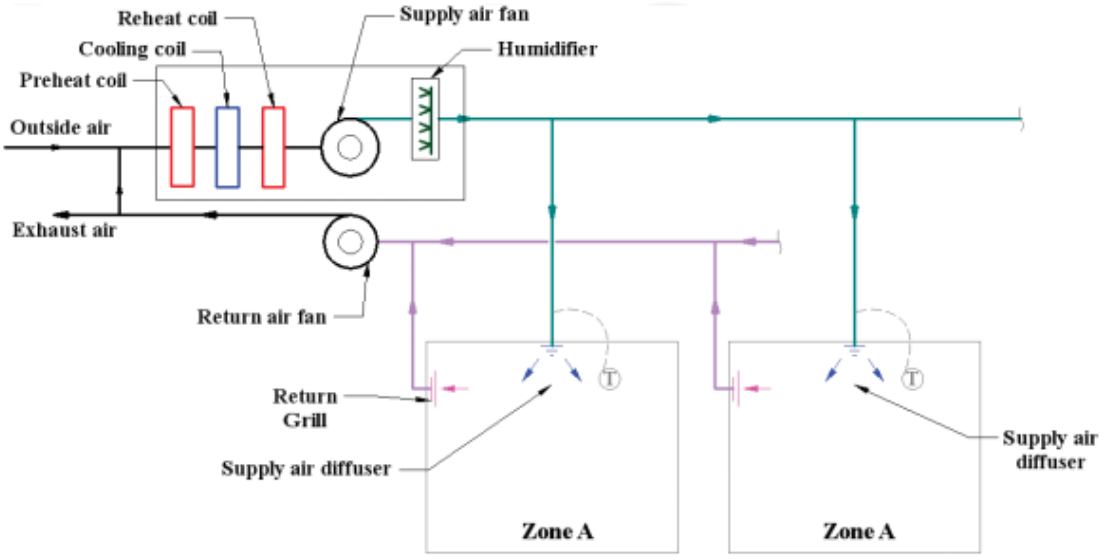

Figure 2.6: All-air HVAC system for a single zone [124].

2.3.2.3.1.2 *Variable-Air-Volume (VAV) Systems*

Traditional air-conditioning systems are based on maintaining air discharge to the building space at constant volume, with load variations met by adjusting the building air temperature. Due to the ever-present demand for energy-efficient systems, variable-volume air-conditioning systems are explored as alternatives to traditional cooling systems [87], Figure 2.7. Variable Air Volume (VAV) systems manage changes in local load conditions by adjusting the air volume delivered to the conditioned space at a constant temperature. VAV systems are suited to buildings with long cooling loads and easily adapt to office partition layouts. However,

buildings with high latent loads may have difficulty in control humidity with VAV systems [87,124].

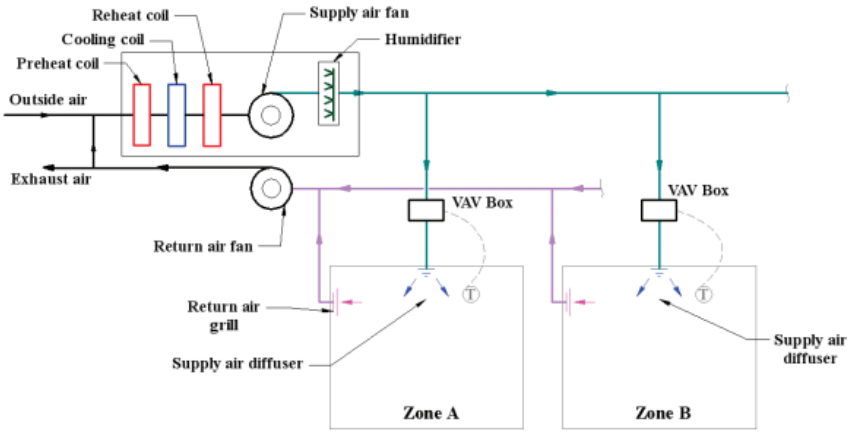

Figure 2.7: All-air HVAC systems with VAV terminal units [124].

2.3.2.3.1.3 *Induction systems*

An all-air induction cooling system may be used where the bulk of the heat output is transferred to the return air to the central plant. With an induction cooling arrangement, the conditioned air is ducted to induction boxes fitted in the ceiling void [87,125]. Each induction box incorporates a damper device and thermostats to enable conditioned airflow to induce a variable proportion of warm air from the ceiling void to the discharge stream. Automatic switching systems may be introduced to minimise the period that heat gains from lighting. Induction cooling systems are easy to maintain and have low sound emissions. However, the induction systems have large duct requirements, thus, higher investment costs [87,124].

2.3.2.3.1.4 *Dual-duct systems*

In a dual duct cooling system, cold and warm air are conveyed via separate ducts and mixed at a junction to reach a desired temperature, Figure 2.8 [124]. Each room that requires cooling has a mixing box with dampers to deliver all cool, warm, or some mixture of both into the building space. Dual duct cooling systems have air delivery rates of five or six changes per hour, compared with the 1.5-2 required to introduce outside air. A dual duct cooling system incorporates air recirculation return to the main plant using return shafts and ducts [124]. An advantage of the dual duct cooling system is that any room can be cooled or heated without zoning the building compartments or changing thermostats. Also, building zones requiring high ventilation rates can be served from the same original plant source. The major disadvantage of

a dual duct cooling system is that the system consumes high energy and requires large spaces for ceiling voids and shafts to accommodate the ductwork size [87,124].

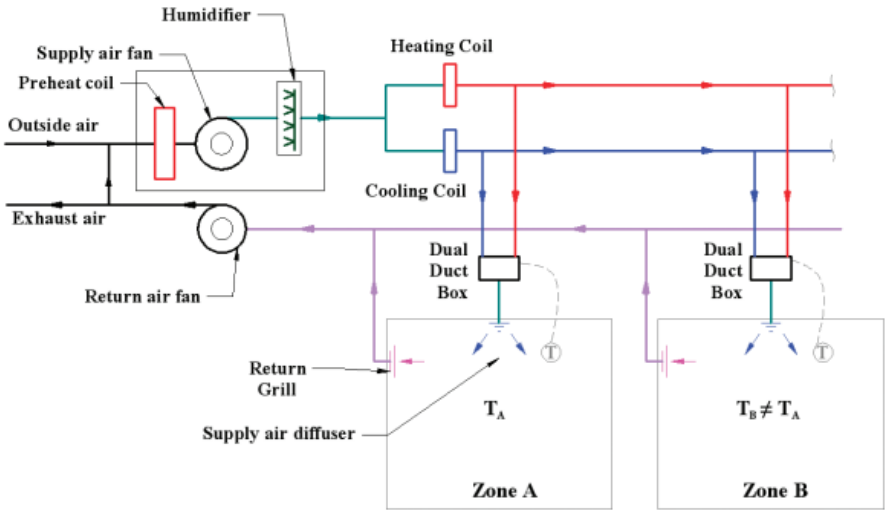

Figure 2.8: All-air HVAC dual-duct system [124].

2.3.2.3.1.5 *Displacement ventilation*

In displacement ventilation, conditioned outdoor air is supplied at low velocity into low-level building spaces to create a pool of cool, fresh air for building occupants. The cooling system works well in open-plan office spaces with low heat gains and where it is not critical to achieve tight control of room or zone temperature [124]. Displacement ventilation systems work best in spaces greater than 2.5m, have moderate heat gains, and are limited to cooling loads up to 100 W/m^2 in localised areas. The benefits of displacement ventilation are better air quality, less cooling demand, and more extended periods of free cooling available in the occupied spaces of the building. In addition, displacement ventilation has simple control with a room thermostat. Nonetheless, displacement ventilation systems cannot be used in the same building space as mixed-flow cooling systems due to the differences in air flow regime requirements and containment issues [87,124].

2.3.2.3.2 Air-water systems

Air-water cooling systems are a hybrid system combining the benefits of all-air and all-water systems. Air-water systems usually have smaller system volumes than all-air systems, and ventilation is introduced to condition the air in the building's internal zone properly. The water medium usually carries the building thermal load by about 80-90% through cooling water, while the air medium conditions the remaining latent load [124]. Air-water cooling systems

have four primary types: fan coils, induction units, heat pump systems, and chilled ceilings [87].

2.3.2.3.2.1 *Fan coil system*

Fan coil units comprise a chassis mounted with a centrifugal or crossflow fan, an air filter, a single water-to-air heat exchange coil, or a pair of such coils, Figure 2.9 [124]. Fan coils have different patterns to suit various mounting positions. One of the most common installation arrangements is where the fan coil is mounted in the ceiling void with the discharge connected to the diffusers. Air recirculation is achieved via the luminaires through the ceiling void, where return air mixes with fresh air supply discharged locally to the fan coil unit intake [87,125].

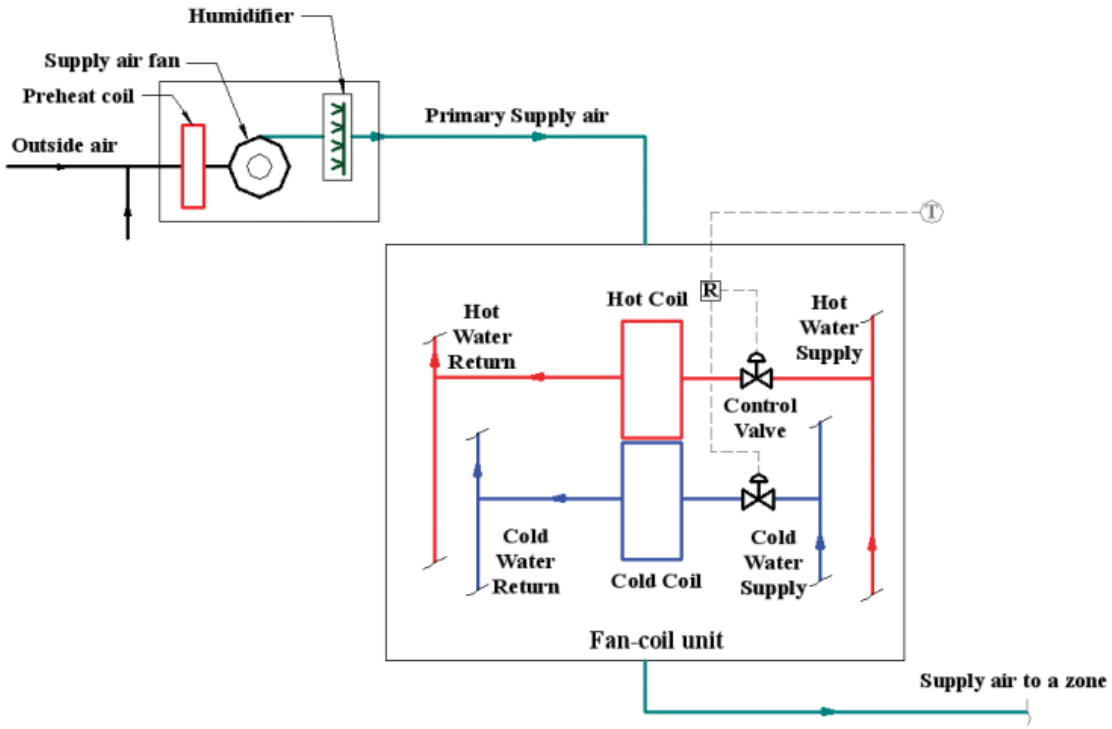

Figure 2.9: An air-water HVAC system uses fan coil units [124].

Fan coil design must meet the ventilation needs of building occupants; as a result, fan coil units must have the capacity to recirculate the zone or room air. The recirculation can be met in the central plant, where the air is prefiltered, conditioned, and introduced via a ducted route, and at the same time, the exhaust air is ducted to an energy recovery unit. Fan coil piping arrangement can be a four-pipe system or a two-pipe system. A four-pipe system connects the cooling, heating flow, and return pipes to independent coils [87,126].

On the other hand, in the two-pipe system, heated water is supplied to a coil in winter, while chilled water is provided to the same coil in summer. The two-pipe system encounters problems

in mid-season where some zones need heating delivered and other spaces require cooling; nonetheless, cooling and heating cannot be delivered simultaneously. Fan coil unit's benefits include high cooling capacity, low capital cost, flexibility to accommodate future changes, and smaller ventilation plant and distribution ductwork than all-air systems [87,122,124,127].

2.3.2.3.2.2 *Induction system*

Induction cooling systems are externally like fan-col units, although they are rarely used today; however, their application is introduced in this section for completeness. In an induction cooling system, primary air is initially conditioned in a central plant and then supplied to zone terminal units under pressure [121,126], Figure 2.10.

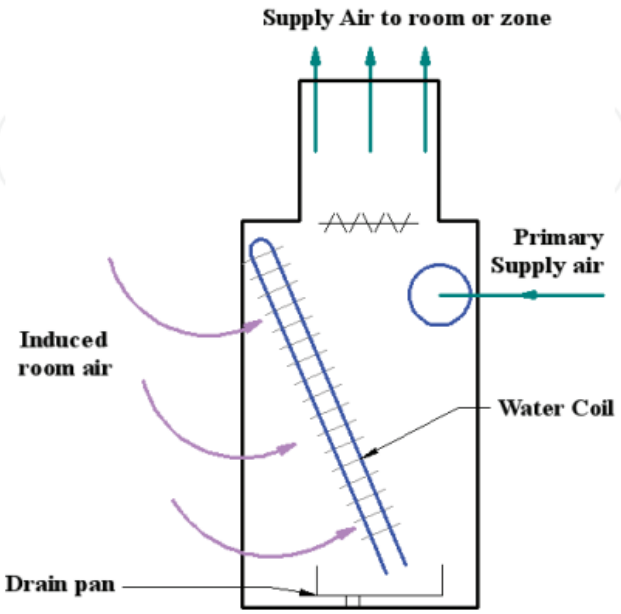

Figure 2.10: Air-water HVAC system using induction units [124].

2.3.2.3.2.3 *Heat pump system*

Water-source heat pumps can save energy for large buildings under extreme cold weather. A centralised water circulating loop can be used as the source and sinks for heat pumps. As a result, heat pumps can act as the primary source of building cooling and heating and are sometimes referred to as reverse-cycle heat pumps [128,129]. The heat pump installation designs can be the floor, ceiling or under-window mounted. A heat pump unit typically comprises a reversible refrigeration compressor, a refrigerant-air coil, a refrigerant-water heat exchanger, a cycle reversing valve, and a refrigerant expansion valve [125,128]. When cooling demand needs to be met in the building space, the refrigerant-air coil becomes the evaporator,

and the condenser rejects heat via the waterside heat exchanger to the circulating water circuit [42,130].

On the other hand, when building heating is needed, the refrigerant-air coil acts as a condenser. In contrast, the refrigerant-water heat exchanger acts as the evaporator by drawing heat from the circulating water circuit. Temperature control is usually achieved using a thermostat to sense the return air temperature sequences between the compressor and the reversing valves. The main drawback of a heat pump system is the lack of ventilation air compared to an all-air cooling system. Also, there can be noise pollution from the indoor units because the compressors can start and stop intermittently [87,124].

2.3.2.3.2.4 *Chilled ceilings*

In the chilled ceiling cooling technique, the building ceiling is cooled by passing chilled water to collect heat in the top or roof compartment so that the HVAC equipment can deal with ventilation and humidity control separately [87]. It is essential in chilled ceiling systems that the temperature entering chilled water be above the room's dew point by at least 1.5K for effective control and to avoid the formation of condensation. Chilled ceiling systems usually have a flow temperature of 14-15 °C and a temperature increase across the exchange device of 2-3 K. Chilled ceiling systems are highly dependent on the dehumidifying capacity of the external air supply to control the zone dew point [87,126]. Many types of cooling surfaces are employed in the industry, including chilled beams, radiant, and convective panels. Radiant and convective panels typically cover large ceiling areas, though both can be accommodated in shallow ceiling voids around 65mm and 250 mm, respectively. Convective systems have higher sensible cooling capacity than radiant panels, 160 W/m^2 and 120 W/m^2, respectively. Chilled beams operate like convective panels, except for using small, finned coils that can incorporate a ventilation air supply. Chilled beams deliver cooling via passive or active methods. The passive beam output is limited to a floor area of 60-80 W/m^2, while active beams can provide up to 150 W/m^2 [87,121,126]. An advantage of chilled ceiling systems is the capacity to offset high cooling loads even without air movement within the building space. However, condensation forming on the chilled ceilings can drip directly into the occupant’s building space [87].

2.3.2.3.3 Direct expansion (DX) systems

Direct expansion (DX) systems use refrigerant directly as the heat transfer working fluid to deliver cooling or heating to the air within the building zone. Two main DX types exist: localised and centralised systems, popularly known as variable refrigerant volume (VRV) [87].

2.3.2.3.3.1 *Local DX systems*

Local DX cooling systems consist of a compressor, air filter, fan, and cooling coil [87,124], Figure 2.11. It may sometimes be fitted with electric resistance heaters to deliver heating during winter months, and outside fresh air may be introduced in some systems. However, it rarely can perform humidification for human thermal comfort. The variety, popularly known as the packaged system, usually has a unit construction frame, consequently benefiting from low initial capital costs [124,126].

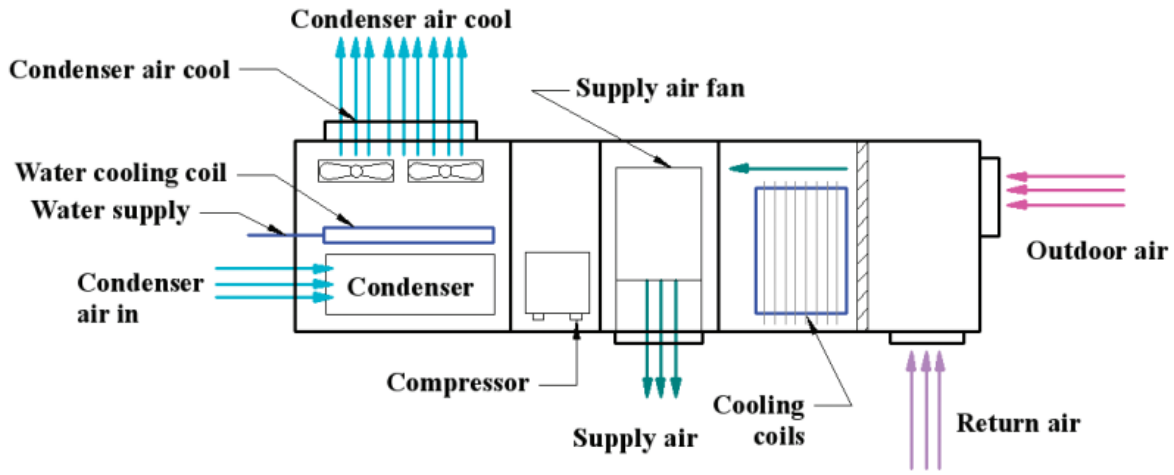

Figure 2.11. Packaged rooftop air-conditioning unit [124].

In another type of DX cooling system, popularly known as the “split type”, the condenser and compressor are fitted remotely outdoors, away from the evaporator within the building space. A split-type system usually has the evaporator fitted through the building wall or the window opening to deliver cooling into the building for human thermal comfort. Small DX cooling systems usually air-cool refrigerators, while water-cooling is applied in larger cooling equipment sizes. Recent DX systems have a hermetic type of compressors to ensure quiet operation for building occupants. A unitary air-conditioner can be a small unit installed in every single room in a building. In contrast, packaged rooftop air-conditioners can be used in large buildings or industrial applications where extensive ductwork may be needed to distribute the air in the building zones [87,124].

2.3.2.3.3.2 *Variable refrigerant volume (VRV) systems*

VRV systems cool or heat buildings using refrigerant as the primary working fluid. The term "variable" refers to refrigerant control to enable independent zonal control to achieve a much more efficient cooling or heating in buildings with many compartments. VRV systems have been popular in the last decade because they are cost-effective, reliable, and efficient at meeting building space cooling and heating demands, as well as water heating needs [131-133]. Although VRV systems use refrigerants with high operating pressures, they offer many benefits, such as high heat transfer, reduced pipe sizes, reduced compressor lubrication and increased operating COPs. The VRV systems consist of multiple indoor units (terminal devices) connected to one or more outdoor components. Each outdoor unit comprises a compressor, refrigerant-air heat exchanger, air circulation fans, and control panel that rejects heat to outdoor air when cooling or absorbs heat from ambient air when heating is required [87,126].

In contrast, the indoor units comprise a refrigerant-air heat transfer coil, filter, fan, and expansion valve. Multiple outdoor units can rotate to provide load sharing and greater plant efficiency. VRV systems operate with a typical operating range of -20 – 13.5 °C in heating and -5 – 43 °C in cooling modes. Despite the many advantages of VRV systems, they come at a higher upfront cost than air cooling systems [87,132].

2.3.2.4 Thermodynamic operation of conventional AC units

Building air conditioning is mainly provided by vapour compression chillers or air conditioning units. Heat pumps that remove heat from a building space or transfer heat into a building apply the vapour compression system [123,134-137]. Different building air conditioning systems will have the same central features, except there could be variations in refrigerants used, the specific mechanical device used, and the system configuration [134-135]. The thermodynamic operation of a vapour compression system is described below.

2.3.2.4.1 Vapour compression cooling system

The vapour compression cycle consists of four main processes: vapour compression, condensation, liquid expansion, and evaporation, Figure 2.12 [134-136,138]. At the beginning of the cooling cycle, a refrigerant vapour at a low temperature and pressure (state 1) flows into a compressor and exits at a higher temperature and pressure (state 2). In the condenser, heat is rejected from the high-temperature refrigerant to an external heat sink, e.g., the ambient air, so

the refrigerant condenses and exits as a liquid (state 3). The refrigerant's pressure, and consequently the temperature, reduces as it flows through the expansion valve. The pressure reduction causes some of the liquid to vapourise. As a result, the refrigerant enters the evaporator as a two-phase flow of liquid and vapour (state 4). Heat gain from the external temperature course evaporates the remaining liquid refrigerant in the evaporator. The resultant vapour then returns to the compressor's inlet, thus completing the cooling cycle [134-136].

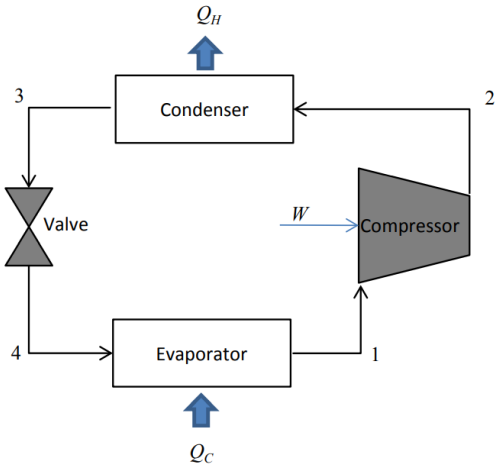

Figure 2.12: Schematic of a vapour compression cooling system [135].

The fundamental laws of thermodynamics, heat transfer, and fluid flow govern the performance of the four main components of the vapour compression cycle [139]. A Carnot cycle is a reversible cycle with maximum thermal efficiency for a given temperature limit, and it can be used as a reference standard to compare actual power cycles. As a result, the Carnot cycle is used to evaluate the best possible performance of vapour compression systems. The COP for a cooling cycle is the ratio of the cooling effect to the cost of work input into the system [135,136]. The COP for a Carnot cooling system is defined in terms of low (L) and high (H) temperature levels using absolute temperature [135]:

$$COP_{Carnot} = \frac{\dot{Q}_L}{\dot{W}_{ideal}} = \frac{T_L}{T_H - T_L} \qquad 2.1$$

The vapour compression cycle processes are different to that of the Carnot cycle. For example, in the vapour compression cycle, the heat rejection does not occur at constant temperature, the expansion process in most machines is reversible, and the compression process is not

isentropic. Nonetheless, the performance of actual vapour compression systems mimics the Carnot relation in equation 2.1. Thus, the COP is inversely proportional to the temperature difference between the low and high-temperature points and directly proportional to the absolute temperature of the low-temperature source. It is conventional to characterise the states of a vapour compression cycle on thermodynamic property coordinates, more commonly on a pressure-enthalpy diagram [135,136].

Open-type compressors are typically used in large air-conditioning systems, and the assumption in processes 1-2 regarding adiabatic compression tends to be valid in open-type compressors. On the other hand, hermetic compressors, used in small-scale and residential air conditioners, have significant heat transfer between the motor and the refrigerant [135,136]. Nonetheless, hermetic compressors are used because of the benefit of quiet operation in residential cooling applications [87].

2.3.2.5 Thermodynamics of the solar diffusion absorption cooling systems

DACC system utilises ammonia-water-hydrogen as a working fluid, where ammonia is the refrigerant, water is absorbent, and hydrogen gas is used as an auxiliary gas [40]. Ammonia (refrigerant) transports energy from a low-temperature source to a high-temperature sink. At the same time, water (absorbent) absorbs the ammonia (refrigerant) at low partial pressure to release it at high pressure [42]. The hydrogen (auxiliary gas) provides pressure equalisation throughout the thermodynamic cycle [40].

A basic layout of the DACC cycle was introduced in Figure 1.1 [40]. Starting a description of the cooling cycle from the absorber component, a reservoir at the base of the absorber contains strong ammonia liquid. The strong ammonia liquid flows by gravity through the solution heat exchanger (SHE) towards the generator/bubble pump. External heat input applied to the generator drives ammonia vapour vertically away from the generator towards the rectifier [40,45].

Water is removed from the weak ammonia-water solution and returned to the absorber through an outer tube of the bubble pump and the SHE to complete the ammonia-water solution loop. The rectifier removes any residual water vapour to ensure that the ammonia vapour's water content is near zero. Any captured water drains down to the outer wall of the generator to mix with an ammonia-water solution, returning to the absorber. Then, the purified ammonia vapour

flows from the rectifier to the condenser. The condenser has a finned tube which rejects heat from ammonia vapour by natural convection to the environment [40,44].

The resulting ammonia liquid (condensate) flows downwards towards the evaporator. Meanwhile, any non-condensed ammonia vapour flows through a gas bypass to the reservoir beneath the absorber. In the evaporator, hydrogen gas flows from the absorber and meets ammonia liquid. The ammonia liquid evaporates due to its low partial pressure compared to hydrogen, as per Dalton's law of partial pressures. The resultant ammonia vapour-hydrogen mixture flows from the evaporator to the absorber via a GHX [43,140].

A small quantity of ammonia vapour is absorbed within the absorber into a liquid solution in the reservoir. The remaining ammonia vapour-hydrogen gas mixture returns from the top section of the absorber, via the GHX, to the evaporator to complete the ammonia vapour-hydrogen gas circulation loop. Gas circulation in the ammonia vapour-hydrogen gas loop is driven by natural convection caused by density differences in ammonia vapour content [141,142].

2.4 Heat sources in the building environment

This section provides a general overview of the main types of heat generators used in the building environment, Figure 2.13. A heat generator is a device that converts fuel or electricity into heat or produces thermal energy to heat interior building space, e.g., a boiler or radiant heater [87]. Examples of energy sources and fuels typically utilised for heating in the built environment include [143]:

- Gas - natural gas, biogas
- Liquid - petroleum-based oil, liquified petrol gas (LPG), biodiesel
- Grid electricity
- Onsite renewable electricity from solar photovoltaic and wind turbines
- Solid biomass
- Waste heat and heat from district heating
- On-site solar hot water
- Heat and electricity from on-site combined heat and power (CHP) plant

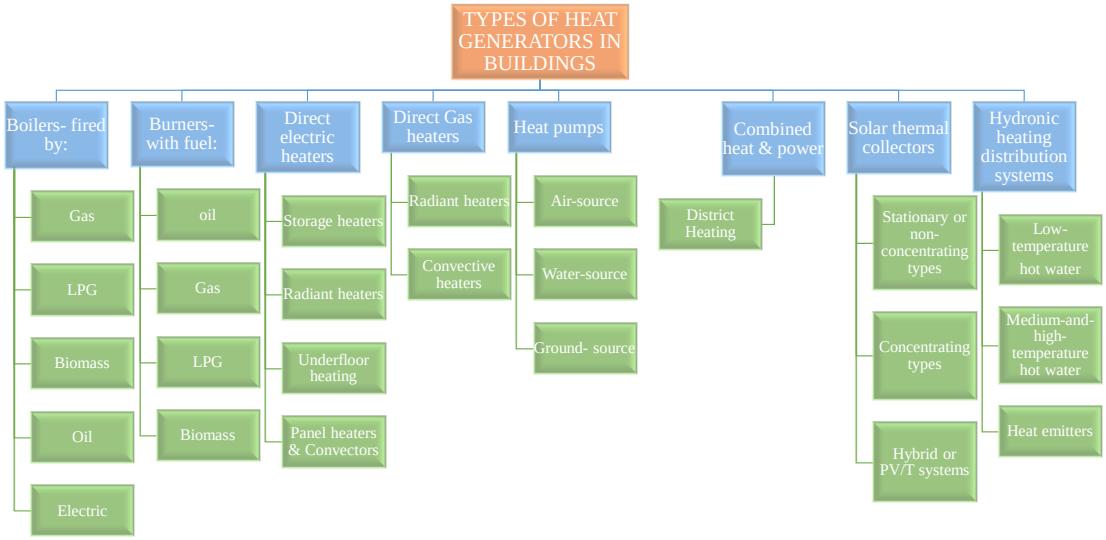

Figure 2.13: Types of heat generators in a building. Compiled from [87].

Space heating systems are grouped into two main types, indirect and direct-fired systems, based on the proximity of the heat generator heat source and heat emitter. In indirect heating systems, a remote heat generator, such as a boiler and CHP plant, produces heat which flows through a fluid transfer medium to several heat emitters, such as radiators. In a direct-fired system, the heat source is located within a heated building zone – e.g., direct electric heaters [87]. The following sections describe the characteristics of different types of heat generators used in the built environment under seven headings illustrated in Figure 2.13.

2.4.1 Boilers: fired by Gas, Oil, LPG, Electric and Biomass.

A boiler is an equipment that converts chemical energy in fuels into heat energy and distributes the heat via hot water medium or steam. Boilers generally use gas and heating oil as fuel in modern residential buildings, while LPG-and-biomass-fired boilers are installed in remote off-grid buildings. Boilers powered by electricity have minimal maintenance requirements and no direct discharge of poisonous gases. Steam boilers use steam as a transport medium primarily for industrial processes rather than the provision of space heating in modern buildings [87,126]. Steam systems demand stringent pressure systems safety requirements, have less thermal efficiencies, and more running costs.

In central building heating systems, the heat generated from a boiler is transported as hot water to heat emitters (e.g., radiators) in interior building space. The cooled water is returned to the boiler and reheated to begin the next heating cycle. In residential buildings, a combination

boiler is a single compact unit that delivers both space heating and hot water service. Moreover, in a condensing boiler, heat from high-temperature (200-250°C) flue gases discharging to the atmosphere are recovered via internal heat exchangers. Thus, condensing boilers can achieve 90% overall efficiency compared with 75% of conventional boilers [87,144].

2.4.2 Hydronic heating distribution systems

Hydronic heating uses liquid as a transport medium to transfer heat from heat generators such as boilers and heat pumps to heat emitters and other building hot water service points. Alternative working fluids such as synthetic and mineral oils may be used in hydronic processes where high temperatures over 250 °C must be achieved. Water heating systems can be categorised according to low, medium, or high flow temperatures. In the United Kingdom, hydronics using water heating systems are classified as [87,126]:

I. Low-temperature hot water systems are used in modern residential buildings because they are safe to operate and do not need to comply with Pressure Systems Safety Regulations 2000. The design temperature is 90 °C, with a differential at the boiler or water heater in the range of 5-20 Kelvin.

II. Medium-temperature hot water systems- design temperature ranges between 90-120 °C, with a differential at boiler or water heater in the range of 25-35 Kelvin.

III. High-temperature hot water systems- are generally used in large commercial buildings and district heating applications where heat must be transported over long distances. The design temperature is above 120 °C, with a differential at boiler or water heater in the range of 45-65 Kelvin.

Two major pipe layout configurations are for distributing heat medium to heat emitter locations within a building: one-pipe circuits and two-pipe circuits [145].

2.4.3 Heat Emitters

Heat emitters distribute heat from engines (e.g., boilers, heat pumps) into interior building spaces through heat radiation, natural or forced convection, and a combination of radiation and convection. Radiators and convectors are prime examples of heat emitters used in residential buildings. Recent building heating equipment manufacturers have supplied varieties of heat emitters that include [87,146]:

- Combined radiant and convective heating- e.g., radiators; column type radiators; panel type radiators; steel radiators.

- Radiant type – typically installed in sports halls, hospital wards and corridors. Heats people and room surfaces by radiation.

- Radiant heating panels are manufactured, rated, and tested according to BS EN 14037.

- Convective - e.g., cased natural convectors and convector skirting heater.

- Combined heating and cooling units – e.g., fan coil units and active beams.

2.4.4 Burners- with fuel: oil, gas, LPG, and biomass

A burner is a device that delivers heat to a building supply airstream by fuel combustion in the air. Fuel is predominantly hydrocarbons, such as oil, gas, and coal. The warm air generated by a burner is blown through ducts and warm-air registers to interior spaces to achieve thermal comfort. Burners applied in residential buildings need to maintain an appropriate draft (typically about 0.5 Pascal) for a given fuel firing rate [87]. Consequently, outlets from flue serving burners must be carefully located to ensure efficient natural draught and safe dispersal of combusted products [147].

2.4.5 Direct Electric heaters

Direct electric heaters are also called unitary systems because their heat source is within the interior building zone. There are four main types of direct electric heaters: storage heaters, radiant-type heaters, underfloor heating, and panel heaters and convectors [87,129,148].

2.4.6 Direct Gas heaters

There are two types of direct gas-fired heaters: radiant heaters and convective heaters. Subsequently, there are two types of gas-fired radiant heaters: radiant overhead tube heaters and radiant plaque heaters. Direct gas-fired heaters are typically mounted close to building roof space to allow uniform heat distribution to people, and reflectors are used to direct heat to appropriate directions and locations. With tube heaters, the gas-air mixture is combusted within a long steel tube to temperatures of approximately 580 °C. On the other hand, the radiant plague types typically operate at temperatures around 900 °C, and they must be installed in well-ventilated rooms because they are not flued [87,128].

2.4.7 Heat Pumps

A heat pump uses mechanical work to move heat from a low-temperature source to a high-temperature reservoir, e.g., from outdoors into interior building space. An electric motor can drive heat pumps with electricity from the national grid, while most heat energy is harnessed from the environment [42,128]. Alternatively, heat pumps can be driven by a gas engine or assisted with heat generated from solar thermal collectors. Heat pumps use working fluids, known as refrigerants, as the transport medium to remove heat from a low-temperature source to a hotter sink. Heat pumps can be used for heating and cooling interior building space for thermal comfort and hot water service. A heat pump in heating mode has four principal components: compressor, condenser, expansion valve, and evaporator [130,149].

Heat pumps may be categorised as air-source (ASHP), water-source (WSHP), or ground-coupled (GSHP), according to where the evaporator coil is drawing heat from outside air, water or directly from the ground. Furthermore, in building applications, the heat pump may be used to heat air (such as space heating) or water (for hot water service or hydronic space heating) [128]. ASHP is easier to maintain due to effortless access to the evaporator; however, they are susceptible to large variations in source temperature. As a result, defrost strategies must be applied to combat low ambient temperatures in cold climate regions [91]. WSHP can extract heat from rivers and aquifers at moderate temperatures (5–10°C); however, embedded impurities in sources can lead to pipework corrosion [150,151]. In GSHP, stable ground temperature and collection efficiency increase with depth [149]. Also, ground thermal response tests must be analysed to clarify groundwater advection effects on the thermal performance of ground heat exchangers [152].

The COP of a heat pump is dependent on the constancy of heat source temperature and heating temperature in a building [153]. Earlier heat pump models cannot supply heat above 60°C, so backup heaters are used to achieve the required temperatures for hot water service. Laboratory and field (in-situ) experimental measurements by Willem et al. [152] indicate that current residential heat pump water heaters (HPWH) have COPs in the range of 1.8-2.5.

2.4.8 Combined Heat and Power

Combined heat and power generation or cogeneration is the simultaneous production of electrical power and heat from a single system. Compared to conventional power stations, CHP recovers some waste heat into useful heat energy for industrial processes, building applications,

and district heating. Thus, CHP has an overall efficiency of 85-90%, while conventional power systems can achieve 40-45% efficiency [154]. A CHP plant typically comprises a conversion device, generator, heat recovery system, and electrical converter [126], [155]. The minimum heating loads that satisfy the most extended CHP running hours are preferred when sizing CHP plants for building use. Thus, a supplementary energy source may be required to cover peak heating demand. District heating is an extended system for distributing heat generated in a centralised location to deliver space heating and hot water service. District heating covers a long distance to several buildings [155].

2.4.9 Solar Thermal Collectors

The solar collectors used for space heating and cooling applications include flat plate collectors, evacuated tube collectors, and compound parabolic collectors, as presented in section 2.2.1.

2.5 Building thermal performance

People spend between 80-90% of their time inside buildings [156,157], so it is critical to deliver good building internal conditions to maintain productivity and avoid impaired occupant thermal comfort, morbidity and even mortality in vulnerable groups such as infants [158-160].

2.5.1 Impact of cooling on performance

Building thermal performance affects interior space energy demand and cooling loads. This section begins with a description of building thermal load calculation methods. After that, the methods of estimating building energy requirements are presented.

2.5.1.1 Estimating cooling load

Cooling load is the sum of sensible and latent heat gains, which must be removed from building space to keep air temperature and humidity at the desired setpoint. In interior building space, sensible heat causes a rise in air temperature. In contrast, a rise in moisture content is due to latent heat. The selection of heating, ventilation, and air-conditioning (HVAC) equipment and system design are based on room-by-room cooling load calculations [123,139]. Also, the maximum cooling load for each building zone must be computed.

Total sensible cooling load is calculated from heat gain from building opaque elements, transparent glazing elements, via infiltration and ventilation, and because of occupancy (people, lights, and equipment). On the other hand, the total latent cooling load is calculated

from three moisture sources: outdoor air infiltration, occupants, and miscellaneous sources such as bathing and cooking. Furthermore, cooling design load calculation methods include the transfer function method, load factor method, heat balance method, radiant time series method [123,135] and admittance method [161]. Cooling load calculation methods consider the contributions of all heat gains.

The following describes the characteristics of heat gains that contribute to building cooling loads. It starts with describing interior building heat gains, followed by heat gains through the building envelope.

2.5.1.1.1 Internal heat sources

Heat gains from people, lighting, and equipment contribute to building cooling loads. The characteristics of heat gains in a building are presented in the following sections.

2.5.1.1.1.1 *Heat gain from people*

Human heat gains depend on physical activity level [162]. The occupants' heat gain consists of sensible and latent heat, each having a distinctive contribution to internal heat gain. The latent heat gain is instantaneous, while sensible heat gain conversion to cooling load is delayed because it is affected by the thermal mass of the internal space. The occupants' heat gain can be separated into convective heat loss to space air and long-wavelength radiative heat loss to the interior building surfaces. Indoor air velocity impacts the ratio of latent to sensible heat from occupants [135,146].

2.5.1.1.1.2 *Heat gain from lighting and equipment*

The heat generated from lighting (e.g., lighting elements or lamps) contributes to cooling loads in internal space. Different lighting systems have corresponding efficiencies and power ratings; thus, heat gain depends on the type of lighting installed. The instantaneous rate of sensible heat gain from lighting may be calculated from the total installed lighting wattage, lighting use factor, and lighting special allowance factor. The lighting use factor is a ratio of wattage in use to the total wattage installed. In contrast, the unique allowance factor is a ratio of actual power consumed by all lighting fixtures to the nominal power consumption of the lamps [139,146].

Alternatively, estimating lighting heat gain from information based on a space area at the building design phase is possible. Heat gain from lighting is separated into long-wavelength radiative and convective components. The radiative fraction is the heat exchange between the

lighting fixture and interior surfaces. At the same time, the convective component is the heat exchange to the space air [123]. Like lighting, heat gain from equipment must be separated into long-wavelength radiation and convection components when calculating resultant cooling loads unless equipment manufacturers advise otherwise [139].

2.5.1.1.2 Heat gains through the building envelope

The heat gains through building envelopes are described in three sub-sections below.

2.5.1.1.2.1 *Heat gain through glazing elements (such as windows and skylights)*

Glazing elements, such as windows, allow building occupants a visual connection to the outdoors and let daylighting and solar radiation heat gain to a building space. Glazing elements are versatile building envelope components used to affect building internal energy performance, and these are achieved by [139]:

- Using glazing to minimise overall building conductive heat loss.
- Using glazing and associated shading design to minimise solar heat gain and related cooling requirements.
- Introduce daylighting in buildings, such as through skylights, to reduce buildings' internal lighting requirements.
- Opening windows as a natural ventilation passive strategy to reject heat from internal building space.

Heat energy flows between windows and the internal building space surfaces via several mechanisms [139,163]:

i. Convective and conductive heat transfer due to a difference in temperature between the indoor and outdoor ambient temperature.
ii. Net long-wavelength radiative heat exchange between glazing elements and internal building surfaces.
iii. Short-wavelength solar heat absorption and reflection by windows and interior building surfaces.

As summarised above, diverse heat sources through glazing elements are key design factors for assessing building thermal performance.

2.5.1.1.2.2 *Heat flux with airflow and moisture transfer*

Infiltration (air inflow) and exfiltration (air outflow) are influenced by wind magnitude and direction, temperature gradient, construction geometry, and occupant use of doors and windows. It is challenging to predict infiltration rates because airflow around buildings is complex and unpredictable [123,139]. Thus, sensible and latent heat gain from infiltration is assessed from standard air values. Air, which is transferred through openings in building walls, carries heat energy, and the transfer mechanism is by convection [123,135]. Consequently, sensible heat in interior building space can be displaced by airflow, affecting the building's thermal performance. Besides, moisture in the surrounding air is essential for human comfort; thus, control is integral to most building air-conditioning systems [121].

Diffusion of moisture through a porous insulating structure such as slabs-on-grade and basement floors causes latent heat gain to buildings. Convection heat transfer aids the moisture transfer mechanism [163]. Moreover, air movement transports not only sensible heat but also the water vapour it contains. Recent studies recommend a combined analysis of heat-air-moisture transfer because separate analysis oversimplifies their effects on building thermal performance [164].

2.5.1.1.2.3 *Transient heat flow through building opaque elements*

The opaque elements of a building envelope include walls, floors, and ceilings. When direct and diffuse radiation falls on building opaque elements, about 50% to 80 % is absorbed. Subsequently, a greater part of the absorbed heat is transmitted through the building element via conduction heat transfer [87]. The heat flow rate depends on the building element's thermal transmittance, also known as the U-value.

Building elements store absorbed heat before it is released into the interior building space, with a time delay. Thus, building cooling loads must be calculated under transient conditions due to, for example, [162]:

- Transmitted solar radiation is absorbed and stored in the internal mass of walls, floors, and slabs and released later with a time lag.
- Internal mass interacts with operational schedules, causing diurnal fluctuations in internal loads such as heat from equipment and lights.
- Heat stored in building thermal mass interacts with interior space control strategies such as diurnal thermostat setup and air volume supply variations.

Consequently, transient heat flow analysis allows the accurate calculation of conduction heat transfer through building opaque elements into interior building surfaces.

2.6 Building thermodynamic modelling techniques

Building design teams use modelling tools to estimate energy consumption and select appropriate HVAC systems. In addition, modelling techniques are used to establish existing building retrofit savings and detect faults in the HVAC system [123]. Three main modelling techniques are used to evaluate building energy consumption and design HVAC systems: forward modelling, data-driven modelling, and gray-box modelling, Figure 2.14.

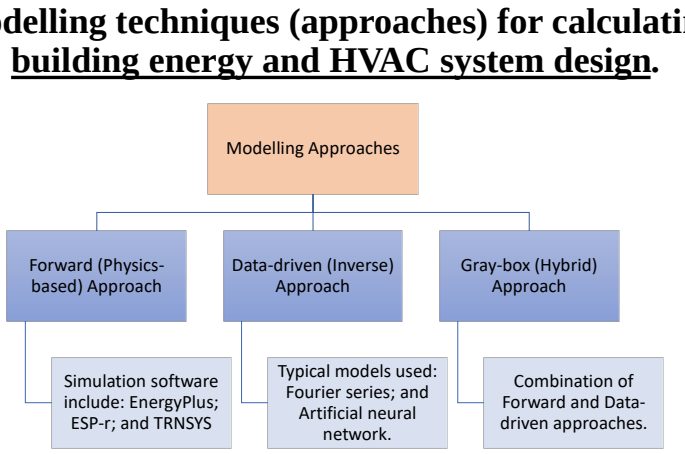

Figure 2.14: Three main modelling approaches evaluate building energy consumption and design the HVAC system.

In the forward modelling (or physics-based/white box) approach, a known structure's behaviour and physical characteristics are described to input parameters to predict design output. Major public-domain building energy simulation codes such as EnergyPlus, ESP-r, and TRNSYS are based on a forward modelling approach [123]. The primary benefit of the forward modelling approach is that the system under study need not be physically built. However, forward modelling relies on a sound understanding of the underlying physics of system behaviour and known physical parameters of an operating system to achieve successful simulation results.

In data-driven modelling, data from system performance are analysed to establish a correlation between the input and output variables, e.g., Fourier series and artificial neural network (ANN) [165]. This modelling approach is well-suited for improving the performance of existing air-conditioning systems. Nonetheless, the data-driven modelling approach relies on adequate

system operational data access. The gray-box (hybrid) model combines forward and data-driven modelling approaches. It has great potential in control applications such as state-space and transfer function models [166,167].

2.6.1 Building Energy Performance Simulation Tools

This section describes two renowned physics-based modelling software, TRNSYS and EnergyPlus and outlines the benefits and limitations of incorporating building information modelling (BIM) into building energy performance tools. Furthermore, building energy simulation tools can be linked with additional modelling tools to improve HVAC system controls and model components of unique cooling systems. Hence, MATLAB and Engineering Equation Solver (EES) are presented.

2.6.1.1 TRNSYS

TRNSYS is a transient energy system simulation program with a modular structure designed to solve complex energy system problems by breaking the problem down into a series of smaller components [168]. TRNSYS has been commercially available since 1975 [169,170], and it is widely used to simulate solar energy applications and conventional buildings. TRNSYS is a flexible energy simulation tool because its platform facilitates the incorporation of mathematical models and has a good interface with other simulation programs. This flexibility allows the utilisation of different design approaches and benefits from a variety of capabilities to the TRNSYS software [171-173].

TRNSYS program is fundamentally a collection of energy or building component models grouped around a simulation engine (solver) to define a specific system [168,172,174]. It comprises a simulation kernel, component models, and a graphical user interface. TRNSYS offers over 80 standard component libraries for many applications, such as solar thermal, solar photovoltaic, HVAC, and hydrogen systems. The components can be as simple as a valve and as complex as a multi-zone building. Simple or complicated parts can be solved independently and linked with other components to solve complex system problems [174].

TRNSYS has a graphical simulation interface (called TRNSYS Simulation Studio) that allows a user to link the outputs from one component to the inputs of another in a unique fashion. The interface consists of a proforma, a bitmap icon, and a brief description of a component, such as direction and rating [175-177]. For complex designs with numerous components, the TRNSYS

simulation studio permits concentrating on one component at a time, going through the model algorithm in detail to minimise errors [169]. The interface allows users to specify inputs and outputs and display appropriate macro connections. Also, the connection of specified inputs is displayed in different colours and styles for easy tracing and to minimise user-induced error [174].

TRNSYS simulation kernel reads and processes a project definition file and utilises its built-in solvers to compute the outputs to complete a dynamic simulation [172,178]. The kernel calls each component in an iterative process until it converges at a defined time step. TRNSYS multi-zone building simulation has advanced capabilities to accurately model large, glazed buildings due to contributions from multiple air nodes, improved radiation model, and processing of effects from view and shading factors.

TRNBuild, the building input description tool of TRNSYS, allows the user to define and input geometric information of buildings as an initial processing step. Simulation inputs such as infiltration and convective heat transfer exchanges are assigned to specified air nodes. In contrast, long and shortwave radiation exchanges are applied to the entire building zone [169]. The simulation time interval can be set as low as 0.1 seconds, though typical timesteps for building energy performance simulations vary from 15 minutes to 1 hour. Calculating heat transfer between a building and the ground has long been uncertain; nevertheless, TRNSYS can simulate ground-coupled heat transfer with high accuracy [169].

Regarding limitations, Trimble SketchUp is the only drawing software that can be used to model three-dimensional features of buildings. Moreover, adequate information about system parameters must be used to produce accurate simulation results. Besides, TRNSYS requires a thorough understanding of the fundamental physics of system phenomena to achieve precise time step convergence and successful simulation results [171].

Baniyounes et al. [179] used TRNSYS software to study a solar-powered desiccant cooling system installed in a Central Queensland University institutional building. The technical and economic performance of the cooling system included energy savings and avoided gas emissions concerning conventional cooling systems developed under a typical meteorological year. The TRNSYS simulation results showed that with a 10 m^2 solar collector area and 0.4 m^3 hot water storage tank volume, the system achieved 0.7 COP and 22% solar fraction during the cooling season. In contrast, when the evacuated solar collector area increased to 20 m^2, and the

hot water storage tank increased to 1.5 m^3, the performance increased accordingly with 1.2 COP and 69% solar fraction [179]. Shrivastava et al. [174] conducted an in-depth study of TRNSYS applications for solar hot water systems for performance analysis and design optimisation. The critical review of TRNSYS simulation of solar water systems showed that average error from area installations ranged from 5% - 10%, and the assumptions used include mass flow rate, draw pattern, stratification, solar collector's heat capacity and direction of heat flow [174]. Ahamed et al. [180] used TRNSYS to model the heating demands in a Chinese solar greenhouse and to quantify the impact of assumptions on heating system design. The modelling results suggested significant errors in predicting the heating load due to the various assumptions, such as a schedule for the thermal blanket, a day-night schedule for moisture gain, and fixed filtration rates [180].

In a TRNSYS simulation study by Al-Saadi et al. [181], a PCM-enhanced building wall was developed and validated under typical United States climates. The simulation result showed a 0.8-15.8 % reduction in cooling loads and up to 4% reduction in heating loads. Also, the results showed that the PCM-enhanced walls delivered maximum savings in peak loads than in annual loads in some climates [181]. Liu et al. [182] used TRNSYS to show that it was feasible to embed a PCM into a mobile refrigeration unit to cool down refrigerated space at -18 °C for 10 h in the local Adelaide, Australia climate. The results showed that the size of the PCM used depends on the PCM's latent heat of fusion and the maximum daily cooling loads [182].

Hou et al. [183] used TRNSYS to study the operational performance of a hybrid ground source heat pump system (GSHP) embedded with a liquid dry cooler and when compared with a conventional ground source heat pump system. The modelling result from the 10-year operational duration showed that the hybrid GSHP systems achieved a higher target minimum temperature of 12.53 °C, which is 0.63 °C lower than the value gained in conventional GSHP systems. In addition, the hybrid system achieved a higher COP of 3.33 compared to COP of 3.23 for conventional systems [183]. Bordignon et al. [184] used TRNSYS to perform an energy analysis of two design configurations (fan coil and cascade systems) of a reversible GSHP delivering heating and cooling to a historical building in Athens and Helsinki. The cascade-cycle configuration showed a seasonal COP of 2.48 for the coldest region of Helsinki, while a higher seasonal COP of 2.86 was achieved for the warmer Athens area. On the other hand, in the radiator configuration, higher overall seasonal COPs were achieved at 3.29 and 4.90 for Helsinki and Athens, respectively [184].

Chargui et al. [177] used the TRNSYS tool to study the performance and effects of changing different parameters of the heating mode of a residential house coupled with a dual-source heat pump. The design study showed that the COP was between 6 and 9 when the outside temperature was around 55 °C, and the heat pump performed better when housed inside a building or under a cover outdoors [177]. Asim et al. [185] used TRNSYS to model a solar-powered absorption cooling system integrated into a building in Pakistan's hot climate. The system utilised a thermally stratified hot water storage tank and a 12 m^2 solar collector that was efficient enough to maintain the cooling room temperature at or below 26 °C [185].

Villa-Arrieta et al. [172] developed a technical-economic model co-simulated with TRNSYS to evaluate the technological and environmental costs of energy systems. The technical-economic model, the Energy Assessment Tool of Energy Projects (EATEP), is an economic calculation procedure adapted from the European standard EN 15459:2007 to operate with TRNSYS. EN 15459:2007 is a European legislative instrument that promotes NetZero energy consumption for buildings. As a result, the EATEP model is applied in TRNSYS to calculate various economic, energetic, and environmental performance indicators to evaluate the best alternatives in several investment options [172].

Asa'd et al. [173] used TRNSYS to investigate the energetic performance of a solar greenhouse connected to a rock-bed thermal storage near Montreal, Canada. To achieve optimum design, the following effects were studied to evaluate their effects on greenhouse indoor temperature: cooling and heating setpoint temperatures, rock bed air flow rate, mechanical outside air ventilation, cover materials, and size of rock-bed thermal storage. The results from the parametric study showed that the rock-bed flow rate and the structure thermal transmittance, also known as U-value, have the dominant effect on the greenhouse indoor temperature [173]. Terziotti et al. [186] used TRNSYS to model the effects of seasonal solar thermal energy storage in a large residential building, where heat is collected and stored during summer and used for heating in winter months. Various bed locations and building efficiencies were configured to determine the most efficient sand-based storage bed system, which achieved up to 91% energy savings [186].

Antoniadis et al. [170] used TRNSYS to model different integration options for optimising a building-integrated solar thermal system with seasonal storage in Thessaloniki, Greece. The building adhered to the latest Greek national building code. The contributions of the solar collector and auxiliary conventional heating systems met the building space heating and

domestic hot water demands. A parametric analysis based on the impact of solar collector types and areas, building integration type, and volume of seasonal storage indicated that it was possible to achieve a seasonal combined solar fraction of up to 39% [170]. Lekhal et al. [187] used TRNSYS to study the thermal performance of an integrated system of a direct solar floor, earth-air heat exchanger and a ventilation device installed in a residential building in Oran, Algeria. The system was adequate based on a control strategy to manage cooling and heating demands when needed. The modelling results showed that the most effective control strategy achieved a 68% total annual energy usage reduction compared to a conventional HVAC system [187].

Khan et al.[188], used TRNSYS to study the performance of two configurations of a solar-assisted single-effect absorption cooling system to meet the 298 kW peak cooling demand during summer conditions for an educational building in Islamabad. In configuration 1, the return fluid from the chiller's generator flows to a hot store. In contrast, in configuration 2, the chiller's generator's return fluid is diverted from the storage tank to an auxiliary heater when the tank temperature is below 110 °C. The key performance factors used for the comparative study were solar fraction, collector efficiency and primary energy savings. In contrast, the design variables optimised in this study include solar collector type and tilt angle, storage tank type and volume. The simulation showed that configuration-2, operating with a flat plate or evacuated tube solar collector, always produced higher primary energy savings than configuration-1. However, there were marginal differences between configuration-1 and configuration-2 when solar fraction and collector efficiency design parameters were used [188]. Altun et al.[189], used TRNSYS to study a solar-powered single-stage absorption cooling system modelled to provide building-scale cooling for the weather conditions of Mugla, Trabzon, Izmir, Konya, Canakkale and Istanbul cities in Turkey. A parametric study was carried out to determine the optimised design. The results showed that operational factors such as solar collector type, area, storage tank volume, collector slope, boiler setpoint temperature, and room thermostat setpoint temperature influenced the building cooling system performance. Besides, based on financial analysis, Izmir city achieved the highest payback period of 10.7 years while Trabzon achieved the highest levelized cooling costs [189].

2.6.1.2 EnergyPlus

According to the International Building Performance Simulation Association, EnergyPlus software is the most used building energy modelling tool. Though EnergyPlus is a standalone

simulation tool, it is also the basis for sophisticated software such as DesignBuilder that can model building water use and daylighting applications. EnergyPlus uses a text-based comma-separated values weather file format called '.epw' (EnergyPlus weather) that comprises hourly weather variables for a specified location. The United States Department of Energy originally developed the weather file. However, the file structure is also applied in other building simulation software such as ESP-r, IES, and TAS [131,158].

EnergyPlus is a modular, structured building energy analysis and thermal load simulation tool used to model energy consumption (such as heating, cooling, ventilation, and lighting) and process loads (such as water use in buildings) [190]. EnergyPlus is based on the popular features and capabilities of two building energy simulation programs: BLAST and DOE-2.1E [191]. EnergyPlus is a free, open-source software funded by the United States Department of Energy's Building Technologies Office. The simulation engine fundamentally reads input and writes output to text files. Building loads are calculated by a heat balance engine at a user-defined time interval (15-minute default) and passed to the building systems simulation module at the same time step. EnergyPlus calculates heating and cooling loads necessary to maintain thermal control setpoints and energy consumption of primary and secondary HVAC plant equipment [131,192].

EnergyPlus simulation manager has two fundamental components: heat and mass balance simulation module and building systems simulation module. EnergyPlus performs heat balances on inside and outside zone surfaces, the zone air, and transient conduction, convection, and radiation effects. The air mass balance module accounts for various air streams, such as infiltration and ventilation and covers convective heat gains and loss. The building systems simulation module manages communication between the heat balance engine and primary and secondary HVAC components such as chillers, fans, and coils. EnergyPlus software, unlike TRNSYS, does not utilise an in-house user interface. Instead, it encodes inputs and outputs as simple encoding text and relies on a third-party graphical user interface to produce desired results. Moreover, there is no capability to calculate the life cycle cost of projects [190,191].

Shen et al. [192] used EnergyPlus to develop an air source, a multi-functional space-conditioning unit with a water heating function that saved energy by recovering waste in the cooling season and delivering dedicated heat pump water heating throughout the year. The research summarised the underlying physics, sub-models, working modes and control strategy

applied. The building energy simulation results for ten United States of America cities indicated that the air source integrated heat pump model delivered more than 50% annual energy savings compared to a baseline heat pump incorporated with an electric water heater [192]. Kang et al.[133], used EnergyPlus to model the performance of a water-source VRF heat pump system integrated with a direct expansion air handling unit. The energy management function in EnergyPlus was used to deliver outdoor unit modelling using an advanced control strategy. In contrast, a prediction model was used to assess the cooling tower, boiler, and pump performance. The validation tests using actual operational data and performance curves showed a 14.5% variability of the errors between measured and simulated values [133].

Boyano et al. [193] used the EnergyPlus simulation tool to study the energy demands and potential energy savings in European office buildings. The simulation was based on several currently available scenarios on a reference office building across three European climatic zones. The simulation results showed that lighting controls bring essential reductions in energy bills. Also, improvements in insulation of building walls and windows and orientation have significant potential to reduce building energy demand. The simulation results indicated higher insulation factors are recommended in cold and medium climates, while well-insulated buildings in warm climatic zones are prone to higher heat gains [193].

Cetin et al. [194] used EnergyPlus simulation software to develop and study the impact of an HVAC on/off controller for energy simulation of a residential and small commercial building. The on/off controller is validated using field data on occupancy schedules and internal lads collected for a house built in California, United States of America (USA). The accurate application of the on/off controller improved the HVAC energy usage with 19% accuracy compared with results without the application of the on/off controller [194]. Kamal et al. [195] applied EnergyPlus to study the effect of strategic control and the cost optimisation of thermal energy storage in large buildings for three thermal energy storage system cases: mixed chilled water storage, stratified chilled water storage, and ice storage. The study utilised strategic controls with six operating modes to provide an average annual shifting of 25-78% of peak electricity demand to reduce 10-17% yearly operation cost and reduce overall system size [195].

Hong et al. [132] used EnergyPlus to develop a model to study the energy performance of VRF systems in heat pump operation mode. The new model, equipped with a detailed description of the underlying physics, enabled advanced controls such as variable fan speeds based on zone

load and temperature, improved part-load conditions, and pipe heat loss calculation using refrigerant flow rate, pipe length and pipe insulation materials. The new model was validated using measured data from field tests, and the modelling results suggested that the new VRF heat pump model provided accurate results for local compliance credits [132]. Seo et al. [131] compared the cooling energy performance between a water-cooled VRF heat pump system and a chiller-based conventional air handling unit (AHU) system in a commercial building. The VRF heat pump system was equipped with a direct expansion air handling unit, and the heating and cooling performance data was developed from diverse operating temperatures and part-load conditions. The modelling results demonstrated that the water-cooled VRF heat pump system could reduce cooling energy by up to 15% compared with the chiller-based conventional AHU system [131].

2.6.1.3 Other building energy performance simulation

More than 400 applications have been developed to analyse building energy performance and assess the environmental impacts of design options [196]. Crawley et al. [191] presented an extensive comparative review of twenty widely used building energy simulation programs regarding overall simulation features, building fabric and fenestration, renewable energy systems, primary and secondary HVAC systems, zone loads, economic and environmental evaluation, and many other factors. The twenty building energy performance software reviewed include BLAST, BSim, DeST, DOE-2.1E, ECOTECT, Energy-10, Energy Express, Ener-Win, EnergyPlus, eQUEST, ESP-r, IDA ICE, IES, HAP, HEED, PowerDomus, SUNREL, Tas, TRACE, and TRNSYS [195].

2.6.1.4 Building information modelling

Building information modelling (BIM) is defined as “the act of creating an electronic development model of a facility for visualisation, engineering analysis, conflict analysis, code criteria checking, cost engineering, as-built product, budgeting, and many other purposes” [197]. BIM is used to produce object-oriented data appropriate for intelligent digital representation of a facility and to analyse facility data to improve the building design process. Preventing data duplication and costly design revisions requires a unified data transfer between BIM and building energy management (BEM). Nonetheless, BIM tools do not always have enough data attributes to support BEM software [198].

2.6.2 Modelling tools linked with Building Energy Performance Simulators

2.6.2.1 Engineering Equation Solver

Engineering Equation Solver (EES; pronounced 'ease') is a general equation-solving program that can numerically solve thousands of coupled non-linear algebraic and differential equations. The program can complete optimisation and uncertainty analyses, perform linear and non-linear regression, convert units, check unit consistency, and generate quality plots [199]. EES is a versatile program with many features. EES has an accurate thermodynamic and transport property database for hundreds of substances, so there is no need to employ external property tables [123].

EES has graphical user input and output capabilities with a diagram window that allows a designer to produce and analyse quantitatively accurate graphs [199]. EES has single and multi-variable optimisation capabilities, which help carry out parametric studies with a spreadsheet-like table. Where a thermodynamic system is not available in the standard TRNSYS component library, it can be developed in EES and then coupled with a TRNSYS model [200]. In this EES-TRNSYS co-simulation exercise, TRNSYS receives information output from EES via text files and dynamic information exchange method [171,200]. Tashtoush et al. [201] used EES to model the performance factors of ejector cooling systems, such as ejector geometry, operating temperatures and pressures, refrigerant type, and primary and secondary flows.

In a separate study by the same authors [200], the TRNSYS simulation studio was used to analyse components such as solar collectors, storage tanks, circulation pumps, and on/off controllers and called on the ejector cooling cycle model created in EES software. Similarly, in another research by Vidal et al. [202], a mathematical model for the solar ejector cooling system was written in EES, while TRNSYS was used to perform a dynamic simulation. TRNSYS component Type 66 was applied to data exchange between EES and TRNSYS.

2.6.2.2 MATLAB

MATLAB is a high-performance programming language tuned for iterative analysis and design processes that directly express matrix and array mathematics. It includes “Live Editor” for creating scripts that combine code, output, and formatted text in an executable notebook [203]. Simulink is a MATLAB-based interactive and graphical programming environment for multi-domain modelling, simulating, and analysing dynamic systems,

including controls. It supports linear and nonlinear systems modelled in continuous time, sampled time, or a hybrid [203]. Simulink allows the connection of components among simple variables, vectors, and matrices and avails several solver options, such as the iterative solving process.

It is possible to convert component models from MATLAB to TRNSYS by adopting a dynamic link library (DLL) in a traditional programming design pattern [178]. Also, MATLAB extension, known as 'real-time workshop,' allows a mechanism to compile Simulink into DLL capable of running an external subsystem's algorithm. Adapting DLL is to 'wrap' the MATLAB function to be compatible with the signature for TRNSYS component functions [204,205].

Building energy performance tools like TRNSYS and EnergyPlus do not provide complex sub-models for advanced control mechanisms. Thus, MATLAB primarily provides enhanced process control [204,205]. Several control methods have been modelled in MATLAB to regulate solar cooling systems to produce optimum system efficiencies within TRNSYS [206-208]. To reduce solar cooling costs and improve cooling COP, MATLAB optimisation toolboxes have been investigated to tune the parameters of existing designs [209,210]. Nonetheless, an intricate MATLAB sub-model requires an excellent system design to produce sophisticated controls in TRNSYS.

2.7 Summary of findings

The primary focus of the literature review is to examine the literature on types of solar energy capture devices, cooling and heating systems, building thermal performance, building use considerations and the thermodynamic modelling techniques applied to study building thermal energy systems. Reviewing these topics draws key conclusions for designing and optimising solar thermally driven building cooling and heating systems.

The non-concentrating solar collectors used in residential building cooling heating systems with high operating temperatures required by a diffusion absorption cooling system are CPC and XCPC. Thus, among the types of solar thermal collectors reviewed, CPC and XCPC solar collectors will be applied in the design to generate the required temperatures. The literature review on solar thermal collectors provides a foundation for further research into the theories and models of using these collectors to generate heat for hot water-fired heating and cooling systems. The review indicates the research focus using solar thermal collectors should improve

efficiency for year-round performance, adapt and optimise the collector system to perform effectively in different regions and climatic, explore potential benefits of hybrid systems that combine thermal collectors with conventional heating systems, effective thermal energy storage solutions necessary to provide heating and cooling during night time or period of low solar availability, integrate the collectors into buildings and HVAC systems for optimal utilisation of the generated heat, and contribute to the economic viability and environmental benefits of solar-powered cooling and heating system.

The review highlighted the main focus of thermal energy storage is improving operational efficiency and reducing the cost of storage material and operation. The promising thermochemical materials are still at the lab stage; thus, the selected thermal storage materials are selected from sensible (e.g., water) and latent heat thermal storage systems (e.g. eutectic salt).

The literature review highlights that currently, there is a high demand for heating energy, primarily from developed nations, such as the United Kingdom. However, the expected socio-economic development of countries and communities in emerging markets and developing economies, such as India, will drive demand for cooling to be at par with heating demand at the turn of the mid-century. Thus, the selection of case study cities will be balanced between cooling and heating-dominated climatic locations.

The review of the heating and cooling systems indicates the types of heat emitters that can be used to deliver space heating and cooling. For example, combined heating and cooling heat emitters such as fan coils can provide heating and cooling for thermal comfort in the building space. A review of the cooling systems indicates that passive cooling techniques, such as implementing efficient thermal insulation in the building envelope, can reduce the building's thermal load before applying mechanical and solar cooling to a building. Moreover, the literature review discussed heating and cooling system types, such as heat pumps, gas boilers, and air conditioners, highlighting the alternatives to the solar-powered DACS during economic comparison analysis.

A review of the building's thermal performance indicates that the design of an efficient building envelope must consider the heat balance consisting of internal building sources and heat gain through the building fabric, such as the walls, floor, roof, and windows. Also, the climatic data is part of the building heat balance; hence, there must be access to local weather data to demonstrate the impact of local weather on building heating and cooling load.

Modelling can be useful for designing solar collector and storage systems and calculating building cooling and heating energy. Of the available building simulation and energy modelling tools, TRNSYS software was selected because of the unique capabilities and flexibility of modelling all types of solar thermal energy devices and single- and multi-zone buildings. Additionally, the EES software has been proven to have in-built thermodynamic properties of the ammonia refrigerant and the water absorber used in the diffusion absorption cooling system. Thus, EES is well placed to define the thermodynamic characteristics compared to MATLAB, which does not have inbuilt thermodynamic properties for ammonia refrigerant [211,212]. Additionally, EES can be used to model design aspects of components, e.g., latent cold storage, whiche8rweee is not readily available in the TRNSYS tool.

The following section presents the methodology applied in this research.

Chapter 3 : Methodology

3.1 Introduction

This Chapter explains the methodology used in this research. TRNSYS software [171] is used to model the solar and storage design and to simulate the building's thermal performance. Additionally, EES software [199] is used to study the thermodynamic modelling of the DACC. The EES modelling results are compared to experimental data published by Najjaran et al. [51].

A description of the solar-powered DACC model is presented in section 3.2. Section 3.3 presents how EES is used to perform the solar-powered DACC thermodynamic modelling. Section 3.4 explains the modelling completed with TRNSYS software. Section 3.5 describes the modelling strategy employed and the case study locations used in the modelling study. The performance parameters investigated are explained in section 3.6. Sections 3.7 and 3.8 explain the economic analysis and the environmental impact assessments of the solar-powered DACS cooling and heating system, respectively.

3.2 Description of the solar-powered diffusion absorption cooling cycle (DACC) model

Figure 3.1 shows the diffusion absorption cooling cycle (DACC) schematic. Detailed component-level designs and modelling are needed to advance the original DACC invented by Von Platen and Munters [41]. The DACC can be thermally driven by energy sources such as waste heat or solar thermal energy [40]. It uses ammonia-water-hydrogen as a working fluid, where ammonia is the refrigerant, water is the absorbent, and hydrogen is the auxiliary gas.

Ammonia transports energy from a low-temperature source to a high-temperature sink. At the same time, water absorbs the ammonia (refrigerant) at low partial pressure and releases it at high pressure [42]. The hydrogen gas provides pressure equalisation throughout the thermodynamic cycle [40,44].

There are eight primary components of the DACC, and the working principle of each component is described below [50].

1. Solar collector
2. Heat pipe
3. Generator
4. Bubble pump
5. Rectifier
6. Condenser
7. Evaporator
8. Cool air chamber
9. Water chamber
10. Convected air via a condenser
11. Absorber
12. Solution heat exchanger

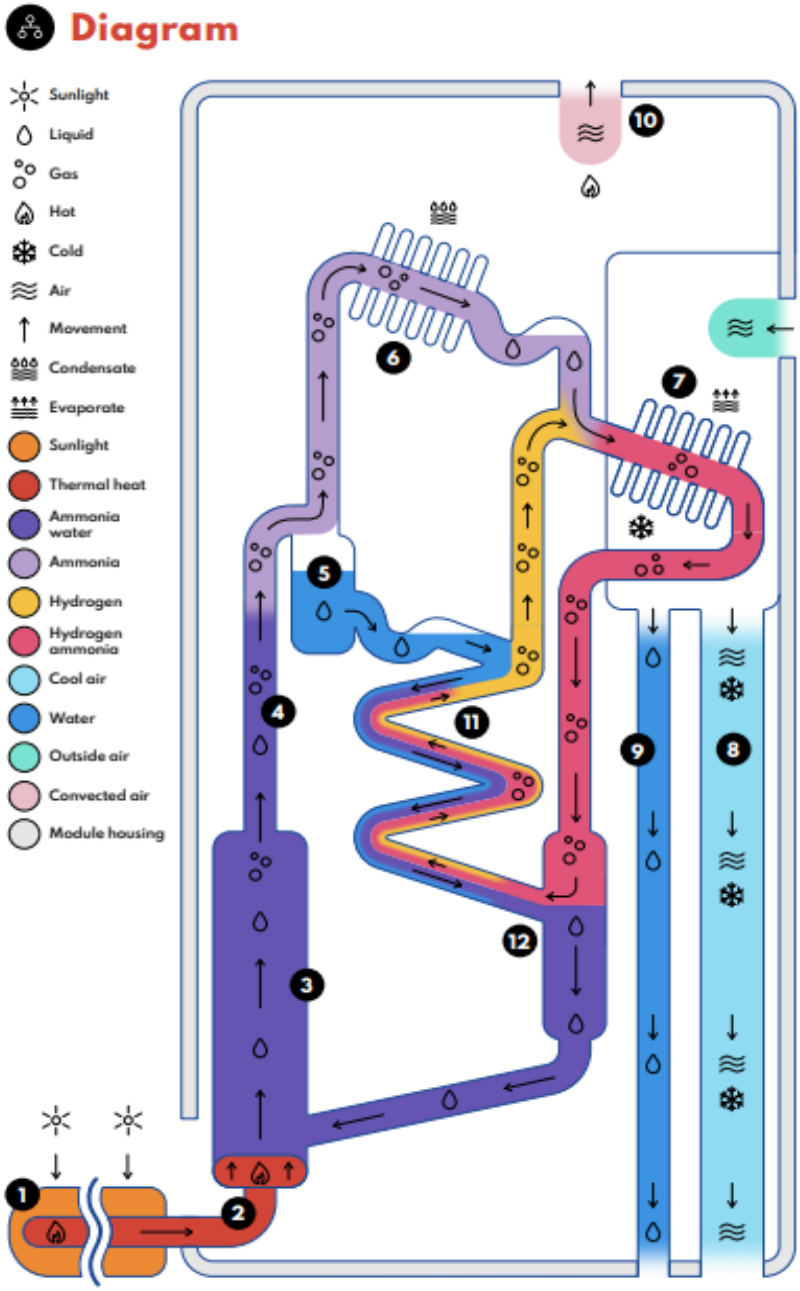

Figure 3.1: Schematic diagram of the DACC cycle from Solar Polar Limited [50].

3.2.1 Absorber

Two circulating loops pass through the absorber, as shown in Figure 3.2. The absorber has a sub-component known as a reservoir, which resides at the bottom of the absorber. The location of the reservoir is such that a refrigerant-rich solution, consisting of ammonia and water, flows from it to the bottom section of the generator via a SHE. Most passive DACC cycles have

serpentine-shaped absorbers that allow counter-flow of two circulation loops: gas (hydrogen-ammonia) and liquid (ammonia-water) [213].

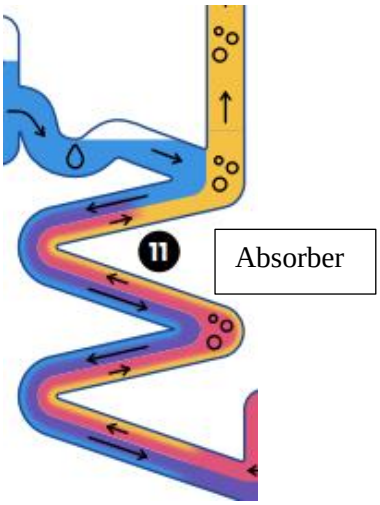

Figure 3.2: Schematic of the absorber.

3.2.2 Solution heat exchanger (SHE)

The solution heat exchanger design absorbs heat from a warm, weak ammonia-water solution returning from the outer space of the generator to the absorber, as shown in Figure 3.3. The absorbed heat is transferred to a strong ammonia-water solution flowing from the solution reservoir through the SHE to the generator's lower part [40,44].

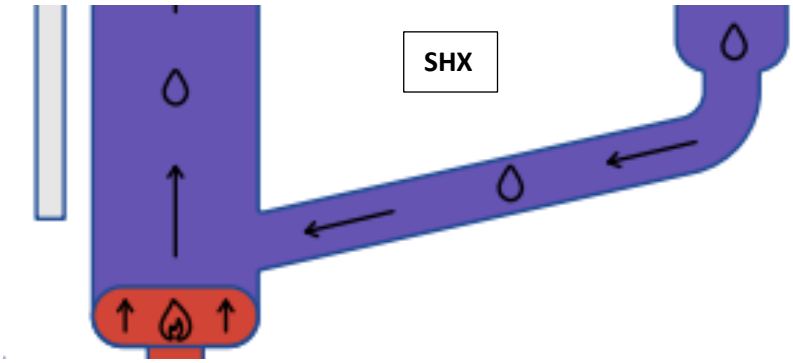

Figure 3.3: Schematic of solution heat exchanger (SHX).

3.2.3 Generator-bubble pump

The generator houses a bubble pump, where refrigerant-rich solution from the absorber is heated to produce refrigerant vapour (ammonia), as shown in Figure 3.4. The shape of the generator allows ammonia vapour bubbles to separate from the ammonia-water solution and subsequently flow towards the rectifier. In conventional DACC designs, the working fluid is actively heated near the base of the generator-bubble pump [214,215]. However, a recent study by Jo et al. and Benhmidene et al. [216,217] has explored distributed heat generation techniques to supply heat to a larger surface area of the generator-bubble pump.

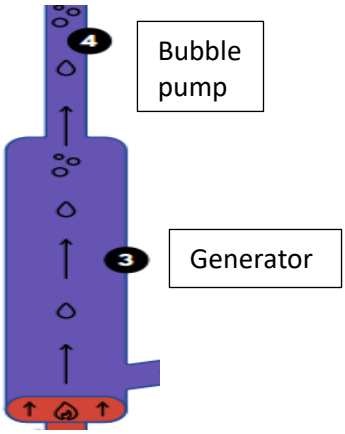

Figure 3.4: Schematic of Generator-bubble pump.

3.2.4 Rectifier

As shown in Figure 3.5, the rectifier has a serpentine shape that removes any remaining water in ammonia vapour and allows it to drain to the generator. Ammonia vapour continues to flow towards the condenser [47].

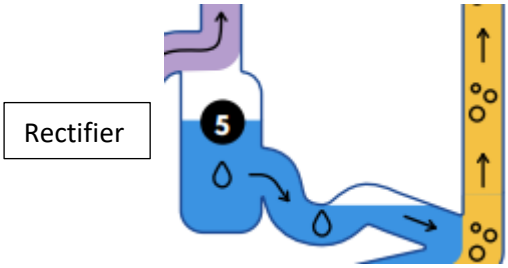

Figure 3.5: Schematic of Rectifier.

3.2.5 Condenser

Figure 3.6 shows the schematic of the condenser. The condenser has fins to increase the surface area to reject heat from ammonia vapour by natural convection to the environment. Thus, ammonia vapour is condensed to ammonia liquid before it flows to the evaporator. A bypass line allows any residual ammonia vapour to flow directly to a reservoir at the top of the absorber [40,44].

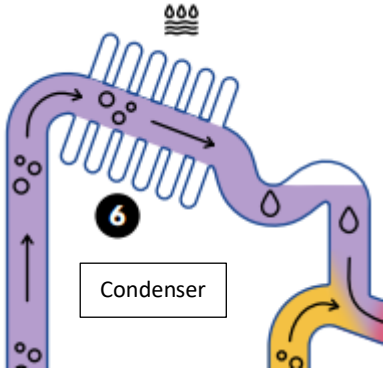

Figure 3.6: Schematic of Condenser.

3.2.6 Evaporator

Figure 3.7 shows the schematic of the evaporator. The shape of the evaporator allows ammonia liquid to flow from the condenser to feed into the evaporator chamber inlet. Then, the ammonia liquid converges into the two-phase ammonia-hydrogen gas mixture. Heat is absorbed from the conditioned space into the evaporator to achieve the desired cooling effect [47].

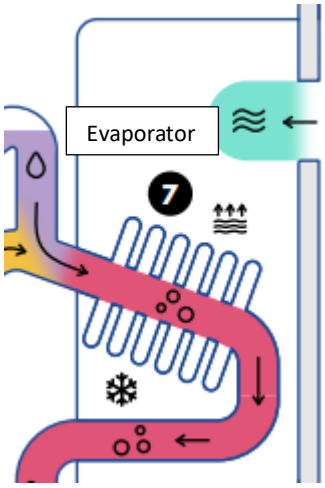

Figure 3.7: Schematic of Evaporator.

3.2.7 Gas heat exchanger (GHX)

Figure 3.8 shows the schematic of the GHX. The gas heat exchanger is designed as a counter-flow heat exchanger to improve the DACC cooling system's efficiency. The GHX is positioned to extract heat from hydrogen and ammonia gas from the absorber towards the evaporator. In addition, GHX is placed between the evaporator and absorber and is driven by gravity-induced pressure differences [218].

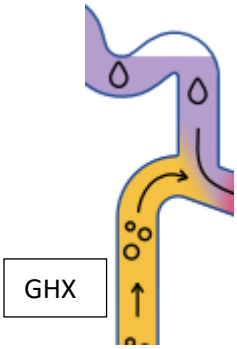

Figure 3.8: Schematic of Gas Heat Exchanger (GHX).

3.2.8 Solar thermal collector

A solar thermal collector can supply the heat source for the generator-bubble pump, as shown in Figure 3.9. A solar thermal collector converts light from the sun into useful heat energy [53]. Most DACC systems in the published literature were predominantly powered with heat from an electric heater and propane gas. Nonetheless, waste heat and solar heat sources can be utilised. The required generator temperature is a major deciding factor for selecting the appropriate solar collector system, i.e., concentrating or non-concentrating solar collector system [54].

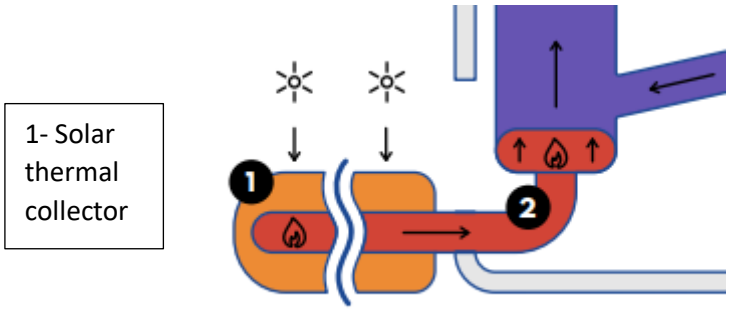

Figure 3.9: Schematic of Solar thermal collector

An external concentrating parabolic solar collector (XCPC) component is the heat source for the solar-powered DACC cooling system. An XCPC solar collector comprises glass evacuated tubes, manifolds of copper head pipes, copper u-tube and aluminium heat spreading fins, CPC reflector, aluminium frame, and rock wool insulation, Figure 3.10 [66]. The heat source temperature for the generator of the DACC cycle operates in the range of 135-230 °C [51,68]. The copper U-tubes serve as the liquid channel inside the collector. The channel structure has less circulating mass and low heat capacity, which enables the solar collector to reach higher temperatures in less time. The CPC reflector is fixed parallel to and underneath the evacuated tube's axis. During operation, beam and diffuse sun rays can be reflected onto the absorber material in the evacuated tube [53,54]. The number of evacuated tubes is usually reduced to minimise heat loss from the solar collector. Likewise, insulation materials, e.g., rock wool, with low thermal conductivity and high-temperature resistance, are used to minimise heat loss to the ambient [65].

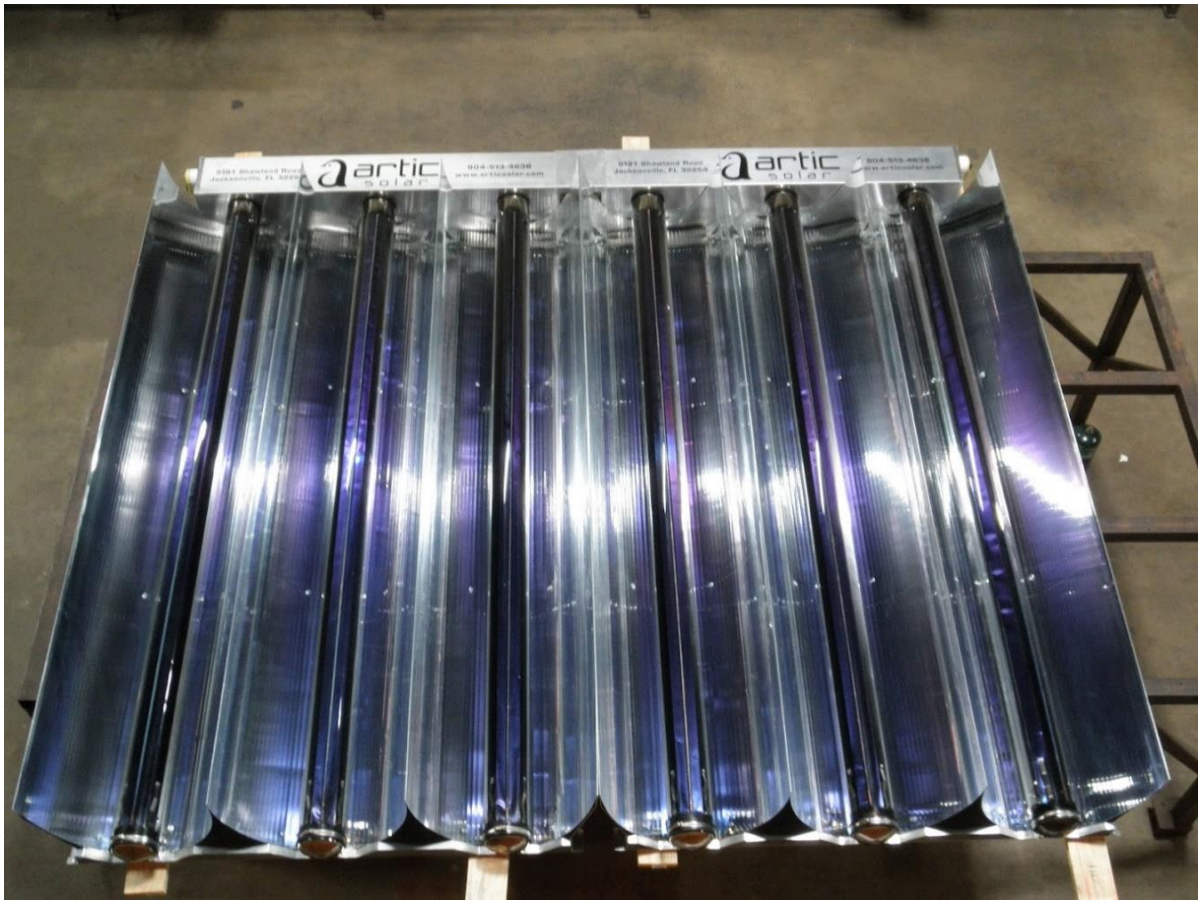

Figure 3.10: Picture of an XCPC medium-temperature collector (taken from Artic Solar [66]).

3.2.9 Summary

Several DACC experimental studies provide valuable system operating details. However, more design information on mass transfer models is needed for components such as the condenser, evaporator, GHX, SHX, solution sub-cooler, and passively circulating gas loop. Experimentally validated component-and-system level design models are needed for DACC systems utilising high temperatures to produce building air-conditioning [49].

3.3 Thermodynamic modelling of the solar-powered, NH_3-H_2O-H_2, DACC cooling system

The thermodynamic model used to study the DACC cooling cycle is based on mathematical equations presented by Starace & De Pascalis [142]. The thermodynamic model is widely cited in the published literature and has relative ease of implementation [51]. Besides, this model is used because it was applied in the accompanying experimental model studied by Najjaran et al. [51,68]. The DACC cooling cycle is studied theoretically with EES modelling software with the energy and mass balance equations presented in this section. Figure 3.11 illustrates the numbered state points in the energy and mass balance equations [51].

3.3.1 Model assumptions:

Using the DACC cooling cycle schematic shown in Figure 3.11, the assumptions used in the modelling of the DACC system are described as follows [32,142]:

- The system operates under steady-state conditions.
- The pressure drops along the pipes are negligible.
- Hydrostatic pressures are negligible.
- The liquid solution (state 3) and the vapour bubbles (state 4) exit the capillary and leave the generator at the same temperature (i.e., $T_3 = T_4$).
- The generator is not wholly thermally insulated, so some of the supplied heat dissipates toward the ambient, depending on a variable heat exchanger efficiency.
- In state 6, the refrigerant flow rate is condensed (i.e., no flow in the gas bypass) and becomes a saturated liquid (i.e., no sub-cooling in the condenser).
- The refrigerant and the rich solution leave the condenser and the reservoir at the same temperature, and the cooling medium is ambient air (i.e., $T_7 = T_{11}$).
- Refrigerant and inert gas mixing at the entrance of the evaporator is adiabatic.

- The refrigerant leaves the GHX in state 10 as a saturated vapour, i.e., the refrigerant is considered pure in the evaporator.
- No absorption takes place inside the reservoir.

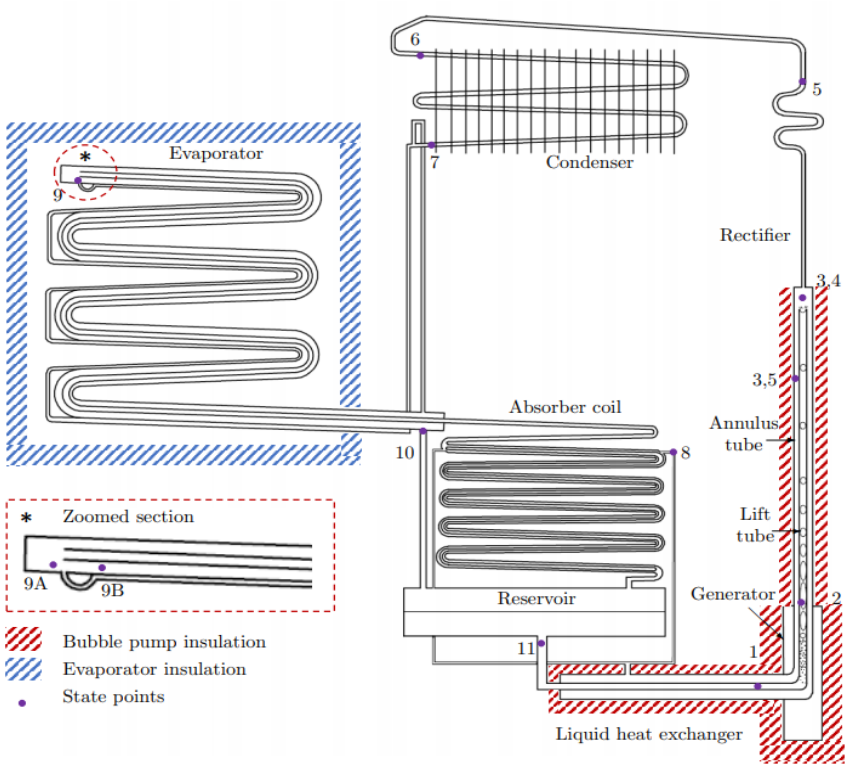

Figure 3.11: Diagram of the DACC cooling system, with numbered state points indicating the processes described in Section 3.2. The zoomed-in section in the bottom left shows the mixing section where the refrigerant meets the inert gas at top of the evaporator [51].

3.3.2 Input parameters used

Table 3.1 presents the state properties of the working fluids at all the cycle state points. Relations between temperature (T), pressure (p), concentration (x), and enthalpy (h) are used to identify each state of the working solutions at each point of the DACC cooling cycle.

The thermodynamic DACC model uses the following input parameters [142]:

- The temperature of the rich solution entering the generator, T_1.
- The temperature reached by the rich solution after heating, T_2.
- The temperature of the weak solution and the vapour leaving the generator, $T_3 = T_4$.
- The temperature of the refrigerant leaving the rectifier, T_6.
- the temperature of the refrigerant leaving the condenser, T_7;

Table 3.1: State properties of the working fluids in the DACC cooling cycle [142]

State	Variable	Value
1	p	$p_1 = p_C$
	h	$h_1 = h_l(T_i, x_1)$
	x	$T_1 = T\ (p_a, x_1) \Rightarrow\ x_1\ (by\ iterations)$
2	p	$p_2 = p_C$
	x	$x_2 = x_{12}$
3	p	$p_3 = p_C$
	h	$h_3 = h_l(T_3, x_3)$
	x	$T_3 = T\ (p_c, x_3) \Rightarrow\ x_3\ (by\ iterations)$
4	p	$p_4 = p_C$
	h	$h_4 = h_v(T_4, y_4)$
	y	$T_4 = T\ (p_c, y_4) \Rightarrow\ y_4\ (by\ iterations)$
5	p	$p_5 = p_C$
	T	$T_5 = T\ (p_c, x_5)$
	h	$h_5 = h_l(T_5, x_5)$
	x	$y_4 = y\ (p_c, x_5) \Rightarrow\ x_5\ (by\ iterations)$
6	p	$p_6 = p_C$
	h	$h_6 = h_v(T_6, y_6)$
	x	$T_6 = T\ (p_c, y_6) \Rightarrow\ y_6\ (by\ iterations)$
7	p	$p_7 = p_C$
	h	$h_7 = h_l(T_7, x_7)$
	x	$x_7 = y_6$
8	p	$T_8 = T\ (p_8, x_8) \Rightarrow\ p_8\ (by\ iterations)$
	T	$h_8 = h_l(T_8, x_8) \Rightarrow\ T_8\ (by\ iterations)$
	x	$x_8 = x_3$
8,ig	p	$p_{8,ig} = p_C$
	h	$h_{8,ig} = C_{p,ig} * T_{8,ig}$
9	p	$p_9 = p_e$
	T	$T_9 = T\ (p_9, x_9)$
	h	$h_9 = h_l(T_9, x_9)$
	x	$x_9 = y_6$
10	p	$T_{10} = T\ (p_{10}, x_{10}) \Rightarrow\ p_{10} = p_e\ (by\ iterations)$
	h	$h_{10} = h_v(T_{10}, y_{10})$
	x	$x_{10} = y_6$
10,ig	p	$p_{10,ig} = p_C - p_e$
	h	$h_{10,ig} = C_{p,ig} * T_{10,ig}$
11	p	$p_a = \dfrac{\dot{m}_r\left[x_r R_{NH_3} + (1 - x_r)\, R_{H_2O}\right]}{\dot{m}_{ig} R_{ig} + \dot{m}_r\left[x_r R_{NH_3} + (1 - x_r)\, R_{H_2O}\right]}\, p_c$
	h	$h_9 = h_l(T_9, x_9)$
	x	$x_9 = y_6$

- the temperature of the refrigerant and the auxiliary gas leaving the GHX, $T_{10} = T_{10,ig}$;
- the operating pressure, P_c;
- the heat supplied to the generator, $\dot{Q}_H$;
- the temperature of the air in the refrigerated chamber, T_{air};
- the refrigerated air mass flow rate, m_{air}.

Using $T_{10} = T_{10,ig}$ determines the temperature of the refrigerant (as saturated liquid) and the auxiliary gas in the evaporator, $T_9 = T_{9,ig}$. The model has specified input variables to produce results that better predict the cooling cycle performance.

3.3.3 Thermal modelling equations for the DACC cycle.

The mass and energy balance equations for various components of the DACC cycle are presented below [142]. The thermodynamic study starts with the energy balance of the generator and the bubble pump and ends with the COP.

3.3.3.1 Generator and bubble pump

The net enthalpy rise of the ammonia-water mixture in the generator-bubble pump equals the difference between the heat supplied to the generator ($\dot{Q}_{gen}$) and the heat loss to the environment ($\dot{Q}_{loss}$). State 1 is a saturated liquid, while vapour-liquid equilibrium is assumed between State 3 (liquid) and State 4 (vapour). The bubble pump and the generator are considered perfectly insulated; the heat dissipation is neglected, and the temperatures T_2=T_3=T_4. The energy balance for the generator and bubble pump is determined as follows [142]:

$$Generator \begin{cases} \dot{m}_1 = \dot{m}_3 + \dot{m}_4 \\ \dot{m}_1 x_1 = \dot{m}_3 x_3 + \dot{m}_4 y_4 \\ \dot{Q}_{gen} - \dot{Q}_{loss} = \dot{m}_3 h_3|_{T_3=T_2} + \dot{m}_4 h_4|_{T_4=T_2} - \dot{m}_1 h_1 \end{cases} \quad 3.1$$

3.3.3.2 Rectifier

$\dot{Q}_{rect}$ is the heat rejected to the environment by the partial condensation of the water fraction from the vapour mixture. Vapour-liquid equilibrium is assumed between the entry vapour mixture (State 4) and the exiting condensate (State 5). State 6 is the near-pure ammonia proceeding to the condenser. The energy balance for the rectifier is determined as follows [142]:

$$Rectifier \begin{cases} \dot{m}_4 = \dot{m}_5 + \dot{m}_6 \\ \dot{m}_6 = \dfrac{y_4 - x_5}{y_6 - x_5}\dot{m}_4 \\ \dot{Q}_{rect} = \dot{m}_5 h_5 + \dot{m}_6 h_6 - \dot{m}_4 h_4 \end{cases} \quad 3.2$$

3.3.3.3 Condenser

Q_{cond} is the heat rejected by the surroundings by condensing the ammonia refrigerant (and any remaining water fraction) at the system condensation pressure. The energy balance for the condenser, $\dot{Q}_{cond}$, is determined as follows [142]:

$$\dot{Q}_{cond} = \dot{m}_6(h_7 - h_6) \quad 3.3$$

3.3.3.4 Evaporator and gas heat exchanger (GHX)

The refrigerant flow rate proceeding to the evaporator is assumed to be equal to that exiting the condenser, $\dot{m}_6 = \dot{m}_7 = \dot{m}_9$. The energy balance for the evaporator considers both the pre-cooling and evaporation processes and the mass flows of refrigerant and inert gas (ig). The vapour at the evaporator outlet (state 10) is assumed to be saturated, so the partial pressures and mass fractions of refrigerant and inert gas are determined from the saturated vapour temperature. Thus, the energy balance for the evaporator, $\dot{Q}_{evap}$, is determined as follows [142]:

$$Evaporator + Gas\ HX \begin{cases} \dot{m}_7 = \dot{m}_9 = \dot{m}_{10} \\ \dot{Q}_{evap} = \dot{m}_9(h_{10} - h_7) + \dot{m}_{ig}(h_{10,ig} - h_{8,ig}) \\ \dot{Q}_{evap} = \dot{Q}_{evap,max} \end{cases} \quad 3.4$$

3.3.3.5 Absorber and reservoir tank

The refrigerant vapour is mixed with inert gas at the bottom (state 10) of the absorber via the reservoir. On the other hand, the weak solution is introduced at the top of the absorber (state 8). As a result, the refrigerant is absorbed into the weak solution to release heat to the environment, while the remaining inert gas exists at the top of the absorber. It is assumed that the inert gas exists at the same temperature as the weak solution, $T_8 = T_{8,ig}$. The energy balance for the absorber, $\dot{Q}_{abs}$, is determined as follows [142]:

$$\dot{Q}_{abs} = \dot{m}_{11} h_{11} - \dot{m}_{10} h_{10} - \dot{m}_8 h_8 + \dot{m}_{ig}(h_{8,ig} - h_{10,ig}) \quad 3.5$$

3.3.3.6 Solution heat exchanger (SHX)

Heat energy is transferred from the refrigerant-weak solution flowing in the outer annulus to the refrigerant-rich solution in the inner tube. The model assumes no heat loss from the SHX to the environment. Thus, the energy balance for the liquid heat exchanger, $\dot{Q}_{shx}$, is determined as follows [142]:

$$Liquid\ HX \begin{cases} \dot{m}_{11} = \dot{m}_1 \\ \dot{m}_8 = \dot{m}_3 + \dot{m}_5 \\ \dot{m}_3 h_3 + \dot{m}_5 h_5 - \dot{m}_8 h_8 = \dot{m}_1 (h_1 - h_{11}) \end{cases} \quad 3.6$$

3.3.3.7 Cycle performance

The coefficient of performance (COP) of the DACC cycle is determined as the ratio of the cooling output power at the evaporator to the heat input at the generator. The COP is calculated [142]:

$$COP = \frac{\dot{Q}_{evap}}{\dot{Q}_{gen}} \quad 3.7$$

3.3.4 Using the EES modelling software to model the DACC sub-system.

The DACC is not included in the standard TRNSYS component library; thus, the EES software is used to develop the mathematical model for the DACC described in section 3.3. The EES modelling results are compared with experimental results for a DACC published by Najjaran et al. [51].

The EES software is used to solve the system of equations described in section 3.3 and to determine the performance of the solar-powered DACS. The EES modelling results include the cooling machine COP, mass flow rates, fluid temperature, generation heat input, and cooling capacity. The properties of ammonia, water and hydrogen have been taken from the EES thermodynamic property library [199].

3.3.4.1 Input information

Using EES to model the DACC requires specifying the input parameters detailed in section 3.3.2. The inputs used have been specified in the published literature by Najjaran et al. [51] and Starace & De Pascalis [142].

3.3.4.2 Analysing the output

A detailed analysis of simulation results is undertaken once an EES design is achieved. For easy detection of patterns and anomalies, it is usually best to change one design characteristic at a time rather than simultaneously change multiple design factors to observe variations. In addition, modifying one design factor at a time allows easy determination of the dominant performance factors [114]. The results are analysed, taking into consideration all the relevant assumptions made.

3.3.4.3 Presenting and recording work

The EES results are exported to Microsoft Excel for post-modelling data processing and analysis, and the results are presented in Chapter 6.

3.4 Modelling in TRNSYS

Figure 3.12 illustrates the fundamental steps in using TRNSYS modelling software [171] to model the solar design for a solar-powered DACS cooling and heating system and simulate the building cooling and heating demand. TRNSYS tool uses the weather values of a typical meteorological year (TMY) file for each location. The various model developments are also illustrated in Figure 3.13.

Suitable components are selected from a component library and set up within the TRNSYS modelling and simulation window [171]. Afterwards, the parameters and the initial values for each component are defined. The appropriate links between components are completed by connecting one component's output to another's input. Besides, the equations feature is used as a function of numerical values and linked to selected inputs and outputs of other components as if it were a standard component. The modelling results can be viewed in charts produced by online plotters and data from in-built printers.

The TRNSYS modelling and simulation consists of two major sub-systems: the solar and storage design and the building's thermal performance simulation. The heat demand of the solar-powered DACS is met with the TRNSYS results for the solar and storage design. On the other hand, TRNSYS is used to simulate the cooling and heating loads of the building. Thus, the solar-powered DACS meets the building's cooling load, while the solar and storage design can meet the building's heating demand. The DACC cooling cycle is modelled with EES and compared with experimental results published by Najjaran et al. [51].

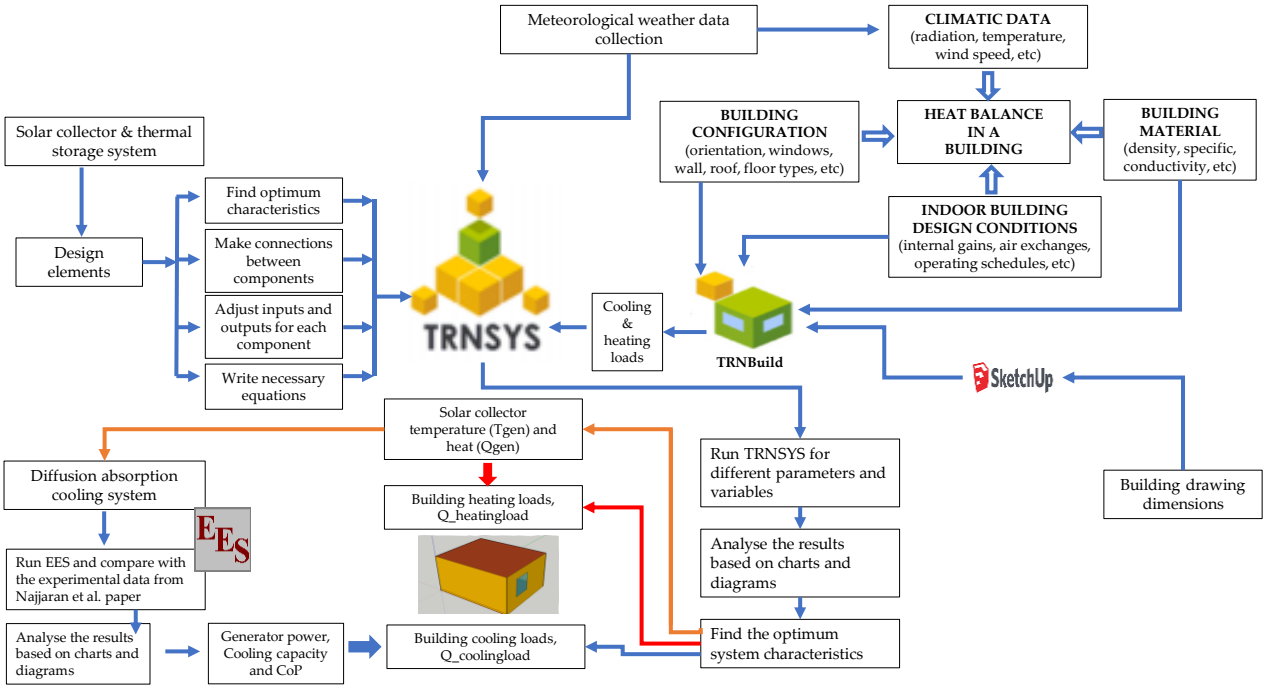

Figure 3.12: Modelling framework in TRNSYS (modified from [219]).

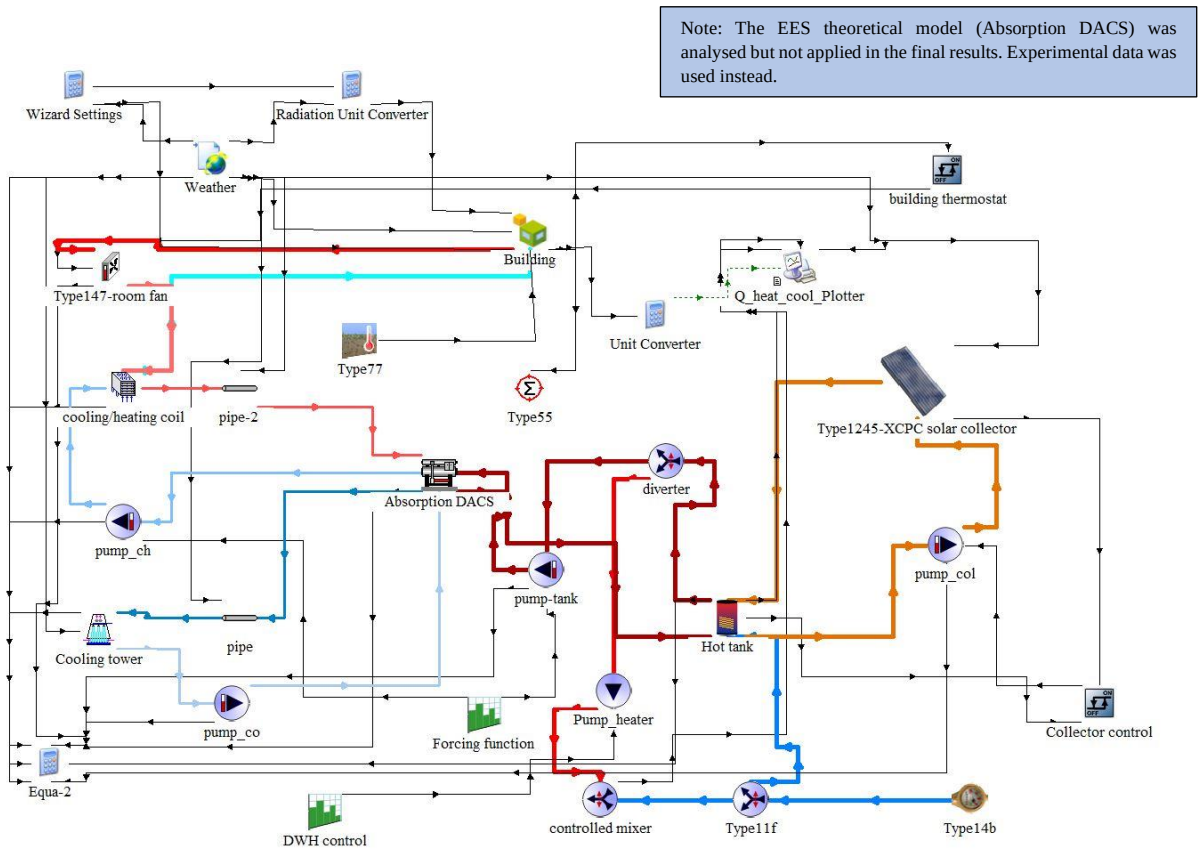

Figure 3.13: Model development in TRNSYS software. EES Theoretical Model (Absorption DACS analysed but not applied in final results; experimental data used instead); discussed in section 3.4.7.

The following assumptions were made in the TRNSYS energy system modelling and building cooling and heating load simulation [32,33,171].

- The pressure drops and the heat energy losses in the in-line piping and valves are assumed to be negligible.
- To model stratification observed in storage tanks, each of the ten nodes of the storage tank is assumed to be isothermal and interacts thermally with above and below nodes through several mechanisms: fluid conduction between nodes and fluid movement (either forced movement from inlet flow streams or natural destratification mixing due to temperature inversions in the tank).

The main components in the TRNSYS design are described below.

3.4.1 Weather data

Solar energy applications and building thermal performance studies require correct climatic data to ensure an accurate design that accounts for the real impact of the environment [53,55]. The environmental factors include solar radiation, ambient air temperature, sky temperature, ground temperature, dew point, wind speed, and relative humidity. The weather data is processed by the Type 99 component, a typical meteorological year (TMY) file for the four case study cities: Tunis, Swansea, Volgograd, and New Delhi. The four cities were selected to cover different climate regions, as shown in Figure 3.14. The Type 99 component reads weather data at regular intervals from a data file, converts it to desired units and creates direct and diffuse radiation outputs for an arbitrary number of surfaces, orientations and inclinations [171].

The typical weather data file is generated from historical data, compiled by comparing the cumulative and empirical distribution functions of diverse meteorological variables within the base dataset. The TMY file is based on average weather over historical basis years, and thus, they are suitable for calculating model outputs such as typical monthly energy usage. Weather data based on historical mean values do not accurately depict design outputs for extreme weather events such as heat waves and drought [158]. However, it is practical to avoid oversizing issues by designing building air conditioning systems to cope with the desired range of historical weather conditions [88,158].

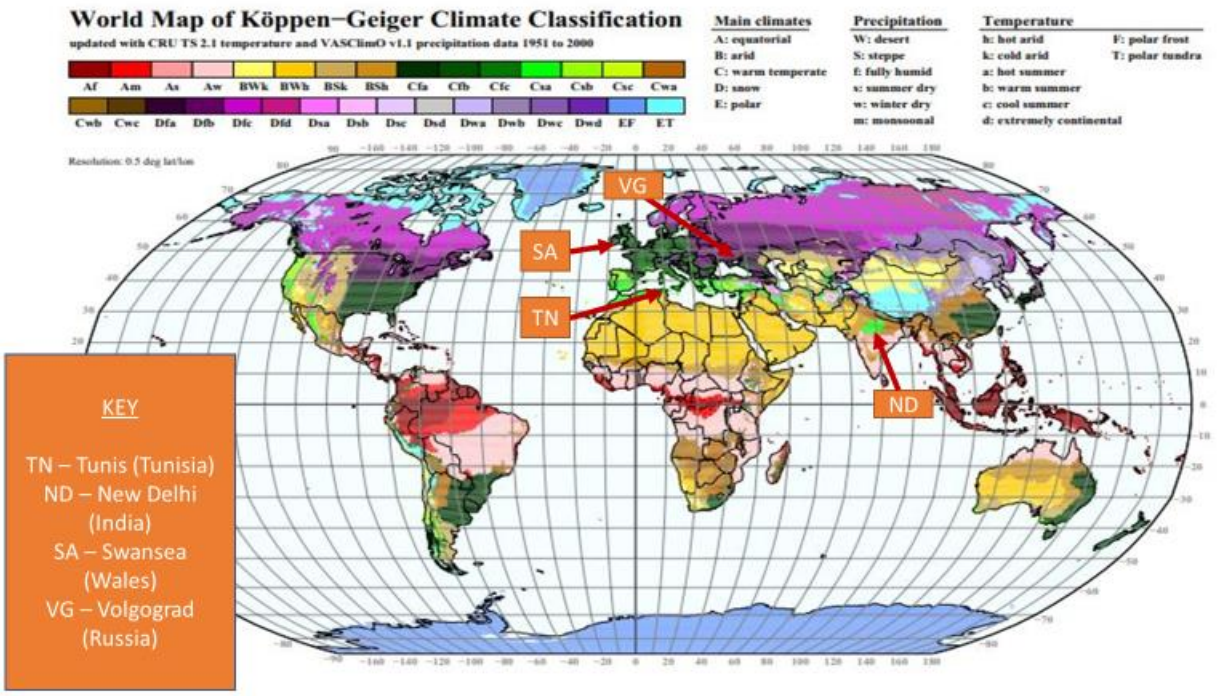

Figure 3.14: The four selected case study cities: Tunis, New Delhi, Swansea, and Volgograd [220].

Tunis, the capital of Tunisia, is located at a 36-degree latitude and a 10-degree longitude [116]. Tunis has a warm, temperate Mediterranean climate characterised by a warm summer temperature, dry summer precipitation and a high solar resource. Volgograd is a city in southwest Russia with a latitude of 48.68 and a longitude of 44.35. In Volgograd, the summers are warm and dry, while the winters are long, freezing, and snowy. New Delhi is the capital of India and has a latitude of 28.58 and a longitude of 77.2. New Delhi's wet season is hot and partly cloudy, and the dry season is warm and mostly clear. Swansea is a city on the south coast of Wales with a latitude of 51.62 and a longitude of 3.94. In Swansea, the winters are long, freezing, and wet, and the summers are comfortable [171,221].

3.4.2 Solar thermal collector

The Type 1245 external concentrating parabolic solar collector (XCPC) component is selected as the heat source for the solar-powered DACS cooling system in the TRNSYS software. An XCPC solar collector comprises glass evacuated tubes, manifolds of copper heat pipes, copper u-tube and aluminium heat spreading fins, concentrating collector reflector, aluminium frame, and rock wool insulation [65]. The heat source temperature for the generator of the DACC cycle operates in the range of 135-230 °C [51,68]. The XCPC solar collector is selected because it has high optical efficiency of around 0.62 and thermal efficiency of about 0.50 at 200 °C

[64,67,222,223]. The impact of boiling the working fluid in the solar collector field was not considered in the thermal analysis of the XCPC in TRNSYS.

The thermal efficiency equation governs the working operation of the solar thermal collector [33]:

$$n = a_0 - a_1 \frac{(\Delta T)}{G} - a_2 \frac{(\Delta T)^2}{G} \qquad 3.8$$

where a_0 is the optical or zero loss efficiency, a_1 and a_2 are the heat loss coefficients, G is the global solar radiation on the solar collector plane, ΔT is the temperature difference between the inlet fluid and ambient temperatures in the ASHRAE standard, and the temperature difference between the mean fluid and ambient temperatures in the European standard [33].

The stationary XCPC has an east-west (E-W) orientation, i.e., the absorber is situated horizontally, and the optics are designed to accept the seasonal swing of sunlight. The E-W orientation produces higher solar concentration with improved performance at a higher operating temperature [67,223].

3.4.3 Storage tank

Type 158 is the storage tank component installed between the solar collector and the DACS to provide a hot water supply buffer store, Figure 3.15. The Type 158 TRNSYS component models a cylindrical liquid storage tank, where hot water from the solar thermal collector is pumped. Besides, a maximum of two flow streams mix, enter or exit the storage tank [171]. The tank is divided into ten isothermal temperature nodes and uses a calculated overall heat loss coefficient in all simulations. Each tank segment acts as a node governed by a tank energy balance as a function of time. Solar heat flows from the top of the buffer storage tank to the generator part of the DACC, while the return flows from the generator to the bottom compartment of the storage tank [33].

The storage tank model accounts for various component interactions with the environment and heat transfers. The environmental temperature calculates storage tank heat loss (or gain) from the top, edge, and bottom areas. The adjacent nodes in the storage tank interact thermally via a conduction heat transfer. The tank model has a maximum of two flow streams which pass into and out of the tank. The tank's inlet and outlet connections are specified as a fraction of the tank height [171].

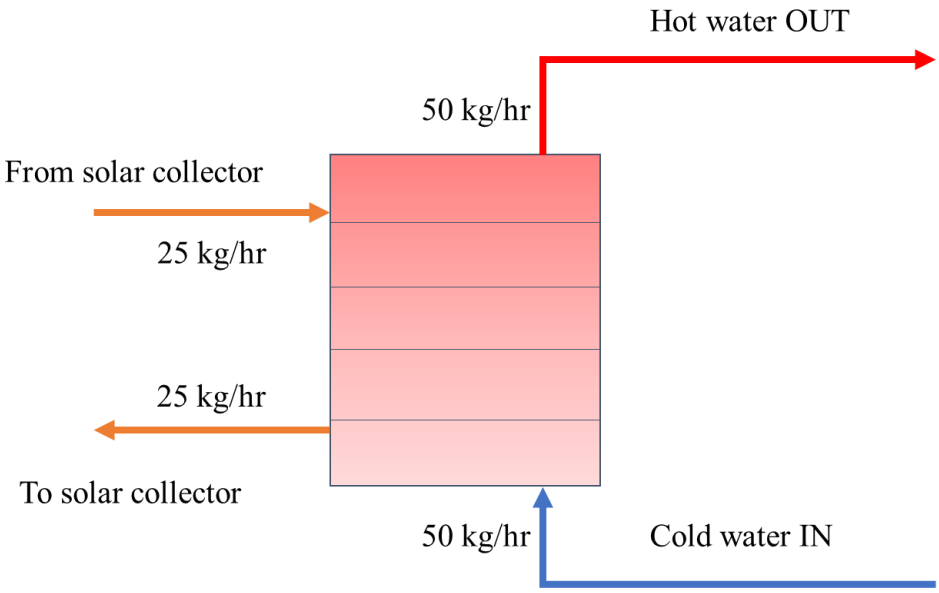

Figure 3.15: Vertically cylindrical storage tank showing example flows [171].

The inlet to the storage tank is assumed to be paired with a corresponding outlet from the storage tank, such that the outlet flow rate is the same as the paired inlet. For example, 50 kg/h flow into inlet connection point 1 causes 50 kg/h to exit the storage tank via outlet point 1. There are instances where a node in the storage tank becomes thermally unstable, i.e., a node has a higher temperature than the adjacent node above. At the end of each time step, the tank model thoroughly mixes any unstable nodes to achieve the tank's fluid stratification [171].

3.4.4 The Building

A building with a floor area of 24.75 m^2 (5.5 m x 4.5 m) is selected for the building simulation design study. The building area or the room is considered a “zone” because it is an area controlled by a dedicated thermostat [122]. The standard building adheres to the 2013 United Kingdom (UK) building regulations [143]. Nonetheless, a comparative building structure suitable for the local climates of the four cities, Tunis, Swansea, Volgograd, and New Delhi, has been selected for the localised design study. The building room temperature is controlled with a room thermostat set at 24 ºC and 20 ºC for cooling and heating, respectively. The building structure drawn with the SketchUp drawing tool [224] is shown in Figure 3.16.

Although the single building is simplistic and is essentially a single room, it was chosen for a number of reasons. It represents the mean space for a primary single occupancy room built in the UK from 2010 onwards [225]. It provides a small surface area to volume ratio for a space, emphasising the building's wall insulative properties. It negates the impact of varying international roofing structures and provides a suitable unit test case that can be scaled to larger

buildings. This building geometry provides the smallest viable dwelling unit, which can be scaled to estimate more complex building structures. This minimum viable dwelling possesses a high surface area to volume ratio, representing a worst-case in terms of heat loss/gain. Energy demand per unit volume is likely to be smaller, and periods of energy deficit are likely shorter for more complex buildings.

(a) Basic single building showing the top, south, and east elevations.	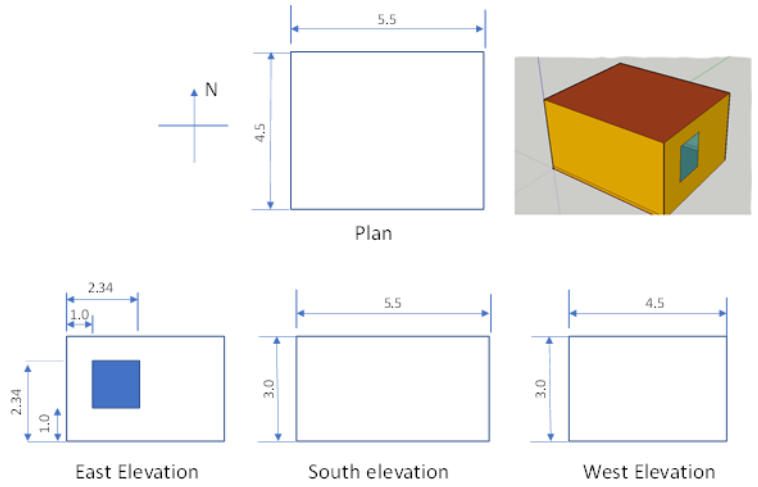
(b) Large (4x single) building showing the top, south, and east elevations.	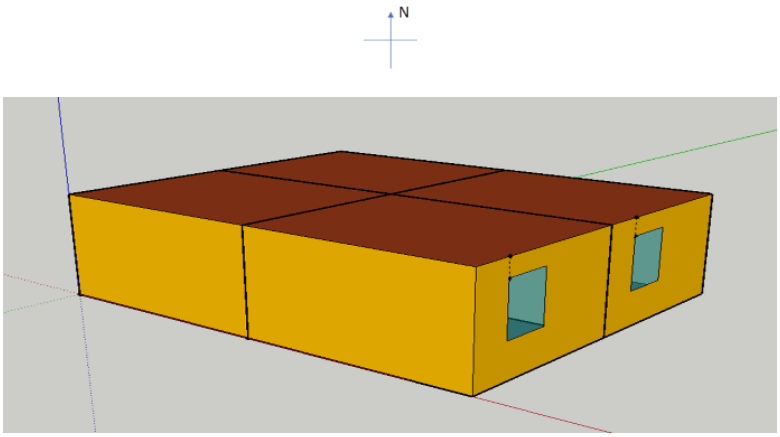

Figure 3.16: Outline of the (a) basic single and (b) large buildings drawn with the SketchUp tool.

Sections 3.4.4.1 and 3.4.4.2 explain how TRNSYS software models the building's thermal performance.

3.4.4.1 TRNSYS building modelling with Type 56 and TRNBuild

The Type 56 component is used to model the thermal behaviour of the building. A separate pre-processing program, TRNBuild, is first executed to use the Type 56 component. TRNBuild, the building input description tool of TRNSYS [171] defines the building characteristics and inputs building geometric information as an initial processing step. In addition, Trimble SketchUp drawing software [224] was used to model the three-dimensional features of the building before exporting the relevant building data into the TRNBuild tool and to the building model Type 56 in the TRNSYS graphical interface. Although the building is a single-zone building, the Type-56 is selected to model the building characteristics because it provides the capability to describe the detailed physics to allow an improved and realistic building description [181].

After selecting the zone construction material, simulation inputs such as infiltration and convective heat transfer exchanges are assigned to specified air nodes. In contrast, long-wave and short-wave radiation exchanges are applied to the entire building zone [169]. The building has a flat roof and is modelled as a single zone without partitions in the interior compartment. The building incorporates insulation in the roof, floor, and walls and the zone is prescribed using input parameters for the walls, roof, floor, and window. The building construction material is selected from the TRNSYS construction library [116]. However, specific material descriptions were amended to suit the preferred building characteristics that match standard building material requirements. In addition, the building characteristics were selected to suit the building's distinctive local climate. In TRNBuild, non-geometric objects, such as building materials, internal heat gains, schedules, cooling, heating, controls, etc., are specified for the project. The orientation of each building surface is defined to include the building surface's azimuth and slope.

TRNSYS calculates the building's cooling and heating loads using the transfer function method (TFM) [171]. The cooling and heating load calculation determines the total sensible thermal load from heat gain or loss from (1) through the building's opaque surfaces (walls, floor, and roof), (2) the transparent window, (3) caused by infiltration, and (4) due to building occupancy. The latent portion of the thermal load is calculated separately and results from moisture sources from outdoor infiltration air, occupants, and miscellaneous sources such as laundry, cooking, and bathing. The variation in air temperature across such surfaces and the solar heat gains incident on the surfaces cause the heat gain via the opaque surfaces. The heat capacity of the

building fabric absorbs the heat gain and, as a result, delays heat gain within the building's internal space [88,139].

TRNSYS software is well suited for TFM because it requires many calculation steps to perform hourly, daily, monthly, and annual energy use. The TFM applies conduction transfer function (CTF) coefficients to the external opaque surfaces and the differences between sol-air and inside space temperature to determine heat gain considering the surfaces' thermal inertia [139]. O'callaghan et al. [226] define the sol-air temperature as the outside air temperature which, in the absence of all radiation changes, gives the same rate of heat entry into the surface as would the combination of incident solar radiation, radiant energy exchange with the sky and outdoor surroundings, convective heat exchange with the outdoor environment, and convective heat exchange with the outdoor air.

The TFM calculation procedure is illustrated in Figure 3.17 [146]. Initially, hourly solar heat gain via glass, transient conduction heat flows through envelope surfaces known as conduction transfer function (CTF) and various internal heat sources are calculated.

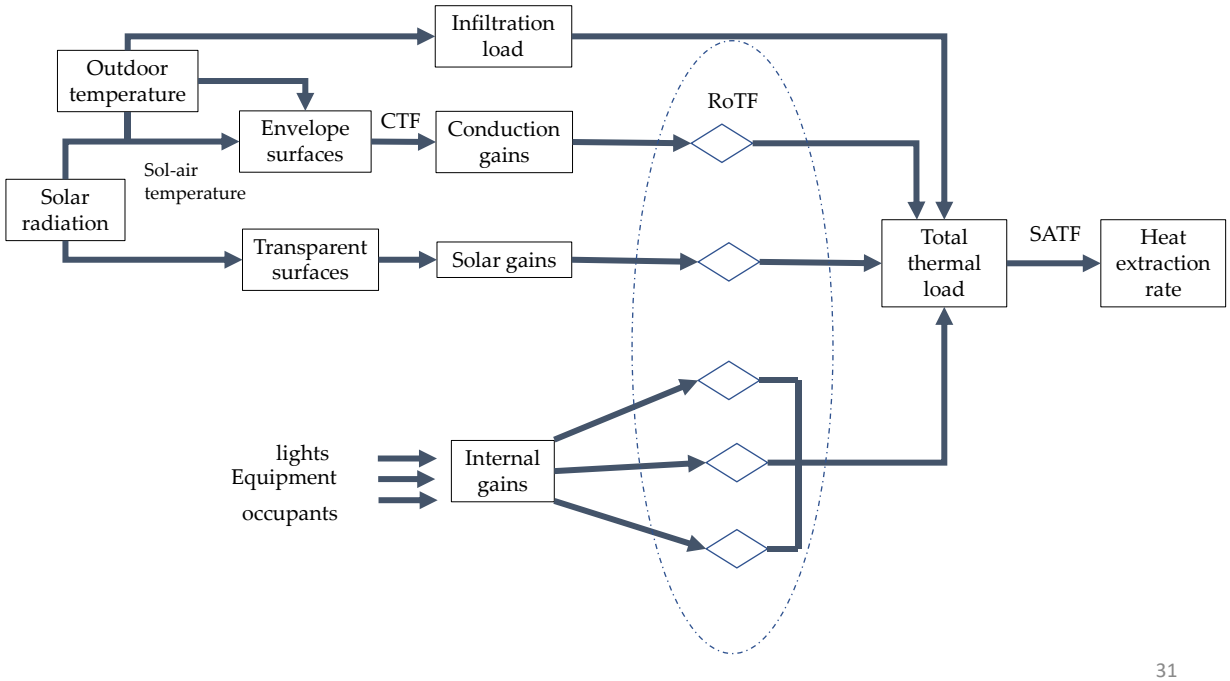

Figure 3.17: Schematic of the transfer function method (TFM). Involves three sets of hourly transfer function (CTF, RoTF, and SATF) coefficients applied during separate iterative calculations in TRNSYS over 24 hours till a periodic steady daily pattern is reached. Only a single envelope surface and a single transparent surface are illustrated in the diagram [146].

Next, the TFM applies a second series of coefficient of room transfer functions (RoTF) to all radiant components of the heat gain and cooling load values, thus accounting for the thermal storage of heat gain before reflecting as a thermal load. The evaluation series considers data from previous and current hours [146]. The RoTF coefficients apply to the spatial geometry, configuration, and mass [88,139] to reflect the building thermal storage effect. As a result, the TFM model calculates the three different types of heat gains and then determines their respective thermal load at constant indoor set point temperature. The component thermal loads are added together to calculate the overall building thermal load [123,135,146].

The following section presents the TFM calculation method employed by the TRNSYS software to determine the building's cooling or heating load.

3.4.4.2 Transfer function method (TFM) calculation procedure used in TRNSYS

The TFM calculation procedure is applied to calculate the thermal load of the building space on an hourly basis to predict resultant system operating conditions, schedules, and control strategies. The equations and sequence of the TFM calculation procedure applied in the TRNSYS software are summarised below [123,135,146]. The building's external heat gain is calculated from the sol-air temperature, t_e, and the 24-hour average sol-air temperature, t_{ea}:

$$t_e = t_0 + \propto I_t/h_0 - \varepsilon\,\Delta R/h_0 \qquad 3.9$$

$$t_{ea} = t_{oa} + \propto/h_o(I_{DT}/24) - \varepsilon\,\Delta R/h_0 \qquad 3.10$$

where t_0 is the current hour dry-bulb temperature, $\propto$ is the absorptance of surface for solar radiation, $\propto/h_o$ is the surface colour factor, I_t is the total incident solar load, $\varepsilon\,\Delta R/h_0$ is the long wave radiation factor, t_{oa} is the 24-hour average dry-bulb temperature, I_{DT} is the total daily solar heat gain. The heat gain through the walls and the roof, $q_{e,\theta}$, is calculated from:

$$q_{e,\theta} = A\left[\sum_{n=0} b_n\left(t_{e,\theta} - n\delta\right) - \sum_{n=1} d_n\left[\left(q_{e,\theta} - n\delta\right)/A\right] - t_{rc} - \sum_{n=0} c_n\right] \qquad 3.11$$

where $b,\ c,\ and\ d$ are conduction transfer coefficients obtained from the design heat transfer coefficient for the roof or wall, θ is the hour for which the calculation is made, δ is the time interval, n is the number of hours for which $b,\ c,\ and\ d$ values are significant, e is an element under analysis for roof or wall, and A is the area of the element under analysis.

The heat gain via the transparent glass, such as the building window, is calculated as $Convective\ q$ heat and solar gain, q :

$$Convective\ heat, q = UA\ (t_o - t_i) \quad 3.12$$

$$Solar\ gain, q = A\ (SC)(SHGF) \quad 3.13$$

where t_i is the inside design temperature in a conditioned space, t_o, is the outdoor environment temperature, U is the design heat transfer coefficients for glass, SC is the shading coefficient, $and\ SHGF$ is the solar heat gain factor by orientation.

The heat gain via the floor is calculated as follows:

$$q = UA\ (t_b - t_i) \quad 3.14$$

where t_b is the temperature in adjacent space, $and\ t_i$ is the inside design temperature in the conditioned space. The internal heat gain from people comes from sensible heat gain, $q_{sensisble}$ and latent heat gain, q_{latent} and is calculated as:

$$q_{sensisble} = N\ (sensible\ heat\ gain) \quad 3.15$$

$$q_{latent} = N\ (latent\ heat\ gain) \quad 3.16$$

where N is the number of people in the building space multiplied by appropriate values of recommended sensible and latent heat gains based on the activity levels of occupants.

The heat gain from light, q_{el} is calculated as:

$$q_{el} = 3.41\ WF_{ul}\ F_{sa} \quad 3.17$$

$$q_{el} = 3.41\ WF_{ul}\ F_{sa}$$

where W is power input from an electrical source or lighting data, F_{ul} is the lighting use factor, $and\ F_{sa}$ is the special allowance factor. The heat gain from an electrical appliance, $q_{sensisble}$, can be calculated from:

$$q_{sensisble} = q_{input}\ F_U F_R \quad 3.18$$

Or

$$q_{sensisble} = q_{input}\ F_L \quad 3.19$$

where q_{input} is the rated energy input from appliances from the manufacturer's data, F_U is the usage factor, F_R is the radiation factor, $and\ F_L$ is the load factor.

The latent heat is zero if the appliance is under the exhaust hood. The ventilation and infiltration air can be calculated as follows:

$$q_{sensisble} = 1.10\ Q\ (t_o - t_i) \tag{3.20}$$

$$q_{latent} = 4840\ Q\ (W_o - W_i) \tag{3.21}$$

$$q_{total} = 4.5\ Q\ (H_o - H_i) \tag{3.22}$$

where Q is the ventilation or infiltration volumetric air flow rate; t_o, t_i are outside, inside air temperature; W_o, W_i are outside, inside air humidity ratio; H_o, H_i are outside, inside air enthalpy.

The sensible load Q_θ, is then calculated from the:

$$Sensible, Q_\theta = Q_{rf} + Q_{sc} \tag{3.23}$$

$$Q_{rf} = \sum_{i=1}\left(v_0 q_{\theta,i} + v_i q_{\theta,i-\delta} + v_2 q_{\theta,i-2\delta} + \cdots\right) - \left(w_i Q_{\theta-\delta} + w_2 Q_{\theta-2\delta} + \cdots\right) \tag{3.24}$$

$$Q_{sc} = \sum_{j=1}\left(q_{c,j}\right) \tag{3.25}$$

where Q_{rf} is the sensible load from heat gain elements having convective and radiative components; v and w are room transfer function coefficients selected per building element type, circulation rate, mass, and fixture type; q_θ equals each of the heat gains of elements having a radiative component; δ is the time interval; Q_{sc} is sensible thermal load from heat gain elements having only convective components; q_c is equal to each j heat gain element having only a convective component.

The latent load, Q_l, is calculated as:

$$Latent\ Q_l = \sum_{n=1}\left(q_{c,n}\right) \tag{3.26}$$

where q_c is equal to each of n latent heat gain elements.

3.4.5 Pump

Type 110 model is a variable-speed pump that delivers fluid from the solar collector to the buffer storage tank. The pump's mass flow rate varies linearly with the control signal setting, and the type 110 pump model sets the downstream flow based on its rated flow rate parameter and the current value of its control signal. When the pump's control signal indicates to be on, the pump's outlet fluid flow rate and the power drawn are set to their respective rated conditions, as specified in the model's parameter list. However, the Type 110 pump does not model pump starting and stopping characteristics because the timeframes in which pumps typically react to control signal changes are shorter than the typical time step used in this modelling study [171].

The temperature of the fluid at the pump's outlet, $T_{fluid,}$, is calculated as follows [171]:

$$T_{fluid,out} = T_{fluid,in} + \frac{Q_{fluid}}{\dot{m}_{fluid}} \qquad 3.27$$

where T_{fluid}, is the temperature of the fluid entering the pump, Q_{fluid}, is the energy transferred from the pump motor to the fluid stream, and $\dot{m}_{fluid}$, is the mass flow rate of the pump's fluid stream.

3.4.6 Control strategy

The solar loop transfers heat from a solar collector to the buffer tank, which supplies heat to the DACS generator. The control scheme that was implemented is summarised below:

1. The solar collector circuit pump is switched on based on the temperature difference between the solar collector and the tank. The collector pump turns on when the temperature difference between the collector outlet and the hot tank inlet exceeds 5 ℃. At the same time, it turns off when the temperature difference between the collector inlet and the hot tank outlet is lower than 2 °C.

2. The building room temperature is controlled with a room thermostat set at 24 ºC and 20 ºC for cooling and heating, respectively.

The Type 2 differential controller model generates a control function used to manage the operation strategy for the solar collector. A high-limit cut-out is included with the Type 2 controller so that the control function is set to zero if the high-limit condition is exceeded [171].

3.4.7 Using the TRNSYS simulation software

The building characteristics, building occupant usage pattern and cooling load components are specified using the TRNBuild component, and the plant and controls are set using standard components in the TRNSYS simulation studio. The cooling rate of the DACS machine equates to the calculated building cooling load. On the other hand, the computed building heating load can be met with the heat generated by the XCPC solar collector. The building thermal demand simulation uses weather data for a typical meteorological year. Thus, the simulation can be performed for a year, monthly, weekly, daily, or hourly [168,171]. The thermal modelling is run with a 1-second simulation time-step. Non-convergence issues are recorded, and further investigation allows simulation issues to be resolved.

3.4.7.1 Using the Experimental Data for the solar-powered DACS

The EES theoretical modelling result based on the thermodynamic mass and energy balance equations [142] is used to generate a data file that details the performance of the diffusion absorption cooling equipment so that the absorption equipment in the TRNSYS simulation window will be applied. However, the calculated EES modelling results based on the thermodynamic mass and energy balance equations did not closely follow the experimental data [51] in the published literature. Finally, the EES model in the TRNSYS simulation window shown in Figure 3.13 was not applied, and the experimental data was implemented for further DACS design presented in Chapter 6, section 6.4.

3.4.7.2 Input information

Careful consideration is applied when choosing the required inputs for detailed building, plant, control, and solar thermal system modelling in the TRNSYS modelling software. A good understanding of the design inputs and parameters is needed to satisfy the development of the design model in the TRNSYS program [227]. The plant configuration defines the individual components utilised in the design study. Each design component is selected from the component's library within the TRNSYS program. Each design component has a list of parameters and inputs that must be confirmed. The building cooling load depicts the size of the DACS machine selected to provide the expected cooling rate.

Artic Solar Manufacturer's datasheet [66] contains information for specifying the inputs and parameters for the XCPC solar collector. At the same time, the thermal characteristics of the building envelope, i.e., the wall, floor, roof, and window, are used from the Chartered

Institution of Building Services Engineers (CIBSE) Environment Guide A [161]. EES software [199] is used to perform thermodynamic modelling of the DACC cooling cycle, and the results include the COP, mass flow rates, fluid temperature, generation heat, and evaporation. The building type is described as a residential building with specific U-values and air-change rates.

3.4.7.3 Analysing the output

A detailed analysis of simulation results is undertaken once there is an achievement of design in TRNSYS. The parameters investigated are described in section 3.6, along with the justification for choosing them. TRNSYS has online plotters that are used to display results from design outputs. Also, design outputs can be exported from the printers to Microsoft Excel spreadsheets where further data analysis is required. For example, the TRNSYS design output, such as solar collector's COP and heat of generation, can be plotted annually, monthly, weekly, daily or hourly. Typically, the annual results help identify system performance for a typical year, while hourly or daily performance analysis shows precise details, design anomalies, and specific patterns [168,169,176].

3.4.7.4 Presenting and recording work

The TRNSYS online plotter component is used to display results from design outputs. Upon a successful simulation run, the online plotter can display the results graphically. The online plot is helpful because the design results can be visualised live as the convergence step is processed [168,171]. As TRNSYS calculates the annual building operative temperature or ambient air temperature, it can be viewed live from, for example, January to December. It is helpful to see visually, for example, if the simulation proceeds well from January to May but then aborts in June, which can be seen visually.

3.5 Modelling strategy used

The modelling strategy illustrates the design logic and process applied to complete the modelling of the solar, storage and DACC design and simulation of a building. The modelling strategy starts with the design goal, which defines the purpose of the modelling assessment. The design process provides the context of all the modelling decisions, such as the calculation methodology used, assumptions made, and the accuracy of the results. The modelling strategy defines the design questions to be answered, translating these into the appropriate models used, modelling objectives, applying simulations, and interpreting results [202,227].

3.5.1 The design goal, logic, and process

The design goal is to model the thermal behaviour of a solar-powered DACS cooling and heating system and simulate the thermal performance of the building. The design process requires using TRNSYS to model the solar and storage design and to simulate the building's thermal performance. Additionally, EES is used to model the DACC and compare it with experimental data.

Figure 3.18 illustrates the modelling strategy used in design logic and process to complete this research. The IEA's design principle for the successful design and operation of solar-powered cooling and heating systems stipulates to "reduce energy demand for cooling and heating systems before applying renewables" [228]. As a result, in Chapter 4, the modelling starts with simulating a standard building where the building envelope has a low thermal transmittance, also known as U-value. Buildings whose thermal characteristics have a low U-value result in reduced thermal energy demand or low combined cooling and heating load [123,161]. A standard building design is replaced with a local building whose envelope has a high U-value to illustrate that building envelopes with low U-value results in reduced thermal energy demand. Thus, the cooling and heating loads for the local building are compared with the standard building in Chapter 4.

In Chapter 5, an energy analysis is performed based on the solar energy capture to illustrate the heating energy available to heat the building based on the building roof space and the solar collector and storage size. In Chapter 6, the cooling engine is modelled using the EES software, where the thermodynamic performance is compared with the experimental data published by Najjaran et al. [51].

Thus, in Chapter 7, the XCPC solar collector and buffer storage tank are designed to meet the DACC's generator heating requirement. TRNSYS is used to complete the solar and storage design to maximise the solar energy capture to meet the required generator temperature. The TRNSYS design incorporates a sensitivity analysis to achieve optimal parameters based on the solar collector area, the fluid mass flow rate in the solar collector, and the storage tank volume. The solar design is complete when an optimised solar and storage system delivers the required generator temperature. Otherwise, backup energy is applied to meet the generator heat load requirement.

Chapter 8 quantifies any backup energy that meets the generator heat load requirement, while Chapter 9 models cold energy storage design. In Chapter 10, an economic analysis is performed

for the completed solar design compared with other heat pump performances. Moreover, an environmental impact assessment is conducted in Chapter 10 based on operational carbon emissions savings achieved due to operating the solar-powered DACS system.

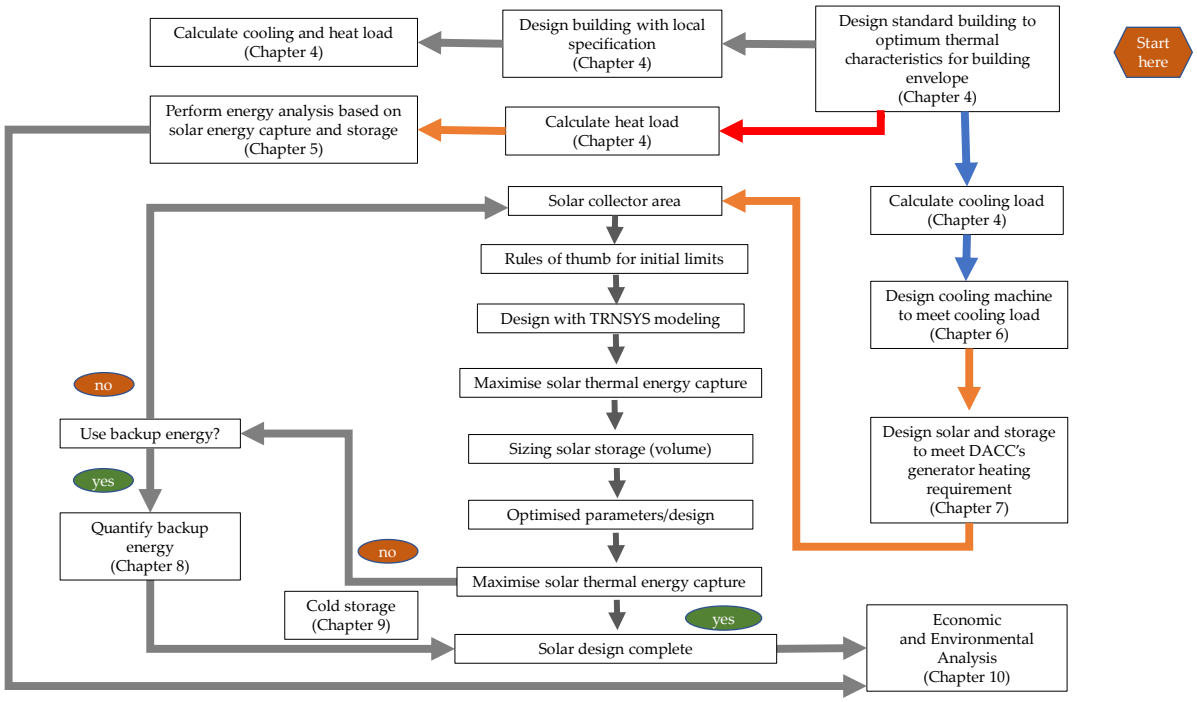

Figure 3.18: Modelling strategy used for the research study.

3.5.2 The case study locations

Chapter 4 compares cooling and heating loads for a standard building with a local building for the climatic locations, while Chapter 5 presents an energy analysis based on solar energy capture and storage, Table 3.2. In Chapters 7 - 9, energy and temperature design are evaluated for how the solar-powered DACS meets the cooling load for New Delhi and Volgograd.

3.5.3 How the experimental data results are used

Najjaran et al. [51] performed experiments with a DACS with a maximum cooling capacity between 100-120 W. The experimental data are compared with the EES modelling results and presented in Chapter 6.

3.6 Performance parameters investigated and their justification.

The parameters influencing the performance of the solar-powered DACS building cooling and heating system are investigated to achieve the optimum characteristics, Table 3.2. The parameter changes while other operational parameters are kept constant to identify any change or impact. Additionally, the parameters of the thermal characteristics of the building envelope

are investigated. The following section presents the justification for choosing each performance parameter—the optimum system benefits from installation costs, space, and reliability. In addition, the optimum system characteristics can be compared for different case study cities.

Table 3.2: Summary of strategy using simulation to identify key design impacts

Chapter	Aim (s)	Parameters varied/assessed	Justification
4	Establish baseline energy demand in each climate	Climate, building regulation compliance (Insulation)	Project aims* : 2,6,8 Literature: [38,139,143,161,162,171,220]
5	Examine energy capture	Days of cooling and heating required, deficit days, lag days, deficit hours/day, watt deficit/day, energy from hot store.	Project aims* : 1,3,4 Literature: [36,53-55,229,230]
6	Evaluate the cooling engine performance.	Generator power, generator temperature, cooling power	Project aims* : 1,2,8 Literature: [40,43-45,51,68,140,141,231]
7	Evaluate how the cooling engine cools a standard building.	Solar collector mass flow rate, solar collector area, thermal energy storage volume.	Project aims* : 1,3,4 Literature: [36-38,51,57,68,230]
8	Evaluates the thermal performance of the solar thermal collector energy capture and hot thermal energy storage.	Backup hours/day, backup energy/day, solar fraction, hot store heat loss.	Project aims* : 1,3,4,5 Literature: [36,37,53,230]
9	Evaluate the thermal performance of cold energy storage as an alternative to hot thermal energy storage.	Cold energy storage capacity, cold store energy loss. Mass of storage material.	Project aims* : 1,4,8 Literature: [73,138,232-234]
10	Perform economic evaluation and environmental impact assessment for the solar-powered DACS.	Payback time, operational carbon emissions and cost compared to heat pump.	Project aims* : 5,8 Literature: [172,189,222,229,233,235-238]

*Project aims listed in section 1.3.

3.6.1 Solar collector area

The solar thermal collector absorbs solar radiation, converts it into heat, and transfers it to a circulating fluid in the collector [54]. The solar collector area is a vital system parameter because the size dictates how much potential heat can be captured from the sun. It is essential to quantify the minimum required solar collector area capable of delivering the necessary heat to drive the absorption cooling system or a heating system [53,239,240]. Excess solar collector size adds costs to the project that must be avoided. Solar-powered systems that have optimum

collector area deliver a minimum system payback period. Thus, excess collector areas more than the optimum value must be avoided because they do not provide financial benefit [53,189]. Financially optimised solar collector areas are presented for the various case study cities.

3.6.2 The mass flow rate of the solar collector

The mass flow rate of fluid in the collector affects the thermal performance of a solar collector. It thus affects the thermal performance of the solar-powered absorption cooling system [31,53,55]. The different case study cities will have different optimum mass flow rates that deliver higher thermal energy from the solar collector. Thus, for each case study location, different collector mass flow rates are modelled to ascertain the optimum thermal performance of the solar collector system [189,240]. For each location, the useful energy gain from the collector is recorded at the optimum collector mass flow rate.

3.6.3 Solar collector efficiency

A collector's efficiency is calculated as the ratio of the collector's useful energy gain to the total energy input for the collector. The collector's total energy input is a product of the incident solar energy and the collector's total surface area. The useful energy produced by the solar collector is equivalent to the difference between the absorbed solar radiation and all heat losses [53]. The collector’s thermal efficiency is an important performance parameter because it allows different collector materials and modifications to be compared for a selected collected area. Thus, though the collector area may be kept the same for all the case study cities, the thermal energy efficiency will differ because different climates have different solar radiation levels [33,60].

3.6.4 Storage tank capacity

A buffer tank stores heat captured by the solar collector so that the heat can be used when there is no sunlight. Besides, there are times when there is sunlight but not enough heat to drive the DACS cooling system. The volume of the storage tank is examined to identify its influence on the heat transfer mechanism between the solar collector and DACS's generator and the potential heat loss to the environment. The storage tank is studied because increasing storage tank size also increases the heat loss potential [55,171]. Thus, it is essential to quantify the optimum tank size to deliver the optimum storage capacity while ensuring minimum heat loss to the environment. In addition, the tank's size impacts the project costs and spatial requirements [189].

One of the IEA’s key principles for the successful design and operation of solar heating and cooling systems is to provide a thermal storage capacity that matches the thermal requirements of solar-driven cooling and heating systems [228]. The solar-powered DACS requires adequate heat to be delivered to the generator to meet cooling demand [40,234].

In an alternative design in Chapter nine, a cold storage tank is used to store the cold generated from the DACS and used later to meet the building cooling demand at night or when there is insufficient energy from the solar collector or hot store. Chapter seven presents the solar collector and hot storage design based on temperature, and Chapter nine presents the cold energy storage design.

3.6.5 Effect of building envelope material

The building's heat balance is affected by climatic, design, material, and building usage data [139,161]. The building cooling and heating loads vary when the building envelope materials change, even when the climatic and building usage data remain the same. Thus, the building materials, i.e., the u-value, are used as performance indicators for investigating the building's thermal performance.

3.6.6 Dynamic behaviour of the solar-powered DACS under different case study locations

The solar-powered DACS cooling system works according to the building cooling load requirements. The building cooling loads are expected to differ for different climatic zones (case study cities). Thus, different cooling systems in various case study cities will perform with various working hours. The major influences on the DACS cooling system's thermal performance include the generator, evaporator, absorber, and condenser operating temperature. For example, the control strategy and the mass flow rate influence the generator operating temperature to match load conditions. The optimum operating conditions of the solar-powered DACS, e.g., flow rate rates and temperatures, must also be determined for the solar thermal collector and the buffer storage tank [33,189].

3.7 Economic analysis

The benefit of adopting a T.E. building design must be proven economically as well as thermodynamically. This limits T.E.'s purely economic installation cost as part of the NetZero Energy Building (NZEB) design stages. Local variations in the unit cost of energy play a key role in determining this economic merit. The financial benefit can be calculated and presented

in Chapter 4 using locally available energy pricing and carbon emissions impact factor. Moreover, the discounted payback time is calculated for the solar-powered diffusion absorption cooling and heating system and compared with the heat pump systems. Payback time is defined differently; however, the most common definition is implemented in this study. The payback time is the time it takes for the cumulative fuel savings to equal the total initial capital investment [53,229]. That is, the time it takes to claw back an investment made into installing the solar thermally driven cooling and heating system through the fuel savings achieved due to utilising the solar-powered cooling and heating system. The payback time can be calculated with or without discounting the fuel savings [229].

3.8 Environmental impact assessment – based on operational CO_2 savings

Using solar-powered cooling systems to replace conventional energy sources delivers primary energy savings and carbon dioxide reduction [55,236,241]. The environmental impact assessment is primarily based on operational CO_2 savings and a reduced carbon footprint due to utilising a solar-powered cooling system instead of conventional energy based on fossil fuels.

Sharma et al. [238] indicate that m_{co2} is the mass of CO_2 emissions calculated using the following equation [238]:

$$m_{co2} = \lambda * \text{Energy consumption (kWh)} \qquad 3.28$$

where λ is the emission conversion factor for the specific climatic location.

3.9 Summary

This Chapter explained how TRNSYS software is used to model the solar and storage design and to simulate the building's cooling and heating loads. Additionally, this Chapter described how EES modelling software is used to study the thermodynamic modelling of the DACC cooling cycle, which will be compared with experimental data in published literature. Fundamentally, EES software proves instrumental in modelling the design aspects of the components that are not available in the TRNSYS component library. The next Chapter presents the building design and the cooling and heating loads simulated with the TRNSYS software.

Chapter 4 : Modelling and Simulation of Building Energy Performance

4.1 Introduction

There is increasing worldwide demand for NetZero Energy Building (NZEB) to reduce buildings' energy consumption and carbon emissions [1,235,237,242-244], and many countries and regions, including the United Kingdom (UK), France, the USA, and the European Union (EU), have set long-term goals to implement NZEB [244]. Wei et al. [244] define NZEB as buildings that generate at least as much energy as they consume annually when tracked at the building site.

Figure 4.1 illustrates the process of achieving a residential NZEB. The fundamental approaches to achieving residential NZEBs are minimising the building energy demand (via improved building design and occupant behaviour) and increasing renewable energy generation. The IEA's first principle for the successful design and operation of solar-powered cooling and heating systems stipulates to "reduce energy demand for cooling and heating systems before applying renewables" [228]. Thus, the initial step for achieving residential NZEBs is to reduce building cooling and heating energy demand before applying renewable energy generation in buildings.

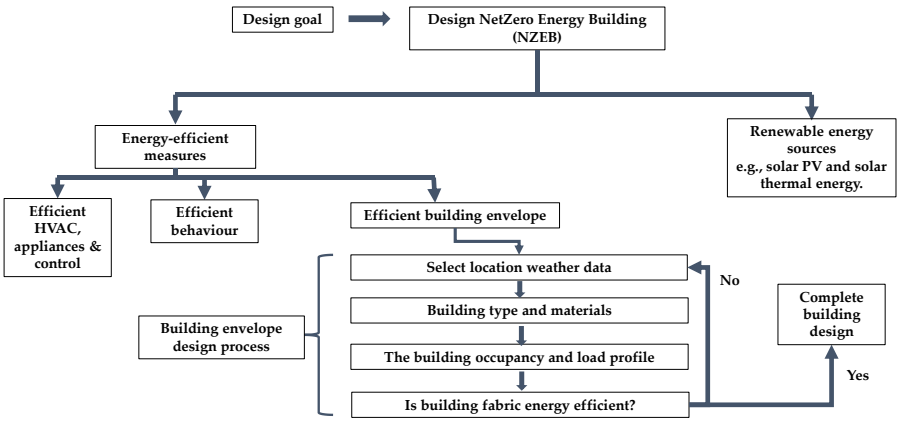

Figure 4.1: Building modelling to achieve residential NZEB (ideas from [146,244]).

This Chapter compares the design process for an energy-efficient standard building with a local building design. An energy-efficient building design focuses on a building's thermal performance such that the building fabric has thermophysical properties that reduce building

cooling and heating energy usage. Solar thermal energy is used in the building cooling and heating system as part of the residential NZEB, discussed in Chapter 5.

This Chapter presents building design for a thermally efficient building envelope that reduces overall building cooling and heating loads. A comparable building is designed with local specifications and compared with the thermally efficient building envelope. The thermally efficient building envelope is referred to as a standard building, while the building with local specifications is called a local building.

Section 4.2 presents the building design specifications, including the building type and materials, geometry, occupancy schedules, and location weather data, applicable to the small and large buildings. Section 4.3 presents results for the building's thermal energy performance, small building (sections 4.3.1 – 4.3.3) and large building (section 4.3.4).

4.2 Data and Methodology

4.2.1 Building design specifications

The building design specifications were input into TRNSYS software to calculate the cooling and heating loads using geometry initially created in SketchUp, as presented in section 3.4.4 and Figure 3.16 [224]. The climatic, design, material, and building usage data affect the building's heat balance, as shown in Figure 4.2.

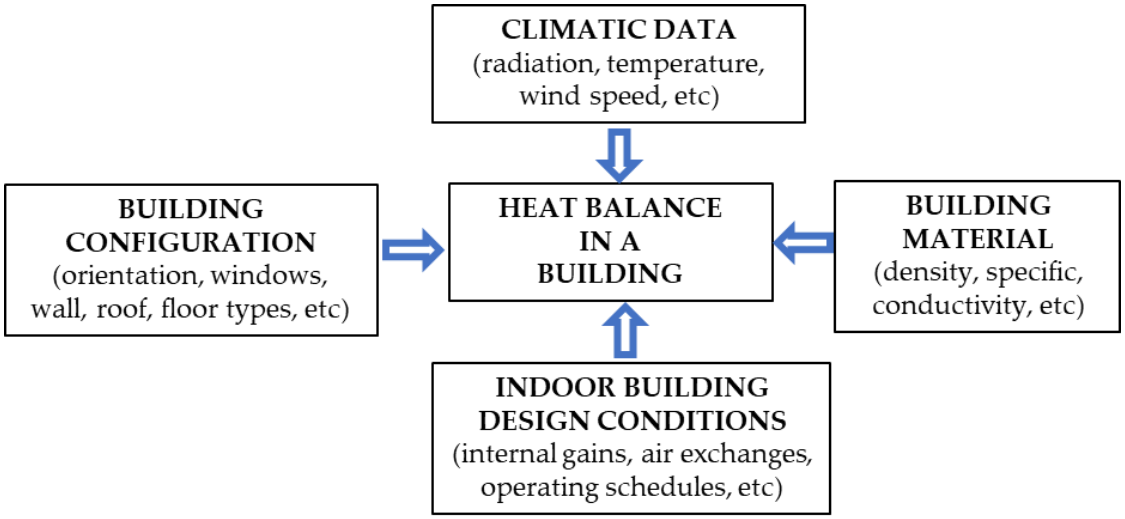

Figure 4.2: The Heat Balance of a building (modified from [146]).

The climatic data include solar radiation, ambient temperature, and wind speed. The building design data consists of the orientation of the building walls, floor, roof, and window; the

building material data includes the material density, conductivity, heat capacity and thermal resistance. Likewise, the building usage data depicts the components of the building's internal heat gains, the air exchange rate, and the ventilation rate [146,171].

4.2.2 The external climatic design information

The building cooling and heating loads are impacted by external climatic factors such as essential weather and solar irradiation. Therefore, four global locations, Tunis (Tunisia), Volgograd (Russia), New Delhi (India), and Swansea (the United Kingdom), were chosen based on their different weather patterns and solar irradiation levels. All were considered in the northern hemisphere, so the building axis orientation could be constant. The weather data required for determining the TE building's thermal energy demand is generated using the Meteornorm weather data file distributed with TRNSYS under license from Meteotest [171]. The meteorological and radiation data is based on monthly values, while Meteornorm calculates hourly values of all parameters using a stochastic model. The resulting time series corresponds to "typical years" applied for system design [245-247]. Table 4.1 lists the case study location's climate, latitude, longitude, elevation, and average summer and winter temperatures [171].

4.2.3 The building envelope's material data

The U-value of the building envelope is the principal factor for determining the building envelope's heat losses and gains [123,161]. The recommended building envelope U-values are stipulated in the Part L of the UK. Building Regulations 2013 [143] are used for the material characteristics of the TE building, Table 4.2. The thermo-physical properties (material data) of the building's walls, floor and roof are specified from the building material data published in the CIBSE Environmental Guide A [161] to meet the required U-values stipulated in the UK building regulations [143]. CIBSE has collated the various material data provided by manufacturers and from other testing results. The thermo-physical properties of the building's walls, floor, roof, and window are specified in TRNBuild as part of simulating the building's thermal performance, and the data are presented in Appendix A.

The thermo-physical properties of the window are specified using a shading coefficient, solar heat transmittance and the U-value. These building material properties do not necessarily represent those present locally in each location but describe a standard building, allowing climate-related demand to be evaluated independently of the building materials. Local socio-

economic factors, building codes, construction techniques and materials may, in practice, prevent the construction of such buildings, but it remains a useful scientific method for establishing the analysis of climatic variations on an idealised energy demand. A local building with thermo-physical properties typical of the local climate is applied to examine how the building envelope material characteristics influence the overall cooling and heating loads.

Table 4.1: Meteornorm weather location for the four case study cities.

Location	Country	Climate	Summer T_{ave} (°C)	Winter T_{ave} (°C)	Latitude [°N]	Longitude [°E]	Elevation [m]
Tunis	Tunisia	Hot summer / mild winter	25.4	12	36.83	10.23	3
Volgograd	Russia	Hot Summer / Cold Winter	22.2	-7.2	48.68	44.35	145
New Delhi	India	Very hot summer / mild winter	31.1	15.7	28.58	77.2	212
Swansea	Wales	Warm summer / Cool winter	15.3	4.6	51.4	-3.35	67

The local building is designed with a high U-value typical for the local climates of the four cities: Tunis, Swansea, Volgograd, and New Delhi, Table 4.2. The local building's thermo-physical properties for Tunis and New Delhi climatic locations are taken from literature published by Boukhris et al. [248] for a case study design for Tunis climate. Radiative and

convective heat transfer mechanisms occur as air-surface barrier heat transfer mechanisms [123,139,161].

Table 4.2: Building envelope thermal characteristics. Full details of each location's wall, floor, roof, and window construction are given in Appendix A.

	Wall	Floor	Roof	Window		
	U- value $W/m^2.K$	U – value $W/m^2.K$	U – value $W/m^2.K$	U-value $W/m^2.K$	Shading Coefficient	Transmittance Light/ solar heat
TE building	0.132	0.105	0.131	1.06	0.75	82% / 65%
Local – Swansea	0.813	1.062	0.739	1.06	0.75	82% / 65%
Local – Tunis	0.201	0.894	0.784	1.06	0.75	82% / 65%
Local – New Delhi	0.201	0.894	0.784	1.06	0.75	82% / 65%
Local – Volgograd	0.813	1.062	0.739	1.06	0.75	82% / 65%

The U-value for the building window is maintained the same for the four climatic zones. The selected building window from the TRNSYS building window data pool [171] has a fixed shading coefficient and a U-value, Table 4.2, meeting the UK Building Regulations 2013 U-value limit [143]. The building window dimensions (1.5 meters x 1.2 meters) meet the minimum width and height criteria such that the building has the same window-to-wall ratio or fixed window number for all climatic locations. Although fixing the U-value for the building windows while varying the U-value for the building's thermal insulation simplifies the analysis in this study, it was chosen for a number of reasons. Maintaining the building window properties constant allows any changes in the building's thermal energy performance to be directly attributed to changes in the thermal insulation U-value. Implementing the same window across the climate zones enables a focused study and straightforward comparisons of

how the building thermal insulation performs in different climates and draws conclusions about the insulative properties. The building window properties do not necessarily represent those present locally in each climatic location but represent a standard building, which allows a focused study on insulation impacts to be evaluated independently of the window properties. Local building codes, socio-economic, construction techniques, and materials may, in practice, prevent the construction of such windows; however, it remains a useful scientific method for evaluating thermal insulation on an idealised energy demand.

4.2.4 The building usage data – internal heat gain

The building energy demand is partly determined by the thermal transmittance, the air exchange rate, and the ventilation rate [123,139] The building's internal heat sources include bodies (human and animal), lighting, computers and office equipment, electric motors, cooking appliances and other domestic equipment [123], specified in Table 4.3. The sensible heat gain has convective components released into the surrounding air and radiative components stored in the building mass [139]. The lights and electrical equipment are scheduled to operate from 06:00 to 22:00 hours, and the building is expected to be occupied by one person during the building use.

Building infiltration, sometimes referred to as residential air leakage, is the introduction of outside air into the building, impacting the air quality within the building. Air leakage rates are specified as airflow rate, Q_i, or air exchange rate (ACH), expressed in equation form [139]:

$$ACH = \frac{3.6\ Q_i}{V} \qquad (1)$$

where Q_i is infiltration air flow rate (L/s); ACH is the air exchange rate (changes/hour); and V is building volume (m^3). The building ventilation rate is selected to be above the minimum air flow rate such that the calculated ACH is within 0.4 -1.0, as recommended by CIBSE [161], Table 4.4.

Table 4.3: Building internal heat gains used for thermal load calculation in TRNSYS.

Source of heat gain/loss type	Convective [kJ/h.m^2]	Radiative [kJ/h.m^2]	Electrical power fraction	Absolute humidity [kg/hr.m^2]
Lights	368.6	92.2	16	0
People	100.8	151.2	0	0.066
Electrical equipment	368.6	92.2	16	0

Table 4.4: Building design data for infiltration and ventilation rate.

Parameter	Value	Unit
Air exchange rate	0.4	ach
Building ventilation rate	8.3	l/s

4.2.5 Large building

A large building is modelled in TRNSYS, which is four times the size of the small building, as shown in Figure 3.16. The TE building and local buildings are each modelled to a large building. Thus, the building material specifications and all other building data are maintained except the new building size. The building partition wall specification is the same as the building's external wall.

4.3 Results

4.3.1 Monthly cooling and heating demand

Analysing the daily cooling and heating loads allows the appropriate selection of the suitable cooling or heating equipment size to maintain the desired temperature and conditions within the building. The energy gains or losses, e.g., from internal heat gains, increase or decrease the temperature of the inner structural mass, furnishings, and zone air. The daily cooling and heating load results for the four climatic locations represented by the four case study cities are presented in Figure 4.3. The overall thermal effect of these gains or losses on the building's

internal zone air is called the load. The cooling load is the energy that needs to be removed from the building's interior space to maintain a zone's thermal condition.

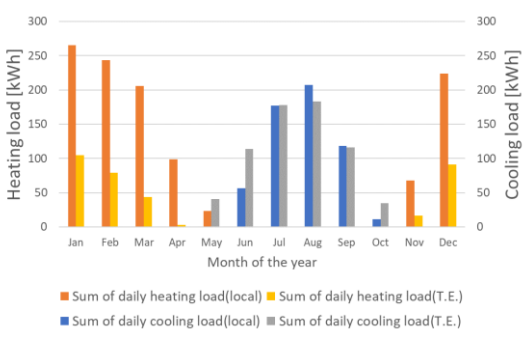

(a) Tunis

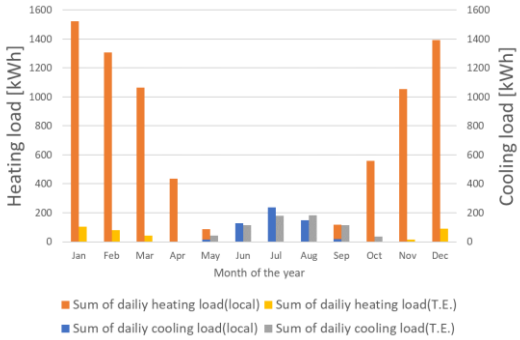

(b) Volgograd

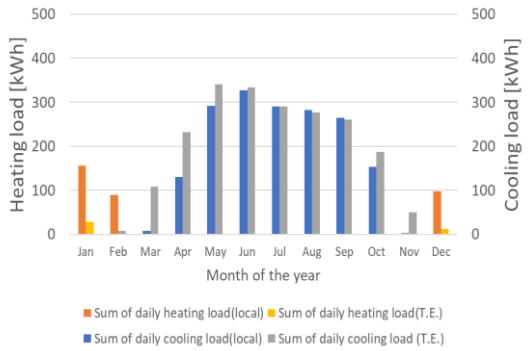

(a) New Delhi

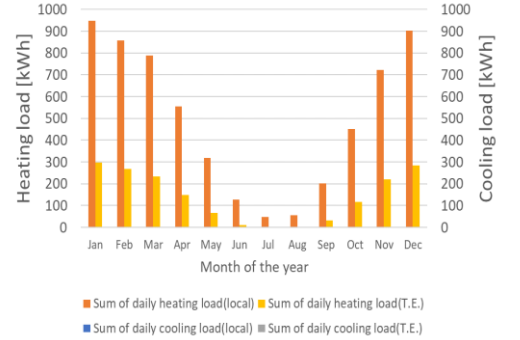

(b) Swansea

Figure 4.3: Monthly cooling and heating loads for TE and local buildings in Tunis, Volgograd, New Delhi, and Swansea.

Likewise, the heating load is the energy that must be added to the building zone to maintain a specified zone condition [135,139]. For Tunis, there is an appreciable reduction in the overall heating load during the winter months by up to 150 kWh per month with the adoption of a TE compared to a building built using local materials. However, during early summer (May – June), the TE building produces an increased energy demand, with cooling required earlier in the year, Figure 4.3(a). For Volgograd, the TE building has a significantly lower energy demand during the Autumn and Winter months, with a peak disparity in energy being around 1400 kWh in January. Only during August is the cooling demand higher for the TE building, Figure 4.3(b). For New Delhi, the building made with local materials provides the lowest cooling energy demands during the long summer months, but the TE building provides a consistently reduced heating load during the short winter, Figure 4.3(c). The reduction in

energy demand for the TE building is evident in the UK climate, where there is a consistent reduction in energy demand across the year, Figure 4.3(d). The relatively cool winter and warm summer mean only heating is required, with no cooling required during the summer months.

4.3.2 Annual cooling and heating consumption

The benefit of adopting thermally efficient building materials and additional solar energy capture devices is most commonly evaluated over an annual cycle such that any carbon saving can be established, and a likely payback period for adopting the technology can be calculated. Figure 4.4 shows the total annual net heating consumption, Figure 4.4 (a) and cooling energy consumption, Figure 4.4 (b), for a local, a TE building and a TE building fitted with solar capture device and cooling machine. Solar energy capture provides a net benefit in all instances, particularly where cooling is required in hot climates. For Tunis, there is a reduction of 77% in the cooling energy consumed over the year, from 667 kWh to 151 kWh.

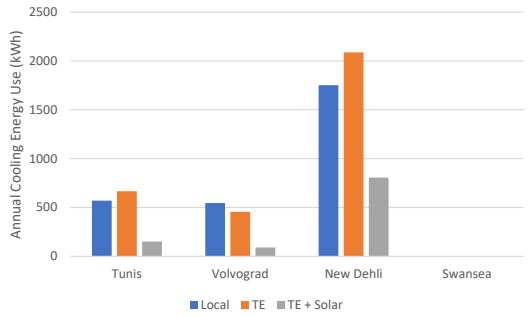

(a) Cooling

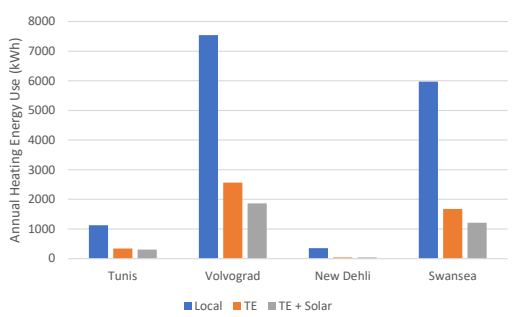

(b) Heating

Figure 4.4: Total annual cooling and heating loads for TE and local buildings for Tunis, Volgograd, New Delhi, and Swansea.

In New Delhi, installing a cooling system reduces the net energy required by building by over 60%, from around 2000 kWh to around 800 kWh. There is also a cooling energy consumption reduction in Volgograd from around 450 kWh to 90 kWh. As expected, building insulation is the primary factor dictating the heating energy consumption during colder winters. This is further reduced by around 28% through the use of solar capture for heating.

4.3.3 Economic and environmental impact analysis

The benefit of adopting a TE building design must be proven economically as well as thermodynamically. This sets the limits of the purely economic installation cost of the TE

building as part of NZEB Stage 1, as well as any further solar-related technology NZEB Stage 2. Local variations in the unit cost of energy play a key role in determining this economic merit. The financial benefit can be calculated using local financial energy pricing, Table 4.5. Likewise, regional variations in the CO_2 emission factors affect the environmental footprint of the building. The operational CO_2 savings can be calculated using the latest published CO_2 emission factors for the climatic locations in Table 4.6.

Table 4.5: Currency exchange rate and local energy costs at each location.

Climatic location	Local currency rate /$ ([249])	Electricity Price $/kWh ([250])	Gas Price $/ kWh ([251,252])
Tunis, Tunisia	3.1	0.067	0.029
New Delhi, India	76.7	0.073	0.057
Volgograd, Russia	82.2	0.630	0.007
Swansea, UK	0.81	0.464	0.167

Table 4.6: Local carbon dioxide emissions factors at each location.

Climatic location	Electricity Emissions $kgCO_2e$/ kWh ([253])	Natural Gas Emissions $kgCO_2e$ / kWh ([253])
Tunis, Tunisia	0.348	0.468
New Delhi, India	0.661	0.951
Volgograd, Russia	0.294	0.476
Swansea, UK	0.187	0.38

Assuming that heating is provided by gas and any cooling is supplied by electricity. An analysis of the total costs and subsequent savings from adopting a TE can be made, Figure 4.5. Although the total power demands are higher in countries with extreme temperatures, this only sometimes translates to economic operational cost, Figure 4.5. The annual cost benefit from adopting a TE design only benefits the building heating for all climatic locations. Although Volgograd has the most elevated building heating due to lower gas prices, the annual heating cost benefit from adopting a TE design is $35 compared to Swansea's $717, Figure 4.5.

(a) Operational cost	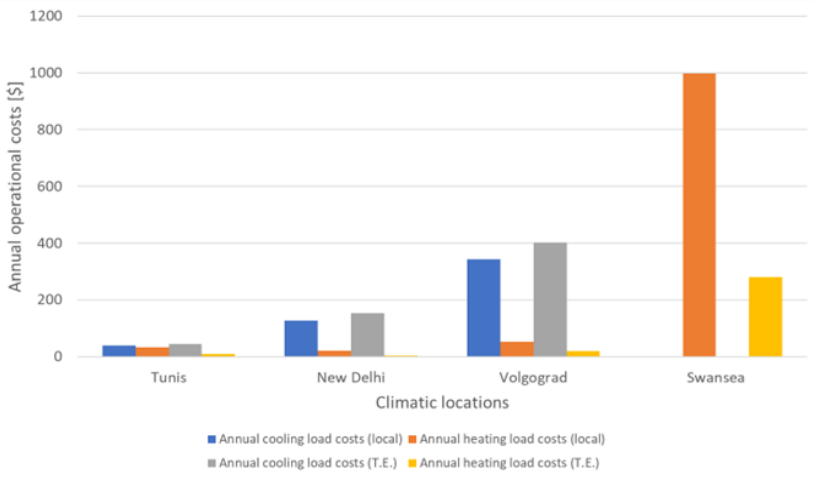
(b) Cost-saving	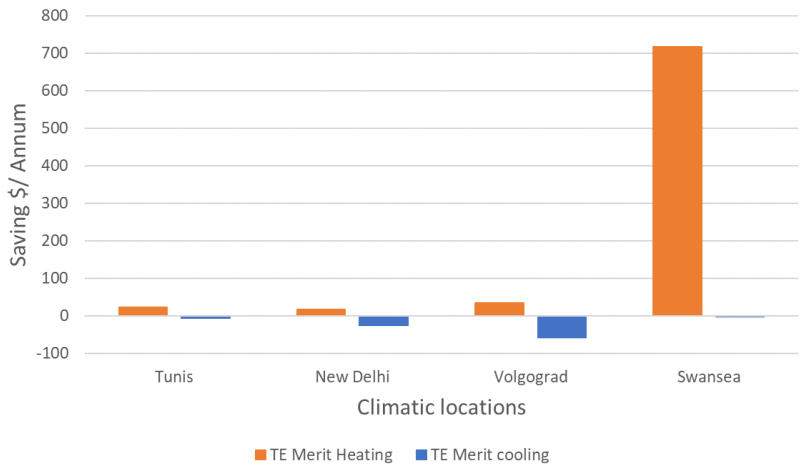

Figure 4.5: Operational cost (a) and cost saving (b) of the annual cooling and heating loads for Tunis, Volgograd, New Delhi, and Swansea.

The reduction in yearly operational costs reflects the local energy costs. An analysis of the total building operational CO_2 savings and subsequent savings from adopting a T.E. building can be made in Figure 4.6. There are annual CO_2 savings from adopting a T.E. design for heating energy for Volgograd and Swansea, at 2405 $kgCO_2$ and 1631 $kgCO_2$, respectively. In contrast, the yearly CO_2 savings from adopting a T.E. design for Tunis and New Delhi are less than 400 $kgCO_2$, Figure 4.6. Volgograd annual total building operational CO_2 emission and savings are higher than Swansea's because the emissions factor is higher for electricity and natural gas, Figure 4.6. Tunis records higher operational savings because of the higher heating energy demand for the local and T.E. buildings than New Delhi. However, Tunis has less carbon emission impact factor than New Delhi, and there are no cooling energy CO_2 savings for the

four climatic locations. The reduction in annual operational CO_2 savings reflects the local CO_2 impact factor.

(a) Operational CO_2 emissions	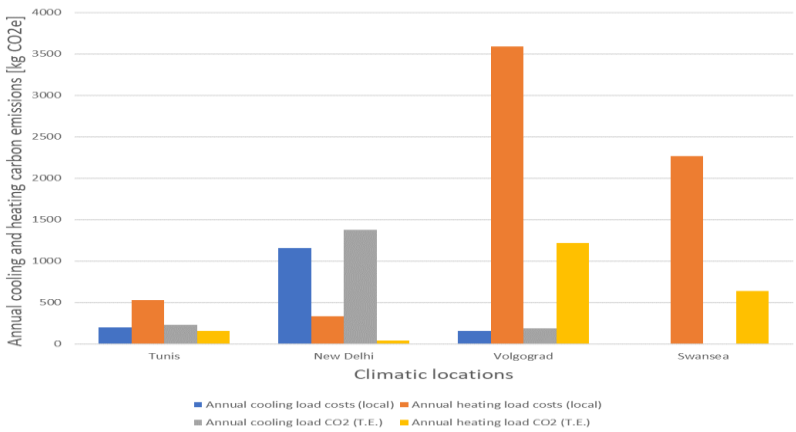
(b) CO_2 Saving	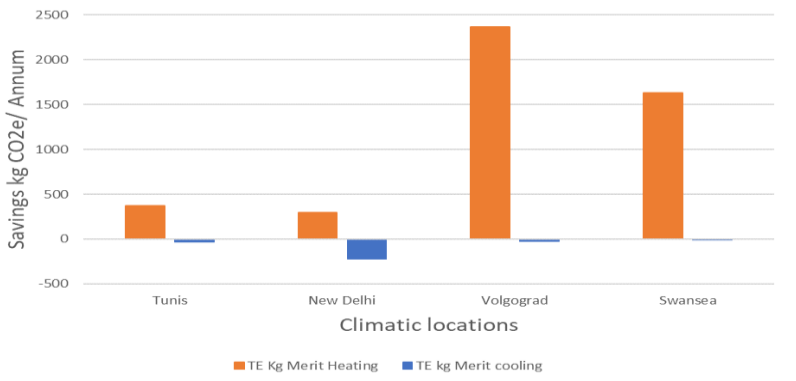

Figure 4.6: Operational CO_2 of the annual cooling and heating loads for Tunis, Volgograd, New Delhi, and Swansea.

4.3.4 Large building

The annual cooling and heating loads per unit surface area for the large and small TE and 'local' buildings for the four climatic regions are shown in Figure 4.7. For all climatic regions and both TE and 'local' buildings, the large buildings deliver a higher annual heating load per unit surface area than the small buildings, while the yearly cooling load per unit surface area for the large building is smaller than the small building. Also, the large TE buildings have less annual cooling and heating loads per unit surface area than the local buildings for all climatic regions. The small local buildings have higher yearly cooling and heating load per unit surface area than the small TE buildings for all climatic regions except for New Delhi, where there is

no change at 19 kWh/ m^2. However, there are differences between the cooling and heating load per unit surface area for the New Delhi small TE and local buildings.

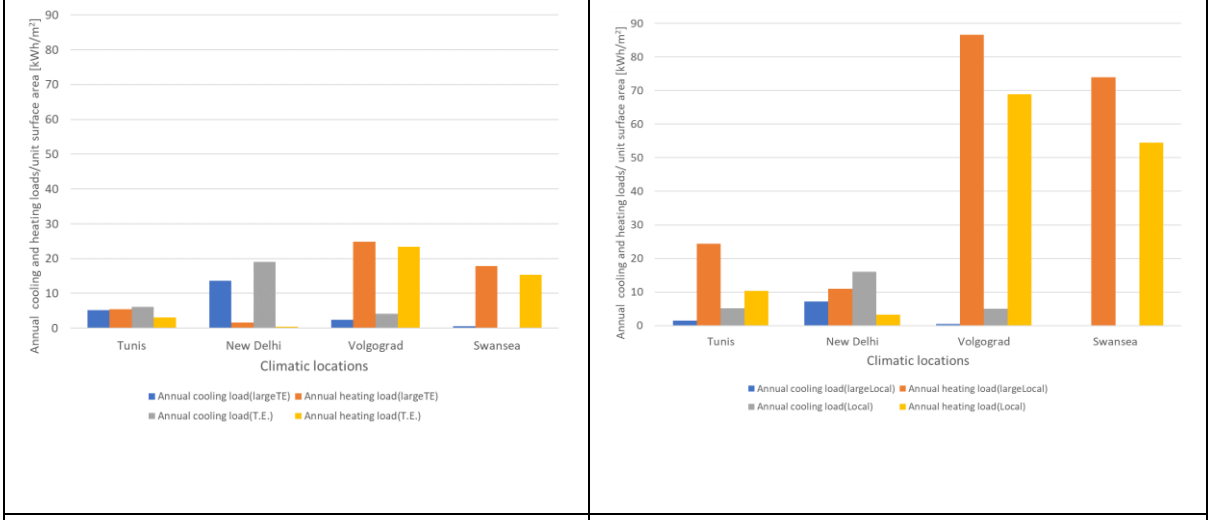

(a) TE building

(b) Local building

Figure 4.7: Annual cooling and heating loads/ surface area for large and small TE and 'local' buildings in Tunis, Volgograd, New Delhi, and Swansea.

Analysis of the monthly cooling and heating loads for the large and small TE and 'local' buildings show the large differences in the building heating loads per unit surface area for all climatic regions, Figure 4.8. For Tunis, the large local building heating load per unit surface area doubles most of the months than that of the small local building, Figure 4.8 (a & b). However, the Tunis TE large and small building heating load per unit surface area remains unchanged except in March and November. For Volgograd, there is only change of 2 kWh/ unit surface area between the large and small TE building heating load, while there is 18 kWh/ unit surface area difference between the large and small local building heating load, Figure 4.8 (c & d). Similarly, for New Delhi, the difference between the large and small 'local' building heating loads is 7 kWh/ unit surface area, and between large and small TE building heating loads is 1 kWh/ unit surface area, Figure 4.8 (e & f).

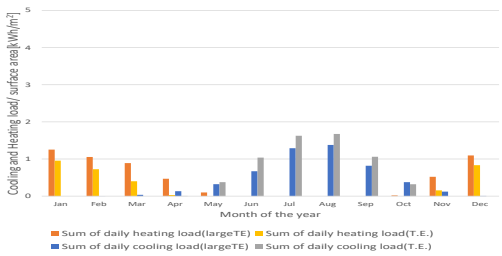

(a) Tunis – TE building

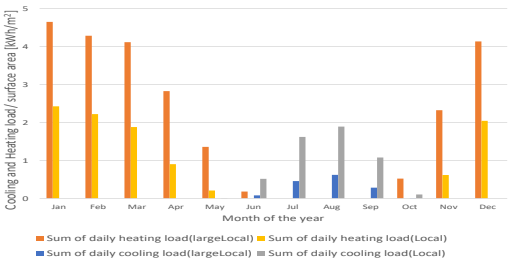

(b) Tunis – Local building

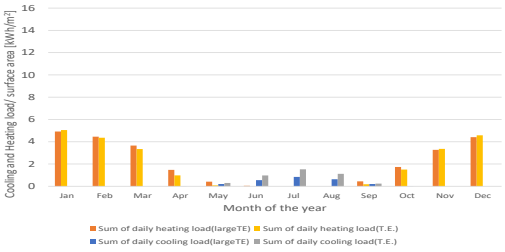

(c) Volgograd – TE building

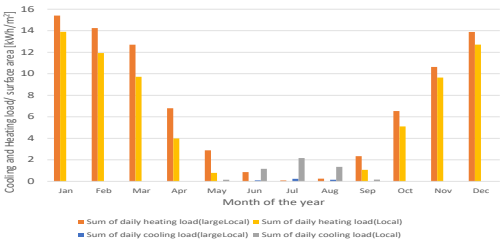

(d) Volgograd – Local building

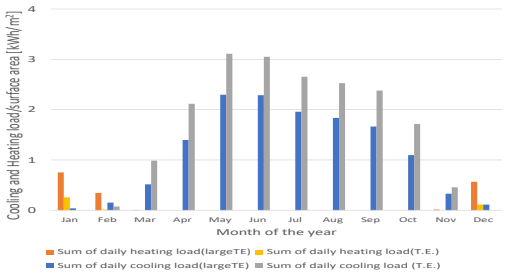

(e) New Delhi – TE building

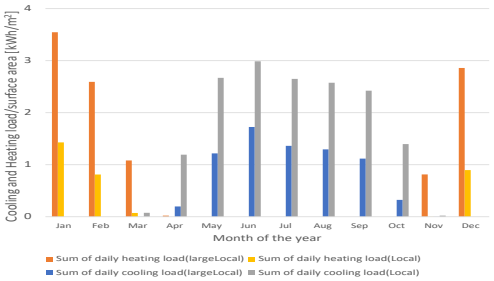

(f) New Delhi – Local building

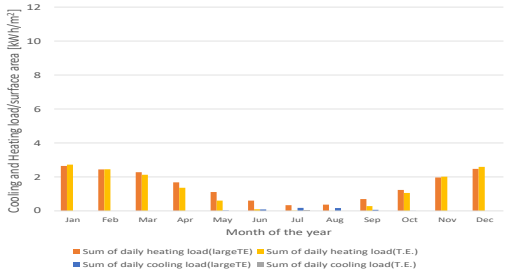

(g) Swansea – TE building

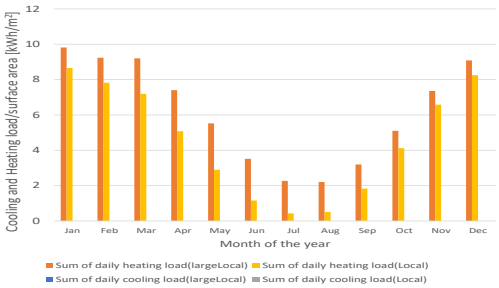

(h) Swansea – Local building

Figure 4.8: Cooling and heating loads/ surface area for large and small TE and 'local' buildings in Tunis, Volgograd, New Delhi, and Swansea.

For Swansea, the difference between the large and small ‘local’ building heating loads is 20 kWh/ unit surface area, and between large and small TE building heating loads is 3 kWh/ unit surface area, Figure 4.8 (g & h).

The results indicate that as the building surface area increases for all large buildings, the cooling load per unit surface area tends to reduce while the heating load per unit surface area increases. Heat transfer in building physics is the cause of this phenomenon. With a large surface area, the cooling load per unit surface area reduces because there is more opportunity for heat transfer between the building envelope surface area and the surrounding environment through heat transfer mechanisms like conduction, convection, and radiation. There is more cooling load per unit surface area reduction for the local building than the TE buildings because, at constant solar radiation and infiltration, well-insulated walls in the TE buildings reduce the heat gain from solar radiation and infiltration and minimise the heat loss via conduction, convection, and radiation to the surrounding environment.

The heating load per unit surface area increases because the larger building surface area exposes a larger building envelope surface area to cold outdoor temperatures, causing more heat loss to the surrounding environment via infiltration, conduction, and radiation. As a result, a higher heating load per unit surface area is recorded because additional energy input is needed to maintain the 20 ℃ room temperature. Like the cooling load, at constant solar radiation and infiltration, the well-insulated walls in the TE building minimise the heat loss through the building envelope via conduction and radiation compared to the local buildings.

4.4 Discussion

Under the current climatic conditions, there is merit in utilising solar thermal collectors coupled with an absorption cooling machine for building cooling and heating. For the simple unit building, it is possible to meet the net daily cooling demand in hotter climates purely by using solar thermal collectors and an absorption cooling machine. Sufficient cooling can be obtained by utilising 60% (Tunis) and 90% (New Delhi) of the roofing space for solar collectors. Thus, there is sufficient scientific merit for a real-world feasibility study of the technology to evaluate the impact of practical issues and thermodynamic losses.

The cost analysis has identified minimal direct operational economic benefit in hot climates from installing improved insulation, consistent with the common practice. The economic case for a solar-driven absorption cooling machine for this installation size is that it will save less

than $200 per annum compared to a conventional system using an electrically-driven equivalent. This saving is derived from local fuel costs, which sometimes, through subsidy, may make the less mature solar thermal systems unattractive compared to conventional photovoltaic (PV) – HVAC systems. This economic consideration is simplistic and ignores several factors. Longer-term sustainability issues such as recycling PV panels at the end of life [254,255] and significant leakage of greenhouse gas refrigerants [256,257] need to be examined. The capital cost of installation at scale is likely to be lower since the key components of a solar-driven system will likely have a lower cost. Being gravity-driven, the solar thermally powered absorption cooling system has few moving parts, and maintenance costs will probably be lower over the lifetime. If energy storage is also examined, the energy storage in an insulated vessel compares favourably with technology such as Lithium-ion batteries from economic and sustainability perspectives. Assessing the system's wider economic and environmental life cycle is a worthy exercise.

The investigation has focussed on a relatively simple unit building, likely different from typical buildings in each climate. Further work should address representative designs with defined building materials and geometries in each location. For example, as the building grows into a larger dwelling, the surface area to volume ratio of the building will reduce with a net decrease in the energy lost per unit volume of the building, but this would be countered by the building's limited roof space footprint, restricting the energy capture opportunity. Further building design investigations could include modification of the building design specification such as the dwelling type, size, occupancy, building envelope material thermal characteristics, building techniques, geometry, climatic zone, and thermal comfort level. A refined model would also need to address the electrical power required for pumps and consider the transient impact of energy capture technology.

A limitation of the heat transfer analysis is that the building surface area assumes equal heat transfer across the building envelope surface area when there will be differences, for example, between the ground and the building floor and differences in the solar gain between the building roof and the walls.

The IEA’s projection of the global energy sector reaching NetZero by 2050 requires minimising energy demand growth through improvements in energy efficiency. It is most prominent in curbing energy demand and emissions by 2030 [258]. This research confirms that building energy efficiency measures yield financial savings depending on local fuel costs and

reduce energy use and emissions. Governments and regulatory agencies could use this research to promote energy-efficient and environmentally friendly building materials and highlight the practical implications of local economic and regulation factors.

4.5 Conclusions

In order to evaluate the energy and economic benefits of adopting NZEB, TRNSYS simulation software was used to determine the cooling and heating demand of a TE building in four climatically varying locations. It has evaluated the energy benefits of a thermally efficient building with lower U values than those locations, with reductions in heating demand by a factor of 3 in colder climates. Increases in cooling demand were observed with the more thermally efficient building materials. Utilising solar-sourced heating and cooling significantly reduces consumption, and hence CO_2, in hot climates and reduces the heating demand during colder periods. The direct financial benefits are more difficult to justify due to the low cost of conventional fuel in some locations.

Chapter 5 : Solar collector heat energy production and storage

5.1 Introduction

Chapter Four discussed calculating standard and local buildings' heating and cooling loads. This Chapter presents the results of the solar power captured by an external concentrating parabolic solar collector (XCPC) in four climatically varying locations in Tunis, Volgograd, New Delhi, and Swansea. The solar collector and storage design are presented in section 5.2, and how TRNSYS is used to calculate the available solar power is presented in section 5.3. The energy performance results are described in section 5.4, followed by a discussion of the results (section 5.5) and the conclusion (section 5.6).

5.2 Materials and Methods

5.2.1 Solar collector and storage system design

Solar thermal collectors convert solar radiation into heat energy and transfer the heat through a fluid in the collector for intended use, such as space heating, hot water service, and space conditioning equipment [60]. The Type 1245 XCPC component is selected as the heat source for the solar-powered DACS system in the TRNSYS software. The XCPC solar collector consists of glass evacuated tubes, manifolds of copper heat pipes, copper u-tube and aluminium heat spreading fins, concentrating collector reflector, aluminium frame, and rock wool insulation [65]. The XCPC solar collector is selected because it has high optical efficiency of around 0.62 and thermal efficiency of about 0.50 at 200 °C [64,67,222,223] and meets the solar-powered DACS's operating temperature range of 135-230 °C [51,68].

The XCPC was primarily selected to meet the temperature requirement of the solar-powered DACS. Nonetheless, the XCPC can generate energy for low-temperature applications such as space heating and domestic hot water service. The stationary XCPC has an east-west (E-W) orientation, i.e., the absorber is situated horizontally, and the optics are designed to accept the seasonal swing of sunlight. The E-W orientation produces higher solar concentration with improved performance at a higher operating temperature [67,223].

The collector efficiency is the ratio of the useful thermal power generated to the available solar power. The parameters of the XCPC are taken from the Artic Solar Limited supplier and are

summarised in the Table 5.1. Widyolar et al. [67] define the useful thermal power from the XCPC can be calculated from:

$$\eta = \frac{Q_{thermal}}{Q_{solar}} \quad 5.1$$

and

$$Q_{solar} = A_{absorber} C_x G \quad 5.2$$

where Q_{solar} is the available solar power (W), $A_{absorber}$, is the area of the absorber of the XCPC (m^2), C_x, is the concentration ratio, and G is the global solar radiation (W/m^2). Also, the effective concentration ratio is the ratio of the collector aperture area, $A_{aperture}$, to the absorbing surface area as follows [67]:

$$C_x = \frac{A_{aperture}}{A_{absorber}} \quad 5.3$$

Artic Solar's XCPC solar collector [66] is used to model solar thermal power. A schematic of the XCPC solar is shown in Figure 5.1, summarising the specification in Table 5.1.

Table 5.1: Artic solar XCPC solar collector specification [66].

Parameter	**Value**
configuration	East-west
aperture area	2.41 m^2
length	2208 mm
width	1220.63 mm
height	295 mm
weight (dry)	37.29 kg
weight (wet)	39.29 kg
fluid volume	2 litres
concentration ratio	1.49X
Outside diameter of the absorber riser tube	8 mm
The thickness of the absorber riser tube	0.75 mm
Absorber Fin Thickness	0.12 mm
Absorber area	1.51 m^2
Flow Pattern	A single U-bend flow tube
Number of risers	3 per collector
Recommended Flow Rate	3.29 litre/minute

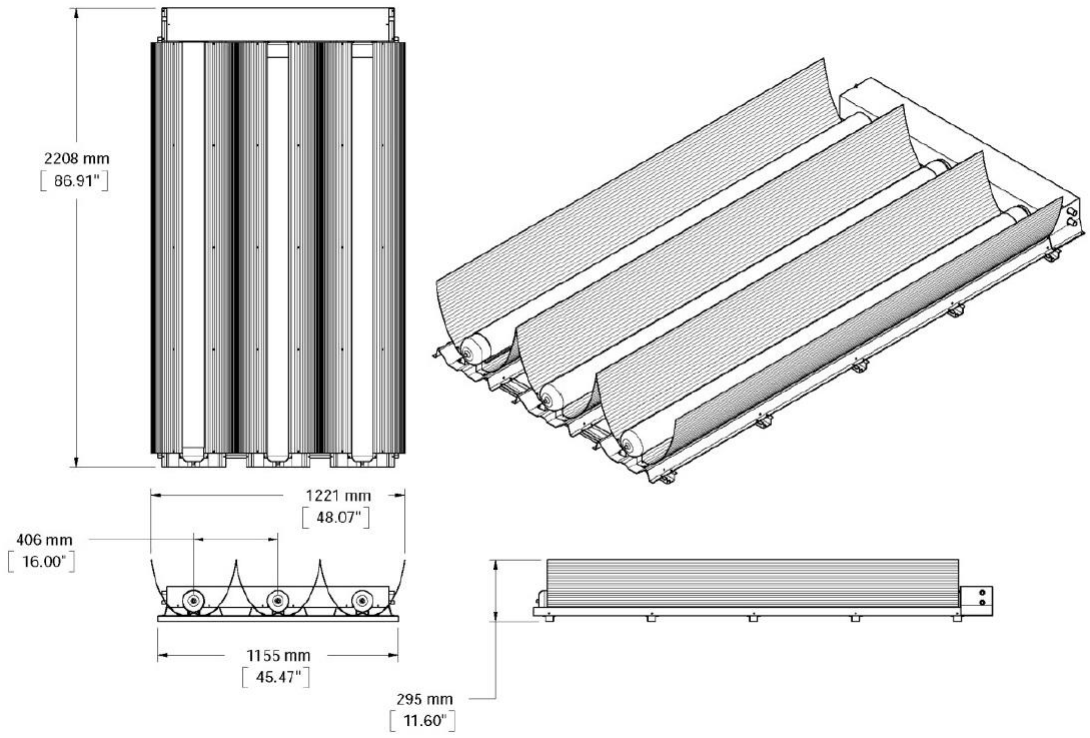

Figure 5.1: Schematic of an XCPC medium-temperature collector (from Artic Solar [66]).

The primary purpose of storage in solar heating and cooling systems is to overcome the mismatch between solar gains and heating and cooling loads [37,55,57]. For thermal energy systems, solar energy is generally stored as liquids, solids, or PCM [57]. Water is the most frequently used storage medium for liquid systems, even though other heat transfer fluids such as oil and water-glycol mixtures may be used. Additionally, the most common application of liquid system thermal storage is the integration of a hot water tank in the heating cycle of heating and cooling systems [53,55,57]. Water tank material includes copper, galvanised metal or concrete tanks, and the typical storage size is about 40-80 litres per square meter of solar collector area [57].

This solar design incorporates a hot water storage tank to store excess heat to be made available when the solar heat from the collector is not sufficient. Nonetheless, in some solar thermally powered cooling systems, such as absorption or adsorption chillers, excess cooling power from the solar-powered cooling systems can be stored in a cold storage unit [37,55]. This Chapter focuses on hot water storage tanks because the emphasis is on the power generated from the solar collector system and how solar heat can be used to meet building heating loads or the heating cycle of a thermally driven cooling system.

5.2.2 TRNSYS simulation model

The total area of a solar collector array depends on the cost, available roof space, and the thermal load to be met by the solar power system. The building roof space area is 24.75 m^2. Sixty per cent of the building roof space is expected to be covered with solar collectors so that the remainder can accommodate other system components such as storage tanks, pipes, pumps and chillers. Table 5.2 lists the parameters of the building and the solar, cooling and heating equipment used for calculating the available solar power and other energy performance calculations. The building roof space fill factor, in Table 5.2, is assumed to be 0.6, which is expressed as a fraction (1 being the total roof area). It is equivalent to 60% of the building's flat roof area being covered by solar thermal collectors.

Artic Solar [66] data indicate the thermal efficiency of the XCPC solar collector when the mean temperature above ambient is 0-200 °C is between 60 - 74 %. As a result, 70 % solar collector thermal efficiency is selected for the solar and storage design. TRNSYS software calculates the global solar irradiance in Watts per square meter. Then, Equation 5.2 is used to calculate the available solar power. The heating power generated from the global solar irradiance is thus calculated using Equation 5.1. In contrast, the available cooling power from the cooling engine is calculated by multiplying the heating power calculated from Equation 5.1 by the cooling engine's COP.

Table 5.2: Artic solar XCPC solar collector specification

Parameter	**Value**
Length of the building roof	5.5 m
Width of the building roof	4.5 m
Building roof space fill factor	0.6
Building available roof area	14.85 m^2
CoP of solar-powered DACS	0.2
The efficiency of the XCPC solar collector	0.7
Room temperature setpoint (cooling)	24 °C
Room temperature setpoint (heating)	20 °C

The heating and cooling loads were calculated for the standard building in Chapter 4. The TRNSYS results are exported to spreadsheets for post-modelling analysis. Below are the fundamental questions solar and storage design would attempt to answer:

1. Can the dwelling's heating and cooling needs be met using Artic Solar's XCPC solar collector?
2. What solar array and storage sizes would be required to achieve question 1?
3. How significant are the heating and cooling power deficits if it is impossible?
4. How can any power deficit be met?

The assumptions used in the modelling of the solar and storage system design are described as follows:

- The modelling focuses only on thermal energy analysis. Thus, any energy captured and stored is useful irrespective of the temperature. Also, the energy captured can be a finite number of small independent stores that can be raised to a desired useful temperature.
- The XCPC solar capture is perfectly designed, aligned and oriented to capture the available solar energy.
- There are no heat losses in transfer pipes in the operating system.
- No pumps and parasitic energy are consumed in the operating system
- A hot water storage tank is used to store excess heat.

5.2.3 Solar energy capture

The potential for direct solar heat capture to provide heating and cooling was evaluated for the TE house, as this is the next logical step after building insulation. The building roof was taken as the location of eight solar capture units, covering from 0.2 to 0.9 of the available area with specifications shown in Table 5.3. An assumption of zero loss and zero transient time was made between the capture location and its use in the building. No diurnal energy storage was assumed such that the net energy capture was reset to zero at midnight at the start of each day. In some ways, this "zero storage" scenario is a worst-case scenario, as some day-to-day energy accumulation would be expected. However, this modelling approach negates any issues related to the heat storage method (sensible, phase change or thermochemical), heat store loss, and buffering transient responses which might arise. The energy captured was used for direct heating using water for heat transfer.

$$Q_{heat} = \eta A_{roof} f Q_{solar} \qquad 5.4$$

where η is solar capture efficiency, A_{roof} is the roof area (m^2), f is the fraction of the roof area covered by solar collectors, and Q_{solar} is the available solar power (W/m^2) from Equation 5.2.

Cooling was achieved using eight cooling machines proven for small-scale cooling [51,68]. The conversion from thermal energy input to cooling output for the cooling machine, effectively the COP, was taken from the literature [51] as 0.2 such that every 1 W/m^2 of solar input resulted in 0.2 W/m^2 of cooling.

$$Q_{cool} = \eta A_{roof} f \beta Q_{solar} \qquad 5.5$$

where β is the cooling system COP. The external concentrating solar collectors (XCPC) were used with a quoted thermal capture to solar irradiance efficiency of 0.7 under ideal conditions, resulting in a power rating of 1.235 KW peak for the 2.41 m^2 solar collector area [66]. These solar collectors can generate hot water at a maximum temperature of 300°C, which is compatible with the absorption cooling system [51]. During the analysis, it was assumed that the mass flow through the solar collectors could be varied such that the cooling engine operated within its range of effective COP of 0.2 [51] with a water supply between 190 - 205 °C. The cost savings produced by adopting direct solar heating and cooling can be calculated by the product of the energy deficit and the unit energy cost. For cooling, this energy comes from an electrical supply, while heating is assumed to come from gas.

Table 5.3: Solar heating and cooling simulation parameters.

Solar Capture parameter	Value
Cooling machine COP (β)	0.2
Energy capture efficiency (η)	0.7
Solar capture as fraction roof area (f)	0.6 fractional area unless otherwise stated (0.2 – 0.9 where varied)

5.3 Solar energy performance results

This section presents the solar energy and storage performance results for the four case study cities: Tunis, Volgograd, New Delhi, and Swansea. The following definitions are used in this section's presentation and analysis of solar energy performance.

- *Deficit days* are the number of days where insufficient energy could be harvested within 24 hours to meet a day's demand.
- *Days where required* – is the number of days where there was a need to control the building room temperature.
- *Lag days* are the number of days with some lag between demand and supply. This number usually equals the days when required, but not always.
- *Deficit hours* are when insufficient energy can be harvested within the hour to meet the hourly load.
- *Power deficit*– is the amount of wattage by which the building's thermal load is over the available solar energy in a given time (e.g. per hour, day, and year).

Figure 5.2 shows the typical year's total heating and cooling deficit hours for the four case study cities: Tunis, Volgograd, New Delhi, and Swansea. Swansea has the highest total heating deficit hours of 4024 hours, followed by Volgograd, Tunis and New Delhi at 3666 hours, 1925 hours, and 432 hours, respectively. In contrast, for cooling, New Delhi has the highest total cooling deficit hours of 4260 hours, followed by Tunis, Volgograd, and Swansea at 1397 hours, 1063 hours, and 0 hours, respectively.

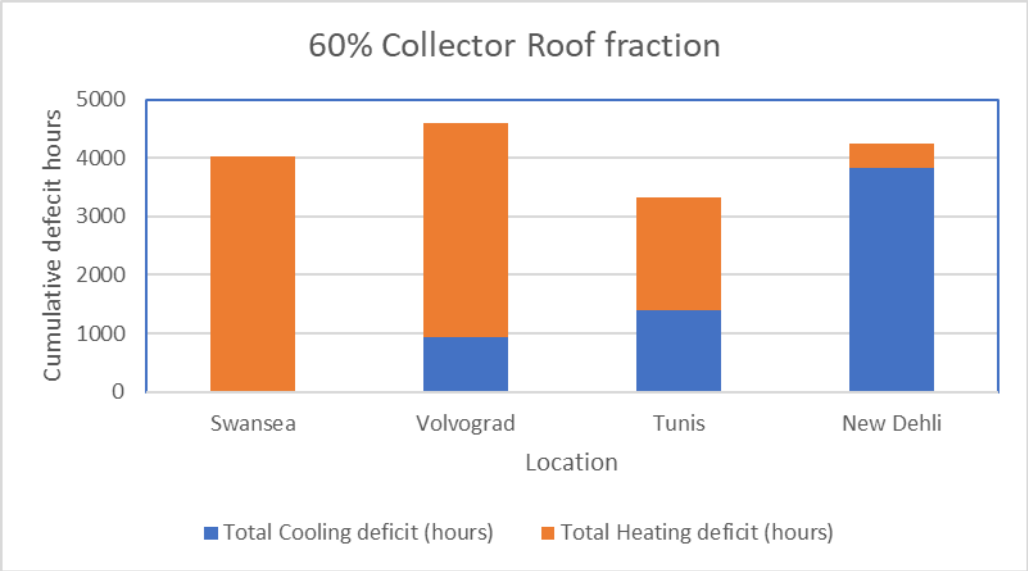

Figure 5.2: Cumulative deficit hours for Tunis, Volgograd, New Delhi, and Swansea.

Figure 5.3 illustrates the typical year's total heating and cooling power deficits for Tunis, Volgograd, New Delhi, and Swansea. Volgograd has the highest total heating power deficit of 1910 kW, followed by Swansea, Tunis and New Delhi at 1212 kW, 301 kW, and 42 kW, respectively. In contrast, for cooling, New Delhi has the highest total cooling power deficit of

945 kW, followed by Tunis, Volgograd, and Swansea at 140 kW, 120 kW, and 0 kW, respectively. Volgograd has more heating power deficit than Swansea, although its heating deficit hours are less than Swansea's.

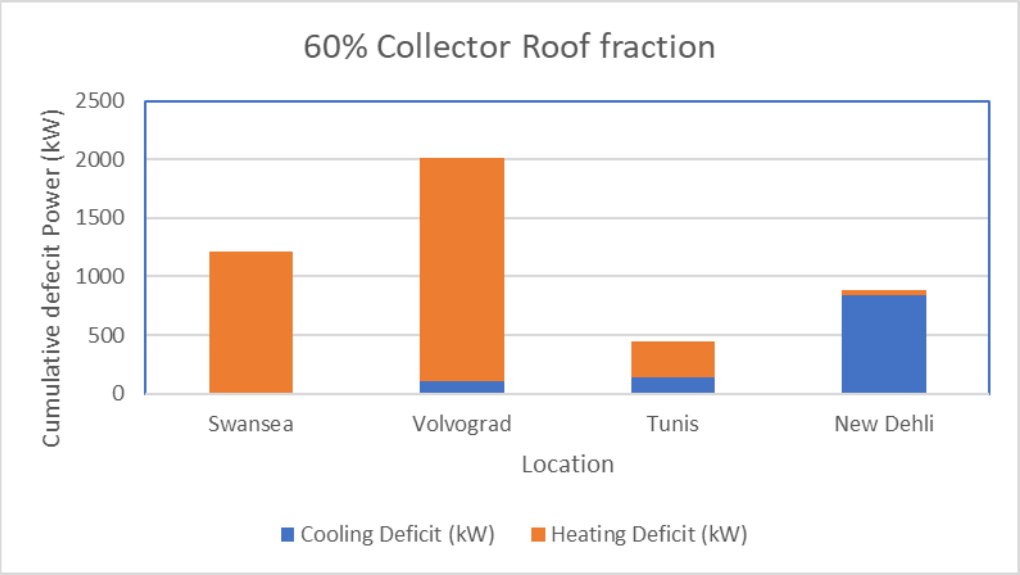

Figure 5.3: Cumulative power deficit for Tunis, Volgograd, New Delhi, and Swansea.

5.3.1 Supply by solar

With a TE building, the second stage of an NZEB can be modelled by adopting solar thermal technology. At a roof coverage of 0.6 fractional area of the solar collector, there is a number of days when there is a net deficit within the day, i.e., less energy is captured than is used, and the number of days where there exists some lag between the demand and the availability of supply, Figure 5.4.

For Tunis, there are no days when there is a net deficit in energy, but there are over 150 days when there is a lag in demand/supply. For Volgograd, there are around 240 days when there is some lag between the demand and supply and a further 70 days when the quantity of energy could be insufficient to heat the building. For Swansea, there are 291 days when there is a lag between the demand and supply and 76 days when there is insufficient energy from the solar supply to meet the heating demand. For New Delhi, cooling is required for 280 days of the year, with most days lag between when cooling is needed and when sufficient solar energy is available to drive the cooling machine. There is also a lag of around 50 days between the early morning heat demand and the availability of solar energy for heating.

Examination of the hourly cooling and heating loads during peak demand times can be useful to determine the root cause of the energy demand. It can also help to identify any storage capability that may be required and the timing of any diurnal lag. Two time periods, February 5-7 (winter) and July 22-24 (summer), were selected to study the hourly heating and cooling loads for the four climatic locations. The winter and summer comparison periods were chosen so that there were three consecutive days of recorded heating and cooling demand, respectively, for all four climatic locations.

Figure 5.5 shows the hourly heating and cooling load, solar power, and ambient temperature variation for Tunis, Volgograd, New Delhi, and Swansea for winter (5-7 February) and summer (22-24 July). The available solar energy for heating and cooling was calculated according to equations 2 and 3. In all instances, sufficient solar-derived power is available in the middle of the day to meet the heating and cooling demand. However, there are considerable differences in the behaviour outside the middle of the day.

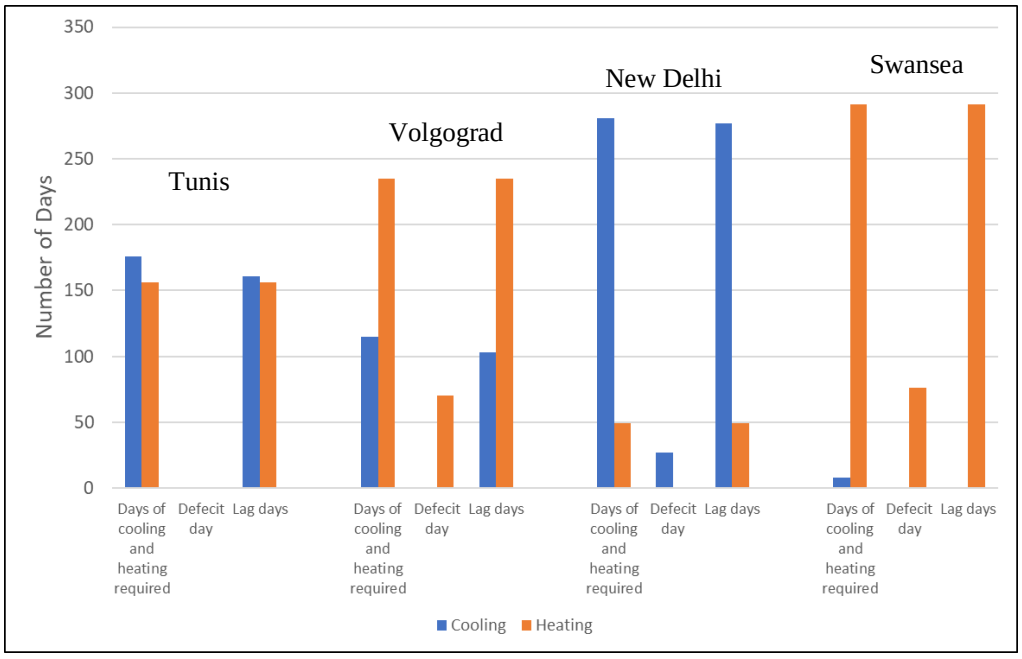

Figure 5.4: Analysis of the number of days with an energy deficit and at least an hour's lag between demand and supply (An area roof fraction of 0.6).

	Winter (5-7th February)	Summer (22-24th July)
Tunis	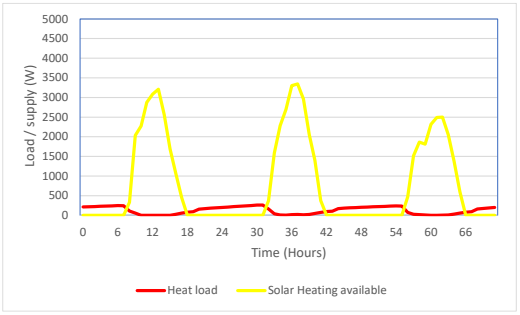 (a)	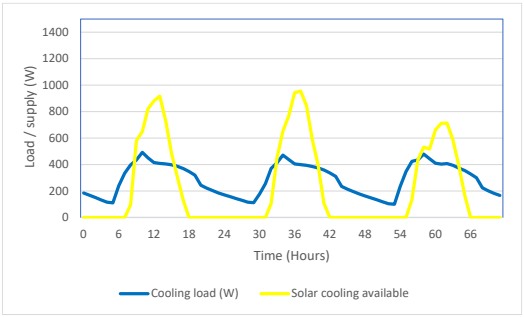 (b)
Volgograd	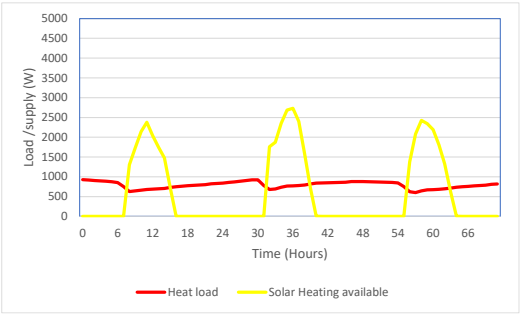 (c)	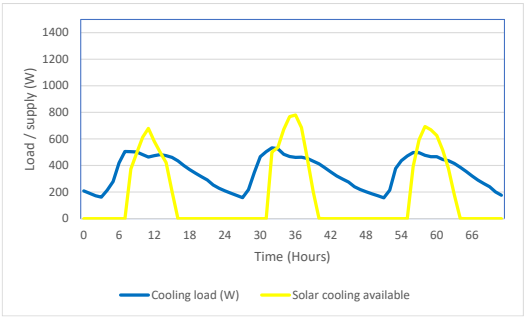 (d)
New Delhi	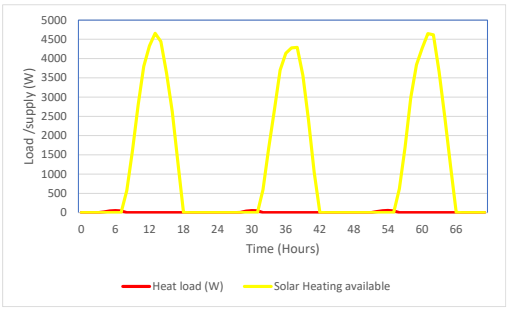 (e)	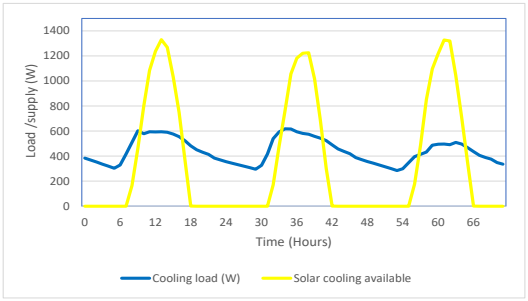 (f)
Swansea	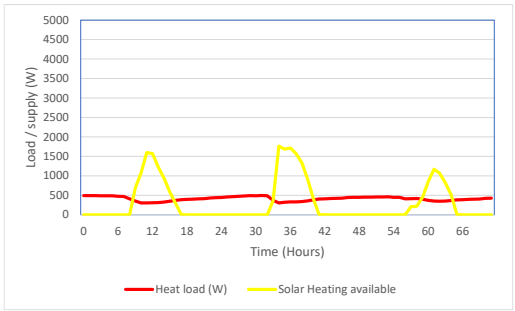 (g)	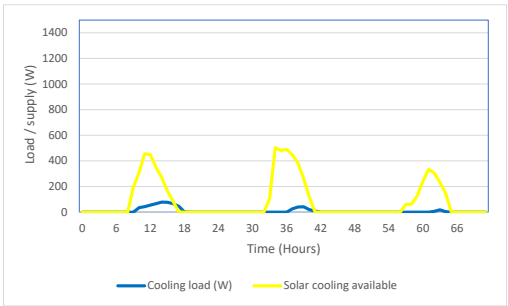 (h)

Figure 5.5: Hourly heating and cooling loads compared to solar availability for TE buildings in Tunis, Volgograd, New Delhi, and Swansea for winter (5-7 February) and summer (22-24 July).

During the winter in Tunis, there is a heating demand which cannot be met by the available solar heating from the early evening to around 6 a.m., Figure 5.5 (a). During summer, there is a continuous demand for cooling in the 200 – 400 W range, but solar can only provide this for around 12 hours a day, Figure 5.5 (b). For Volgograd, there is a more continuous winter heating demand of approximately 1000 W throughout the day and night, which can only be met by solar for around 8 hours daily, Figure 5.5 (c). A similar lack of supply is created during summer when the cooling demand exceeds the available solar supply for all but 4 hours around mid-day, Figure 5.5 (d). For New Delhi, there is minimal heat demand/supply lag of around 80 W in a winter morning while there is a continuous 400 – 600 W cooling demand, which is met by the solar supply for around 12 hours a day, Figure 5.5 (e & f). For Swansea, a continuous winter heating load of around 500 W is required, which is met by solar supply for approximately 5 hours around mid-day, while the summer cooling load is readily surpassed by the available solar-powered cooling machine supply, Figure 7 (g & h).

The primary cause of the temporal lag mismatch is cooling or heating at the start of each day as temperatures rise before sufficient solar energy is available to heat or cool the building. In heating and cooling, increasing the fraction of the roof covered by the roof area can, in some instances, reduce the number of deficit days, but it does not eradicate issues where demand is greater than the supply, Figure 5.6. For Tunis, the deficit days can be reduced to zero with 0.6 fractional roof space dedicated to solar collectors, Figure 5.6 (a). Zero deficit cooling days can be achieved for Volgograd with only 0.5 fractional roof space allocated to solar collectors. However, there are always over 40 days per year when the solar collectors will not meet the heating demand, irrespective of the size of the solar collector, Figure 5.6 (b).

This lag can be associated with the low local temperatures and the limited sunlight available during the coldest winter months. Extending the solar collector size to 0.95 fractional area of the available roof space eventually results in the entire year's cooling demand being met in New Delhi, but an area fraction of 0.25 means a cooling deficit for around half the year, Figure 5.6 (c). The challenge of meeting the heat demand in Swansea follows a similar pattern to Volgograd, with a plateau of about 40 days when there is insufficient energy captured to heat the building, irrespective of the area of the solar collectors, Figure 5.6 (d). The surplus cooling energy during summer would be best stored as a cooling liquid within the building to meet any daily temporal lag between supply and demand, e.g., late evening or early morning. Storing as a cooled liquid is less challenging than storing at temperatures > 190 °C; from a safety perspective, temperature differences (hence losses) are lower, and a more significant dynamic

response will be achieved. The sizing and design of the storage will be examined in a later chapter.

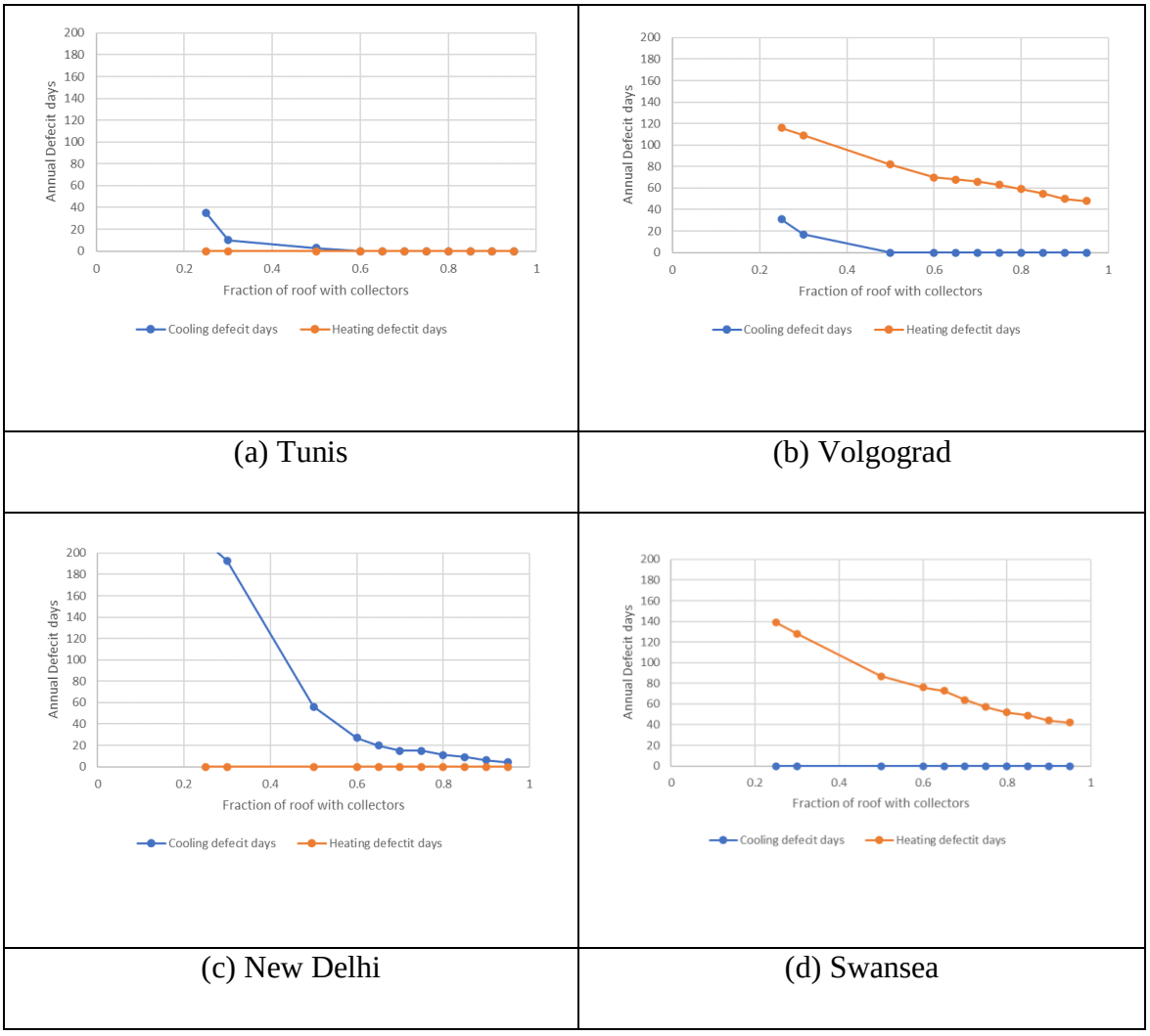

Figure 5.6: The impact of scaling the roof collector on the number of deficit days.

5.3.2 Deficit hours/day and Watt deficit/day

Figure 5.7 presents the deficit hours per day for the T.E. building in the four climatic zones in a typical meteorological year from Jan. 1 to Dec. 31. For Tunis, the heating deficit hours occur only in winter and spring, not summer because there is no heating load from May to October, Figure 5.7 (a). For Volgograd, the number of deficit hours for heating is more prominent in winter, and there are no deficit hours in summer from mid-May to early September, Figure 5.7 (b). For New Delhi, the heating deficit hours occur only in winter (December to February) when there is a recorded heating load in the building, Figure 5.7 (c).

For Swansea, as expected, the number of deficit hours for heating is more prominent in winter and less in summer because the building heating demand is higher in winter than in summer, Figure 5.7 (d). Figure 5.8 shows the power deficit per day for the four climatic locations. Tunis and New Delhi have no power deficits throughout the year due to the available solar power to meet the heating demand in 24 hours, Figure 5.8 (a & c). For Volgograd, of the 70 days where power deficits were recorded, 0.6 – 20 kWh would be required to meet the building heating demand from November to January, Figure 5.8 (c). For Swansea, of the 76 days where power deficits were recorded, 0.4 – 10 kWh would be required to meet the building heating demand from November to February, Figure 5.8 (d).

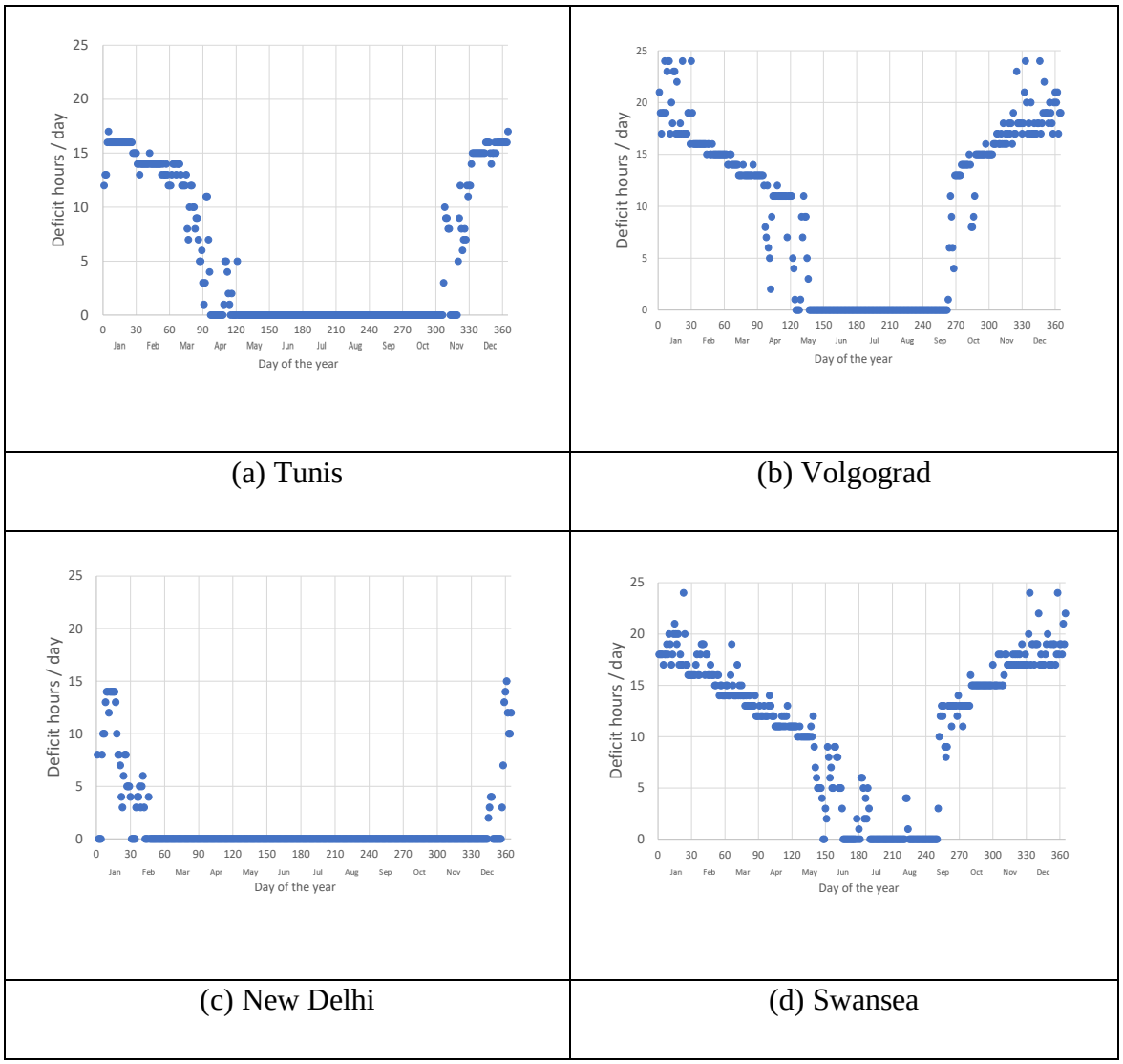

(a) Tunis

(b) Volgograd

(c) New Delhi

(d) Swansea

Figure 5.7: Deficit hours per day for heating over the year.

Figure 5.9 shows the peak heating demand time for the four climatic zones. Most of the peak heating deficit occurs in the evening, with the pronounced deficits occurring between 0 and 7

a.m. For Volgograd and Swansea, no cooling peak is shown because there are no cooling deficit days, as shown in Figure 5.4.

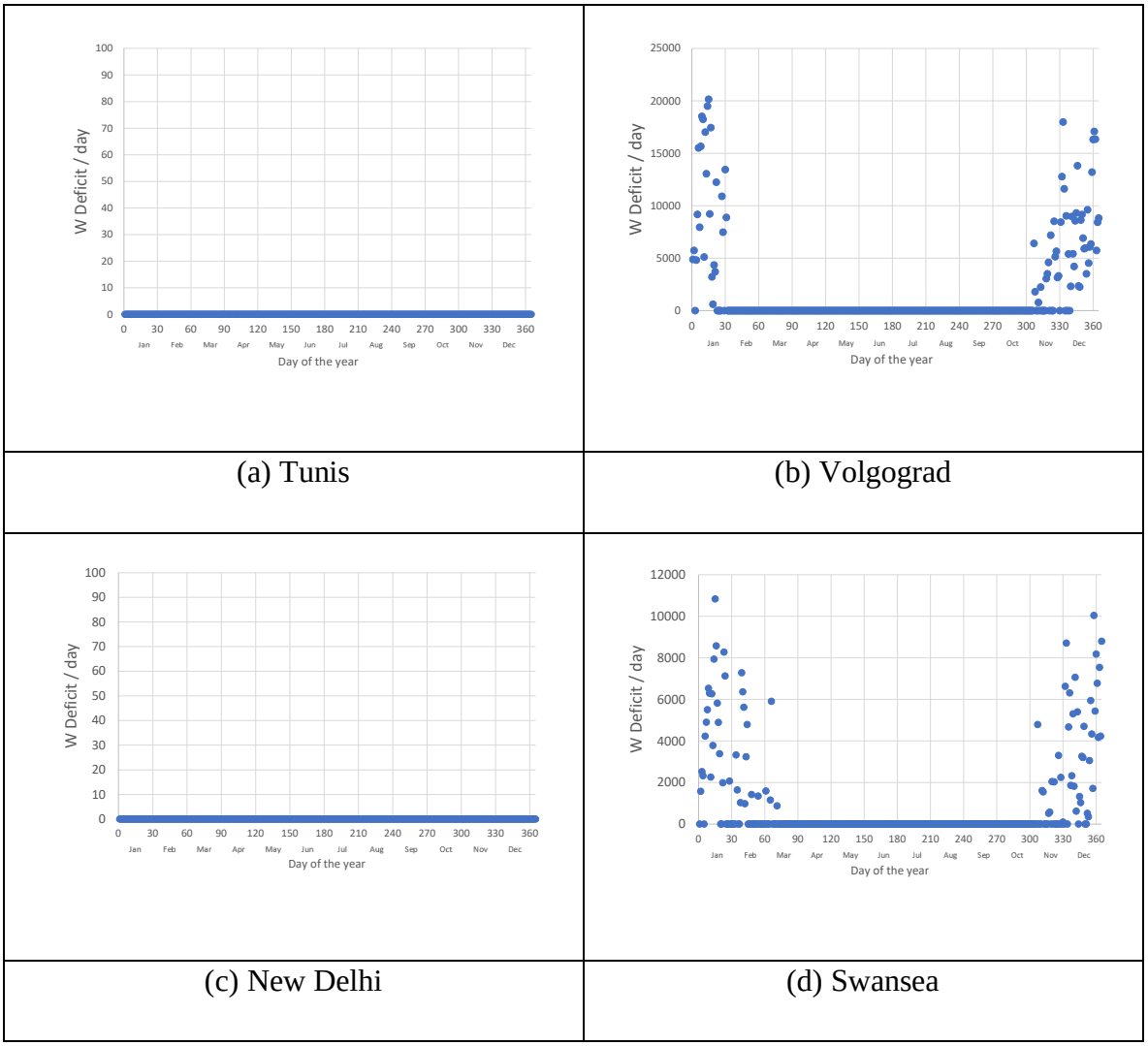

Figure 5.8: Power deficit per day over the year.

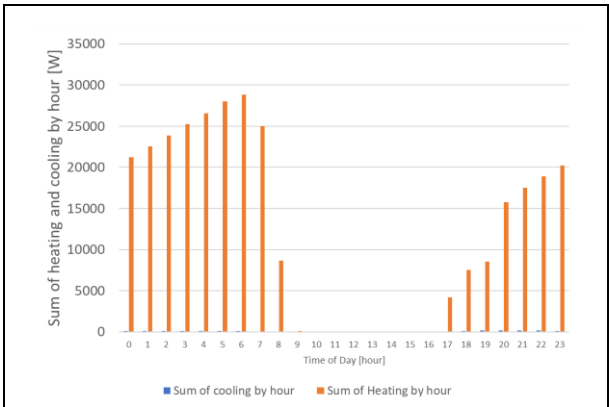

(a) Tunis

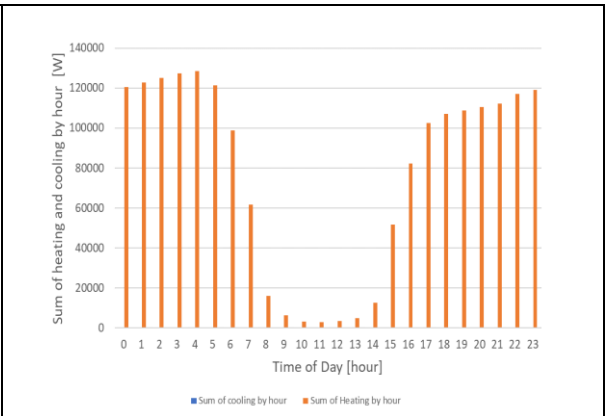

(b) Volgograd

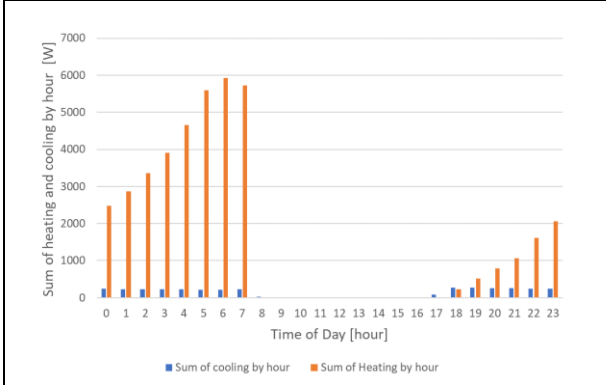

(c) New Delhi

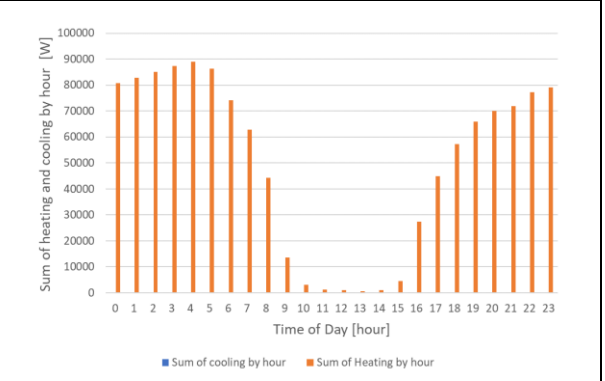

(d) Swansea

Figure 5.9: Hourly heating and cooling time of the day for the four climatic regions.

5.3.3 Energy from the hot thermal store

Figure 5.10 shows the cumulative energy captured in a perfectly insulated storage tank for the four climatic zones. For Tunis, the total annual heating load demand from the building is 339 kWh; 237757 times more stored solar energy is available than the heating demand, even under different modelling start dates of January and July, Figure 5.10 (a). For all climatic locations, the energy stored for the July modelling start date starts higher than the January start date because of the high solar irradiance levels providing the heat source to the storage medium. For Volgograd, the total annual heating load demand from the building is 2566 kWh.

Well over 22581 times more stored solar energy is available than the heating demand for the different modelling start dates of January and July, Figure 5.10 (b). New Delhi's total annual

heating load demand from the building is 42 kWh; thus, more stored solar energy is available than the heating load for the different modelling start dates of January and July, Figure 5.10 (c). Swansea's total annual heating load demand from the standard building is 1677 kWh, approximately four times more stored solar energy available than the heating demand, even under different modelling start dates of January and July, Figure 5.10 (d).

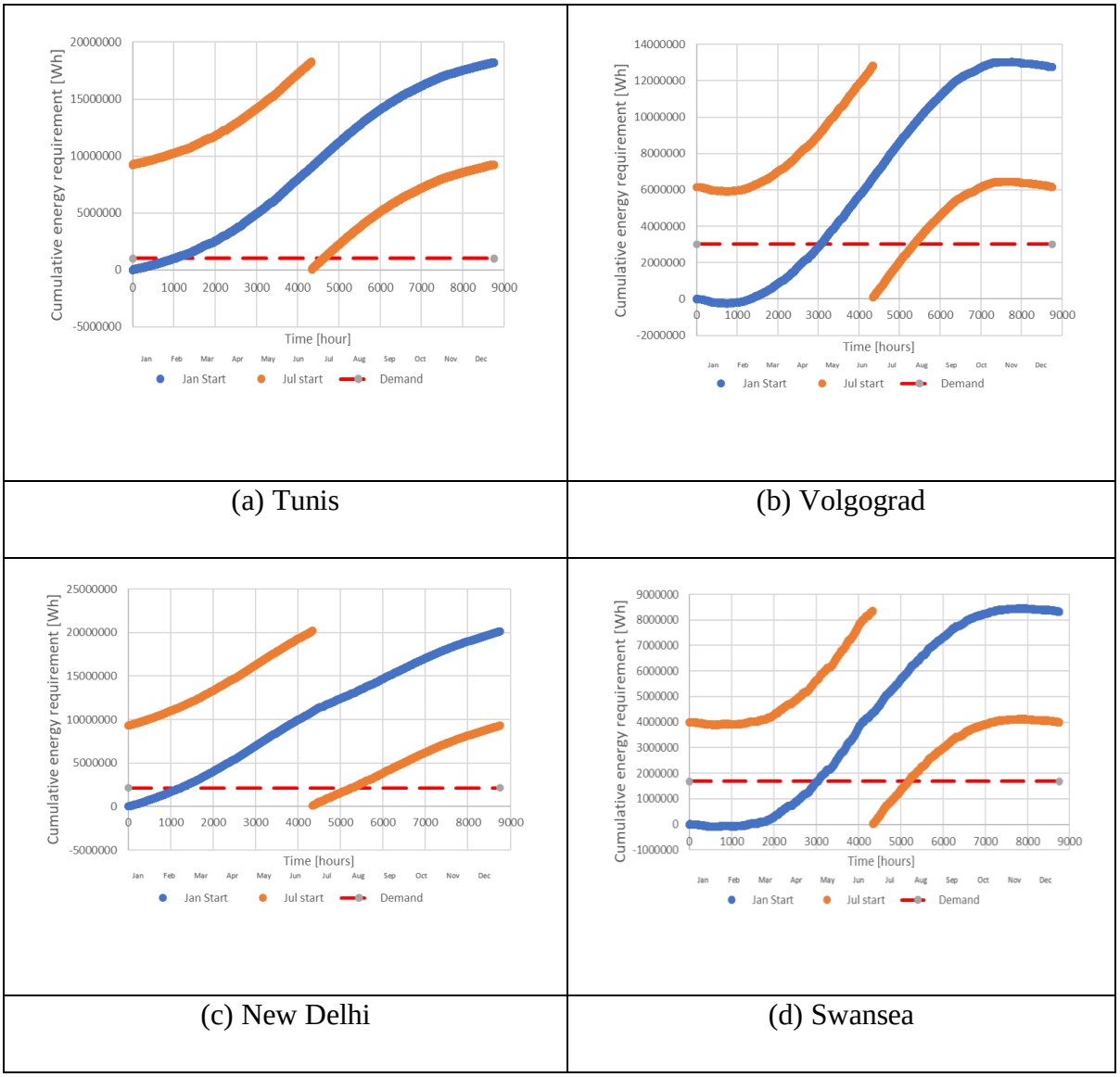

Figure 5.10: Cumulative heat energy available for a perfect thermal energy store over the year.

5.4 Discussion

TRNSYS modelling software has been used to model the heat production from a solar and storage design that meets a standard building's cooling and heating loads for Tunis, Volgograd, New Delhi, and Swansea climates. The solar collector and storage system design includes the

type and sizing of an XCPC solar collector, water as the heat transfer fluid, and a water-based thermal store. The performance analysis was based on the heat energy production of the solar collector and storage design.

The results showed that TRNSYS software could calculate the heat energy generation of XCPC solar collectors. Theoretical models presented by Widyolar et al. [67] allowed the calculation of the XCPC solar collector's thermal energy outputs from the TRNSYS-modelled solar irradiance for the local climate. In any case, the design approach was to investigate how well the heat energy produced by the solar collector can be used to meet the standard building's heating and cooling loads. The main emphasis has been on meeting the building's heating demand, even though some comparable results for cooling are presented. This is because the energy analysis that does not consider the equivalent temperature will be more relevant for heating with low temperature (below 90 °C) than the solar-powered DACS, which needs high temperature (above 166 °C). Thus, Chapter Seven explores the temperature analysis for solar heat production for solar-powered DACS.

As expected, the predominantly cold climates, Swansea and Volgograd, had higher heating deficit hours than the mostly hot climates, New Delhi and Tunis. Likewise, mostly hot climates, New Delhi and Tunis, recorded higher cooling deficit hours than the predominantly cold climates, Swansea and Volgograd. Although Swansea recorded the highest total heating deficit hours of 4024 hours compared to Volgograd's 3666 hours, Volgograd recorded the highest total heating power deficit of 1910 kWh compared to Swansea's 1212 kWh. Volgograd's total heating power deficit results in a higher magnitude than Swansea's because the building's annual heating load is higher for Volgograd (2566.6 kWh) than for Swansea (1677 kWh).

Tunis has a high total heating deficit hours, about 52% of that of Volgograd, and the total heating power deficit is 15.7% of that of Volgograd. This is because solar heat is more available in Tunis in the winter than Volgograd. Besides, most of the Tunis deficit hours occur at night with a low heating power deficit, compared to Volgograd's large amounts of heating power deficits during the daytime with less available solar power. Additionally, Tunis has no heating deficit days compared to Volgograd's recorded 70 heating deficit days in the year.

The energy analysis for the four case study cities indicates that peak heating and cooling mainly occur between 0:00 and 07:00. Therefore, the indoor heating temperature setting of 20 °C can be lowered to reduce the building's heating load, or warm clothing

can be worn in the building space. For Tunis and New Delhi, the design analysis showed that the solar collector sizing could be increased to cover the building roof space to meet all the building's heating and cooling needs.

In contrast, for Swansea and Volgograd, covering all the building roof space with solar collectors could meet the building cooling demand but have 40 and 48 annual heating deficit days, respectively. As a result, it was necessary to incorporate thermal energy storage for Swansea and Volgograd solar design to meet all the building's heating loads. Thermal storage provides stored energy capable of meeting the heating demands of Swansea and Volgograd. However, the analysis is limited because it is based on the thermal store being a perfect thermal store with no account for the practical heat loss expected in energy storage systems. Future solar and storage design must include the heat loss rates typical of water-based thermal storage systems.

Solar design has been applied to a standard building in four case studies of climatic regions. However, the design methodology applies to large buildings such as high-rise apartments, offices, hospitals, warehouses, and schools. Further solar design investigation can include modification of the solar collector type and efficiency, concentration ratio collector aperture and absorber area and how that impacts the solar thermal energy performance. Further investigation can include design modifications such as using diverse performance figures of various cooling engines and modifying the building's room temperature setpoints.

5.5 Conclusion

TRNSYS modelling software has been used to model the heat production from a solar and storage design that meets a standard building's cooling and heating loads for Tunis, Volgograd, New Delhi, and Swansea climates. The conclusions drawn from the study are:

1. It is possible to calculate the solar heat energy generated from an XCPC solar collector using the data from solar irradiation recorded from TRNSYS software.
2. Swansea recorded the highest total heating deficit hours than Volgograd. However, Volgograd's total heating power deficit is of a higher magnitude than that of Swansea because the building's annual heating load is higher for Volgograd than for Swansea.
3. Tunis's total heating deficit hours is 52% of Volgograd's. However, the total heating power deficit is at a lower value of 15% than that of Volgograd because solar heat is

more available for Tunis in the winter than for Volgograd, and Tunis has no heating deficit days compared to Volgograd's recorded 70 heating deficit days.

4. For Tunis and New Delhi, the building's roofing space has enough area to cover the solar collector and meet all the building's heating and cooling power needs.
5. For Swansea and Volgograd, the solar collector area can be increased to cover the building's roof space and meet all the building's cooling loads. Nonetheless, thermal storage is needed to generate enough energy to meet the Swansea and Volgograd buildings' heating energy demands.

Chapter 6 : Diffusion absorption cooling engine performance

6.1 Introduction

Chapter 5 presented the results for the solar power captured by an XCPC solar collector in four climatically varying locations in Tunis, Volgograd, New Delhi, and Swansea. This Chapter presents the thermodynamic modelling of the solar-powered DACS and compares the modelling results with experimental data in published literature. Also, this Chapter presents the optimum generator temperature and power to meet the building's cooling demand. The modelling results are presented in section 6.3. The modelling results are compared to the literature in section 6.4 before the conclusion in section 6.5.

6.2 How the solar-powered, NH_3-H_2O-H_2 DACS cooling system is modelled

This section presents how a new model of NH_3-H_2O-H_2, DACS cooling cycle, is developed using EES modelling software. The thermodynamic model used to study the DACC cooling cycle is based on mathematical equations presented by Starace and De Pascalis [142]. The thermodynamic model is widely cited in the published literature and has relative ease of implementation. This model is used because it was applied in the accompanying experimental model studied by Najjaran et al. [51].

Mass balances are written for each DACS component as detailed in the equations presented in section 3.2.2.3, and the assumptions used in modelling the DACS are presented in section 3.2.2.1. The thermodynamic equations, the model inputs and the mass, ammonia, and energy balances of each component are presented in Appendix B.

Creating the diffusion absorption cooling cycle's thermodynamic model in EES can be challenging when writing many equations to prevent errors. The thermodynamic equations are entered in EES, component by component, to minimise complexity in modelling the DACS cooling cycle. It is standard practice in EES to break many equations into smaller subsections that can be checked more efficiently [114]. The sequence of the thermodynamic modelling procedure applied in EES is illustrated in Figure 6.1 and described in this section.

The thermodynamic model of the NH_3-H_2O-H_2 diffusion absorption chiller is based on the steady-state conditions of the mass and energy balances. The DACS cooling cycle consists of a generator, rectifier, condenser, evaporator, gas heat exchanger, absorber, reservoir tank, and solution heat exchanger [141]. The purpose of the modelling is to determine the capacity of the

generator and evaporator, the mass flow rates in the cycle, the pressure and enthalpy of each state point, and the CoP of the DACS system. The lowest generator temperature below which the cooling process will not operate is determined from the EES results. It is a good practice in EES to specify the unit system utilised at the start of the modelling steps [114,123].

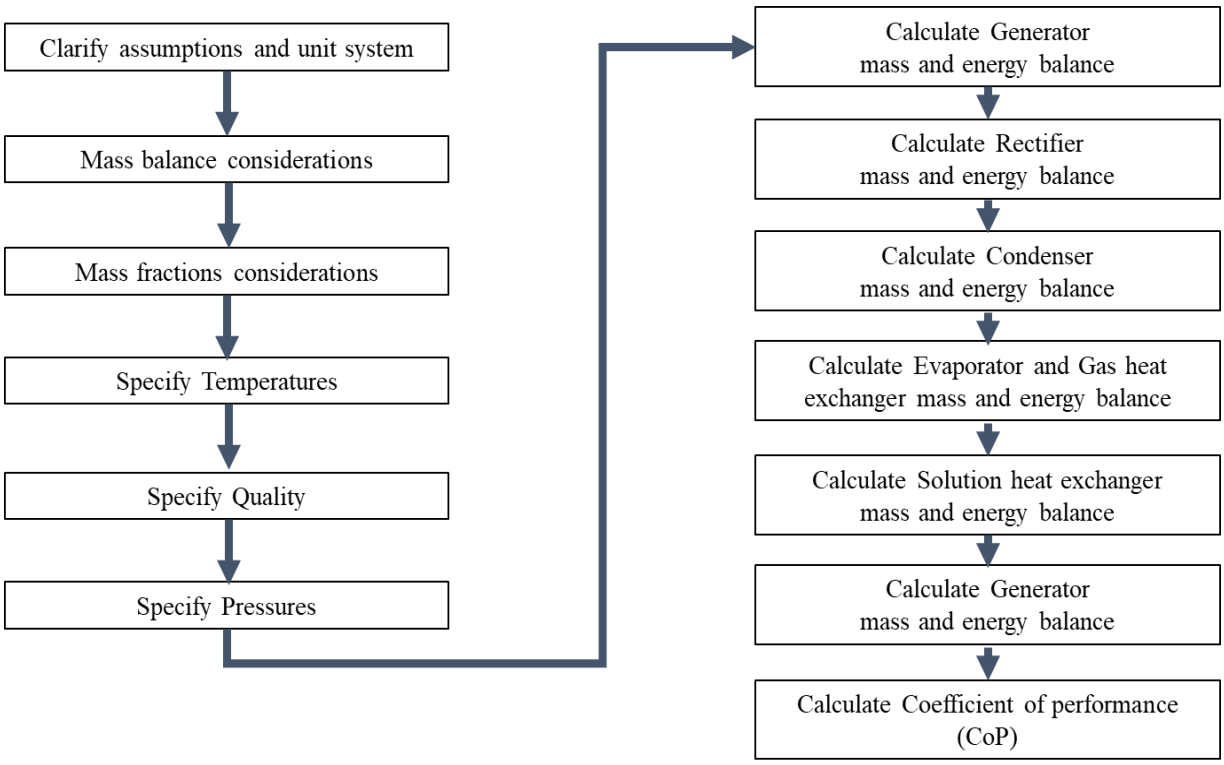

Figure 6.1: Schematic representation of the thermodynamic modelling procedure applied in EES.

6.2.1 Model inputs – mass balance, mass fraction, temperature, quality, and pressure

The fundamental strategy in mass balance analysis is to use the mass fractions from the known values in the literature and then solve the mass balances based on the known/assumed mass fractions to calculate the unknown mass flow rate. For each component in the cooling cycle, a number of mass balances are written equivalent to the number of species in the working fluid. The mass fractions of the streams are defined by other constraints in the respective component model equations, as detailed in the energy balances and heat transfer equations. For the theoretical analysis in EES, the mass fractions of all the streams are assumed to be known. Likewise, the temperature, quality and pressure data are known based on Najjaran et al. [51] paper.

In addition, the solution mass flow rate in the generator and the temperature of fluids in the stream are assumed to be known. The DACS components are treated as having a single inlet and output. The solution heat exchanger falls into this category because the different streams in the exchanger do not mix. The working stream composition is assumed to not change across the component, so the inlet and outlet mass flow rates are equal. Pressure losses are neglected; thus, two pressure levels exist in the cooling cycle [51]. The low pressure is determined by the saturation conditions at the evaporator exit [45,142], and it is calculated from EES property relations for temperature, mass fraction, and quality. The high pressure is defined by the saturation conditions at the generator exit towards the condenser [142], determined from EES property relations based on temperature, mass fraction, and quality.

The model inputs are computed in a few lines under the sub-heading of mass balance, mass fraction, temperature, quality, and pressure. That way, errors are minimised, and it is easy to trace and rectify any issues in the model as it is being developed [114].

6.2.2 Mass, ammonia, and energy balances for each component

The next step is to write the energy balances. The energy balance is written for each DACS component, and it accounts for the energy flowing in and out from the cooling system with mass flow rates and heat transfer mechanisms. An inter-joining of adjacent state points exists that couples between DACS components and enables systems equations to be solved simultaneously in EES [259]. The thermodynamic set of steady-state equations is non-linear, coupled, algebraic equations. Thus, the equations are coupled in that the operating conditions in one component affect the adjacent component (or components) through the changes in state points and flow rate. The assumption that the working fluid exiting the generator and bubble pump, the absorber and the condenser are saturated liquid and the fluid exiting the evaporator is a saturated vapour ignores sensible heat effects and simplifies the modelling [142].

The mass and ammonia balances precede the energy balance assessment for the component modelling. The mass balance is based on the mass flow rates for the state point; the ammonia balance is based on a combination of mass flow rate and mass fraction or quality. For example, the ammonia balance for the generator is based on the derivation based on mass flow rate and mass fraction. At the same time, the ammonia balance for the rectifier is derived from the mass flow rate, quality, and mass fraction [141,142].

Herold et al. [260] have demonstrated that the Newton-Raphson calculation method can be used to solve algebraic equations because it can be formulated in multiple dimensions such that each unknown cycle variable represents one dimension. A fundamental requirement of the method is the number of equations equals the number of unknowns, and there must be an initial guess value for each unknown. In this modelling, the guess values are the known inputs from the experimental research paper. Each iteration in the Newton-Raphson method brings the entire system closer to a solution by calculating a correction to each unknown. Where the problem is formulated in vector notation, the unknowns can be represented in vector form, such that the correction at each iteration is a correction vector [114,123].

Linearisation of the set of equations based on the guess values computes the correction vector. The numerical linearisation is achieved by evaluating the derivative of each equation for the independent variables. Two limitations of using the Newton-Raphson calculation method in solving the sets of nonlinear algebraic equations are multiple solutions and lack of convergence from a specific guess value. Firstly, solving non-linear equations can lead to multiple possible solutions. Thus, when the EES iterative solver converges on a solution, care must be taken to examine whether the solution is valid for the problem of interest. The second issue is the divergence of the iteration, which can occur when the guess values for the independent variables are far from a solution [114].

EES is incorporated with the required property data for ammonia, water, and hydrogen [199]. The specific enthalpy values are related to other state-point variables such as temperature, pressure, mass fraction and quality. As a result, the specific enthalpy for each state is used to evaluate the energy balance. The specific enthalpy values rely on the thermodynamic state, which depends on the operating conditions of the adjacent state points. For example, the specific enthalpy can be determined since the temperature, pressure, and quality at state 3 (generator exit) are known. Likewise, the known mass fraction, pressure, and quality at state 5 (rectifier exit) allow the specific enthalpy at that point to be calculated [114].

The specific enthalpy calculation for the other DACS components follows a similar fashion, except for the state points for the inert gas at the top of the absorber ($h_{8,ig}$) and at the evaporator exit ($h_{10,ig}$). Starace and De Pascalis [142] suggest that the evaporator and the GHX can be treated as a single control volume, and the specific enthalpy, $h_{10,ig}$, can be deduced from the product of the specific heat of hydrogen and the temperature at the evaporator exit. Likewise, $h_{8,ig}$, is determined from the product of the specific heat of hydrogen and the corresponding

temperature measured at the absorber entry. Besides, to determine $h_{10,ig}$ and $h_{8,ig}$, it is assumed that the refrigerant temperature equates to the auxiliary gas temperature at the GHX exit and the absorber entry. The modelling ends with calculating the coefficient of performance (CoP), the ratio of the evaporator cooling output power to the generator heat input [51,142].

6.3 Simulated performance evaluation

This section presents and discusses the results showing the DACS system performance using the thermodynamic equations presented by Starace and De Pascalis [142] for different boundary conditions [16]. Research by Jakob et al. [16] indicates that the rich solution in the thermally driven bubble pump strongly depends on the generator heating temperature and the external heating circuit mass flow rate. Also, the generator temperature affects the internal bubble pump temperature and, as a result, the corresponding enthalpies.

The modelling results for the DACS illustrate its thermodynamic performance under steady-state design conditions. The COP of the DACS is defined as the ratio of the useful cooling effect produced to the energy input required, Equation 3.7. The evaporator delivers the cooling capacity while the heat energy input is achieved at the generator compartment. The modelling results comprise the COP and cooling capacity with the corresponding generator power, Figure 6.2.

The COP increases to a peak value of 0.3 as the generator increases from 258 W to 407 W. After that, the COP reduces to 0.01 as the generator power increases from 407 W to 658 W. It is seen that the cooling capacity increases from 13 W to 114 W as the generator power increases from 258 W to 407 W and then reduces to 7 W as the generator power increases from 407 W to 658 W. Najjaran et al. [51] suggest that at higher generator power, there is higher water vapour content carried from the rectifier through the condenser to the evaporator, consequently reducing the achievable cooling output. The excessive heat is rejected in the rectifier at lower generator power, resulting in condensation and a lower flow rate of the ammonia refrigerant delivered via the condenser to the evaporator, consequently reducing the achievable cooling output.

The system pressure is assumed to be constant at a given generator power. However, during operation, the system pressure is expected to decrease by as much as 15-20 % based on the continuous supply of heat at the generator [51].

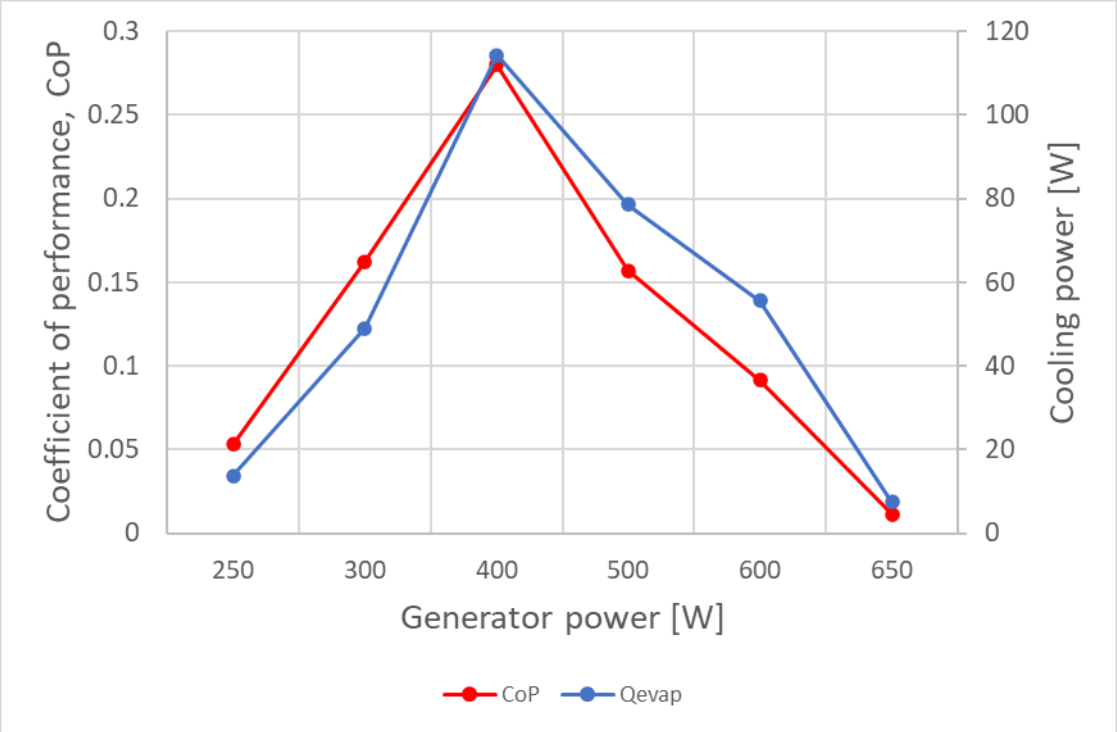

Figure 6.2: Simulated DACS system generator power plotted against coefficient of performance (CoP) and the cooling power from the evaporator (Q_{evap}).

6.4 The model comparisons with published literature

Many studies have been published on the theoretical and experimental energy performance of the DACS cooling cycle. This section presents the key findings from such theoretical simulations and experimental results published in the literature. Some of the main work and results are summarised in Table 6.1.

Yildiz and Ersoz [231] performed theoretical and experimental analyses of an ammonia-water DACC cycle with helium as the auxiliary gas based on energy balances and the coefficient of performance (CoP). Their research used the REFPROP software to model ammonia-water solution thermodynamic properties at various components. It demonstrated that heat gain occurs in the evaporator and generator components as the heat losses occur in the absorber, condenser, rectifier, and solution heat exchanger (SHX). Yousfi et al. [261] performed experiments with a DACS chiller at varying generator temperature, cooling water and chilled water temperatures and demonstrated that increasing the generator temperature does not always increase the CoP and suggested this could be due to the system heat and mass transfer limitations and irreversibility.

Table 6.1: Summary of main published work

Authors	Main work	Main results
Yildiz and Ersoz [231]	Theoretical and experimental analyses of NH_3-H_2O-He DACS cycle based on mass and energy balances and CoP.	Temperature and pressure are the dominant determinants of the DACS system's characteristics. Cooling capacity and CoP were 10 W and 0.19, respectively.
Yousfi et al. [261]	Theoretical and experimental analyses of NH_3-H_2O-H_2 DACS cycle investigating the influence of varying generator temperature, cooling water and chilled water temperatures.	Operating DACS at low generator temperature and controlling chiller cooling capacity is preferable. The inlet temperature of the water-cooled condenser affects the total system pressure and efficiency of ammonia condensation. Cooling capacity and CoP were 4.5 kW and 0.45, respectively.
Mansouri et al. [140]	Numerical simulations of NH_3-H_2O-H_2 DACS cycle using Aspen-plus simulation software.	The Aspen-plus simulation tool was used to show three primary pressure levels for the components in the cooling cycle. Optimal CoP of 0.16 at a generator temperature of 167 °C with a power supply of 46 W.
Chaves et al. [259]	Numerical simulations and experimental study of NH_3-H_2O-H_2 DACS cycle based on mass and energy balances.	The ambient temperature influences the operating temperature in the evaporator, rectifier, generator, reservoir, and condenser. It is preferable to operate DACS at low generator temperatures.
Pérez-García et al. [43]	Theoretical modelling and experimental study of NH_3-H_2O-H_2 DACS cycle focussed on determining component outlet temperatures, bubble pump fluid mass flows and the system.	The geometrical characteristics of the DACS influence the operational conditions of each component of the cooling cycle. The maximum recorded CoP was 0.15.
Jacob et al. [16]	Development, experimentation, and simulation of a solar-powered NH_3-H_2O-He DACS for air-conditioning application.	The bubble pump's rich solution mass flow rate highly depends on the generator temperature and the heating source's fluid mass flow rate. It is preferable to operate DACS at low generator temperatures. Cooling capacity and CoP were 2.5 kW and 0.38, respectively.
Najjaran et al. [51]	Theoretical analysis and experimental evaluation of NH_3-H_2O-H_2 DACS cycle of a 100 W cooling capacity DACS unit under varying heating source power and generator temperature.	It is preferable to operate DACS at low generator temperatures. The measured cooling output ranged between 24 and 108W, with CoP between 0.11 and 0.26; a peak CoP of 0.26 was recorded at the 300 W generator heat source.

Also, their research indicates that it may be possible that the total surface area in the evaporator chamber is not utilised for the liquid ammonia such that residual ammonia liquid falls directly into the absorber chamber. Furthermore, their research demonstrates that inlet cooling water temperature directly affects the total system pressure and high efficiency of ammonia condensation and lower heat rejection temperature in the condenser (less than 24 °C) is preferred because there is high-purity ammonia liquid reaching the evaporator to improve the cooling output.

Mansouri et al. [140] used an Aspen-Plus modelling software to predict the steady-state operation of DACS and three primary pressure levels for the components in the cooling cycle. The evaporator, GHX, and absorber had a low-pressure level (< 5 bar); the solution heat exchanger was at a mid-pressure level (around 10 bar); and the generator, rectifier, and condenser were at a high-pressure level (> 20 bar). Chaves et al. [259] performed numerical simulations using EES software. Their results indicate that the ambient temperature influences the operating temperature in various components such as the evaporator, rectifier, generator, reservoir, and condenser. Like Yousfi et al., their results indicated that the refrigerator's performance increases as the generator's power decreases.

Pérez-García et al. [43] used EES software to undertake theoretical modelling along with an experimental study of a small capacity DACS that demonstrated the impact of geometrical characteristics and operational conditions of the different components of the cooling cycle. Jacob et al. [16] presented the development, experimentation and simulation of a solar heat-powered ammonia-water DACS. They showed that for a thermally driven bubble pump, the rich solution mass flow rate in the bubble pump is highly dependent on the generator temperature and the heating source's fluid mass flow rate. Also, the generator temperature influences the various specific enthalpies of the components.

Najjaran et al. [51] performed a detailed experimental evaluation of a 100 W cooling capacity DACS unit. The heating source varied between 150 and 700 W, resulting in a corresponding generator temperature range of 175 to 215 °C. The measured cooling output ranged between 24 and 108W, with CoP between 0.11 and 0.26, the highest CoP recorded at a 300 W generator heat source. The cooling output increases as the generator heat input increases from 103 W to 400 W, after which it plateaus to a maximum value of 103 W ± 5 W, followed by a decrease in cooling output at generator inputs greater than 650W. Likewise, the measured CoP reaches a peak value of 0.26 at a generator heat source of 300 W. Their results are in sync with the

previous observation of this theoretical research study, where higher generator temperature does not lead to higher CoP throughout the design. Their research suggests that the possible reason for this phenomenon is that excess heat makes it difficult to be rejected in the rectifier, causing progressively higher water vapour to the condenser and evaporator, limiting the resultant cooling output.

Figure 6.3 shows the cooling power plotted against the generator power from the experimental results received from Najjaran et al. [51]. The maximum cooling output is recorded when the generator heat input is between 500 and 650 W.

(a) Cooling power	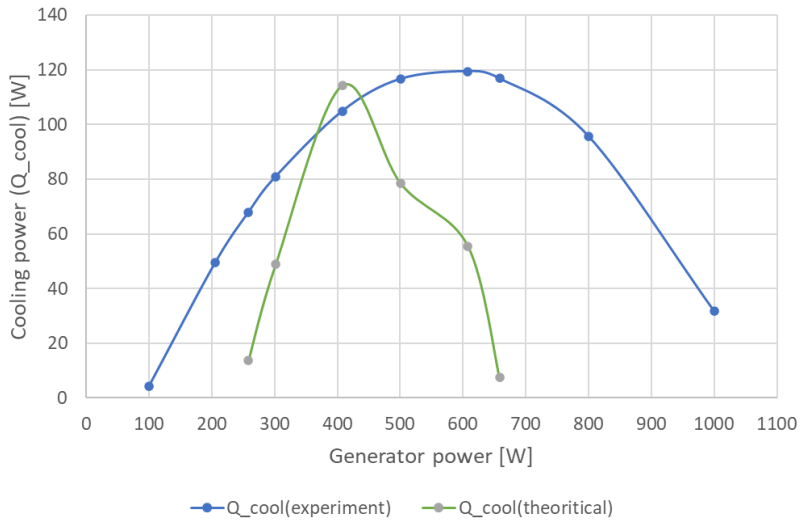
(b) COP	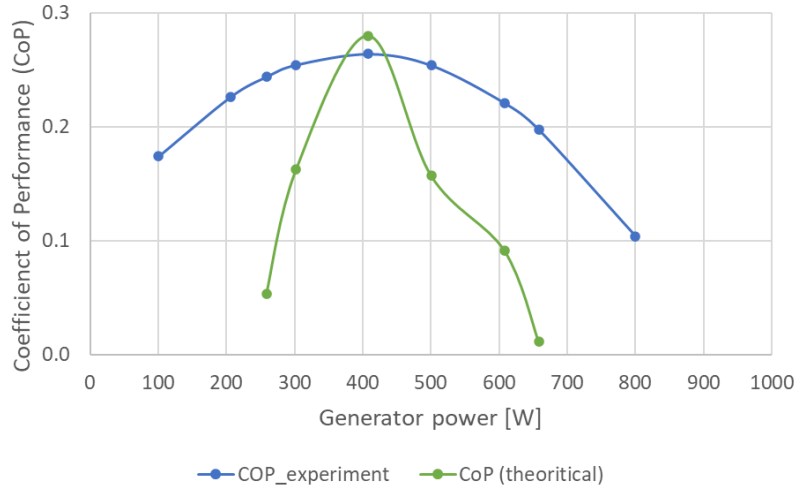

Figure 6.3: Comparing the generator power and the cooling capacity and coefficient of performance (CoP) (theoretical results from this study and experimental data received from [51]).

Figure 6.4 shows the cooling power plotted against the generator temperature, where the maximum cooling capacity is recorded for the generator temperature between 190 and 205 °C. The manufacturer's stated system pressure is 22 bar, yet the pressure was not measured in the experimental setup. The EES modelling results agree with other theoretical study patterns, e.g., smaller generator power capable of achieving high cooling capacity and heat gain to the generator and evaporator from the building's cooling demand. The calculated EES modelling results based on Starace and De Pascalis thermodynamic model did not closely follow the experimental data in the published literature [51]. Likewise, other theoretical studies [141,262,263] do not closely follow the experimental data in the published literature [51]. The theoretical modelling results outside the peak generator power are poor, under-predicting the cooling power and the COP.

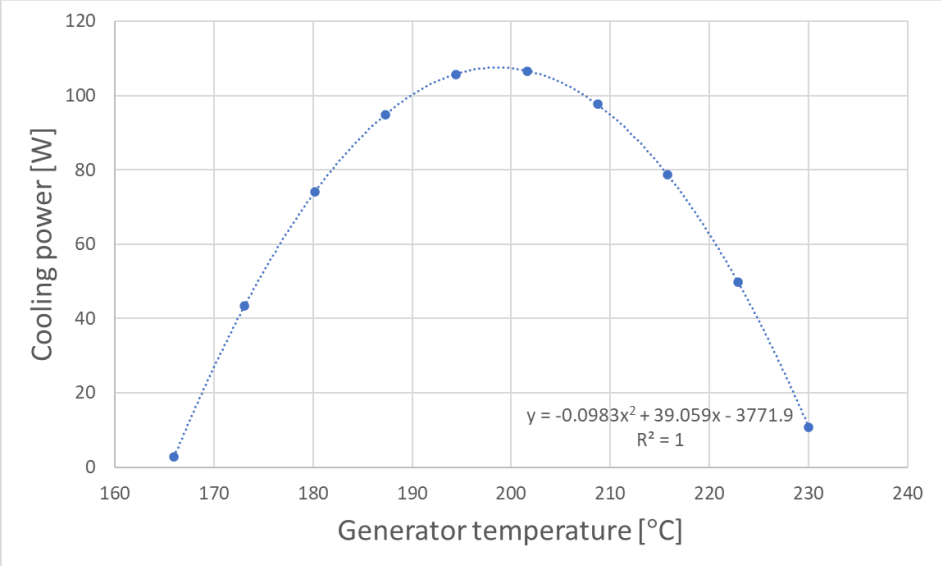

Figure 6.4: Experimental DACS system cooling power plotted against generator temperature (data received from [51]).

Practical DACS cooling engines involve simultaneous, complex multi-component heat and mass transfer processes, each with unique thermophysical properties of the refrigerant (NH_3), absorbent (H_2O), and inert gas (H_2) working fluids [43,45,46]. Theoretical modelling of an absorption refrigeration unit by Micallef et al. [264] suggests the limitations in the simplicity of the mass and heat transfer equations, such as the inability to simultaneously change each variable, influences accurately predicting the nonlinear behaviour and temperature and mass concentration gradients. The working fluids of the DACS cooling engine could develop non-ideal gas behaviour deviating from the liquid mixture behaviour predicted by Raoult's Law

[136], affecting the cooling engine system performance deviating from the static vapour pressures [46,217,218] assumed in the simple mass and heat transfer theoretical models. Any deviation in the DACS's operating pressure will likely impact the modelling performance, considering that Yildiz and Ersoz's [231] research indicates that system operating pressure and temperature are the dominant determinants of the DACS system's characteristics.

Moreover, the simplified mass and heat transfer thermodynamic equations do not adequately account for the critical geometric surface irregularities [218,265,266], such as the wick structures in the absorber and evaporator, and the local surrounding conditions [51,261], e.g., the humidity, ambient temperature, and wind speed, that could influence component performance in practice or experiments. A theoretical thermodynamic model such as the DACS cooling engine's accuracy depends on the reliability of the thermophysical property data [43,44,141], including density, thermal conductivity, viscosity, and solubility of NH_3-H_2O mixtures. Whist EES software [199] in-built functions for the thermodynamic and transport properties of the NH_3-H_2O-H_2 working fluids were used, and the experimental measurement could be used to accurately determine the real thermophysical properties together, particularly at equilibrium. Coquelet et al. [267] suggest developing experimentation equipment utilising small sample quantities and in-situ analysis techniques is essential.

6.5 Conclusion

The EES software is an effective tool for modelling the diffusion absorption cooling cycle using thermodynamic equations. The EES modelling results compare well to other patterns, such as the expected heat gain pattern in the evaporator and generator, showing that smaller generator power can achieve high cooling capacity. However, the EES modelling results do not follow closely with the experimental data in published literature, which could be due to factors such as the impact of geometrical characteristics and operational conditions such as mass flow rate, total system pressure, the efficiency of ammonia condensation, and lower heat rejection temperature. As a result, the experimental data is used for the subsequent design of the solar collector and storage tank systems needed to meet the building cooling loads.

Chapter 7 : Solar collector and storage design for a diffusion absorption cooling engine in New Delhi and Volgograd

7.1 Introduction

Chapter 6 identified the generator's temperature and power needed to meet a building's cooling demand. This Chapter presents the design approach for determining the optimum dimensioning and sizing of solar collectors and storage required to meet the generator temperature or power requirements identified in Chapter 6. Thus, this section presents the design philosophy for the solar and storage part of the solar-powered DACS system. Section 7.2 explains the design methodology used to complete the solar and storage design modelling. Section 7.3 presents the results of the solar and storage design, followed by the discussion of the results and the conclusion in sections 7.4 and 7.5, respectively.

7.2 Methodology

7.2.1 The design approach and dimensioning

This section presents the rationale for choosing an optimised solar energy capture and storage to meet the required generator temperature or power for building cooling. Henning [37,55] proposes designing a solar capture and storage system implies dimensioning and sizing the solar collector and heat storage units. As a result, this design aims to maximise the energy generation based on solar collectors and storage as practically as possible. Any lag in the heat demand can be explored with an auxiliary heating source. Figure 7.1 illustrates the connection between the DACS, solar collector, hot store, and heat exchanger delivering cold air to the building.

Figure 7.2 shows the design approach for the solar collector and heat storage systems required for the solar-powered DACS. The design uses the solar collector area specified by the manufacturer Artic Solar in their technical specification datasheet [66]. The Artic Solar XCPC solar collector datasheet indicates the solar collector can achieve temperatures over 200 °C at more than 50% efficiency and has a 2.41 m^2 collector aperture area. After selecting the minimum solar collector, the next step is to apply the rule of thumb to determine the required storage volume [55].

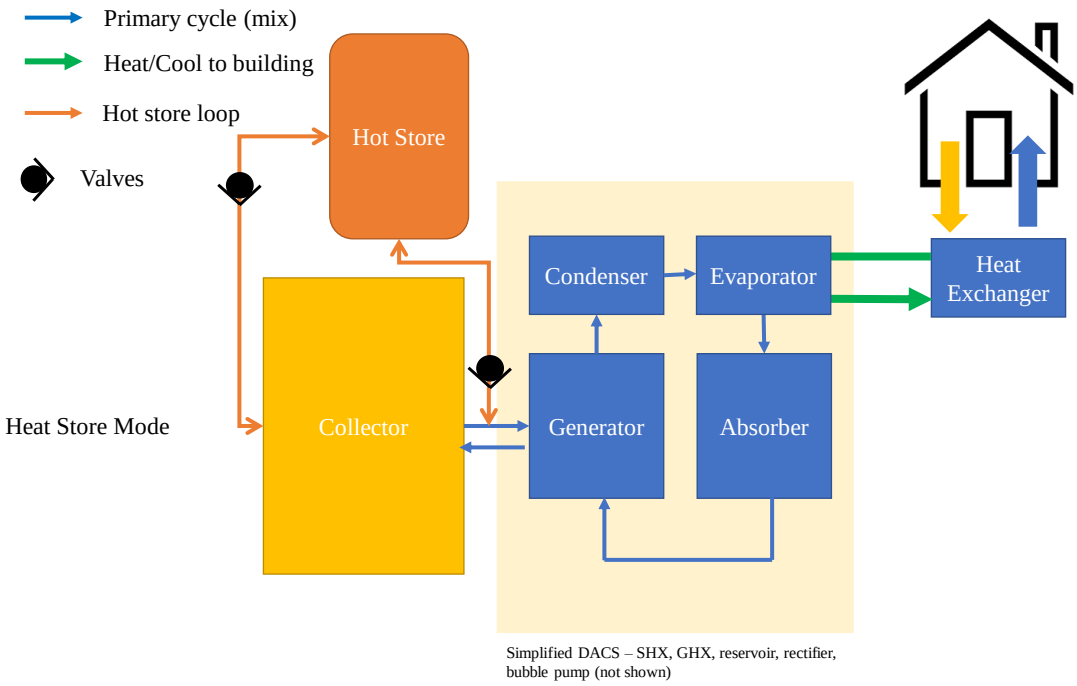

Figure 7.1: Schematic showing the connections between the solar collector, DACS, hot store, and heat exchanger delivering cold air to the building.

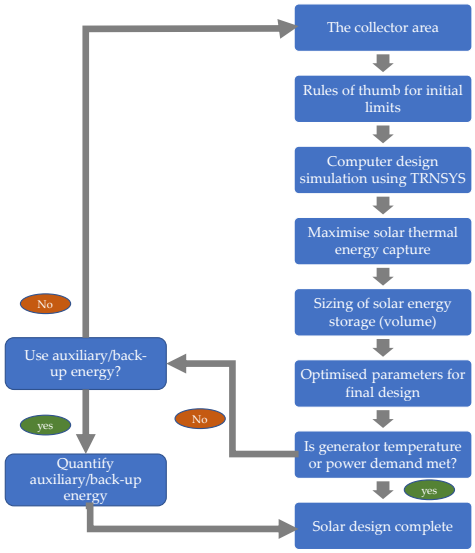

Figure 7.2: The design approach for the solar collector and heat storage systems.

A buffer storage system is employed in the solar design to store the solar fluid from the collector and return the stored liquid to the generator component of the DACS when needed. Mugnier et al. [230] suggest that a typical hot water storage volume for an absorption cooling system ranges from 10 – 50 litres/m^2 of collector area; the lower end of the range is recommended for solar cooling and to minimise heat loss. Based on Mugnier et al. [230]

recommendation, the lowest end of 10 litres/m^2 of the collector area is selected as the starting point for the computer design simulation in the TRNSYS software. TRNSYS software is applied for solar design because it has the unique capabilities to model solar collector and thermal energy systems [171,174,268]. The parameters investigated are summarised in Table 7.1. Figure 7.3 illustrates the strategy based on the mass flow rate, the storage tank volume, and the optimum collector and tank temperature needed for optimum COP and cooling capacity, presented in Chapter 6.

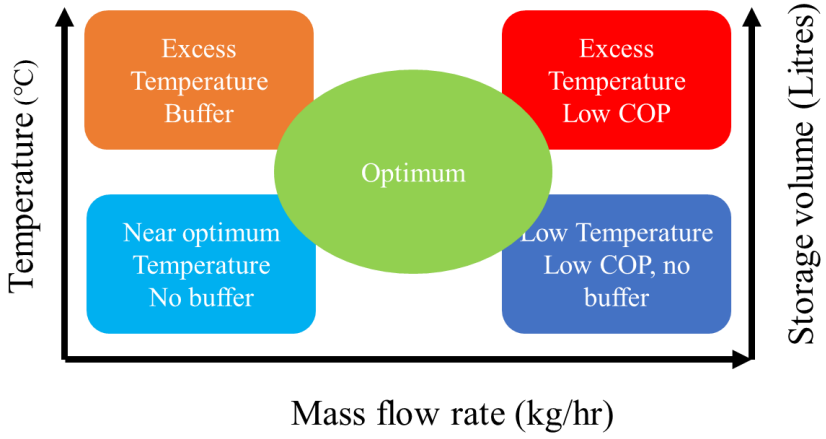

Figure 7.3: Explanation of the reason for the modelling study.

Table 7.1: Parameters investigated in the solar and storage design

Parameters investigated	Operating range/ results	Justification
Solar collector mass flow rate	0.1 – 100 kg/hr	Literature: [37,55,66,171]
Solar collector area	2.41 – 4.82 m^2	Literature: [37,55,66,171]
Solar collector volume	2 litres/ collector area	Literature: [37,55,66,171]
Thermal energy storage volume	2-20 litres/m^2 of the solar collector area	Literature: [37,55,230]
Solar collector temperature	results recorded	Literature: [37,53-55,57,228,230]
Heat storage tank temperature	results recorded	Literature:[37,53-55,57]

The optimisation strategy employed in TRNSYS is to maximise the solar thermal energy yield by modifying the fluid mass flow rate to achieve higher solar fluid temperatures needed to drive the DACS's generator. Thus, a range of fluid mass flow rates is used in the TRNSYS simulation to determine the ideal solar collector and heat storage temperatures. The mass flow rates used

in the simulation study were 0.1 - 100 kg/h, and resultant solar fluid temperatures were recorded.

7.2.2 Solar energy yield maximisation using the mass flow rate

The rate of useful energy gain, Q_u, by the solar collector fluid is calculated from the equation [171]:

$$Q_u = \dot{m}c_p(T_{out} - T_{in}) \qquad 7.1$$

where $\dot{m}$, is the mass flow rate of the fluid exiting the solar collector (kg/hr), c_p, is the specific heat of the solar fluid (J/kg°C), T_{out}, is the temperature of the fluid exiting the solar collector array (°C), and T_{in}, is the inlet temperature of the solar collector array (°C).

Thus, the mass flow rate of the solar fluid can be calculated from Equation 7.1. The energy source from the sun does not always match the times when heat is required at the generator to meet the building's cooling demand. As a result, the generated heat from the solar collector is stored in a small buffer thermal store. The buffer store is applied to deliver a uniform temperature for the generator to meet cooling demand at night or during the day. The heat source for the generator is then supplied from the buffer store rather than directly from the solar collector.

Firstly, the TRNSYS modelling starts with the lowest possible solar collector aperture area of 2.41 m^2. Then, the results for a higher solar collector area of 4.82 m^2 are used for the TRNSYS modelling, and the results are presented. Once the optimum fluid mass flow rate is recorded, the next step is to use the chosen mass flow rate to model various sizes of the heat storage system.

7.2.3 Sizing the volume of the buffer storage tank

The buffer storage volume ranging from 2-20 litres/m^2 of the solar collector area is modelled to determine the optimum generator temperature, and results are presented in section 7.3.2. The simulation is completed over a year to analyse the results for the peak cooling demand days. Like the mass flow rate, the TRNSYS modelling starts with the lowest possible solar collector aperture area of 2.41 m^2. Then, the results for a higher solar collector area of 4.82 m^2 are used for the TRNSYS modelling, and the results are presented.

The result based on the optimal volume is recorded as the optimised design parameter. The ideal generator temperature published in Najjaran et al. [51] work is compared with the

optimised modelling result. The solar design is complete if the optimised design meets the required generator temperature. Other design routes can be pursued where the solar power output does not meet the necessary generator temperature or power demand. Auxiliary energy or backup energy may meet any shortfall in the demand for generator energy. Alternatively, the solar design process can be restarted by amending the solar collector area as practically as possible until all the generator temperatures or power are met. The research strategy employed focused on solar and storage design.

7.3 Results

7.3.1 Solar energy yield maximisation using the mass flow rate

The target operating temperature for the solar collector and the buffer storage tank is between 190 and 205 °C, as discussed in Chapter 6. The energy assessments presented in Chapter 5 indicate the available energy as the heat source for cooling. However, the temperature assessments provide a balanced approach to assessing how high temperatures can be generated, transferred and stored to meet the heat source requirements. The temperature assessments help to highlight practical safety considerations, thermodynamic limitations, efficiency and losses, and material and design constraints.

Figure 7.4 shows the results of the fluid mass flow rates and the corresponding maximum tank temperature and collector temperature for New Delhi and Volgograd at collector areas 2.41 m^2 and 4.82 m^2. For New Delhi, the highest collector temperatures are recorded as 300 °C at different mass flow rates of 0.1 kg/hr and 1 kg/hr, while the highest maximum tank temperature is recorded as 181 °C at the 1kg/hr mass flow rate. For the 4.82 m^2 New Delhi collector area, the 5 kg/hr mass flow rate generates the highest tank and solar collector fluid temperature. For Volgograd, the 2.41 m^2 collector area results show that the highest collector temperatures are recorded as 300 °C at different mass flow rates of 0.1 kg/hr and 1 kg/hr, and the highest maximum tank temperature was 201 °C at the mass flow rate of 5 kg/hr. For the 4.82 m^2 Volgograd collector area, the 5 kg/hr mass flow rate generates the highest tank and solar collector fluid temperature.

There are practical implications with operating with water at 300 ℃ because the water well above its boiling point of 100 ℃ behaves differently depending on the pressure conditions. The water at that temperature becomes a superheated liquid, which may exhibit properties of liquid and gas phases, significantly depending on the pressure conditions, leading to unique solvent

properties [136,199,269]. Higher operating pressures of around 85 bar [136,269] are needed to maintain water in a liquid state, and the water is less dense and flows easily than at room temperatures. The water's thermal conductivity and specific heat capacity remain high, making it an efficient heat transfer medium and storing heat effectively at elevated temperatures [136,269]. Handling superheated water at high temperatures and pressure poses significant safety risks, which require adequate safety measures and fail-safes to prevent accidents [53,87,126].

Additionally, substantial energy, e.g., from using pumps [38,87], may be needed to maintain the water at high pressure and temperature to achieve the expected generator temperature in the 190 – 205 °C range for each location. Materials that can withstand the corrosive nature of hot water must be selected, which could increase the cost and complexity of design, equipment, and containment.

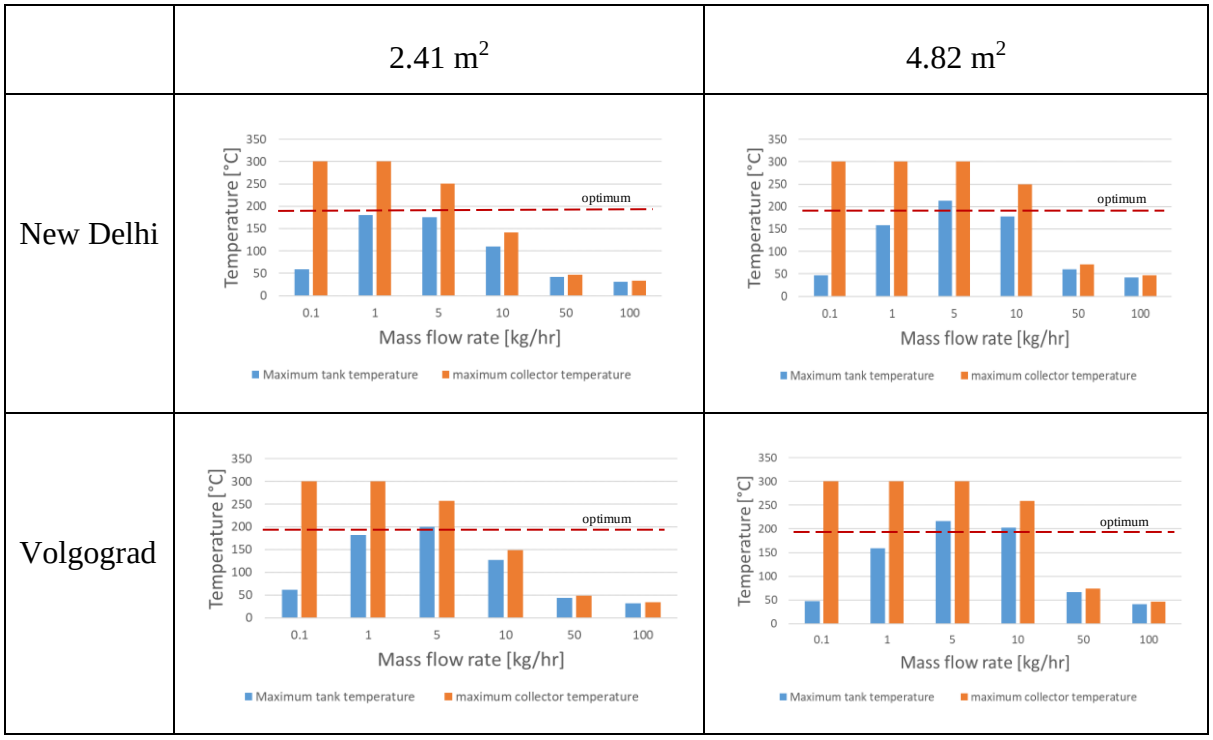

Figure 7.4: Fluid mass flow rates and the corresponding maximum tank and collector temperature for New Delhi and Volgograd at 2.41 m^2 and 4.82 m^2 collector areas.

7.3.2 Sizing the volume of the buffer storage tank

Figure 7.5 shows the results of the buffer tank volume and the corresponding maximum tank temperature and collector temperature for New Delhi and Volgograd at collector areas 2.41 m^2 and 4.82 m^2. For New Delhi, the 2.41 m^2 collector area results show that the maximum collector temperatures remained at 300 °C. In contrast, the recorded maximum tank temperature

gradually reduces from 232 °C to 153 °C when the buffer tank volume increases from 4.82 - 48.2 litres. For the 4.82 m^2 New Delhi collector area, the maximum collector temperatures remained at 300 °C, while the recorded maximum tank temperature gradually reduced from 247 °C to 186 °C when the buffer tank volume increased from 9.64 to 96.4 litres. The results show that a smaller buffer storage tank delivers higher tank temperatures in both collector areas, 2.41 m^2 and 4.82 m^2. The results are as expected because the solar collector temperature does not influence the size of the volume of the storage tank used. Thus, the solar fluid mass flow rate impacts the recorded solar collector temperature.

	2.41 m^2	4.82 m^2
New Delhi	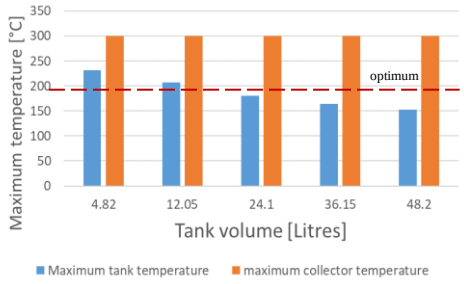	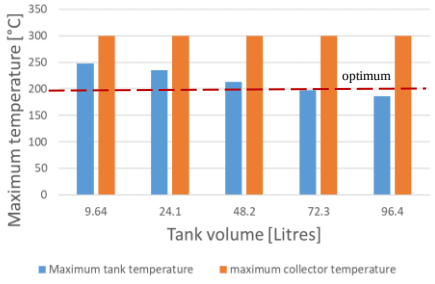
Volgograd	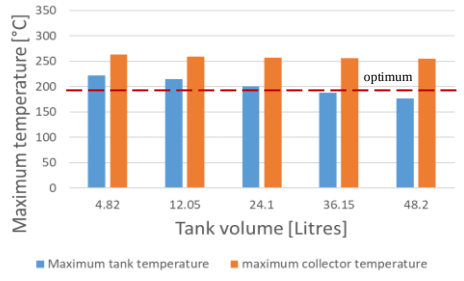	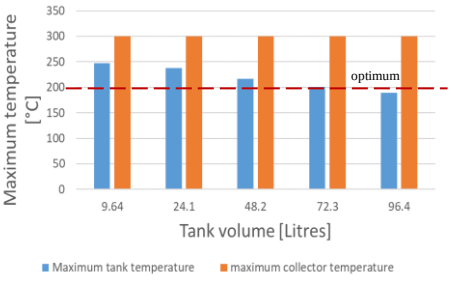

Figure 7.5: The buffer tank volume and the corresponding maximum tank and collector temperatures for New Delhi and Volgograd at collector areas are 2.41 m^2 and 4.82 m^2, respectively.

For Volgograd's 2.41 m^2 collector area, the maximum collector temperatures were in a small range of 255-263 °C, while the recorded maximum tank temperature gradually reduced from 222 °C to 176 °C when the buffer tank volume increased from 4.82 to 48.2 litres. For the 4.82 m^2 Volgograd collector area, the maximum collector temperatures remained at 300 °C, even as the various buffer tank volume maximum temperatures were reduced from 248 °C to 189 °C. Like New Delhi, the results are as expected because the solar collector temperature does not influence the size of the storage tank volume. Figure 7.6 shows the maximum solar collector

and tank temperatures and the optimum storage tank volume for small and large collector areas, 2.41 m^2 and 4.82 m^2, respectively, for New Delhi and Volgograd. The results show that small mass flow rates (below 10 kg/hr) can achieve the optimum collector and tank temperature for both New Delhi and Volgograd.

New Delhi

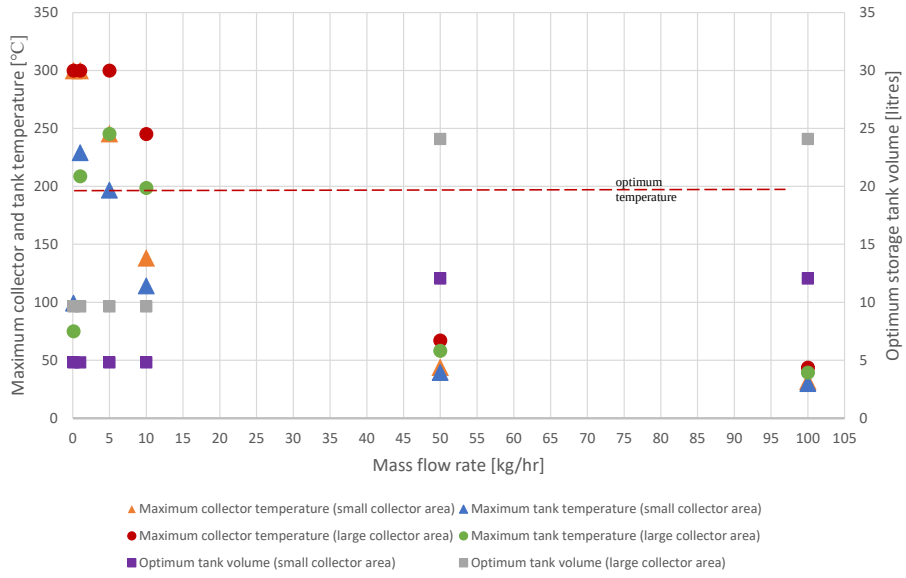

Volgograd

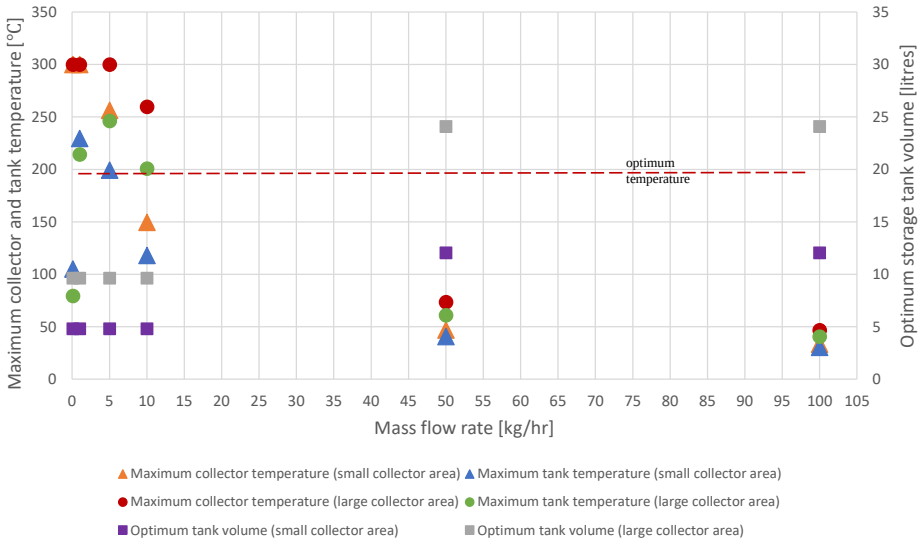

Figure 7.6: The maximum solar collector and tank temperatures and the optimum storage tank volume for New Delhi and Volgograd at collector areas 2.41 m^2 (small) and 4.82 m^2 (large).

At the same time, small buffer tank sizes (2 litres/m^2 of the solar collector area) can achieve the optimum storage tank sizes and achieve the optimum DACS generator temperature. Also,

operating at large mass flow rates (> 10 kg/hr) requires large storage tank volumes, although it does not generate high collector or tank temperatures.

7.3.3 Justification for selecting the optimum solar collector area, buffer tank volume, and fluid mass flow rate

For New Delhi, the 2.41 m^2 solar collector is the selected collector area because it requires a low mass flow rate (1 kg/hr) and a smaller tank volume (4.82 litres) to deliver maximum tank temperatures of 232 °C, Table 7.2. The 4.82 m^2 solar collector is not selected because it needs a higher mass flow rate (5 kg/hr) and tank volume (9.64 litres) to deliver maximum tank temperatures of 247 °C. The 4.82 m^2 solar collector area achieves a maximum tank temperature of 247 °C, greater than the 232 °C maximum tank temperature recorded in the 2.41 m^2 solar collector. Nonetheless, the maximum tank and collector temperature of the 2.41 m^2 solar collector are still above the expected generator temperature in the 190 – 205 °C range.

Table 7.2: Optimum operating window for selected parameters to achieve expected generator temperature in the 190 – 205 °C range for each location.

	Mass flow rate	Storage volume	Maximum collector temperature	Maximum storage tank temperature	Collector area
Unit	kg/hr	litres	℃	℃	m^2
New Delhi	1	4.82	300	232	2.41
Volgograd	5	4.82	300	222	2.41

For Volgograd, the 2.41 m^2 solar collector has an optimum mass flow rate and buffer tank volume of 5 kg/hr and 4.82 litres, respectively, while the 4.82 m^2 solar collector has an optimum mass flow rate and buffer tank volume of 5 kg/hr and 9.64 litres, respectively. The 4.82 m^2 solar collector area achieves a maximum tank temperature of 248 °C, greater than the 222 °C maximum tank temperature recorded in the 2.41 m^2 solar collector. However, the 2.41 m^2 solar collector is selected because it needs a smaller tank volume and mass flow rate, and the 222 °C maximum tank temperature and up to 300 °C collector temperature are still above the expected generator temperature in the 190 - 205°C range. Like New Delhi, the small collector area and buffer tank volume for the Volgograd climate means less capital and operating costs and less space needed within or around the residential building.

7.4 Discussion

TRNSYS modelling software has been used to model the solar collector and storage design to meet the high-temperature requirements for a solar-powered DACS to meet the standard building's cooling demand in New Delhi and Volgograd. The sensitivity analysis of the solar collector and storage design confirmed that the mass flow rate of solar fluid, the solar collector area, and the buffer storage tank influence the optimum generator temperature that can be generated.

The Volgograd and New Delhi results show that the small, single XCPC solar collector unit, 2.41 m^2, is sufficient to reach the required operating temperature range of 190- 205 °C for the DACS's generator. Consequently, the small solar collector area needed a small buffer storage volume. As a result, a small collector area and buffer tank volume mean less space required for installation and fewer capital costs for the operating system.

The results show that the solar collector achieves higher operating temperatures at low fluid mass flow rates. The solar collector temperature reduces as the fluid mass flow rates increase. Thus, the fluid mass flow rates must be operated below 10 kg/hr for New Delhi and Volgograd to achieve high collector operating temperatures. The XCPC solar collector reaches higher operating temperatures at low fluid mass flow rates because the fluid spends more time in the collector, allowing it to absorb more heat from the sun, leading to a higher rise in temperature.

The buffer tank achieves lower temperatures than the solar collector because the solar fluid is fed to the diffusion absorption cooling engine from the buffer tank. The optimum mass flow rate is between 1 and 5 kg/hr when high amounts of heat from the solar collector are transferred to the buffer tank. As the mass flow rate increases, the buffer tank temperature reduces significantly because the high mass flow rate causes less heat from the solar collector to be transferred to the buffer tank.

At fixed solar fluid mass flow rates, increasing the buffer storage tank volume does not affect the maximum solar collector temperature but influences the tank's maximum temperature. This phenomenon happens because as the buffer tank size increases, the solar heat from the collector has a larger volume to fill, thus reducing the tank temperature.

In practice, a control system linking the variable speed pump must be installed to control the solar collector's output temperature and the buffer tank to reach the desired 190-205 °C. A variable speed pump may need to increase its rate to reduce the collector output temperature to

the optimum range of 190-205 °C. Likewise, a variable speed pump may be necessary to reduce its speed to increase the buffer tank temperature to meet the desired operating temperature of 190-205 °C.

Further economic analysis is needed to ascertain a cost comparison between a solar-driven system and a solar and storage system to meet the temperature requirements of the DACS's generator. The economic analysis will be critical in solar-assisted systems that may use backup energy to meet all the building cooling demands. A small buffer storage tank volume of 4.8 litres could be embedded in the DACS's generator to save space and minimise heat, such as in tank-in-tank energy storage systems. Alternatively, the buffer tank between the XCPC collector header and the DACS's generator can be installed. However, tank-in-tank storage systems would have issues with adequate maintenance access.

The solar and storage design has been applied to New Delhi and Volgograd climatic regions. Nonetheless, the design methodology can be used in other hot climate regions with significantly high summer cooling demand for residential buildings or offices. Further solar design investigation can include modification of the solar collector types to high-temperature solar collectors alternatives [53,54] such as concentrating solar collectors, parabolic trough collectors, and linear Fresnel reflectors. Moreover, the solar design methodology can be applied to other solar thermally powered cooling systems [32,188,189], such as single-stage and double-stage absorption cooling systems.

7.5 Conclusion

TRNSYS modelling software has been used to model the solar collector and storage design to meet the temperature requirements for the generator part of a solar-powered DACS in New Delhi and Volgograd. The following conclusions are drawn from this study:

1. It is possible to calculate the temperature of the solar fluid in an XCPC solar collector and a buffer storage tank using TRNSYS software.
2. For Volgograd and New Delhi, a small, single XCPC solar collector unit, 2.41 m^2, mass flow rates between 1-5 kg/hr, and 4.8 litres buffer volume is sufficient to reach the required operating temperature range for the DACS's generator of 190-205 °C.
3. For Volgograd and New Delhi, the fluid mass flow rates must be operated below 10 kg/hr to achieve high collector operating temperatures. The optimum mass flow rates to reach higher buffer tank temperature are 1-5 kg/hr.

4. Increasing the buffer storage tank volume does not influence the solar collector's temperature or power at a fixed solar fluid mass flow rate.
5. The hot water storage volume for a DACS ranges from 2 – 10 litres/m^2 of collector area; the lower end is recommended to minimise heat loss and save on space and costs.

Chapter 8 : Solar energy capture and storage and backup energy performance

8.1 Introduction

Chapter Seven presented the optimum solar collector and storage design to generate the required generator temperature to maximise solar energy capture and storage. This Chapter explains the strategy and the design approach needed to meet the deficit between the building cooling energy demand and the cooling energy that the solar-powered DACS system can produce. Thus, this section quantifies the backup energy required and identifies the variation of the backup hours per day throughout the year. Section 8.2 explains the methodology used to complete the solar and storage design modelling. Section 8.3 presents the results of the solar and storage design, followed by the discussion of the results and the conclusion in sections 8.4 and 8.5, respectively.

8.2 Methodology

8.2.1 Strategy for how the lag is to be met

The primary motivation for deploying solar air-conditioning systems is to save primary energy usage from fossil fuels and lower the running costs for the user [31]. The solar-powered DACS is designed to meet all the cooling energy demands throughout the year, Figure 8.1 (a).

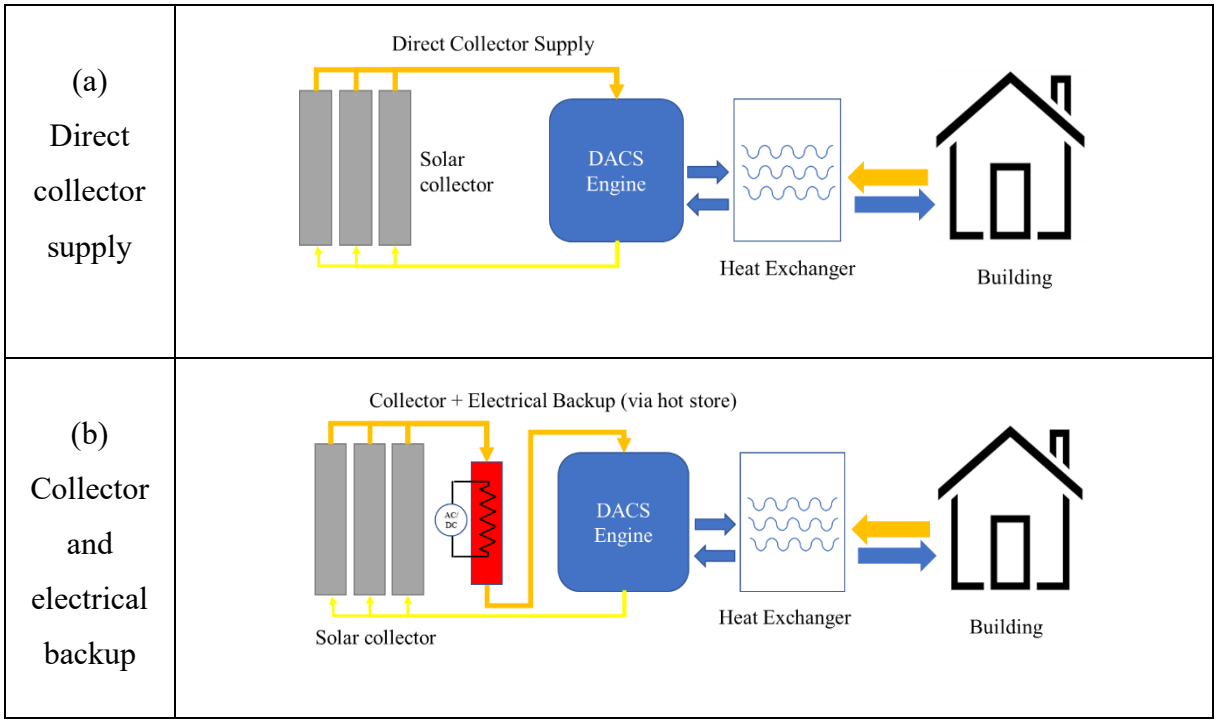

Figure 8.1: Schematic for direct solar collector supply and electrical backup via hot store to DACS.

As a result, any shortfall in the heat requirements to meet the building cooling demand is expected to be generated with backup energy. For the building cooling process, there are times when the temperature in the solar collector is insufficient to drive the DACS for reasons such as inadequate solar insolation and cloudy days. There are days when some heat is available from the solar collector, and the backup electrical energy, Figure 8.1 (b), must be used to fulfil the heat requirements of the DACS generator. For example, the temperature in the solar collector or storage is 110 °C, and backup heat must be applied to increase the fluid temperature to, e.g., 190 °C, depending on the cooling demand.

8.2.2 System design, input, and assumptions

The inputs used in the solar and storage design are summarised in Table 8.1, and the justification for the selected values is presented in Chapter 7 (section 7.3.3 and Table 7.2). Chapter Seven discussed the solar and storage design parameters, fluid mass flow rate, solar collector area, and buffer tank volume. The solar collector volume is 2 litres, as confirmed by the equipment supplier, Artic Solar [66], and the selected specific heat of water used for the modelling study is 1.16 Wh/kg.K [31].

Table 8.1: Inputs used in the solar and storage design

	New Delhi	Volgograd
Hours of cooling load annually	6200	2275
Mass flow rate	1 – 6 kg/hr	
Solar collector area	2.41 m^2	
Solar collector volume	2 litres	
Buffer tank volume	4.82 litres	
Specific heat of water	1.16 Wh/kg K	

The backup energy consumption is calculated for the design using a buffer tank and directly via solar collector (no storage), each completed for New Delhi and Volgograd. The following control strategy must be implemented in the solar-powered DACS and the electrically driven backup heat source.

1. The pump which moves the solar collector fluid is switched on only when a set temperature difference between the collector outlet and the buffer tank is reached.
2. When there is a cooling demand on the DACS, the stored heat in the buffer tank delivers the heat requirement for the generator if the minimum tank temperature meets the required generator tank temperature.

3. When there is a cooling demand on the DACS, but the buffer tank's temperature is below the required generator temperature. The auxiliary heat source is activated to meet the cooling demand.

The backup energy required is assumed to be electrically generated by supplying electrical energy to the solar fluid in the solar collector or the buffer tank. The backup energy is calculated based on the hot water heat requirement, Q_{HW} [31]:

$$Q_{HW} = V_{HW} C_w \triangle T \qquad 8.1$$

where V_{HW}, is the average hot water quantity (litres), C_w, is the specific heat capacity of water (=1.16 Wh/kg K), and $\triangle T$, is the temperature difference between hot and cold water (° C).

The backup heating is supplied via an electrical heating device. The electrical heater is thermally controlled and designed to accept preheated water from the solar collector or heat fluid in the buffer tank. The electrical heater heats as much as is required to reach a set exit temperature. The experimental data presented in Chapter 6, supplied by Najjaran et al. [51], indicates that a generator temperature setting of 190 °C delivers a cooling capacity of 100 W from the DACS chiller. Thus, a temperature of 190 °C is used as the temperature setting for the electrical heater to deliver backup energy when required. Hence, each solar-powered DACS can deliver 100 W of cooling power. The distribution of the number of cooling loads for New Delhi and Volgograd is shown in Figure 8.2. As a result, eight and five solar-powered DACS will be required to meet an 800 Wh (New Delhi) and 500 Wh (Volgograd) cooling load, respectively.

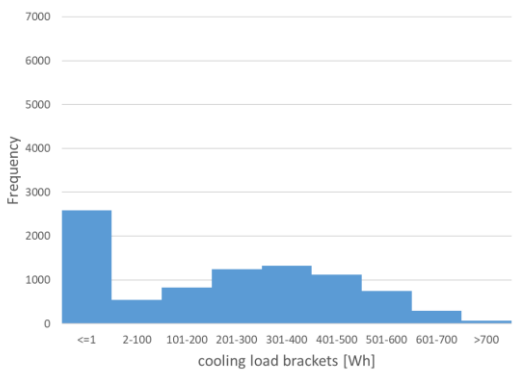

New Delhi

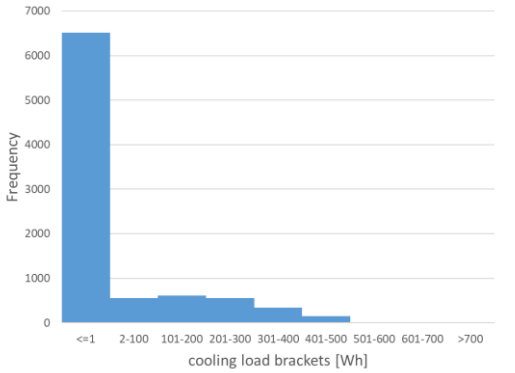

Volgograd

Figure 8.2: Frequency distribution of the number of cooling loads in a year in New Delhi and Volgograd.

8.3 Modelled Results and Energy Performance

8.3.1 Backup hours/day

Table 8.2 shows the number of hours with temperature recordings in the collector or the buffer tank below the 190 °C temperature setting (deficit hours), New Delhi. When the buffer tank is used to boost the temperature of the solar collector and supply the heat source to the generator, there are 3693 hours where a deficit is recorded. In contrast, when heat is provided directly from the solar collector, there are 3930 hours where a deficit is recorded. The electrically powered backup heating is applied to supply the extra heat required to achieve the 190 °C temperature setting. The total recorded energy consumed for the buffer tank and directly via the solar collector is 3829 kWh and 3696 kWh, respectively. By comparison, more auxiliary energy is consumed directly with the solar collector than via a buffer tank.

Also, Table 8.2 shows the hours with temperature recordings in the collector or the buffer tank below the 190 °C temperature setting (deficit hours), Volgograd. When the buffer tank is used to boost the temperature of the solar collector and supply the heat source to the generator, there are 1818 hours where a deficit is recorded. When heat is provided directly from the solar collector, there are 1716 hours where a deficit is recorded. The electrically powered backup heating is applied to supply the extra heat required to achieve the 190 °C temperature setting. The total recorded energy consumed (Wh) for the buffer tank and directly via the solar collector is 1499 kWh and 1091 kWh, respectively. By comparison, more backup energy is consumed via a buffer tank than directly with the solar collector.

Table 8.2: The hours with temperature deficits (backup hours) and the total backup energy consumed for New Delhi and Volgograd.

	New Delhi		Volgograd	
	Buffer tank	Solar collector	Buffer tank	Solar collector
Total backup hours in a year (hours)	3693	3930	1818	1716
Total backup energy (kWh)	3829	3696	1499	1091

Figure 8.3 shows the backup hours per day for the buffer tank and directly via a solar collector for New Delhi and Volgograd. The backup hours per day for the buffer tank and via solar collector change similarly, though the solar collector has more total backup hours in a year. As expected, New Delhi has more backup hours per day in the summer months from June to

September than in February, March, October, and November. For Volgograd, all the backup hours per day occur when there is a cooling load in the summer months from May to September.

	Buffer tank	Solar collector
New Delhi	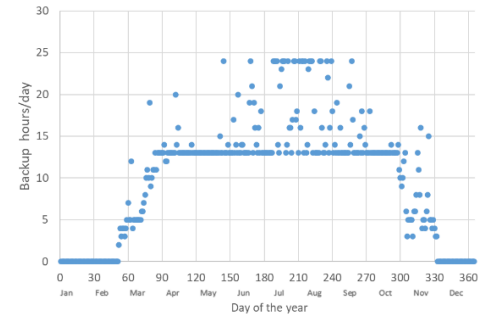	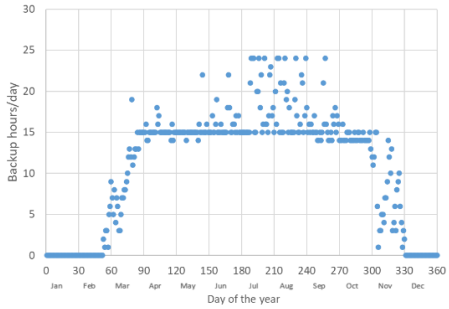
Volgograd	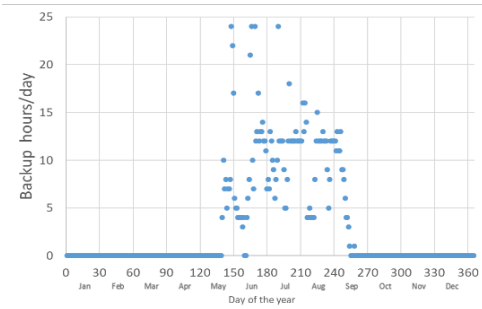	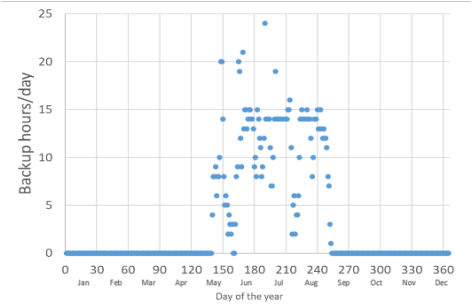

Figure 8.3: Backup hours/day via buffer tank and solar collector for New Delhi and Volgograd.

8.3.2 Backup energy/day

Figure 8.4 shows the backup energy per day for the buffer tank and directly via a solar collector, New Delhi and Volgograd. For New Delhi, the maximum backup energy consumed for the buffer tank was 81 kWh recorded in July, while the maximum backup energy consumed for the solar collector was 33 kWh recorded in July.

For Volgograd, the maximum backup energy per day consumed for the buffer tank is 44 kWh, recorded in July, while the maximum backup energy consumed for the solar collector is 25 kWh, recorded in July. The backup deficit hours per day are similar for the buffer tank and the solar collector. However, the backup energy per day for the buffer tank is significantly larger than the backup energy for the solar collector because the buffer storage tank volume (4.82 litres) is larger than the solar collector volume (2 litres).

	Buffer tank	Solar collector
New Delhi	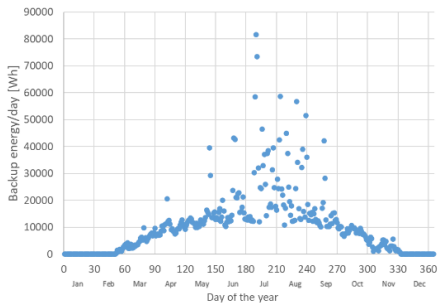	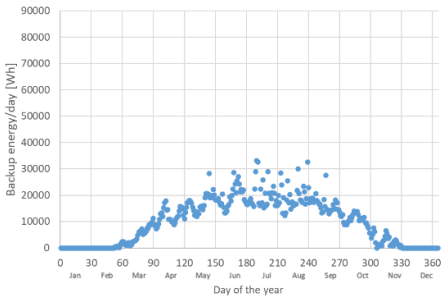
Volgograd	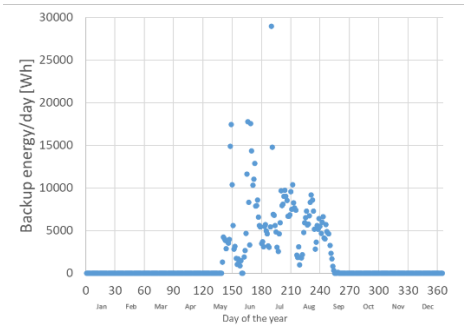	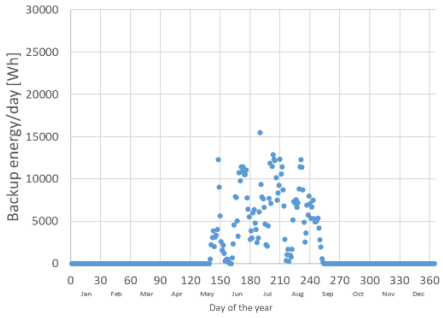

Figure 8.4: Backup energy/day via buffer tank and solar collector for New Delhi and Volgograd.

8.3.3 Solar fraction

The solar fraction is calculated to determine the percentage of the generator's heat requirement generated by the solar collector and buffer tank. Figure 8.5 illustrates the solar fraction for a number of solar collectors and the corresponding buffer tank at different mass flow rates. For both climatic locations of New Delhi and Volgograd, larger buffer tanks required high mass flow rates to deliver higher solar fractions. In comparison, all the solar collector areas had the highest solar fraction at a lower mass flow rate of 1 kg/hr. The buffer tank delivers a higher solar fraction than the solar collector for all collector areas, primarily due to the tank's capacity to optimise performance by smoothing out the variability of the solar radiation and the tank temporarily storing hot water to be used at night when there is a cooling load. The solar fraction is calculated by determining the deficit hours in a year when the cooling load is not met.

When the design focus is to maximise solar fraction for the buffer tank, the mass flow rate is kept constant to suit the buffer tank, Figure 8.6. The deficit hours for the buffer tank reduce as the solar fraction increases. Maximising the solar collector's solar fraction uniformly reduces the buffer tank's solar fraction as the deficit hours increase and the collector area increases.

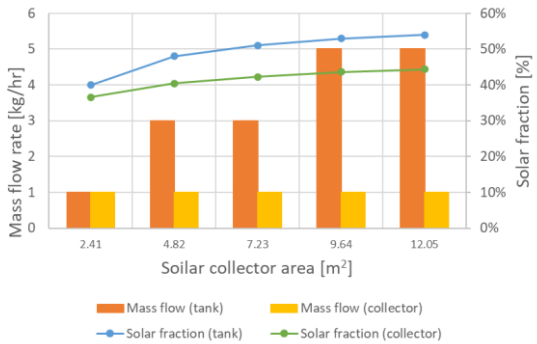

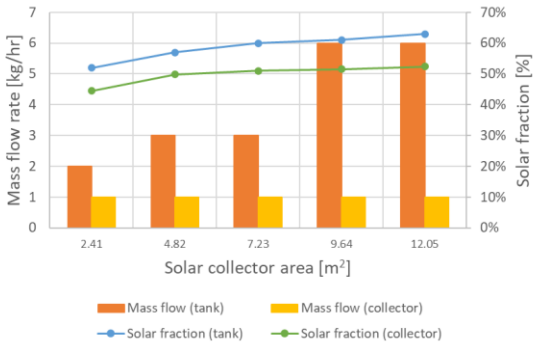

New Delhi	Volgograd

Figure 8.5: Mass flow rate and solar fraction for various solar collector areas and buffer tanks for New Delhi and Volgograd.

	Buffer tank	Solar collector
New Delhi	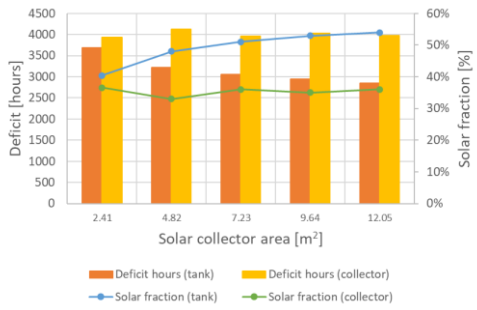	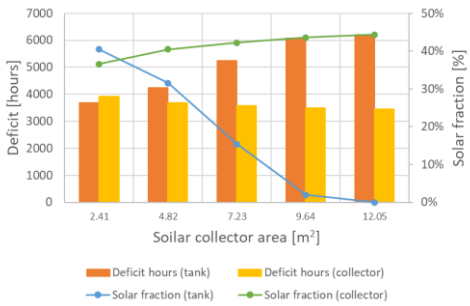
Volgog-rad	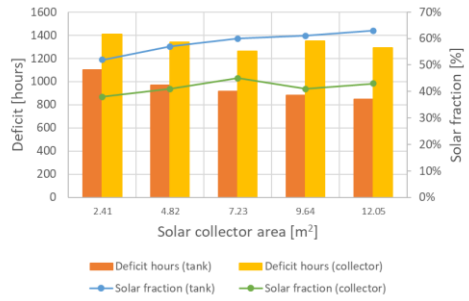	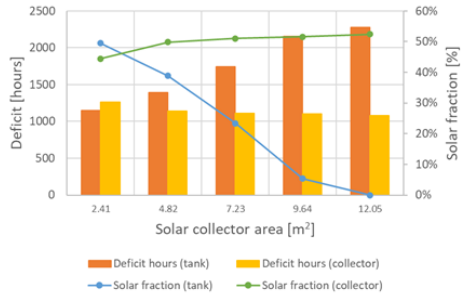

Figure 8.6: Deficit hours and solar fraction at fixed mass flow rate (1kg/hr) for various solar collector area and buffer tank for New Delhi and Volgograd.

For New Delhi, the 7.23 m^2 solar collector area incorporating a buffer tank must be selected to meet a minimum of 50% solar fraction. Thus, two DACS units, each with a 7.23 m^2 solar

collector area incorporating a buffer tank, will be sufficient to meet all the building cooling loads in New Delhi. For Volgograd, a 2.41 m^2 solar collector area embedded with a buffer tank delivers a minimum of 50% solar fraction. Thus, two DACS units, each with a 2.41 m^2 solar collector area incorporating a buffer tank, will be sufficient to meet all the building cooling load in Volgograd.

8.3.4 Hot store heat loss

The solar fraction for the buffer tank is limited because there is a significant heat loss from the buffer tank to the environment, Figure 8.7. For Volgograd, the temperature for fluid in the buffer tank reduces from 221 °C at 20:00 hours to 121 °C at 10:00 hours the next day, indicating a 100 °C temperature reduction over 10 hours through the night when there is a cooling load. Subsequent periods from 20:00 to 10:00 hours the next day show a similar 100 °C temperature reduction pattern over time. Similarly, New Delhi has a typical 100 °C temperature reduction from 20:00 to 10:00 hours the next day when there is cooling demand. Such a significant 8 °C temperature reduction per hour encourages cold energy storage. For example, the energy from the hot store at 20:00 hours is used to generate cooling and stored to be used later in the evening till the morning when the solar collector generates enough heat.

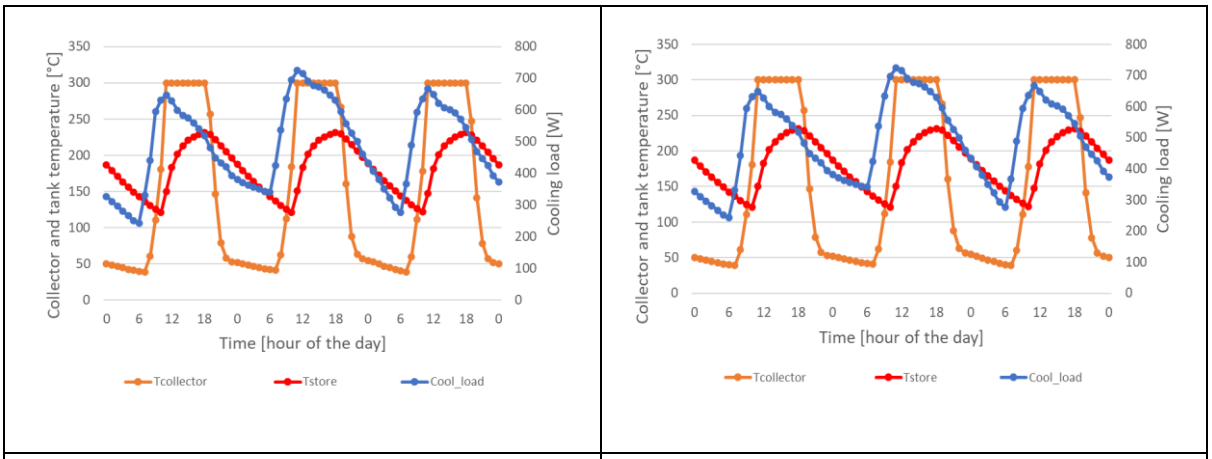

New Delhi	Volgograd

Figure 8.7: Solar collector and buffer tank temperature and cooling load variation over three days (12-14 June), New Delhi and Volgograd.

8.4 Discussion

This Chapter presented the amount of backup electrical energy required to meet the deficit between the building's cooling load and the cooling power supplied by a solar-powered DACS.

The results compared the needed backup energy from a solar collector and backup energy from a buffer storage tank for two case study cities, New Delhi and Volgograd. The volume of the buffer storage tank is more than twice that of the solar collector. Consequently, the backup energy required for the buffer tank is significantly larger than that the solar collector needs. The total backup hours of the solar collector are higher than that of the buffer tank. Thus, a reduced buffer storage tank for solar-powered DACS is essential when backup energy is to be utilised.

The results show that solar collector and storage design, which purely considers the optimum generator temperature, will be inadequate until the amount of backup energy to be applied is factored in a balanced energy supply analysis. Nonetheless, using backup energy in the solar-powered DACS improves the cooling system's reliability. The backup energy design has been applied to New Delhi and Volgograd climatic regions. The design methodology can be used in other hot climate regions with significantly high summer cooling demand for residential buildings, offices, or building types.

Further investigation can include modification of the backup heat sources, such as gas-fired heaters, and cost and environmental impact analysis of the solar-powered DACS cooling with or without the backup energy system. Incorporating the hot store in the solar thermally driven, hot-water fired DACS compared to cooling with conventional, electrically powered AC system offers advantages in energy efficiency from using renewable energy from the sun, reduced operational carbon impact and reliance on fossil fuels, and suitable for cooling in off-grid areas. However, the hot water fired DACS may require additional hot water distribution in building types, and they have a lower cooling capacity [40,68] than the conventional AC system [79,123,139] for a wide range of climates and building types.

8.5 Conclusion

The following conclusions are drawn from this study:

1. For both New Delhi and Volgograd, the backup energy required for the buffer tank is significantly larger than that needed for the solar collector, primarily due to the volume of the buffer storage tank being more than twice that of the solar collector.
2. For New Delhi and Volgograd, the buffer tank system requires more backup energy than the solar collector. However, the buffer tank system for New Delhi has fewer total

backup hours in a year than the solar collector. In contrast, for Volgograd, the buffer tank system has fewer total backup hours in a year than the solar collector.

3. Applying backup energy in a solar-powered DACS system helps the cooling system meet all the building cooling load, thus improving the cooling system's reliability. Incorporating backup electrical energy is energetically and economically advantageous for direct solar collector use than the buffer tank, and could potentially maximise the benefits for buildings with large solar fraction and high thermal loads.
4. Using a small buffer store of 2 litres/ m^2 of solar collector area, the solar fraction was between 40-65 %.

Chapter 9 : Cold energy storage

9.1 Introduction

The optimised solar and storage system modelled with TRNSYS was presented in Chapter 7, and in Chapter 8, electrical backup energy was used to meet the lag in cooling demand. This Chapter evaluates cold energy storage as an alternative to the hot storage analysis previously presented. The methodology used is described in section 9.2. The results are presented in section 9.3, followed by the discussion and conclusion in sections 9.4 and 9.5, respectively.

9.2 Methodology

9.2.1 System description and design logic

Cold energy storage, as utilized in the building cooling application, is the storage of cooling capacity in a storage medium at temperatures below the nominal temperature of the building space [125]. Figure 9.1 illustrates the connection between the chiller, solar collector, cold store, and heat exchanger delivering cold air to the building. Three operating modes are implemented in the cold storage design. Firstly, during the charging process, the cooling capacity generated by the chiller's evaporator is stored in the cold storage device. Secondly, the cooling capacity from the evaporator can be used directly by the heat exchanger to meet the building's cooling demand. Thirdly, during the discharge process, the stored cooling capacity of the cold storage device is delivered to the heat exchanger.

Figure 9.2 illustrates the combined cooling and heating where a hot store is added to the cold store mode (Figure 9.1). Cold and hot storage allows for efficient utilisation of surplus energy from the solar collector, reducing energy wastage to balance the supply of solar energy and cooling and heating. Combining cold and hot storage enhances flexibility in varying cooling and heating demands. However, using cold and hot stores requires space around the residential building.

Figure 9.3 illustrates the cooling and cooling storage logic applied in the operating system. The logic starts with an assessment of the difference between demand and supply. Where the deficit is not tolerable, the cold store is used if available, or electrical backup is used to cover the deficit. On the other hand, where demand exceeds the supply, the cooling capacity is stored in the cold store until the cold store is full. Alternatively, excess solar energy supply past the cold storage capacity is stored in the hot store or sent to a dump heat exchanger.

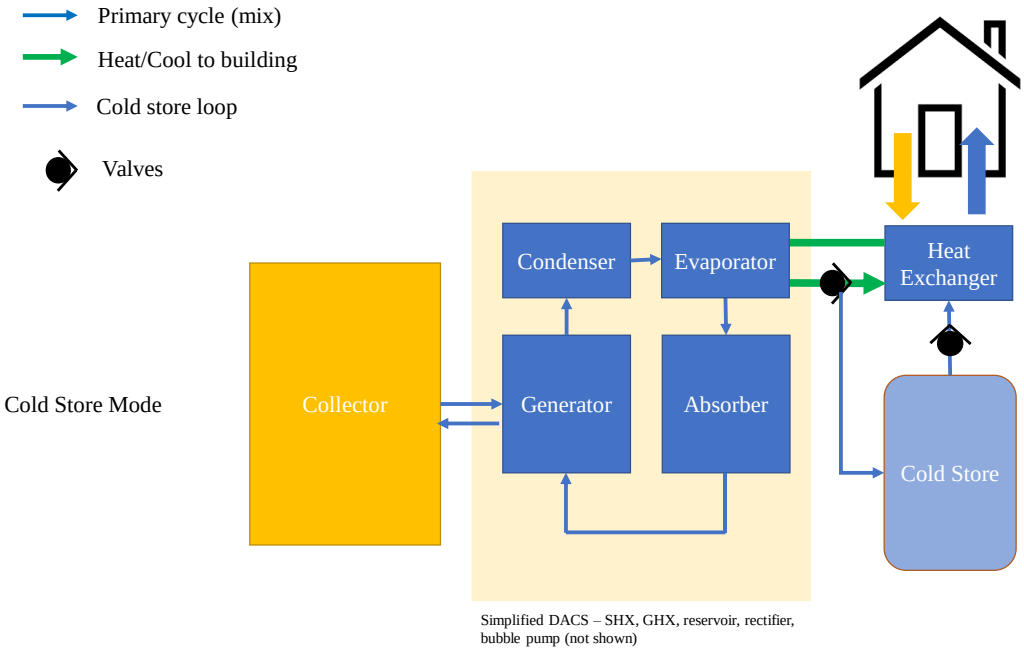

Figure 9.1: Schematic showing the connections between the solar collector, DACS, cold store, and heat exchanger delivering cold air to the building.

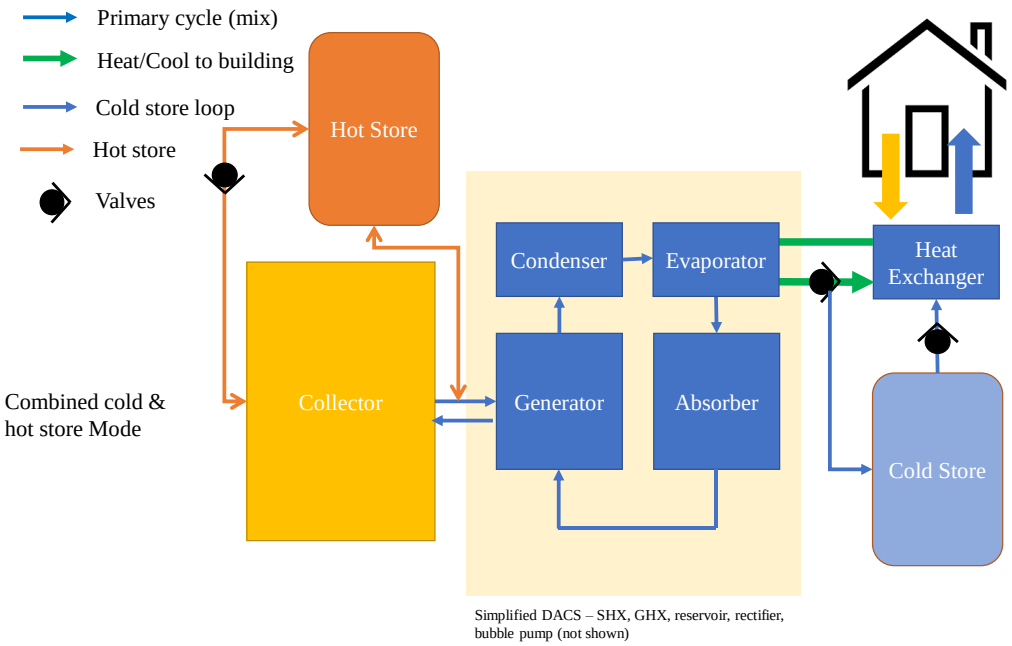

Figure 9.2: Schematic showing the connections between the solar collector, DACS, cold store, and heat exchanger delivering cold air to the building.

Figure 9.4 illustrates the piping scheme for the chiller, cold storage, and air handler, where the locations of the valves and pumps are indicated. While charging the cold store, valve V2 closes,

and valve V1 opens, so the chiller pumps cooling capacity via pump P1 and valve TWV1 to the cold store.

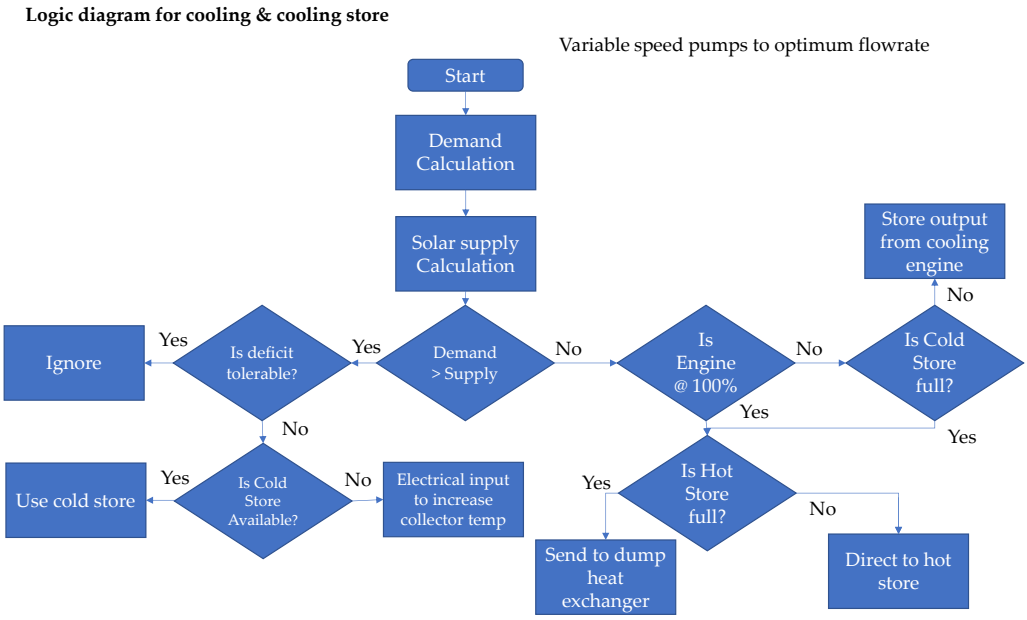

Figure 9.3: Logic diagram for cooling and cooling storage.

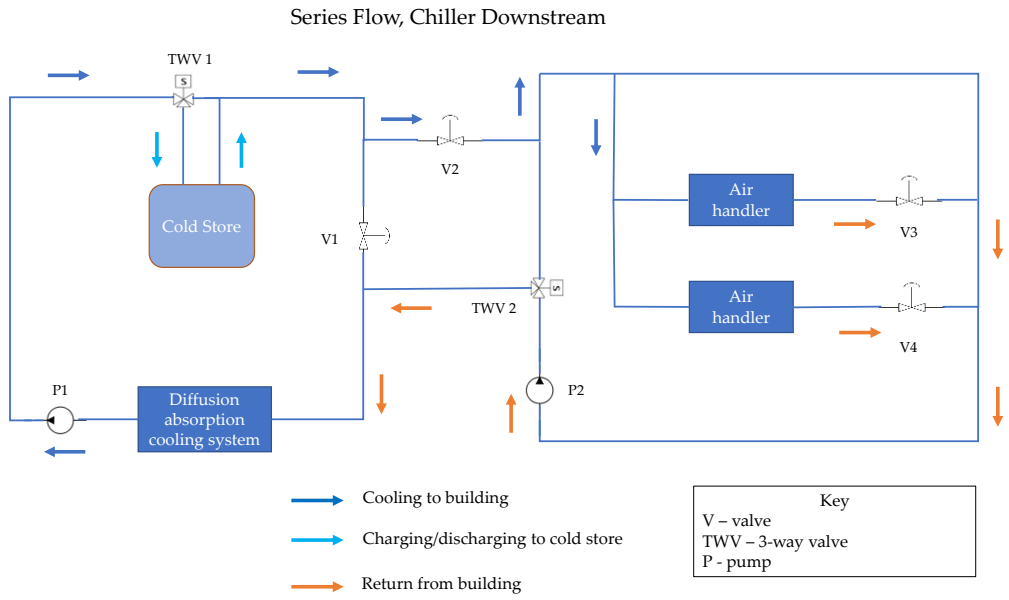

Figure 9.4: Piping scheme for the DACS, cold storage, and air handler (adapted from ASHRAE handbook [125]).

During discharge of the cold store, pump P1 is utilised to pump the cooling capacity from the cold store to the air handlers via valve V2 open and V1 closed. During direct cooling from the

chiller to the handlers, TWV1 closes the cold store, valve V1 is closed, and valve V2 opens. In the three scenarios, the return from the air handlers to the chiller is via valves V3 and V4 and through pump P2 and three-way valve TWV 2.

9.2.2 Cold storage capacity

In sensible heat storage (SHS), thermal energy is stored by utilising the heat capacity and changing the temperature of the material during the charging and discharging processes [71]. The amount of sensible thermal energy stored in the storage tank for cooling is determined [72]:

$$Q_{sc-shs} = mC_p(T_f - T_i) \qquad 9.1$$

where Q_{sc-shs} is the sensible heat energy stored for cooling (J), C_p is the specific heat capacity of the medium (kJ/kg·K), m is the amount of storage material (kg), T_f is the final temperature of the storage medium (°C), and T_i is the initial temperature of the storage medium (°C). The energy stored for the SHS system, Q_{sc-shs}, is equal to the amount of heat stored for cooling calculated as:

$$Q_{sc} = k\,(E_a - E_d) \qquad 9.2$$

where E_a is the available energy for cooling (J), E_d is the building energy demand (J), and k is the coefficient of performance of the cooling system. Thus, Equations 9.1 and 9.2 can be used to calculate the mass of material stored with the known amount of heat stored.

Latent heat storage (LHS) is based on the heat absorption or release when a storage material changes phase from liquid to solid or liquid to gas or vice versa [70,71]. The storage capacity of the LHS with a material that undergoes a phase change is determined [72]:

$$Q_{sc-lhs} = m\left[C_{sp}(T_m - T_i) + a_m \triangle h_m + C_{lp}(T_f - T_m)\right] \qquad 9.3$$

where Q_{sc-lhs} is the latent heat energy stored for cooling (J), C_{sp} is the average specific heat between T_i and T_m (J·kg^{-1}·K^{-1}),), C_{lp} is the average specific heat between T_m and T_f (J·kg^{-1}·K^{-1}), m is the amount of storage material (kg), T_f is the final temperature of the medium (°C),), T_m is the melting temperature from the medium (°C), T_i is the initial temperature of the storage medium (°C), a_m is the fraction melted, and $\triangle h_m$ is the heat of fusion per unit mass

(J/kg). Likewise, Q_{sc-lhs} is equal to Q_{sc}, thus, the mass of stored LHS material can be calculated from Equations 9.2 and 9.3.

9.2.3 Model of the cold store heat loss

There is potential for a cold storage tank with the stored cooling capacity to lose or gain heat with the surrounding environment. Thus, the cold store heat loss is modelled [233]:

$$Q_{loss} = k_{cst} A_{cst} (T_{env} - T_{cst}) \qquad 9.4$$

where Q_{loss} is the cold store heat energy loss between the cold storage tank and the environment (W), k_{cst} is the heat loss coefficient of the cold tank (W/m^2°C), A_{cst} is the heat transfer area of the cold storage tank (m^2), T_{env} is the environment temperature around the cold storage tank (°C), and T_{cst} is the temperature of the cold storage medium (°C). The heat transfer coefficient and the tank transfer area must be reduced as much as possible and are constant for a given cold store.

9.3 Results

The potential cooling energy is calculated from the energy stored due to the net heat collected from the solar collector, Figure 9.5. The cumulative energy stored for cooling is determined by the difference between the building's cooling energy demand and the energy available from the solar collector. Throughout the year, there are over 142 MJ and 123 MJ running total of potential cooling energy that can be stored or used for New Delhi and Volgograd's eight and five diffusion absorption cooling systems, respectively.

Calculating the heat loss of the cold storage medium is essential to determine how long it will take for the cold storage to lose thermal energy over time. The cooling engine requires a minimum of 60 litres of cold storage per square meter of collector area for the SHS system [234]. In contrast, the LHS system storage size is selected to be a third of the SHS system [71].

Figure 9.6 shows the heat energy loss from the cold store, with a U-value of 0.27 W/m^2°C, as a function of the ambient temperature for the SHS and the LHS systems. For an SHS system with a cylindrical tank volume of 144 litres and at an ambient temperature of 25 °C, it takes about 10-20 days to lose the heat energy from the cold store temperature of -5 °C. For the LHS system with a cylindrical tank volume of 48 litres and at an ambient temperature of 25 °C, it takes about 10-20 days to lose the heat energy from the cold store temperature of -5 °C.

New Delhi	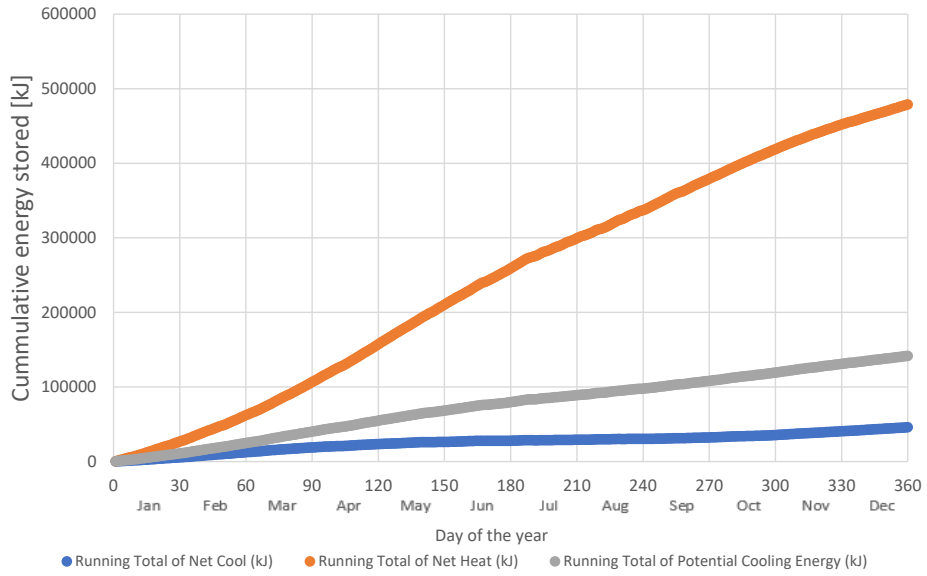
Volgograd	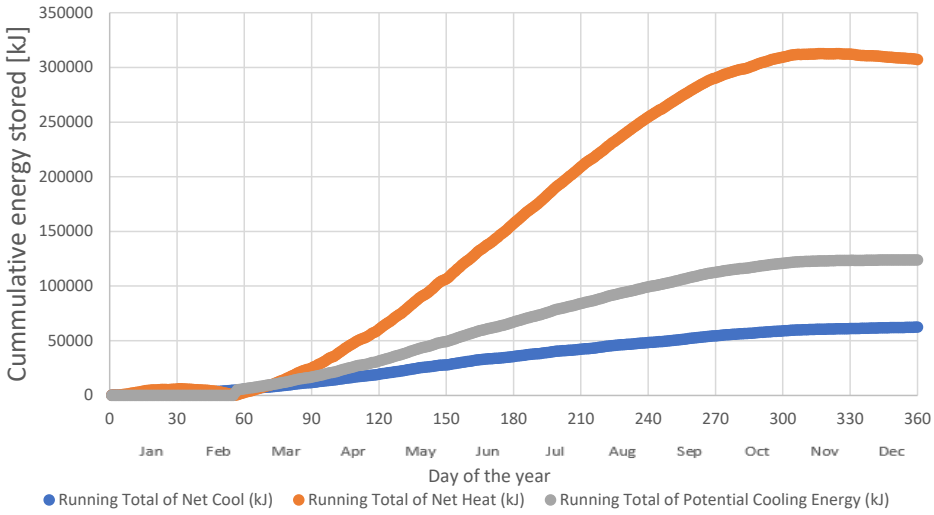

Figure 9.5: Cumulative energy for net cooling, net heating, and potential cooling energy for New Delhi and Volgograd.

Figure 9.7 shows the mass of cold storage material and the energy stored for LHS and SHS. The sizing strategy is that the cooling system operates with the cooling engine running at full capacity using the cold store for 24 hours to meet the building cooling load. Excess cooling is stored when the chiller output exceeds the building load. On the other hand, when the chiller output is less than the building load, the cold store meets the deficit requirement. The building energy analysis in Chapter Four indicated that the maximum daily cooling load for New Delhi

and Volgograd TE buildings ranged between 28800 and 50400 kJ daily. As a result, for the New Delhi LHS cold storage medium, 200 kg of storage material can be used to meet the daily cooling load demand throughout the year. 500 kg of cold storage material is needed for the New Delhi SHS cold storage medium to meet the daily cooling load throughout the year. For the Volgograd LHS cold storage material, 120 kg of storage material can be used to meet the daily cooling load demand. In contrast, 270 kg of cold storage material is needed for the SHS cold storage medium to meet the daily cooling load throughout the year.

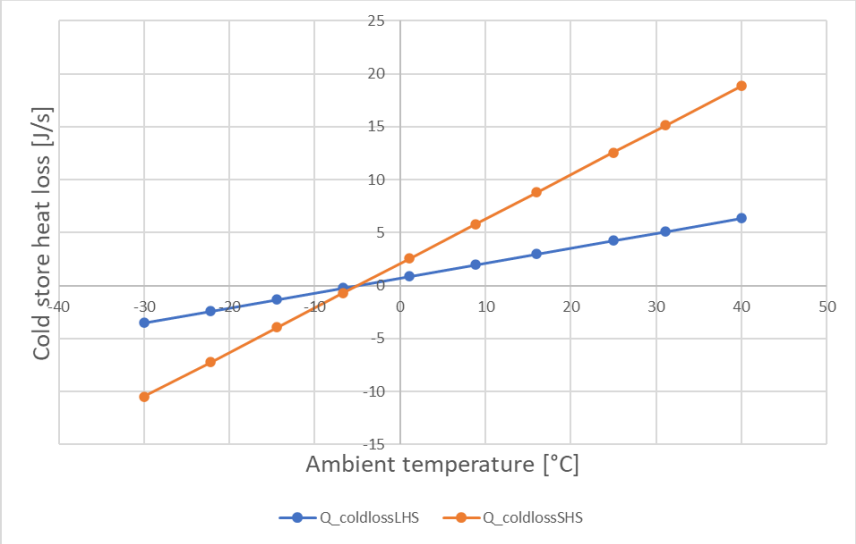

Figure 9.6: Cold store heat loss with a variation of the environment's temperature for SHS and LHS.

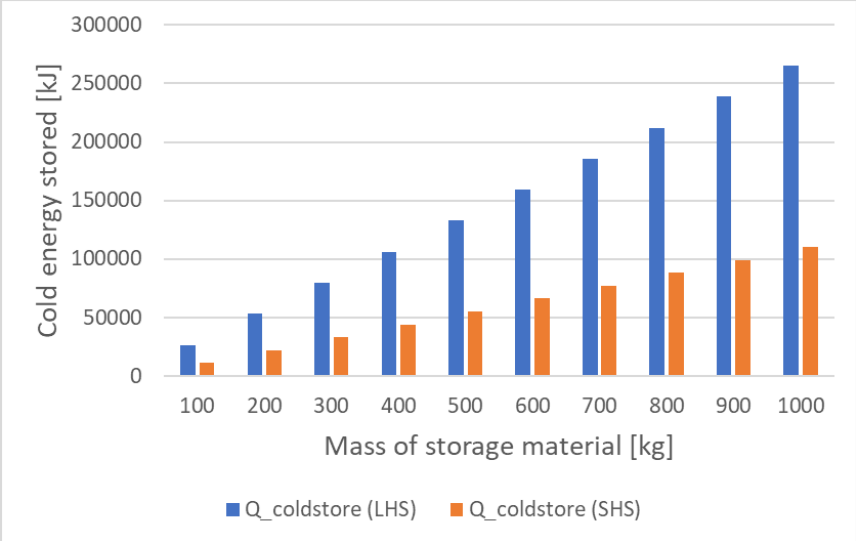

Figure 9.7: The mass of cold storage material and the energy stored for LHS and SHS.

9.4 Discussion

From an energy source, the solar collector perspective, sufficient cooling energy can be stored in the SHS cold store or LHS cold storage medium. The SHS storage material's mass is larger than that of the LHS storage medium because LHS stores 3-14 times more heat per unit volume than SHS, such as water [71,72]. LHS system has less cold tank energy loss rate than the SHS because of the smaller tank volume and surface area exposed to the environment.

Nonetheless, LHS systems must exhibit desirable thermodynamic, kinetic, and chemical properties such as high thermal conductivity, high density, high fusion heat, suitable phase change temperature range, compatibility with tank construction, and not be flammable [72,73,232].

Ethylene glycol and water mixture are selected as the fluid for the SHS system to avoid freezing in the cold storage tank at -5 °C temperature at the target store [270]. On the other hand, a eutectic water-salt solution (e.g., Na_2CO_3-H_2O, wt.% of salt 0.059) is chosen as the material for the LHS system due to its high fusion heat (310.23 kJ/kg) and suitable phase change temperature range (-2.1 °C) [232]. However, eutectic water-salt solution as phase change materials are prone to issues such as phase separation, supercooling, and corrosion between the material and the storage container [72,73,232]. The unit mass costs of the nitrate salts are moderate (0.4-0.9 $/kg) compared to the alternative storage material, glycols (2 $/kg) [69,70]. Low heat loss at low ambient temperatures suggests that storing the cold tank on the ground will lose less energy over time. Also, when excess cold air from the absorption cooling system is not needed to cool the building, such cold can be dumped around the cold tank to minimise heat loss.

The practical application of the LHS in the cold energy storage would need a heat exchanger such as screw, shell and tube, and module PCM heat exchangers [271], between the phase change material and the energy transfer medium via the cold store to the air handler units. The sizing of the cold storage tanks is between 120-500 litres compared with domestic hot water tanks sizing of 90 litres/person/day and residential cold water cisterns with a minimum capacity of 230 litres [126]. The cold store can be situated within or outside the residential building. However, underground installations save space, and there could be advantages with temperature control compared to storing to ambient air temperature [271]. The cold storage tank's material, less than 100 m^3, is likely rectangular and typically made of galvanised sheet

steel [55]. Further development of this research will include characterising the discharge phase of the storage unit for dynamic analysis and the thermal effects of different system geometries and heat transfer coefficients.

9.5 Conclusion

This Chapter provides a fundamental study on storing cold energy using a sensible and latent heat energy storage medium. The energy capacity is the same as that of a solar collector system; however, the mass of storage material differs. The material stored for the LHS system is smaller than that for the SHS system, dictating a smaller space requirement and heat loss. However, several phase change material issues, such as phase separation, supercooling, and corrosion, must be addressed for the LHS system to deliver a reliable operation.

Chapter 10 : Economic evaluation and environmental impact assessment

10.1 Introduction

The optimised solar and storage system modelled with TRNSYS was presented in Chapter 7, and in Chapter 8, electrical backup energy was used to meet the lag in cooling demand. This Chapter presents the economic evaluation and the environmental impact of the solar-powered DACS system with cold storage for building cooling and direct heating from solar collectors for building heating. The financial and environmental evaluation criteria and method are presented in section 10.2. The results are presented in section 10.3, followed by the discussion and conclusion in sections 10.4 and 10.5, respectively.

10.2 Economic and environmental evaluation method

The benefit of adopting a solar-powered DACS must be proven economically and according to avoided operational CO_2 emissions, as well as thermodynamically. Local variations in the unit cost of energy play a key role in determining this economic merit. The financial benefit and avoided carbon emissions can be calculated using locally available energy pricing and carbon impact factors (Table 4.5 and 4.6). It is assumed that electrically powered heat pumps power heating and cooling.

Using solar thermal energy avoids using electricity and natural gas to meet building cooling and heating demands. Table 10.1 lists the solar fraction for cooling and heating for all the climatic locations.

Table 10.1: Solar fraction for cooling and heating at each location

	Cooling energy (via cold store) solar fraction	Heating energy solar fraction
Tunis, Tunisia	100%	100 %
New Delhi, India	100 %	100 %
Volgograd, Russia	100 %	70 %
Swansea, UK	100 %	74 %

The payback time is when the cumulative fuel savings equal the total investment [229], as defined in section 3.7.1. The discounted payback time is used because the calculation discounts the fuel savings. The discounted payback time, n_P, is calculated using the equation [229]:

$$n_P = \frac{\ln\left[\frac{C_s(i_F - d)}{FLC_{F1}} + 1\right]}{\ln\left(\frac{1 + i_F}{1 + d}\right)} \qquad 10.1$$

where F is the solar fraction, L is the load (kWh), C_{F1} is the first-year unit energy cost delivered from fuel, and it is the product of fuel heating value and heater efficiency (/kWh), C_s is the total cost of the solar system, i_F is the fuel inflation rate, and d is the annual market discount rate.

10.3 Results

10.3.1 Annual operational costs of solar-powered DACS compared to heat pumps.

The operational costs for implementing a solar-powered DACS and the heat pumps to deliver the cooling and heating demands for a T.E. building are shown in Figure 10.1. Electricity is assumed to cover any backup energy and the power for the heat pumps (HPs).

There are no operational costs for the solar-powered DACS because all the cooling energy is provided by solar thermal energy via cold storage. On the other hand, the operating costs for the heat pumps, as expected, reduce with increasing HP's coefficient of performance. Volgograd HPs have higher cooling costs because of the high costs of electricity price coupled with the high cooling energy consumption. New Delhi HPs have the second-highest cooling costs due to the higher cooling energy than Tunis and Swansea. Swansea has the lowest cooling cost due to the small cooling energy demand.

For heating costs, Volgograd and Swansea climatic locations incur costs to meet the T.E. building heating demand via DACS. Besides, DACS costs for Volgograd are higher than Swansea's due to higher heating energy and electricity costs. The operational heating costs for Swansea and Volgograd are less than HP, with COPs up to 3. HP operational heating costs for Tunis and New Delhi are below $25.

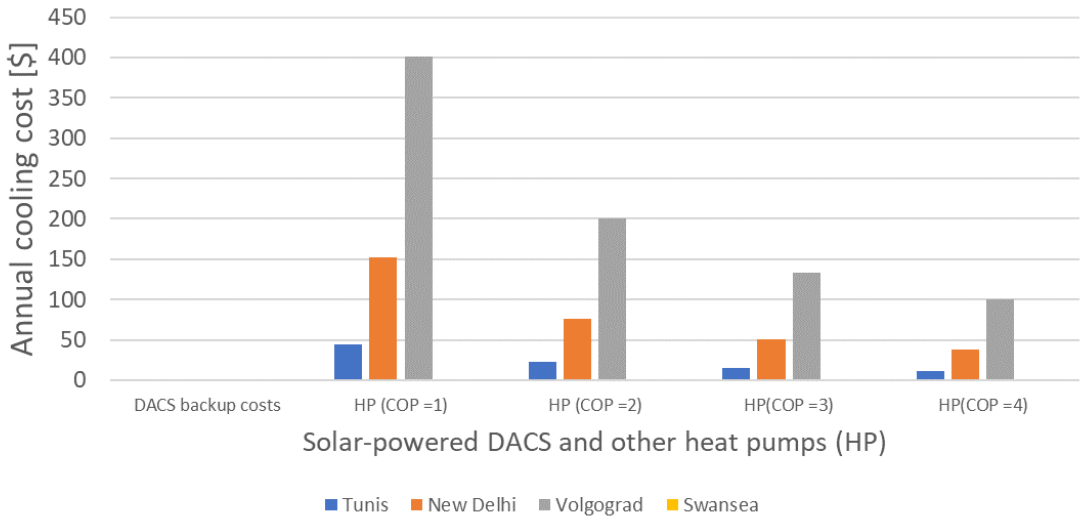

(a) Cooling cost

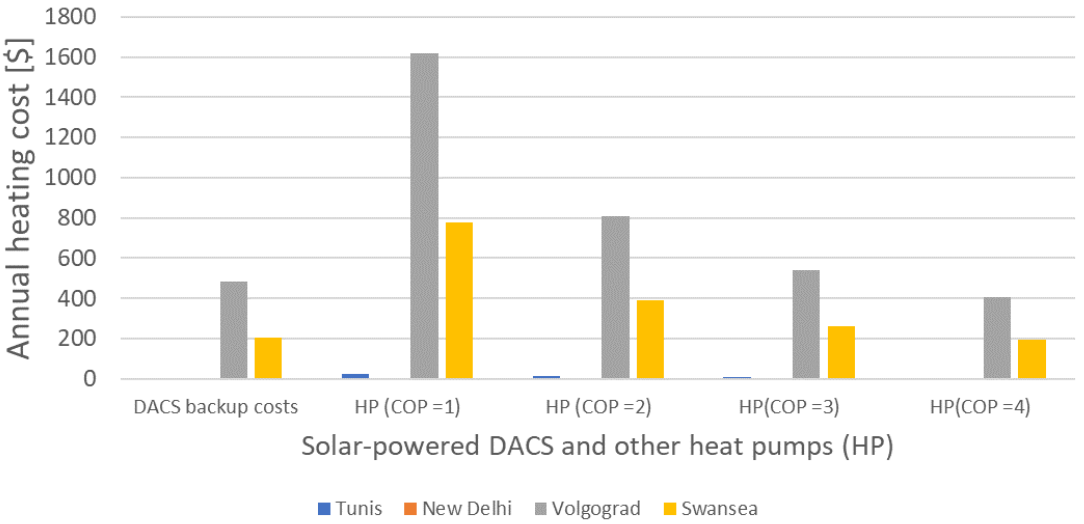

(a) Heating cost

Figure 10.1: Comparing the operational energy consumption of the solar-powered DACS and other heat pumps for Tunis, Volgograd, New Delhi, and Swansea.

10.3.2 Annual operational carbon emissions of solar-powered DACS compared to heat pumps.

The operational carbon emissions for a solar-powered DACS compared to the heat pumps used to deliver the building cooling and heating demand for a T.E. building are shown in Figure 10.2. Like the operational costs, there are no cooling operational carbon emissions for the DACS because all the cooling energy is provided by solar energy. Moreover, operational carbon emissions for the heat pumps, as expected, reduce with increasing HP's coefficient of

performance. New Delhi HPs have higher cooling carbon emissions because of the high carbon emission factor and cooling energy consumption. Tunis HPs have the second-highest cooling carbon emissions due to the higher cooling energy and emission factor than Volgograd and Swansea. Swansea has the lowest cooling operating carbon emissions due to the smallest cooling energy demand.

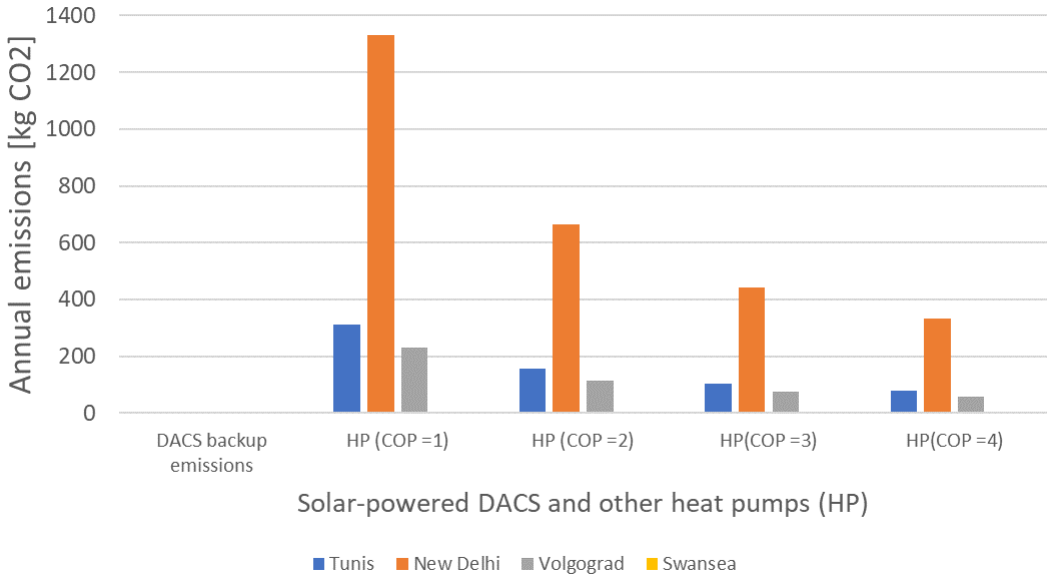

(a) Cooling carbon emissions

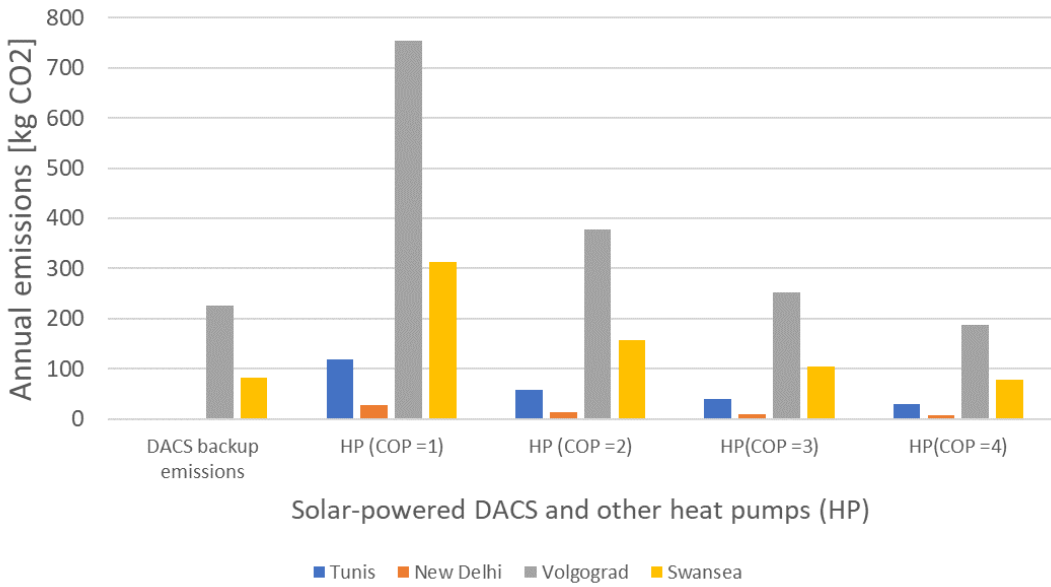

(a) Heating carbon emissions

Figure 10.2: Comparing the operational carbon emissions of the solar-powered DACS and other heat pumps for Tunis, Volgograd, New Delhi, and Swansea.

For heating costs, Volgograd and Swansea climatic locations emit operational carbon to meet the T.E. building heating demand via DACS. Besides, DACS operational carbon emissions for Volgograd are more than twice that of Swansea due to higher heating energy and electricity emission factors. The heating operational carbon emissions for Swansea and Volgograd are less than all the HP, except the HP (COP =4) that emits 4 $kgCO_2$ than the DACS. Due to high heating energy, Tunis HPs have the third largest carbon emissions than New Dehli. New Delhi has the lowest HP operational heating emissions, below 29 $kgCO_2$.

10.3.3 Payback time

Table 10.2 presents the discounted payback time for the four climatic locations based on cooling and heating loads. The costs of the solar-powered DACS comprise equipment costs (€9,724) and installation costs (€7,000). The equipment costs were taken from estimates suggested by Altun and Kilic [189], and the installation costs were taken from low-end estimates reported in the industry for air source heat pump installation costs [272].

The payback time for the cooling-dominated climates, Tunis and New Delhi, is higher than the heating-dominated climates, Swansea and Volgograd, because of the high cost of electricity. The higher the building's thermal energy and higher energy prices, the lower the payback time. The DACS payback compares with air source heat pumps, which are reported to have payback between 3 to 15 years, depending on the local electricity cost and subsidy level [273].

Table 10.2: Discounted Payback time for combined cooling and heating at each location

	Payback time, discounted (years)	Cooling and heating loads (kWh)
Tunis, Tunisia	12.7	1006
New Delhi, India	6.77	2130
Volgograd, Russia	0.84	3203
Swansea, UK	2.13	1678

10.4 Discussion

The solar-powered DACS, despite the effective COP of 0.2, saves on the operational cooling costs for all climatic locations, with the most significant savings made at small heat pump COPs for Volgograd, New Delhi and Tunis. The most significant operational cost savings are made for heating for Volgograd and Swansea due to the high heating energy and electricity costs for

both zones. These operational cost savings are likely to be pronounced in extreme cold climates like Volgograd, where air source heat pumps are likely to operate with COPs between 1 and 2 in extreme cold climate conditions in the winter [274]. In that case, though there are DACS backup costs, over $1100 can be saved when HP COP =1 and $323 when HP COP =2. For Swansea, where the mean air source heat pump in winter is likely between 2 and 3 [274], similar costs are incurred when comparing the DACS backup costs with those of the HPs. Hot thermal storage implemented in the DACS heating systems presents the opportunity to increase the DACS solar fraction, thereby reducing the DACS backup costs and improving the cost competitiveness with HP COPs greater than 3.

From the environmental impact perspective, the DACS avoids cooling operational carbon emissions in all climatic locations, which contributes to the decarbonisation of the energy supply system. Likewise, for the heating system, the DACS potential to reduce operating carbon emissions increases as the building energy increases and HP COPs are low. Thus, the solar-powered DACS has a significant potential to reduce the 28% of global energy-related CO_2 emissions in buildings [3,5]. This environmental impact assessment is based on the assumption that HPs are powered by electricity from fossil fuel primary energy sources. Thus, the environmental impact of the HPs could be improved when the electricity powering the HPs is supplied from renewable energy sources such as solar photovoltaics. Nonetheless, the operating carbon savings apply to combustion or gas-powered (fossil fuel) heating systems that have an efficiency of less than 1 [135,144].

The payback time for the cooling-dominated locations is not likely to be improved for air source heat pumps with COPs similar to those around 1.172 [275] to the alternative air conditioners. Similarly, the payback of heat pumps during very cold winter efficiency is likely to be similar to the alternative gas boilers (efficiency around 85%) [87,144], thus reducing the heat pump's annual energy savings. At constant fuel inflation and discount rates, bigger buildings with higher thermal loads will likely have lower payback times than calculated in this research because more solar savings will be achieved. The equipment and installation costs for the solar-powered DACS are likely to be lower than the estimated prices taken from published literature. As the DACS technology matures, the uptake increases to the mass market and installers become familiar with the system; there is likely a cost reduction in capital costs compared to current costs. Additionally, the solar-powered DACS are likely to qualify for the financial support currently benefited by heat pumps in some parts of the world, lowering uptake

costs. Future economic analysis can incorporate operational costs such as maintenance, inspection, and local financial incentives.

10.5 Conclusion

Utilising solar-sourced heating and cooling leads to a significant reduction in energy fossil fuel consumption, and hence CO_2, in hot climates and reduces the heating demand during colder periods. The direct financial benefits are more difficult to justify because of the low cost of conventional fuel in some locations.

The operating cost and carbon emissions analysis has shown that the solar-powered DACS significantly contributes to decarbonising the energy supply system and providing cost savings. Thus, the research has shown that energy analysis of heating and cooling energy systems must include environmental and economic analysis.

Payback time analysis shows that buildings with higher thermal loads will likely have higher solar savings, leading to an improved payback period.

Chapter 11 : Discussion

This thesis has focussed on studying the design of a solar-powered diffusion absorption cooling and heating system to meet building cooling and heating demand for a TE building in four case study locations in New Delhi, India, Volgograd, Russia, Tunis, Tunisia, and Swansea, UK. The research has highlighted many scientific and practical issues, from designing and operating solar-powered diffusion absorption cooling and heating systems to meeting building cooling and heating loads. This Chapter collates the individual Chapter discussions so that the overall implications of the research findings can be made.

11.1 Modelling and simulation of building energy performance

New buildings and some existing buildings must have thermally efficient envelopes and are likely to require renewable energy systems to reduce thermal energy consumption and achieve the NetZero goals for 2030 and beyond. The research demonstrates the benefits of adopting thermally efficient building envelopes. In hot climates, the use of TE buildings can result in a reduction of over 70% in fossil fuel consumption for cooling, while in colder climates, the reduction in heating consumption can be around 28%.

Cost analysis reveals that in some countries, the direct economic benefits of installing thermally insulating materials and adopting sustainable technology may be minimal. Local fuel costs, often influenced by subsidies, discourage the use of such materials as the reduction in energy costs is not significant enough to offset the additional construction expenses, resulting in long payback periods. However, this economic consideration oversimplifies the broader local and global costs associated with higher CO_2 emissions, such as flood defence, crop irrigation, and land loss. It also overlooks the local advantages of price stability, energy security, and improved cash flow for building occupants.

Further analysis is needed to examine representative buildings that reflect typical homes in each climate, considering various design aspects such as building materials, geometries, and construction techniques. As buildings increase in size, the surface area to volume ratio decreases, leading to reduced energy loss per unit volume. Further investigation of building design can encompass modifications in dwelling type, size, occupancy, thermal characteristics of building envelope materials, building techniques, geometry, climatic zone, and desired thermal comfort level. Efficient behaviour should be considered, including occupant habits, room temperature settings, and efficient building envelope components such as windows,

walls, roof, and flooring. A refined model should also address the electrical power requirements for pumps and account for the transient effects of energy capture technology.

The IEA's projection of the global energy system reaching NetZero by 2050 includes curbing energy demand through energy efficiency improvements. This research indicates that building energy efficiency through the thermal envelope could yield financial savings as well as reduce energy usage and avoid carbon emissions.

11.2 Solar heat energy production and storage

The heat energy generated by the XCPC solar collector was modelled to meet the heat source requirement for meeting the TE building's cooling and heating loads for Tunis, Volgograd, New Delhi, and Swansea climatic regions. The emphasis has been on assessing the heat energy generated from the solar collector to meet the building's heating demand, though comparable results for cooling were presented.

As expected, the predominantly cold climates recorded high heating power deficits, while the predominantly hot climates recorded high cooling deficits. Comparing the predominantly cold climates, Swansea and Volgograd, the Volgograd heating deficit is higher than that of Swansea because of the higher heating load. Although, Swansea recorded higher deficit hours than Volgograd. The heating power deficit for Tunis and New Delhi occurs at night because there is some solar radiation in the day to meet the heating demand in the day.

The peak heating and cooling loads mainly occur between 0:00 and 06:00 for the four case study locations. Thus, the 20 °C indoor temperature setting can be lowered to reduce the building's heating load, or warm clothing can be worn in the building space at nighttime.

It was enough to meet all the building's heating and cooling needs for Tunis and New Delhi by covering the building roof space with solar thermal collectors. In contrast, for Swansea and Volgograd, covering all the building roof space with solar collectors could meet the building cooling demand but have 40 and 48 annual heating deficit days, respectively. Therefore, it was necessary to incorporate thermal energy storage to meet the heating demands for Swansea and Volgograd. However, the thermal analysis is limited because it does not account for the heat loss rates typical of water-based thermal storage systems.

11.3 Cooling engine performance

The EES modelling software was used to model the diffusion absorption cooling system, demonstrating the software's capability to model thermally driven engines based on thermodynamic models. The EES modelling results agree with other theoretical study patterns, such as smaller generator power capable of achieving high cooling capacity and heat gain to the generator and evaporator from the building's cooling demand.

Nonetheless, the calculated EES modelling results did not closely follow the comparative experimental data in the published literature [51]. The possible reasons for this mismatch could be due to the impact of geometric characteristics of the experimental setup and other operational conditions such as system pressure, the mass flow rate in the cooling system and from the solar heat source, the efficiency of ammonia, and the heat rejection temperature in the absorber and condenser.

Thus, the experimental data is used for the subsequent design of the solar collector and storage systems needed to meet the cooling load of the TE building. Analysis of the experimental results indicates that the optimum temperature for supplying heat to the generator is 190-205 °C.

11.4 Solar collector and storage design to meet generator temperature requirements

The optimum operating temperature for the solar-powered DACS falls in a medium to high-temperature range of 190-205 °C. Thus, TRNSYS is used to model the solar collector and storage design to meet the temperature requirements of the DACS's generator, which is applied to the building cooling demand for New Delhi and Volgograd. New Delhi was selected because it has the highest annual cooling load, and Volgograd was chosen because while it has a predominantly cold climate, it has a significant cooling load during summer.

The sensitivity study on the solar and storage design confirmed that the solar collector area, mass flow rate, and storage tank size affect the optimum generator operating temperature. For Volgograd and New Delhi, a single XCPC solar collector unit, 2.41 m^2, can reach the required optimum operating temperature for the DACS generator. Consequently, a small collector area implies a small buffer tank volume can be utilised in the system design to save space and have fewer capital costs.

The solar collector achieves higher operating temperatures at low fluid flow rates. Additionally, the solar collector temperature reduces, as the fluid mass flow rate increases; thus, no more than 10 kg/hr mass flow rates are recommended to achieve higher operating temperatures for New Delhi and Volgograd climatic regions. The solar collector reaches high operating temperatures at low mass flow rates because, at low flow rates, there is high solar fluid residence time in the collector to allow more time to absorb more heat from the sun to reach higher temperatures. At low flow rates, the fluid flows through the solar collector at low velocity; thus, the heat transfer coefficient between the fluid and the collector decreases, leading to a lower overall heat transfer rate. As a result, there is a trade-off between achieving higher operating temperatures and maintaining a higher heat transfer rate that requires a higher fluid mass flow rate.

The buffer storage tank achieves a lower maximum temperature than the solar collector throughout the various mass flow rates. This phenomenon occurs because the solar fluid is fed from the buffer tank to the diffusion absorption cooling engine, thus reducing the temperature in the buffer tank through the process. New Delhi and Volgograd's optimum mass flow rate to achieve the highest buffer tank temperature is 1-5 kg/hr.

At a fixed fluid mass flow rate, increasing buffer storage size does not influence the maximum solar collector temperature. However, increasing the tank's size reduces its maximum temperature because the solar collector fills a larger volume, and the draw of heat from the absorption cooling engine further reduces the tank temperature.

Practical operation requires adopting a variable speed pump and control system to regulate the solar collector's output temperature so that the collector and the buffer tank achieve the desired optimum operating temperature range. The buffer tank can be installed inside the generator compartment to save installation space and minimise heat loss. However, such tank-in-tank storage systems would have issues with adequate access for maintaining the tank. The solar and storage design can be applied to other climatic regions and different solar collector types, e.g., concentrating solar collectors, parabolic trough collectors, and other solar thermally powered cooling systems.

11.5 Solar energy capture and storage and backup energy performance

Based on the collector and buffer tank temperature assessments, the calculated energy deficits for New Delhi and Volgograd climatic locations were assessed against meeting such deficits

with backup electrical energy. The backup energy required for the buffer tank is significantly larger than that needed for the solar collector, primarily because the buffer tank volume is more than twice the size of the solar collector. However, in New Delhi's case, the collector's total backup hours are longer than those of the buffer tank. Thus, reducing the buffer storage volume is essential where backup energy is utilised.

The temperature assessment of the heat from the solar collector and thermal storage design suggests backup energy may be required to meet generator temperature requirements. However, the heat energy assessment in Chapter 5 indicates enough energy is available to drive the DACS's generator. As a result, the next step in the design is to pursue cold energy storage so that all the available energy from the solar collector is converted to cooling energy used directly by the building air handlers or stored for later use.

For New Delhi and Volgograd climatic locations, the hot storage tank achieves 40-65% solar fraction for each DACS unit. As a result, backup energy may be used to deliver the remainder of the energy to meet all the building cooling loads.

11.6 Cooling energy storage

When the cooling energy from the DACS's evaporator is stored for later use, sufficient cooling energy is available throughout the year, which is a significant improvement to using the thermal hot store. The two cooling energy storage systems designed are based on sensible heat cold storage and latent heat cold storage medium. The LHS storage medium stores more than three times more energy per unit volume than the SHS storage medium; thus, a smaller LHS storage size can be used. Moreover, using a smaller LHS storage size has less cold tank energy loss rate because the small tank volume has a smaller surface area exposed to the surroundings.

The SHS system has an ethylene glycol and water mixture as the working fluid to avoid freezing in the cold store at the -5 °C temperature from the DACS's evaporator. In contrast, an eutectic water-salt solution was chosen as the material for the LHS system due to its high heat of fusion and appropriate phase change temperature range. During the practical application of the LHS, additives and other measures must be implemented to avoid issues such as phase separation, supercooling, and corrosion between the material and the storage container.

The LHS cold storage application requires exchangers, such as the shell and tube and module heat exchangers [271], between the PCM and the energy transfer medium transporting via the cold store. The cold storage tank size for the climatic regions ranges between 120-500 litres for

the LHS and SHS cold storage systems, which compares with residential hot water tanks sizing of 90 litres/person/day and cold water cisterns minimum capacity of 230 litres [126]. Additionally, the modelled cold storage volume compares with DACS systems applied in refrigeration systems with cold storage volume up to 200 litres [51]. The cold store materials are likely rectangular and made of galvanised sheet steel [55].

Further research development of the cold storage design includes the discharge phase characterisation for dynamic analysis and the thermal effects of various system geometries and heat transfer coefficients.

11.7 Economic evaluation and environmental impact assessment

The building energy cost analysis revealed that in certain countries, there may be limited immediate economic advantages associated with installing T.E. materials in buildings and adopting sustainable technology. This situation can be attributed to local fuel costs, which, at times, are kept low through subsidies. As a result, the incentive to embrace thermally insulating materials is diminished, as the reduction in energy expenses is relatively small, necessitating extended periods to recover the likely additional construction expenditures.

The most significant cooling cost savings occur in places like Volgograd, New Delhi, and Tunis at low heat pump COPs. Meanwhile, the DACS yields substantial heating cost savings in Volgograd and Swansea due to high heating energy demands and electricity costs. These savings are most noticeable in extremely cold climates, such as Volgograd, where air source heat pumps are reported to be likely to operate with COPs between 1 and [274]. Nonetheless, for mild cold climates such as Swansea, where heat pumps are said to likely operate with COPs between 2 - 3 [274], the costs are comparable between DACS backup and heat pumps.

Hot thermal storage in the heating systems can increase the DACS combined cooling and heating solar fraction, reducing backup costs and enhancing cost competitiveness. The DACS helps reduce operational carbon emissions associated with cooling in all climate locations, contributing to decarbonising 28% of global energy-related CO_2 emissions in buildings [3,5]. Regarding heating, the DACS's ability to lower carbon emissions is evident with increasing building energy demand and depends on the primary energy source used to generate electricity for the alternative heat pump system.

The discounted payback times for Tunis, New Delhi, Volgograd, and Swansea are 12.7, 6.8, 0.8, and 2.1 years, respectively. Higher building thermal energy and higher energy prices result

in lower payback time. Besides, the discounted payback time for the solar-powered diffusion absorption cooling and heating system compared with residential air source heat pumps is reported to have paybacks typically between 3 – 15 years, depending on the local energy costs and subsidy level [273]. Larger buildings with higher thermal loads will likely have lower payback time because more annual solar savings will be achieved. Moreover, as the uptake of the DACS increases and installers become familiar with installing the system, the capital installation costs are likely to reduce over time. Also, the DACS are likely to qualify for regional financial incentives, lowering the cost of uptake and reducing the payback.

Chapter 12 : Conclusions and Future Work

This Chapter summarises the main conclusions of this research study. The recommendations for future work are presented based on the findings of this research.

12.1 Summary of the main conclusions

A modelling study has been performed for designing and optimising a solar-powered diffusion absorption cooling and heating system to meet building cooling and heating demand for a TE building in four case study locations in New Delhi, India, Volgograd, Russia, Tunis, Tunisia, and Swansea, UK. The following conclusions can be stated as a result of the study.

1. In order to evaluate the energy, economic, and environmental benefits of adopting NZEB, TRNSYS simulation software was used to determine the cooling and heating demand of a TE building in four climatic locations. It has evaluated the energy benefits of a thermally efficient building with lower U values than that used locally in each location, with reductions in heating demand by a factor of 3 in colder climates. Increases in cooling demand were observed with the more thermally efficient building materials. The direct financial benefits are more difficult to justify due to the low cost of conventional fuel in some locations.
2. The heat production from the XCPC solar collector on the TE building can be calculated using solar irradiation data recorded from the TRNSYS software and collector efficiencies for a given climatic location. Comparing the predominantly cold climates, climatic locations with higher building heating loads have higher heating power deficits, even though they may have lower deficit hours. The availability of solar radiation in winter months reduces the total heating deficit hours, e.g., Tunis's total heating power deficit is 52% of that of Volgograd; however, the total heating deficit hours is at a lower value of 15.7% than that of Volgograd.
3. For hot climatic locations, i.e., New Delhi and Tunis, the building roof space has enough area to accommodate the solar collectors to meet all the TE building’s heating and cooling requirements. For the cold climates of Swansea and Volgograd, the solar collectors installed on the building roof are sufficient to cover the building cooling demand. However, thermal energy storage is needed to meet the building’s heating energy demands.
4. The EES software can model the diffusion absorption cooling system using thermodynamic equations. The modelling results follow the expected pattern in the

evaporator and the generator, e.g., smaller generator power can achieve high cooling capacity. However, the EES modelling results do not closely follow the experimental data from published literature. The possible reasons for this anomaly are the impact of geometrical characteristics of the experimental setup and other practical operating conditions that are assumed to be constant in the theoretical model, such as the total system pressure, heat rejection temperature in the absorber and condenser, efficiency of ammonia condensation, and the mass flow rate of the working fluid. Analysis of the experimental data indicates the optimum operating temperature for the solar-powered DACS is 190-205 °C.

5. TRNSYS can be used to calculate the fluid temperature in the XCPC solar collector and buffer storage tank, and a sensitivity analysis confirms that the solar fluid mass flow rate, the solar collector area, and the buffer tank volume influence the optimum generator temperature.
6. For New Delhi and Volgograd climatic regions, the solar collector achieves higher operating temperatures and small collector power at low fluid flow rates (no more than 10 kg/hr). The hot buffer storage tank reaches a lower temperature than the solar collector because the solar fluid is fed from the buffer tank to the diffusion absorption cooling engine. The buffer tank inside the generator section saves installation space and minimises heat loss to the ambient. Smaller hot buffer tank sizes (up to 10 litres per m^2 of the solar collector area) are recommended to achieve the optimum generator operating temperatures when the solar collector operates at the recommended mass flow rates of up to 10 kg/hr. The practical operation of the solar and storage design requires adopting a variable speed pump and control system to regulate the fluid flow in the solar collector.
7. The temperature assessments from the solar collector and the hot buffer tank design indicate backup energy is an option to meet any shortfall. However, backup energy use discourages using buffer tanks because the tank size is at least twice that of the solar collector. The backup energy assessment indicates the need to keep the buffer tank size smaller to minimise the cost of heating the fluid and raise the temperature to the optimum range where needed.
8. Using a small hot buffer store of 2 litres/m^2 of solar collector area, the solar fraction achieved for the solar collector and hot storage system was between 40-65 %.
9. When a cold energy storage system is employed in the design, sufficient cooling energy is available throughout the year for the climatic regions. Using a latent heat storage

medium can be advantageous over sensible heat storage because the LHS storage medium stores more than three times more energy per unit volume than the SHS storage medium and causes less cold tank heat loss. However, the practical application of LHS requires appropriate measures to deal with potential operational issues with phase separation, supercooling, and corrosion between the material and the storage container.

10. Using solar-derived heating and cooling results in a substantial decrease in the consumption of fossil fuels for energy and, consequently, reduces CO_2 emissions in warm regions. Additionally, it lessens the need for heating during colder seasons. The direct financial benefits are more challenging to justify due to the low cost of primary fuel, such as natural gas, in some climatic regions. Nonetheless, the economic benefits of the DACS are more evident than those of the electrically powered heat pumps. Also, the DACS plays a significant role in decarbonising building cooling and heating energy systems.

12.2 Future work

This research has shown several areas for further investigation and design improvements that can be examined in further studies.

1. This work evaluated the energy benefits of a thermally efficient building with lower U values of the building materials than that used locally in each location. Still, other building energy reduction techniques exist, such as passive cooling and thermally efficient windows. A further examination of thermally efficient buildings can focus on implementing passive cooling techniques in the building envelope, such as using selective and reflective coatings on the exterior building walls, solar shading of the outer building surfaces, or incorporating phase change materials into building construction materials.
2. The thesis has demonstrated that optimum solar and storage design is required to meet the high-temperature requirements (190-205 °C) of the DACS generator. There is an opportunity for expanding the understanding of the solar and storage design and the diffusion absorption cooling system to apply to other solar-powered absorption cooling system variants, e.g., Libr-H_2O single-stage absorption cooling systems operating under low temperatures (below 100 °C).
3. The condenser of the diffusion absorption cooling engine is designed to be air-cooled to ambient temperature for theoretical and experimental studies. There is a scope to

potentially apply a water-cooled heat rejection system, including a heat exchanger, to improve the efficiency of the condenser and absorber heat rejection.

4. The thesis has demonstrated the four different climatic locations impact the heating and cooling loads of the TE building. The weather datasets from Meteornorm in TRNSYS are based on a typical year and a ten-year average of the weather data. There is an opportunity to establish new building thermal system design based on data sets that factor in the impact of climate change.
5. The work on the cold energy storage demonstrated that enough cooling energy is available for the climatic locations studied, and the hot thermal store can be implemented as a tank-in-tank in the generator compartment. There may be an opportunity to expand on understanding cold and hot storage for long-term storage, such as seasonal energy storage. Also, the surplus energy from the solar collector can be used for domestic hot water applications.
6. There is a scope for additional work to establish how the cooling energy directly from the evaporator or indirectly from the cold store can be integrated into existing and new buildings.
7. There is a scope for investigating how the coefficient of performance and the cooling capacity of the solar-powered DACS can be improved for the solar fraction, the operating energy cost savings and the avoided carbon emissions.

Appendices

Appendix A: Specifications for each building envelope

Table 1: Thermo-physical properties of the TE building wall (Net U-value = 0.132 W/m^2.K)

Material (layer)	Thickness	Thermal conductivity	Heat capacity	Density	Thermal resistance
	x	λ	Cp	ρ	R
	m	kJ/h.m·K	kJ/kg.K	kg/m^3	m^2.K/W
Internal surface resistance	-	-	-	-	0.13
Plasterboard finish	0.015	0.25	1	900	0.06
Concrete block (hollow, mediumweight)	0.15	0.62	0.84	1040	0.242
Mineral wool Insulation	0.06	0.042	1.03	12	1.429
Drained cavity (air-gap)	0.015	-	-	-	0.18
Brick (burned)	0.115	0.75	0.84	1300	0.153
External surface resistance	-	-	-	-	0.04

Table 2: Thermo-physical properties of the TE building roof with U-value = 0.131 W/m^2.K

Material (layer)	Thickness	Thermal conductivity	Heat capacity	Density	Thermal resistance
	x	λ	Cp	ρ	R
	m	kJ/h.m·K	kJ/kg.K	kg/m^3	m^2.K/W
Internal surface resistance	-	-	-	-	0.13
Plasterboard finish	0.015	0.25	1	900	0.06
Mineral wool Insulation	0.08	0.042	1.03	12	1.905
Concrete (cast, dense, reinforced)	0.2	1.9	0.84	2300	0.105
Roof tiles	0.004	0.84	0.8	1900	0.005
External surface resistance	-	-	-	-	0.04

Table 3: Thermo-physical properties of the TE building floor with U-value = 0.105 $W/m^2.K$

Material (layer)	Thickness	Thermal conductivity	Heat capacity	Density	Thermal resistance
	x	λ	Cp	ρ	R
	m	kJ/h.m·K	kJ/kg.K	kg/m^3	$m^2.K/W$
Internal surface resistance	-	-	-	-	0.17
Floor covering (vinyl)	0.004	0.17	0.9	1390	0.024
cement screed	0.06	1.4	0.65	2100	0.043
Insulation (mineral wool, quilt)	0.1	0.042	1.03	12	2.381
Concrete (cast, dry, heavyweight)	0.18	1.3	0.84	2000	0.138
tiles - sandstone tiles	0.02	1.2	0.84	2000	0.017
External surface resistance	-	-	-	-	0.04

Table 4: Thermal insulation glass performance data for window with U-value = 1.06 $W/m^2.K$

Window glass pane	Light (%)		Solar radiant heat (%)				Total shading coefficient	U value $[W/m^2.K]$
	Transmittance	Reflectance	Transmittance	Reflectance	Absorptance	Total solar heat transmittance		
Optitherm S3 Double insulating Glass	82	11	57	26	17	65	0.75	1.06

Table 5: Thermo-physical properties of the local building (Tunis and New Delhi) wall with U-value = 0.201 W/m^2.K

Material (layer)	Thickness	Thermal conductivity	Heat capacity	Density	Thermal resistance
	x	λ	Cp	ρ	R
	m	W.m·K	J/kg.K	kg/m^3	m^2.K/W
Internal surface resistance	-	-	-	-	0.13
Mortar	0.025	1.4	1.08	2200	0.01785714
Stone	0.15	1.4	0.84	2200	0.107
Insulation	0.04	0.038	1.4	20	1.053
Brick	0.065	0.47	0.94	700	0.18
Cement motar	0.025	1.4	1.08	2200	0.018
External surface resistance	-	-	-	-	0.04

Table 6: Thermo-physical properties of the local building (Tunis and New Delhi) roof with U-value = 0.784 W/m^2.K

Material (layer)	Thickness	Thermal conductivity	Heat capacity	Density	Thermal resistance
	x	λ	Cp	ρ	R
	m	kJ/h.m·K	kJ/kg.K	kg/m^3	m^2.K/W
Internal surface resistance	-	-	-	-	0.13
Lime mortar	0.02	1.15	1.08	1900	0.0173913
Brick	0.16	0.94	0.9	820	0.170
Concrete	0.15	1.75	0.96	2300	0.086
Cement mortar	0.025	1.4	1.08	2200	0.018
Felt	0.005	0.2	0.92	1080	0.025
External surface resistance	-	-	-	-	0.04

Table 7: Thermo-physical properties of the local building (Tunis and New Delhi) floor with U-value = 0.894 W/m^2.K

Material (layer)	Thickness	Thermal conductivity	Heat capacity	Density	Thermal resistance
	x	λ	Cp	ρ	R
	m	kJ/h.m·K	kJ/kg.K	kg/m^3	m^2.K/W
Internal surface resistance	-	-	-	-	0.17
Mosaic	0.02	0.5	0.79	1700	0.040
Cement mortar	0.02	1.4	1.08	2200	0.014
Sand	0.03	0.33	0.79	1700	0.091
Concrete	0.05	1.75	0.84	1600	0.029
Stone	0.15	1.67	0.84	2250	0.090
External surface resistance	-	-	-	-	0.04

Table 8: Thermo-physical properties of the local building wall (Swansea and Volgograd) with U-value = 0.813 W/m^2.K

Material (layer)	Thickness	Thermal conductivity	Heat capacity	Density	Thermal resistance
	x	λ	Cp	ρ	R
	m	W/m·K	kJ/kg.K	kg/m^3	m^2.K/W
Internal surface resistance	-	-	-	-	0.13
Cement plaster finish	0.01	0.72	0.84	1760	0.01388889
Brick (burned)	0.2	0.75	0.84	1300	0.267
Cement plaster finish	0.01	0.72	0.84	1760	0.018
External surface resistance	-	-	-	-	0.04

Table 9: Thermo-physical properties of the local building (Swansea and Volgograd) roof with U-value = 0.739 W/m^2.K

Material (layer)	Thickness	Thermal conductivity	Heat capacity	Density	Thermal resistance
	x	λ	Cp	ρ	R
	m	kJ/h.m·K	kJ/kg.K	kg/m^3	m^2.K/W
Internal surface resistance	-	-	-	-	0.13
Cement plaster finish	0.01	0.72	0.84	1760	0.01754386
Concrete block (hollow, mediumweight)	0.16	0.62	0.84	1040	0.242
Concrete (cast, dense, reinforced)	0.04	1.9	0.84	2300	0.021
Roof tiles	0.03	0.84	0.8	1900	0.036
External surface resistance	-	-	-	-	0.04

Table 10: Thermo-physical properties of the local building (Swansea and Volgograd) floor with U-value = 1.062 W/m^2.K

Material (layer)	Thickness	Thermal conductivity	Heat capacity	Density	Thermal resistance
	x	λ	Cp	ρ	R
	m	kJ/h.m·K	kJ/kg.K	kg/m^3	m^2.K/W
Internal surface resistance	-	-	-	-	0.17
Floor covering (vinyl)	0.003	0.17	0.9	1390	0.018
cement screed	0.06	1.4	0.65	2100	0.043
Concrete (cast, dry, heavyweight)	0.2	1.3	0.84	2000	0.154
External surface resistance	-	-	-	-	0.04

Appendix B: EES modelling inputs and equations for the DACS.

```
$UnitSystem SI C kPa kJ mass

"Input parameters from the problem statement"

"Mass balances"
m_dot[1]=0.001114 [kg/s]                                "mass flow rate from absorber to generator"
m_dot[1]=m_dot[2]                                       "mass balances"
m_dot[1]=m_dot[11]                                      "mass balances"
m_dot[3]=0.4*m_dot[1]                                   "mass balances"
m_dot[7]=m_dot[6]                                       "mass balances"
m_dot_ref=m_dot[6]                                      "mass balances"

"Mass fractions"
x[1]=0.28                                                "refrigerant mass fraction"
x[1]=x[2]                                                "refrigerant mass fraction"
x[1]=x[11]                                               "refrigerant mass fraction"
x[3]=0.65                                                "refrigerant mass fraction"
x[3]=x[5]                                                "refrigerant mass fraction"
x[6]=0.994                                               "refrigerant mass fraction"
x[6]=x[7]                                                "refrigerant mass fraction"
x[8]=0.20                                                "refrigerant mass fraction"
x[9]=0.975                                               "refrigerant mass fraction"
x[9]=x[10]                                               "refrigerant mass fraction"

"Temperatures"
T[2]=128[C]                                              "temperature at entry of generator"
T[3]=173[C]                                              "temperature at entry of generator is equal to point 3"
T[3]=T[4]                                                "temperature at entry of generator is equal to point 4"
T[4]=T[5]                                                "temperature at entry of generator is equal to point 5"
T[7]=51[C]                                               "temperature at exit of condenser"
T[11]=41[C]                                              "temperature at exit of absorber"
T[10]=29[C]                                              "temperature at exit of evaporator"
T[10]=T[9]                                               "temperature at exit of evaporator is equal to entry of evaporator"

"Quality"
Q[11]=0                                                  "quality of liquid exiting absorber reservoir entering LHX"
Q[1]=0                                                   "quality of liquid exiting LHX and entering generator"
Q[2]=Q[1]                                                "quality of liquid at entry of generator"
Q[4]=0.7                                                 "quality of vapour at exit of generator"
Q[3]=Q[1]                                                "quality of liquid at exit of generator"
Q[8]=0                                                   "quality of liquid returning from rectifier and through LHX"
Q[6]=0.95                                                "quality at exit of rectifier"
Q[5]=Q[4]                                                "quality of vapour towards rectifier"
Q[7]=0                                                   "quality of liquid at exit of condenser"
Q[10]=0.975                                              "quality at exit of evaporator"
Q[9]=0.975                                               "quality at entry of evaporator"
```

```
"Pressures"
P_high=pressure(NH3H2O,T=T[2],x=x[2],Q=Q[2])        "pressure at generator to condenser at high level"
P_low=pressure(NH3H2O,T=T[9],x=x[9],Q=Q[9])         "pressure at evaporator exit at low level using state 10"
P[1]=P_high                                         "set all pressures"
P[2]=P_high
P[3]=P_high
P[4]=P_high
P[5]=P_high
P[6]=P_high
P[7]=P_high
P[8]=P_high
P[9]=P_low
P[10]=P_low
P[11]=P_high
```

Figure 1: The model inputs in the EES modelling window are mass balance, mass fraction, temperature, quality, and pressure.

```
"Mass, ammonia, and energy balances of each component"


"GENERATOR"
m_dot[1]=m_dot[3]+m_dot[4]                                  "mass balance equation"
m_dot[1]*x[1]=m_dot[3]*x[3]+m_dot[4]*x[4]                   "Ammonia mass balance equation"
Q_gen=m_dot[3]*h[3]+m_dot[4]*h[4]-m_dot[1]*h[1]             "energy balance equation"
h[3]=enthalpy(NH3H2O,T=T[3],P=P[3],Q=Q[3])                  "specific enthalpy at state 3"
h[4]=enthalpy(NH3H2O,T=T[4],P=P[4],Q=Q[4])                  "specific enthalpy at state 4"
h[1]=enthalpy(NH3H2O,x=x[1],P=P[1],Q=Q[1])                  "specific enthalpy at state 1"

"RECTIFIER"
m_dot[4]=m_dot[5]+m_dot[6]                                    "mass balance equation"
m_dot[6]=((Q[4]-x[5])/(Q[6]-x[5]))*m_dot[4]                   "mass balance equation"
Q_rect=m_dot[5]*h[5]+m_dot[6]*h[6]-m_dot[4]*h[4]              "energy balance equation"
h[6]=enthalpy(NH3H2O,x=x[6],P=P[6],Q=Q[6])                    "specific enthalpy at state 6"
h[5]=enthalpy(NH3H2O,T=T[5],P=P[5],Q=Q[5])                    "specific enthalpy at state 5"

"CONDENSER"
Q_cond=m_dot[6]*(h[7]-h[6])                                    "energy balance equation"
h[7]=enthalpy(NH3H2O,x=x[7],T=T[7],Q=Q[7])                     "specific enthalpy at state 7"

"EVAPORATOR plus GHX"
m_dot[7]=m_dot[9]                                                    "mass balances"
m_dot[7]=m_dot[10]                                                   "mass balances"
m_dot_ig=0.425*m_dot_ref                                             "mass balances"
Q_evap=m_dot[9]*(h[10]-h[7])+m_dot_ig*(h_ig[10]-h_ig[8])           "energy balance equation"
h[10]=enthalpy(NH3H2O,x=x[10],T=T[10],Q=Q[10])                   "specific enthalpy at state 10"
h_ig[10]=C_p_ig*T_ig[10]                                             "specific enthalpy at state 10 inert gas"
T_ig[10]=299[K]                                                      "temperature of inert gas at state 10-assumed =T[10]"
C_p_ig=14.31                                                         "specific heat of hydrogen gas"
h_ig[8]=C_p_ig*T_ig[8]                                                  "specific enthalpy at state 8 inert gas"
T_ig[8]=299[K]                                                       "temperature of inert gas at state 8-assumed = T[10]"

"SOLUTION HEAT EXHANGER"
m_dot[8]=m_dot[3]+m_dot[5]                                               "mass balance equation"
m_dot[3]*h[3]+m_dot[5]*h[5]-m_dot[8]*h[8]=m_dot[1]*(h[1]-h[11])          "energy balance equation"
h[11]=enthalpy(NH3H2O,T=T[11],P=P[11],Q=Q[11])                           "specific enthalpy at state 11"

"ABSORBER"
Q_abs=m_dot[11]*h[11]-m_dot[10]*h[10]-m_dot[8]*h[8]+m_dot_ig*h_ig[8]-m_dot_ig*h_ig[10]     "energy balance equation"

"REFRIGERANT RATIO"
f=m_dot_r/m_dot_ref                                                      "mass flowrates ratio"
m_dot_r=m_dot[1]                                                        "refrigerant mass flow rate"

"COEFFICIENT OF PERFORMACE"
COP=Q_evap/Q_gen                                          "COP of Diffusion absorption cooling machine"
```

Figure 2: Mass, ammonia, and energy balances of each component.

Appendix C: TRNSYS simulation results

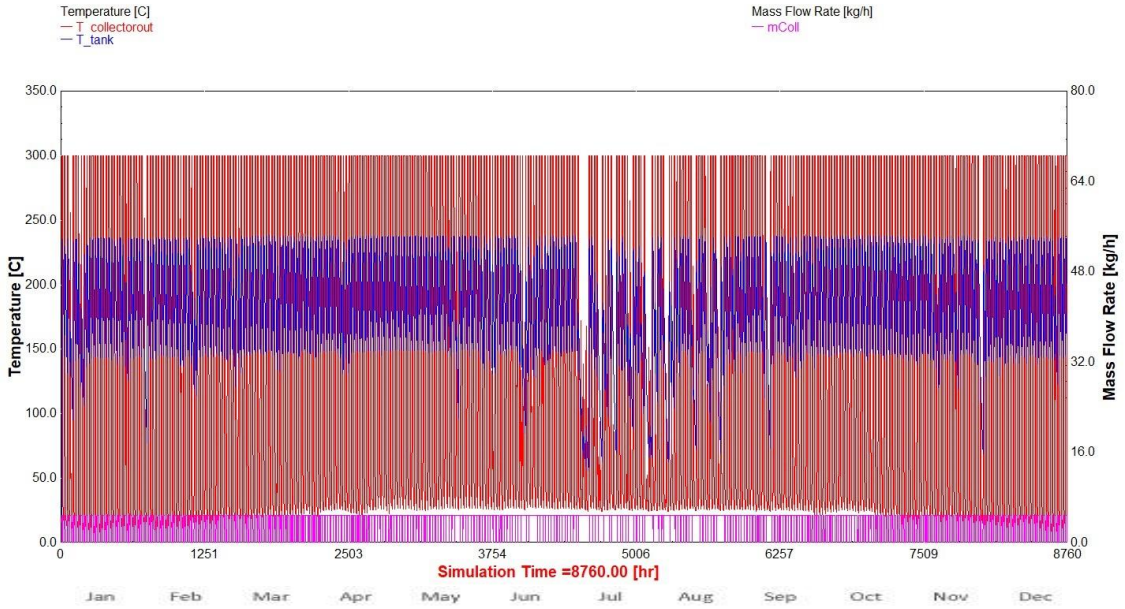

Figure 1: XCPC solar thermal collector performance, Tunis.

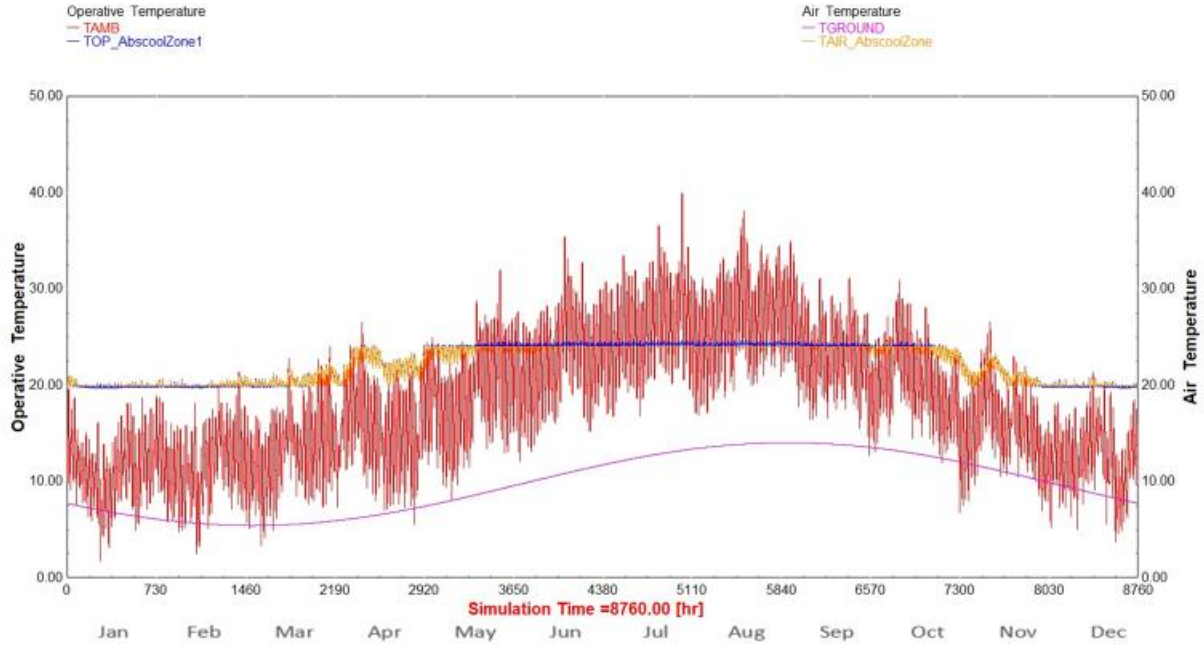

Figure 2: Building operative and ground temperature, Tunis.

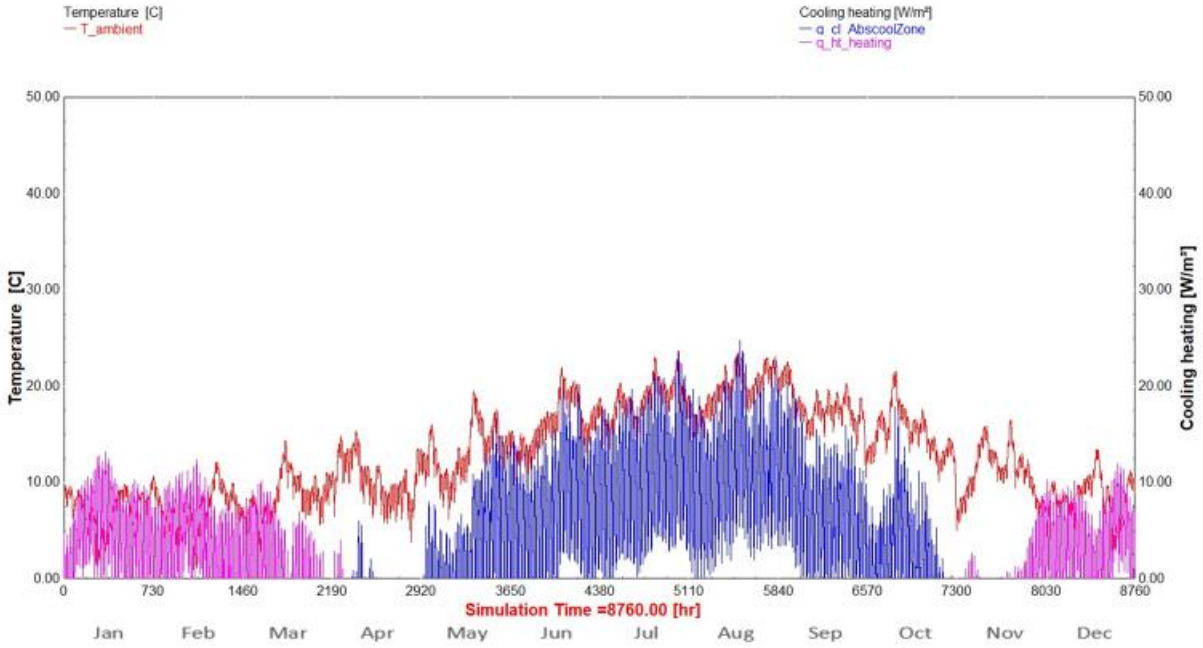

Figure 3: Building cooling and heating demand and ambient temperature, Tunis.

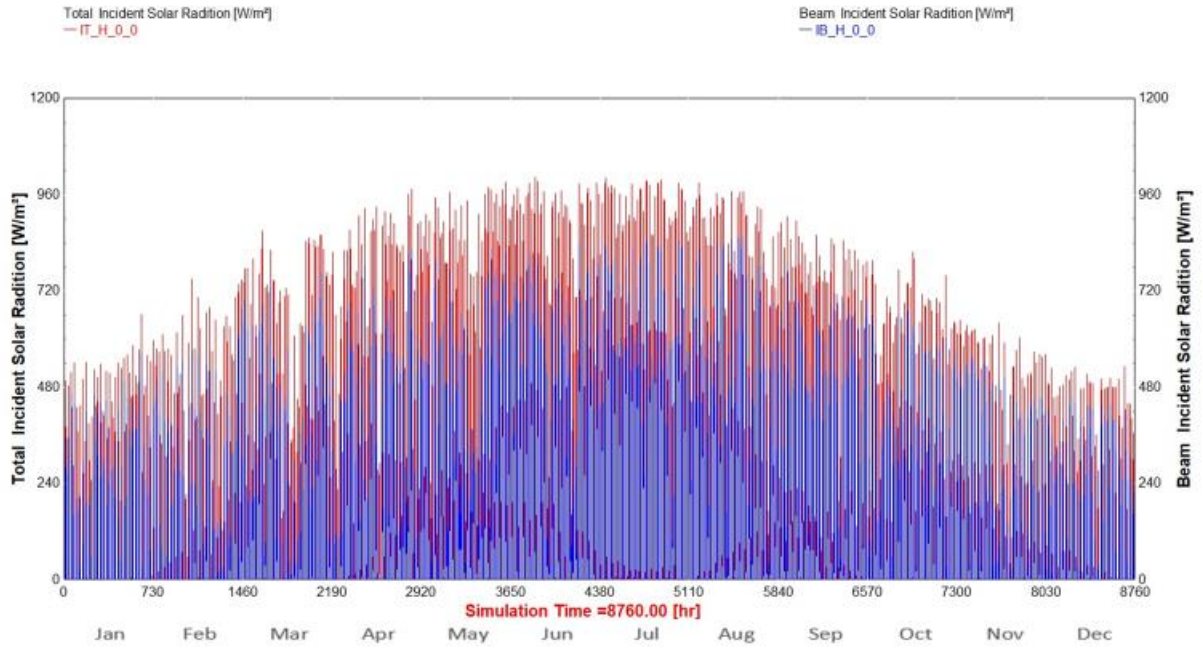

Figure 4: Total and beam horizontal solar radiation, Tunis

References

[1] International Energy Agency, “Buildings - Sectoral overview,” Paris, Sep. 2022. Accessed: November 1, 2023. [online]. Available: https://www.iea.org/reports/buildings

[2] International Energy Agency, “Heating,” Paris, Sep. 2022. Accessed: November 1, 2023. [online]. Available: https://www.iea.org/reports/heating

[3] International Energy Agency, “IEA: World Energy Outlook 2020,” Paris, France, 2020. Accessed: November 1, 2023. [online]. Available: https://www.iea.org/reports/world-energy-outlook-2020

[4] International Energy Agency, “Cooling,” Paris, 2020. Accessed: November 1, 2023. [online]. Available: https://www.iea.org/reports/world-energy-outlook-2020

[5] International Energy Agency, “The Future of Cooling Opportunities for energy-efficient air conditioning Together Secure Sustainable.” Accessed: November 1, 2023. [Online]. Available: www.iea.org/t&c/

[6] G. R. McGregor, P. Bessemoulin, K. Ebi, and B. Menne, “Heatwaves and Health: Guidance on Warning-System Development,” 2015. Accessed: November 1, 2023. [Online]. Available: https://dro.dur.ac.uk/28811/1/28811.pdf

[7] A. Mastrucci, E. Byers, S. Pachauri, and N. D. Rao, “Improving the SDG energy poverty targets: Residential cooling needs in the Global South,” Energy Build, vol. 186, pp. 405–415, Mar. 2019, doi: 10.1016/j.enbuild.2019.01.015.

[8] T. E. Downing, N. Eyre, R. Greener, and D. Blackwell, “Projected Costs of Climate Change for Two Reference Scenarios and Fossil Fuel Cycle,” Oxford: Environmental Change Unit, pp. 1–48, 1996.

[9] T. E. Downing, R. A. Greener, and N. Eyre, “The Economic Impacts of Climate Change, Assessment of Fossil Fuel Cycles for the Extern Project,” Environmental Change Unit and Eyre Energy Environment, pp. 1–48, 1995.

[10] M. Santamouris and D. Kolokotsa, “On the impact of urban overheating and extreme climatic conditions on housing, energy, comfort and environmental quality of vulnerable population in Europe,” Energy Build, vol. 98, Jul. 2015, doi: 10.1016/j.enbuild.2014.08.050.

[11] A. Sakka, M. Santamouris, I. Livada, F. Nicol, and M. Wilson, “On the thermal performance of low-income housing during heat waves,” Energy Build, vol. 49, Jun. 2012, doi: 10.1016/j.enbuild.2012.01.023.

[12] D. Kolokotsa and M. Santamouris, “Review of the indoor environmental quality and energy consumption studies for low-income households in Europe,” Science of the Total Environment, vol. 536. Elsevier, pp. 316–330, Dec. 01, 2015. doi: 10.1016/j.scitotenv.2015.07.073.

[13] M. Santamouris, “Cooling Energy Solutions for Buildings and Cities,” World Scientific, 2019. pp. 1-250, doi: 10.1142/10901.

[14] M. Santamouris, C. Cartalis, A. Synnefa, and D. Kolokotsa, “On the impact of urban heat island and global warming on the power demand and electricity consumption of buildings—A review,” Energy Build, vol. 98, Jul. 2015, doi: 10.1016/j.enbuild.2014.09.052.

[15] A. Al-Alili, Y. Hwang, and R. Radermacher, “Review of solar thermal air conditioning technologies,” International Journal of Refrigeration, vol. 39. Elsevier Ltd, pp. 4–22, 2014. doi: 10.1016/j.ijrefrig.2013.11.028.

[16] U. Jakob, U. Eicker, D. Schneider, A. H. Taki, and M. J. Cook, “Simulation and experimental investigation into diffusion absorption cooling machines for air-conditioning applications,” Appl Therm Eng, vol. 28, no. 10, pp. 1138–1150, Jul. 2008, doi: 10.1016/j.applthermaleng.2007.08.007.

[17] M. Santamouris and D. Kolokotsa, “Passive cooling dissipation techniques for buildings and other structures: The state of the art,” Energy Build, vol. 57, Feb. 2013, doi: 10.1016/j.enbuild.2012.11.002.

[18] L. W. Davis and P. J. Gertler, “Contribution of air conditioning adoption to future energy use under global warming,” Proc Natl Acad Sci U S A, vol. 112, no. 19, pp. 5962–5967, May 2015, doi: 10.1073/pnas.1423558112.

[19] M. A. Mcneil, V. E. Letschert, and E. Org, “Title Future Air Conditioning Energy Consumption in Developing Countries and what can be done about it: The Potential of Efficiency in the Residential Sector”, Lawrence Berkeley National Laboratory, [online], 2008, https://escholarship.org/uc/item/64f9r6wr

[20] N. Zhou, N. Z. Khanna, D. Fridley, J. Romankiewicz, and E. O. Lawrence, “Development and implementation of energy efficiency standards and labeling programs in China: Progress and challenges,” 2013.

[21] K. J. Lomas, “Dwelling and household characteristics’ influence on reported and measured summertime overheating: A glimpse of a mild climate in the 2050’s,” Build Environ, vol. 201, Aug. 2021, doi: 10.1016/j.buildenv.2021.107986.

[22] R. Gupta, “Monitoring and modelling the risk of summertime overheating and passive solutions to avoid active cooling in London care homes,” Energy Build, vol. 252, Dec. 2021, doi: 10.1016/j.enbuild.2021.111418.

[23] S. Choi, J. Oh, Y. Hwang, and H. Lee, “Life cycle climate performance evaluation (LCCP) on cooling and heating systems in South Korea,” Appl Therm Eng, vol. 120, pp. 88–98, 2017, doi: 10.1016/j.applthermaleng.2017.03.105.

[24] H. Lee, S. Troch, Y. Hwang, and R. Radermacher, “Évaluation du LCCP de diverses options de cycle à compression de vapeur et de frigorigènes à faible GWP,” International Journal of Refrigeration, vol. 70, pp. 128–137, Oct. 2016, doi: 10.1016/j.ijrefrig.2016.07.003.

[25] G. Li, “Investigations of life cycle climate performance and material life cycle assessment of packaged air conditioners for residential application,” Sustainable Energy Technologies and Assessments, vol. 11, pp. 114–125, Sep. 2015, doi: 10.1016/j.seta.2015.07.002.

[26] L. Zhao, W. Zeng, and Z. Yuan, “Reduction of potential greenhouse gas emissions of room air-conditioner refrigerants: A life cycle carbon footprint analysis,” J Clean Prod, vol. 100, pp. 262–268, Aug. 2015, doi: 10.1016/j.jclepro.2015.03.063.

[27] H. Wang, L. Zhao, R. Cao, and W. Zeng, “Refrigerant alternative and optimization under the constraint of the greenhouse gas emissions reduction target,” J Clean Prod, vol. 296, May 2021, doi: 10.1016/j.jclepro.2021.126580.

[28] J. L. Boot, “Overview of alternatives to CFCs for domestic refrigerators and freezers,” International Journal of Refrigeration, vol. 13, no. 2, Mar. 1990, doi: 10.1016/0140-7007(90)90008-K.

[29] S. Benhadid-Dib and A. Benzaoui, “Refrigerants and their environmental impact substitution of hydrochlorofluorocarbon HCFC and HFC hydrofluorocarbon. Search for an adequate refrigerant,” in Energy Procedia, Elsevier BV, 2012, pp. 807–816. doi: 10.1016/j.egypro.2012.05.096.

[30] R. Ciconkov, “Refrigerants: There is still no vision for sustainable solutions,” International Journal of Refrigeration, vol. 86. Elsevier Ltd, pp. 441–448, Feb. 01, 2018. doi: 10.1016/j.ijrefrig.2017.12.006.

[31] Deutsche Gesellschaft fur Sonnenenergie, “Planning and Installing Solar Thermal Systems, A guide for installers, architects and engineers,” Second. London, Washington DC: Earthscan, 2010.

[32] J. Cerezo, R. J. Romero, J. Ibarra, A. Rodríguez, G. Montero, and A. Acuña, “Dynamic simulation of an absorption cooling system with different working mixtures,” Energies (Basel), vol. 11, no. 2, Feb. 2018, doi: 10.3390/en11020259.

[33] M. S. A. Khan, A. W. Badar, T. Talha, M. W. Khan, and F. S. Butt, “Configuration based modeling and performance analysis of single effect solar absorption cooling system in TRNSYS,” Energy Convers Manag, vol. 157, pp. 351–363, Feb. 2018, doi: 10.1016/j.enconman.2017.12.024.

[34] A. Prieto, U. Knaack, T. Klein, and T. Auer, “25 Years of Cooling Research in Office Buildings: Review for the Integration of Cooling Strategies into the Building façade (1990–2014),” Renewable and Sustainable Energy Reviews, vol. 71. Elsevier Ltd, pp. 89–102, 2017. doi: 10.1016/j.rser.2017.01.012.

[35] A. Prieto, U. Knaack, T. Auer, and T. Klein, “Feasibility study of self-sufficient solar cooling fa ade applications in different warm regions,” Energies (Basel), vol. 11, no. 6, p. 121693718, Jun. 2018, doi: 10.3390/en11061475.

[36] P. Kohlenbach and U. Jakob, “Solar Cooling: The Earthscan Expert Guide to Solar Cooling Systems,” Illustrated. Routledge, 2014.

[37] H. M. Henning and J. Döll, “Solar Systems for Heating and Cooling of Buildings,” Energy Procedia, vol. 30, 2012, doi: 10.1016/j.egypro.2012.11.073.

[38] G. Grossman, “SOLAR-POWERED SYSTEMS FOR COOLING, DEHUMIDIFICATION AND AIR-CONDITIONING,” Solar Energy, Volume 72, Issue 1, Pages 53-62, 2002. doi.org/10.1016/S0038-092X(01)00090-1.

[39] H. Z. Hassan and A. A. Mohamad, “A review on solar-powered closed physisorption cooling systems,” Renewable and Sustainable Energy Reviews, vol. 16, no. 5. pp. 2516–2538, Jun. 2012. doi: 10.1016/j.rser.2012.02.068.

[40] J. L. Rodríguez-Muñoz and J. M. Belman-Flores, “Review of diffusion-absorption refrigeration technologies,” Renewable and Sustainable Energy Reviews, vol. 30. pp. 145–153, 2014. doi: 10.1016/j.rser.2013.09.019.

[41] B. C. Von Platen and C. G. Munters, “Diffusion Absorption Refrigerator,” 1, 1928

[42] W. Wu, B. Wang, W. Shi, and X. Li, “An overview of ammonia-based absorption chillers and heat pumps,” Renewable and Sustainable Energy Reviews, vol. 31. Elsevier Ltd, pp. 681–707, 2014. doi: 10.1016/j.rser.2013.12.021.

[43] V. Pérez-García, J. L. Rodríguez-Muñoz, J. M. Belman-Flores, C. Rubio-Maya, and J. J. Ramírez-Minguela, “Theoretical modeling and experimental validation of a small capacity diffusion-absorption refrigerator,” International Journal of Refrigeration, vol. 104, pp. 302–310, Aug. 2019, doi: 10.1016/j.ijrefrig.2019.05.014.

[44] A. Taieb, K. Mejbri, and A. Bellagi, “Theoretical analysis of a diffusion-absorption refrigerator,” Int J Hydrogen Energy, vol. 41, no. 32, pp. 14293–14301, Aug. 2016, doi: 10.1016/j.ijhydene.2016.06.180.

[45] J. Chen, K. J. Kim, and K. E. Herold, “Performance enhancement of a diffusion-absorption refrigerator Am61ioration de la performance d’un r6frig6rateur ii diffusion-absorption,” Int J. Refrig. Vol. 19, No. 3, pp. 208-218, 1996.

[46] A. Taieb, K. Mejbri, and A. Bellagi, “Detailed thermodynamic analysis of a diffusion-absorption refrigeration cycle,” Energy, vol. 115, pp. 418–434, Nov. 2016, doi: 10.1016/j.energy.2016.09.002.

[47] A. Zohar, M. Jelinek, A. Levy, and I. Borde, “Performance of diffusion absorption refrigeration cycle with organic working fluids,” International Journal of Refrigeration, vol. 32, no. 6, pp. 1241–1246, Sep. 2009, doi: 10.1016/j.ijrefrig.2009.01.010.

[48] H. Wang, “A new style solar-driven diffusion absorption refrigerator and its operating characteristics,” in Energy Procedia, Elsevier BV, 2012, pp. 681–692. doi: 10.1016/j.egypro.2012.05.083.

[49] A. S. Rattner and S. Garimella, “Low-source-temperature diffusion absorption refrigeration. Part I: Modeling and cycle analysis,” International Journal of Refrigeration, vol. 65, pp. 287–311, May 2016, doi: 10.1016/j.ijrefrig.2015.10.010.

[50] Solar Polar Ltd, “Cooling Solutions,” Accessed: November 1, 2023. [online]. Available: https://www.solar-polar.co.uk/solutions.

[51] A. Najjaran, J. Freeman, A. Ramos, and C. N. Markides, “Experimental investigation of an ammonia-water-hydrogen diffusion absorption refrigerator,” Appl Energy, vol. 256, Dec. 2019, doi: 10.1016/j.apenergy.2019.113899.

[52] U. Jakob, “RECENT DEVELOPMENTS OF SMALL-SCALE SOLAR OR WASTE HEAT DRIVEN COOLING KITS FOR AIR-CONDITIONING AND REFRIGERATION.” SolarNext AG. Accessed: November 1, 2023. [online]. Available: https://solarnext.de/downloads/09HPC820_Berlin.pdf

[53] J. A. Duffie and W. A. Beckman, “Solar Engineering of Thermal Processes,” 4th ed. John Wiley & Sons, 2013, pp. 1-1258.

[54] S. A. Kalogirou, “Solar thermal collectors and applications,” Progress in Energy and Combustion Science, vol. 30, no. 3. pp. 231–295, 2004. doi: 10.1016/j.pecs.2004.02.001.

[55] H. M. Henning, “Solar-Assisted Air-Conditioning of Buildings: A Handbook for Planners,” 1st ed., vol. 1. Springer Verlag GmbH, 2003.

[56] G. A. Florides, S. A. Tassou, S. A. Kalogirou, and L. C. Wrobel, “Review of solar and low energy cooling technologies for buildings,” Renewable and Sustainable Energy Reviews, Volume 6, Issue 6, 2002. [Online]. Available: www.elsevier.com/locate/rser

[57] S. A. Kalogirou and G. A. Florides, “Solar space heating and cooling systems,” in Comprehensive Renewable Energy, vol. 3, Elsevier Ltd, 2012, pp. 449–480. doi: 10.1016/B978-0-08-087872-0.00313-9.

[58] X. Zhang, X. Zhao, J. Xu, and X. Yu, “Characterization of a solar photovoltaic/loop-heat-pipe heat pump water heating system,” Appl Energy, vol. 102, pp. 1229–1245, 2013, doi: 10.1016/j.apenergy.2012.06.039.

[59] S. Vaishak and P. V. Bhale, “Photovoltaic/thermal-solar assisted heat pump system: Current status and future prospects,” Solar Energy, vol. 189. Elsevier Ltd, pp. 268–284, Sep. 01, 2019. doi: 10.1016/j.solener.2019.07.051.

[60] L. Evangelisti, R. De Lieto Vollaro, and F. Asdrubali, “Latest advances on solar thermal collectors: A comprehensive review,” Renewable and Sustainable Energy Reviews, vol. 114. Elsevier Ltd, Oct. 01, 2019. doi: 10.1016/j.rser.2019.109318.

[61] A. Shafieian, M. Khiadani, and A. Nosrati, “A review of latest developments, progress, and applications of heat pipe solar collectors,” Renewable and Sustainable Energy Reviews, vol. 95. Elsevier Ltd, pp. 273–304, Nov. 01, 2018. doi: 10.1016/j.rser.2018.07.014.

[62] M. B. Elsheniti, A. Kotb, and O. Elsamni, “Thermal performance of a heat-pipe evacuated-tube solar collector at high inlet temperatures,” Appl Therm Eng, vol. 154, pp. 315–325, May 2019, doi: 10.1016/j.applthermaleng.2019.03.106.

[63] W. He, Y. Su, Y. Q. Wang, S. B. Riffat, and J. Ji, “A study on incorporation of thermoelectric modules with evacuated-tube heat-pipe solar collectors,” Renew Energy, vol. 37, no. 1, pp. 142–149, Jan. 2012, doi: 10.1016/j.renene.2011.06.002.

[64] L. Jiang, B. Widyolar, and R. Winston, “Characterization of Novel Mid-temperature CPC Solar Thermal Collectors,” in Energy Procedia, Elsevier Ltd, 2015, pp. 65–70. doi: 10.1016/j.egypro.2015.02.098.

[65] G. Ma, Z. Yin, X. Liu, J. Qi, and Y. Dai, “Developments of CPC solar evacuated glass tube collector with a novel selective coating,” Solar Energy, vol. 220, pp. 1120–1129, May 2021, doi: 10.1016/j.solener.2020.08.052.

[66] Artic Solar, “External Concentrating Parabolic Collector (XCPC).” Artic Solar, Jacksonville, pp. 1–2. Accessed: November 1, 2023. [online]. Available: https://articsolar.com/

[67] B. Widyolar, L. Jiang, J. Ferry, and R. Winston, “Non-tracking East-West XCPC solar thermal collector for 200 celsius applications,” Appl Energy, vol. 216, pp. 521–533, Apr. 2018, doi: 10.1016/j.apenergy.2018.02.031.

[68] A. Najjaran, A. A. Harraz, J. Freeman, and N. Mac Dowell, “Numerical and experimental investigation of diffusion absorption refrigeration systems for use with low-temperature heat sources,” 2018.

[69] G. Alva, L. Liu, X. Huang, and G. Fang, “Thermal energy storage materials and systems for solar energy applications,” Renewable and Sustainable Energy Reviews, vol. 68. Elsevier Ltd, pp. 693–706, Feb. 01, 2017. doi: 10.1016/j.rser.2016.10.021.

[70] K. Pielichowska and K. Pielichowski, “Phase change materials for thermal energy storage,” Progress in Materials Science, vol. 65. Elsevier Ltd, pp. 67–123, 2014. doi: 10.1016/j.pmatsci.2014.03.005.

[71] I. Dinçer and R. Marc A., “Thermal Energy Storage : Systems and Applications,” John Wiley & Sons, Incorporated, 2010.

[72] A. Sharma, V. V. Tyagi, C. R. Chen, and D. Buddhi, “Review on thermal energy storage with phase change materials and applications,” Renewable and Sustainable Energy Reviews, vol. 13, no. 2. pp. 318–345, Feb. 2009. doi: 10.1016/j.rser.2007.10.005.

[73] H. Selvnes, Y. Allouche, R. I. Manescu, and A. Hafner, “Review on cold thermal energy storage applied to refrigeration systems using phase change materials,” Thermal Science and Engineering Progress, vol. 22. Elsevier Ltd, May 01, 2021. doi: 10.1016/j.tsep.2020.100807.

[74] L. Shilei, Z. Neng, and F. Guohui, “Eutectic mixtures of capric acid and lauric acid applied in building wallboards for heat energy storage,” Energy Build, vol. 38, no. 6, pp. 708–711, Jun. 2006, doi: 10.1016/j.enbuild.2005.10.006.

[75] P. Pardo, A. Deydier, Z. Anxionnaz-Minvielle, S. Rougé, M. Cabassud, and P. Cognet, “A review on high-temperature thermochemical heat energy storage,” Renewable and Sustainable Energy Reviews, vol. 32. pp. 591–610, Apr. 2014. doi: 10.1016/j.rser.2013.12.014.

[76] D. Gielen and M. Taylor, “Modelling industrial energy use: The IEAs Energy Technology Perspectives,” Energy Econ, vol. 29, no. 4, pp. 889–912, Jul. 2007, doi: 10.1016/j.eneco.2007.01.008.

[77] D. Ürge-Vorsatz, L. F. Cabeza, S. Serrano, C. Barreneche, and K. Petrichenko, “Heating and cooling energy trends and drivers in buildings,” Renewable and Sustainable Energy Reviews, vol. 41. Elsevier Ltd, pp. 85–98, 2015. doi: 10.1016/j.rser.2014.08.039.

[78] A. Abela, L. Hamilton, R. Hitchin, A. Lewry, and C. Pout, “Study on Energy Use by Air-Conditioning: Final Report BRE Client Report for the Department of Energy & Climate Change, HPR218-1001-June 2016 Contents.” Accessed: November 1, 2023. [online]. Available: www.nationalarchives.gov.uk/doc/open-government-licence/

[79] M. Santamouris, “Cooling the buildings – past, present and future,” Energy Build, vol. 128, pp. 617–638, Sep. 2016, doi: 10.1016/j.enbuild.2016.07.034.

[80] A. Alahmer and S. Alsaqoor, “Simulation and optimization of multi-split variable refrigerant flow systems,” Ain Shams Engineering Journal, vol. 9, no. 4, pp. 1705–1715, Dec. 2018, doi: 10.1016/j.asej.2017.01.002.

[81] A. Alahmer and S. Ajib, “Solar cooling technologies: State of the art and perspectives,” Energy Convers Manag, vol. 214, Jun. 2020, doi: 10.1016/j.enconman.2020.112896.

[82] C. Baldwin and C. A. Cruickshank, “A review of solar cooling technologies for residential applications in Canada,” in Energy Procedia, Elsevier Ltd, 2012, pp. 495–504. doi: 10.1016/j.egypro.2012.11.059.

[83] W. Johnston, “Solar Air Conditioning: Opportunities And Obstacles In Australia,” 2006. Accessed: November 1, 2023. [online]. Available: www.issinstitute.org.au

[84] D. Urge-Vorsatz, K. Petrichenko, M. Staniec, and J. Eom, “Energy use in buildings in a long-term perspective,” Curr Opin Environ Sustain, vol. 5, no. 2, Jun. 2013, doi: 10.1016/j.cosust.2013.05.004.

[85] L. D. D. Harvey, K. Korytarova, O. Lucon, and V. Roshchanka, “Construction of a global disaggregated dataset of building energy use and floor area in 2010,” Energy Build, vol. 76, Jun. 2014, doi: 10.1016/j.enbuild.2014.03.011.

[86] J. K. Carson, “Refrigeration: Theory And Applications,” Nova Publishers, 2013.

[87] D. Oughton and A. Wilson, “Faber and Kell’s Heating and Air-conditioning of Buildings,” 11 edition. Routledge, 2015.

[88] R. and A. C. Engineers. “American Society of Heating, 2009 ASHRAE handbook : fundamentals, “American Society of Heating, Refrigerating and Air-Conditioning Engineers, 2009.

[89] D. K. Bhamare, M. K. Rathod, and J. Banerjee, “Passive cooling techniques for building and their applicability in different climatic zones—The state of the art,” Energy and Buildings, vol. 198. Elsevier Ltd, pp. 467–490, Sep. 01, 2019. doi: 10.1016/j.enbuild.2019.06.023.

[90] N. B. Geetha and R. Velraj, “Passive cooling methods for energy efficient buildings with and without thermal energy storage-A review,” 2012. https://www.semanticscholar.org/paper/Passive-cooling-methods-for-energy-efficient-with-A-Geetha-Velraj/eabe66ea2769d2651e5c688ac24d1aa6ca685a42

[91] N. M. Nahar, P. Sharma, and M. M. Purohit, “Studies on solar passive cooling techniques for arid areas.” Energy Conversion and Management, vol. 40, issue 1, pg. 89-95, 1999, doi.org/10.1016/S0196-8904(98)00039-9.

[92] R. Tang and Y. Etzion, “Cooling performance of roof ponds with gunny bags floating on the water surface as compared with a movable insulation,” Renew Energy, vol. 30, no. 9, pp. 1373–1385, Jul. 2005, doi: 10.1016/j.renene.2004.10.008.

[93] B. P. Jelle, D. Arasteh, and C. Kohler, “State-of-the-Art Highly Insulating Window Frames-Research and Market Review Project report 6-2007 SINTEF Building and Infrastructure Project report no 6 Arild Gustavsen 1) 2) State-of-the-Art Highly Insulating Window Frames-Research and Market Review special agreement with SINTEF Building,” 2007. [Online]. Available: www.sintef.no/byggforsk

[94] J. W. Lee, H. J. Jung, J. Y. Park, J. B. Lee, and Y. Yoon, “Optimization of building window system in Asian regions by analyzing solar heat gain and daylighting elements,” Renew Energy, vol. 50, pp. 522–531, Feb. 2013, doi: 10.1016/j.renene.2012.07.029.

[95] A. Kirimtat, B. K. Koyunbaba, I. Chatzikonstantinou, and S. Sariyildiz, “Review of simulation modeling for shading devices in buildings,” Renewable and Sustainable Energy Reviews, vol. 53. Elsevier Ltd, pp. 23–49, Jan. 05, 2016. doi: 10.1016/j.rser.2015.08.020.

[96] C. Amaris, M. Vallès, and M. Bourouis, “Vapour absorption enhancement using passive techniques for absorption cooling/heating technologies: A review,” Applied Energy, vol. 231. Elsevier Ltd, pp. 826–853, Dec. 01, 2018. doi: 10.1016/j.apenergy.2018.09.071.

[97] A. Jayalath, L. Aye, P. Mendis, and T. Ngo, “Effects of phase change material roof layers on the thermal performance of a residential building in Melbourne and Sydney,” Energy Build, vol. 121, pp. 152–158, Jun. 2016, doi: 10.1016/j.enbuild.2016.04.007.

[98] F. Goia, M. Perino, and V. Serra, “Improving thermal comfort conditions by means of PCM glazing systems,” Energy Build, vol. 60, pp. 442–452, 2013, doi: 10.1016/j.enbuild.2013.01.029.

[99] F. Jomehzadeh et al., “A review on windcatcher for passive cooling and natural ventilation in buildings, Part 1: Indoor air quality and thermal comfort assessment,” Renewable and Sustainable Energy Reviews, vol. 70. Elsevier Ltd, pp. 736–756, 2017. doi: 10.1016/j.rser.2016.11.254.

[100] B. Costelloe and D. Finn, “Indirect evaporative cooling potential in air-water systems in temperate climates.” Energy and Buildings, vol. 35, no. 6, pp. 573-591, 2003. doi.org/10.1016/S0378-7788(02)00161-5.

[101] M. Zeyghami, D. Y. Goswami, and E. Stefanakos, “A review of clear sky radiative cooling developments and applications in renewable power systems and passive building cooling,” Solar Energy Materials and Solar Cells, vol. 178, pp. 115–128, May 2018, doi: 10.1016/j.solmat.2018.01.015.

[102] S. Vall and A. Castell, “Radiative cooling as low-grade energy source: A literature review,” Renewable and Sustainable Energy Reviews, vol. 77. Elsevier Ltd, pp. 803–820, 2017. doi: 10.1016/j.rser.2017.04.010.

[103] M. Zeyghami, D. Y. Goswami, and E. Stefanakos, “A review of solar thermo-mechanical refrigeration and cooling methods,” Renewable and Sustainable Energy Reviews, vol. 51. Elsevier Ltd, pp. 1428–1445, Aug. 03, 2015. doi: 10.1016/j.rser.2015.07.011.

[104] A. Ghafoor and A. Munir, “Worldwide overview of solar thermal cooling technologies,” Renewable and Sustainable Energy Reviews, vol. 43. Elsevier Ltd, pp. 763–774, Feb. 05, 2015. doi: 10.1016/j.rser.2014.11.073.

[105] K. R. Ullah, R. Saidur, H. W. Ping, R. K. Akikur, and N. H. Shuvo, “A review of solar thermal refrigeration and cooling methods,” Renewable and Sustainable Energy Reviews, vol. 24. pp. 499–513, 2013. doi: 10.1016/j.rser.2013.03.024.

[106] J. Guo and H. G. Shen, “Modeling solar-driven ejector refrigeration system offering air conditioning for office buildings,” Energy Build, vol. 41, no. 2, pp. 175–181, Feb. 2009, doi: 10.1016/j.enbuild.2008.07.016.

[107] J. M. Abdulateef, K. Sopian, M. A. Alghoul, and M. Y. Sulaiman, “Review on solar-driven ejector refrigeration technologies,” Renewable and Sustainable Energy Reviews, vol. 13, no. 6–7. pp. 1338–1349, Aug. 2009. doi: 10.1016/j.rser.2008.08.012.

[108] A. Allouhi, T. Kousksou, A. Jamil, P. Bruel, Y. Mourad, and Y. Zeraouli, “Solar driven cooling systems: An updated review,” Renewable and Sustainable Energy Reviews, vol. 44. Elsevier Ltd, pp. 159–181, 2015. doi: 10.1016/j.rser.2014.12.014.

[109] E. Wali, “Optimum working fluids for solar powered Rankine cycle cooling of buildings,” Solar Energy, vol. 25, no. 3, pp. 235–241, 1980, doi: https://doi.org/10.1016/0038-092X(80)90330-8.

[110] N. Kalkan, E. A. Young, and A. Celiktas, “Solar thermal air conditioning technology reducing the footprint of solar thermal air conditioning,” Renewable and Sustainable Energy Reviews, vol. 16, no. 8. pp. 6352–6383, Oct. 2012. doi: 10.1016/j.rser.2012.07.014.

[111] I. Sarbu and C. Sebarchievici, “Review of solar refrigeration and cooling systems,” Energy and Buildings, vol. 67. pp. 286–297, 2013. doi: 10.1016/j.enbuild.2013.08.022.

[112] A. Al-Alili, Y. Hwang, and R. Radermacher, “Review of solar thermal air conditioning technologies,” International Journal of Refrigeration, vol. 39. Elsevier Ltd, pp. 4–22, 2014. doi: 10.1016/j.ijrefrig.2013.11.028.

[113] A. Shirazi, R. A. Taylor, G. L. Morrison, and S. D. White, “Solar-powered absorption chillers: A comprehensive and critical review,” Energy Conversion and Management, vol. 171. Elsevier Ltd, pp. 59–81, Sep. 01, 2018. doi: 10.1016/j.enconman.2018.05.091.

[114] K. E. Herold, R. Radermacher, and S. A. Klein, “Absorption Chillers and Heat Pumps,” 2nd ed. CRC Press, 2016.

[115] A. Shirazi, R. A. Taylor, G. L. Morrison, and S. D. White, “Solar-powered absorption chillers: A comprehensive and critical review,” Energy Conversion and Management, vol. 171. Elsevier Ltd, pp. 59–81, Sep. 01, 2018. doi: 10.1016/j.enconman.2018.05.091.

[116] M. Balghouthi, M. H. Chahbani, and A. Guizani, “Feasibility of solar absorption air conditioning in Tunisia,” Build Environ, vol. 43, no. 9, pp. 1459–1470, Sep. 2008, doi: 10.1016/j.buildenv.2007.08.003.

[117] J. Sun, L. Fu, and S. Zhang, “A review of working fluids of absorption cycles,” Renewable and Sustainable Energy Reviews, vol. 16, no. 4. pp. 1899–1906, May 2012. doi: 10.1016/j.rser.2012.01.011.

[118] G. A. Florides, S. A. Kalogirou, S. A. Tassou, and L. C. Wrobel, “Design and construction of a LiBr-water absorption machine,” Energy Convers Manag, vol. 44, no. 15, pp. 2483–2508, Sep. 2003, doi: 10.1016/S0196-8904(03)00006-2.

[119] T. Berlitz, H. Plank, F. Ziegler, and R. Kahn, “An ammonia-water absorption refrigerator with a large temperature lift for combined heating and cooling,” International Journal of Refrigeration, vol. 21, no. 3, pp. 219-229, 1998. doi.org/10.1016/S0140-7007(98)00018-8.

[120] M. J. P. Bogart, “Pitfalls in ammonia absorption refrigeration,” International Journal of Refrigeration, vol. 5, no. 4, pp. 203–208, 1982, doi: https://doi.org/10.1016/0140-7007(82)90020-2.

[121] T. D. Eastop, “Mechanical Services for Buildings,” 1st ed. Longman, 1992. pp. 1-263.

[122] W. Grondzik, “Air-conditioning system design manual,” 2nd ed. BH Press, 2001, pp. 1-401.

[123] R. H. Howell, “Principles of heating ventilating and air conditioning : a textbook with design data based on the 2017 ASHRAE handbook of fundamentals,” 8th ed. ASHRAE, 2017, pp. 1-593.

[124] S. Seyam, “Types of HVAC Systems,” in HVAC System, InTech, 05 November 2018. Accessed November 1, 2023, [online] Available: doi: 10.5772/intechopen.78942.

[125] ASHRAE, “ASHRAE Handbook 2016: HVAC Systems and Equipment: SI Edition,” 2016th ed. Atlanta: ASHRAE, 2016, pp. 10-992.

[126] F. Hall and R. Greeno, “Building Services Handbook, 8th edition. Routledge,” 2013, pp. 768.

[127] Mike. Price, and Ken. Butcher, “Chartered Institution of Building Services Engineers: TM43 Fan coil units.” CIBSE, 2008, pp. 1-47.

[128] I. Staffell, D. Brett, N. Brandon, and A. Hawkes, “A review of domestic heat pumps,” Energy and Environmental Science, vol. 5, no. 11. pp. 9291–9306, Nov. 2012. doi: 10.1039/c2ee22653g.

[129] J. Sarkar, S. Bhattacharyya, and M. R. Gopal, “Simulation of a transcritical CO2 heat pump cycle for simultaneous cooling and heating applications,” International Journal of Refrigeration, vol. 29, no. 5, pp. 735–743, 2006, doi: 10.1016/j.ijrefrig.2005.12.006.

[130] M. Song, S. Deng, C. Dang, N. Mao, and Z. Wang, “Review on improvement for air source heat pump units during frosting and defrosting,” Applied Energy, vol. 211. Elsevier Ltd, pp. 1150–1170, Feb. 01, 2018. doi: 10.1016/j.apenergy.2017.12.022.

[131] B. Seo, Y. B. Yoon, B. H. Yu, S. Cho, and K. H. Lee, “Comparative analysis of cooling energy performance between water-cooled VRF and conventional AHU systems in a commercial building,” Appl Therm Eng, vol. 170, Apr. 2020, doi: 10.1016/j.applthermaleng.2020.114992.

[132] T. Hong, K. Sun, R. Zhang, R. Hinokuma, S. Kasahara, and Y. Yura, “Development and validation of a new variable refrigerant flow system model in EnergyPlus,” Energy Build, vol. 117, pp. 399–411, Apr. 2016, doi: 10.1016/j.enbuild.2015.09.023.

[133] W. H. Kang et al., “Modeling, calibration, and sensitivity analysis of direct expansion AHU-Water source VRF system,” Energy, vol. 199, May 2020, doi: 10.1016/j.energy.2020.117435.

[134] J. K. Carson, “Refrigeration: Theory And Applications.” Bookboon, 2013, pp. 1-128.

[135] J. W. Mitchell and J. E. Braun, “Principles of Heating, Ventilation, and Air Conditioning in Buildings”, 1st ed. Wiley, 2012, pp. 1-595.

[136] M. A. Boles and Y. A. Cengel, “Thermodynamics: An Engineering Approach”, 5th ed. McGraw-Hill, 2005, pp. 1-963.

[137] M. G. Gado, S. Ookawara, S. Nada, and I. I. El-Sharkawy, “Hybrid sorption-vapor compression cooling systems: A comprehensive overview,” Renewable and Sustainable Energy Reviews, vol. 143. Elsevier Ltd, Jun. 01, 2021. doi: 10.1016/j.rser.2021.110912.

[138] T. Hu, J. Liu, J. Chang, and Z. Hao, “Development of a novel vapor compression refrigeration system (VCRS) for permafrost cooling,” Cold Reg Sci Technol, vol. 181, Jan. 2021, doi: 10.1016/j.coldregions.2020.103173.

[139] ASHRAE, “2017 ASHRAE Handbook -- Fundamentals (SI)”, 2017th ed. Ashrae, 2017, pp. 1-1000.

[140] R. Mansouri, M. Bourouis, and A. Bellagi, “Steady-state investigations of a commercial diffusion-absorption refrigerator: Experimental study and numerical simulations,” Appl Therm Eng, vol. 129, pp. 725–734, Jan. 2018, doi: 10.1016/j.applthermaleng.2017.10.010.

[141] A. Zohar, M. Jelinek, A. Levy, and I. Borde, “Numerical investigation of a diffusion absorption refrigeration cycle,” International Journal of Refrigeration, vol. 28, no. 4, pp. 515–525, Jun. 2005, doi: 10.1016/j.ijrefrig.2004.11.003.

[142] G. Starace and L. De Pascalis, “An advanced analytical model of the Diffusion Absorption Refrigerator cycle,” International Journal of Refrigeration, vol. 35, no. 3, pp. 605–612, May 2012, doi: 10.1016/j.ijrefrig.2011.11.007.

[143] UK 2013 building regulation, “Approved Document L1A: Conservation of fuel and power in new dwellings,” Accessed: November 1, 2023. [online].

www.planningportal.co.uk/info/200135/approved_documents/74/part_l_-_conservation_of_fuel_and_power.

[144] CIBSE, “CIBSE Guide B: Heating, Ventilating, Air Conditioning and Refrigeration”, 1st ed. Chartered Institution of Building Services Engineers (CIBSE), 2001, pp. 1-369.

[145] D. A. SNOW, “Plant Engineer’s Reference Book,” 1st ed. Butterworth-Heinemann Ltd, 1991, pp. 1-672.

[146] A. T. Reddy, J. F. Kreider, P. S. Curtiss, and A. Rabl, “Heating and Cooling of Buildings: Principles and Practice of Energy Efficient Design,” 3rd ed. CRC Press, 2016, pp. 1-900.

[147] Glen Dimplex UK Limited, “Heat generators.” Accessed: Nov. 01, 2023. [Online]. Available: https://product-portal.gdhv.com/sites/default/files/assets//Heat_Pump_Brochure.pdf

[148] G. Schwank, “Functioning principle of gas-fired tube heaters.” Accessed: Nov. 01, 2023. [Online]. Available: https://schwank.co.uk/products/heating-solutions/tube-heaters/

[149] S. Marinelli, F. Lolli, R. Gamberini, and B. Rimini, “Life Cycle Thinking (LCT) applied to residential heat pump systems: A critical review,” Energy and Buildings, vol. 185. Elsevier Ltd, pp. 210–223, Feb. 15, 2019. doi: 10.1016/j.enbuild.2018.12.035.

[150] J. Luo, J. Rohn, W. Xiang, D. Bertermann, and P. Blum, “A review of ground investigations for ground source heat pump (GSHP) systems,” Energy and Buildings, vol. 117. Elsevier Ltd, pp. 160–175, Apr. 01, 2016. doi: 10.1016/j.enbuild.2016.02.038.

[151] I. Sarbu and C. Sebarchievici, “General review of ground-source heat pump systems for heating and cooling of buildings,” Energy and Buildings, vol. 70. pp. 441–454, Feb. 2014. doi: 10.1016/j.enbuild.2013.11.068.

[152] H. Willem, Y. Lin, and A. Lekov, “Review of energy efficiency and system performance of residential heat pump water heaters,” Energy and Buildings, vol. 143. Elsevier Ltd, pp. 191–201, May 15, 2017. doi: 10.1016/j.enbuild.2017.02.023.

[153] K. Alanne and A. Saari, “Sustainable small-scale CHP technologies for buildings: The basis for multi-perspective decision-making,” Renewable and Sustainable Energy Reviews, vol. 8, no. 5. pp. 401–431, Oct. 2004. doi: 10.1016/j.rser.2003.12.005.

[154] L. Dong, H. Liu, and S. Riffat, “Development of small-scale and micro-scale biomass-fuelled CHP systems - A literature review,” Applied Thermal Engineering, vol. 29, no. 11–12. pp. 2119–2126, Aug. 2009. doi: 10.1016/j.applthermaleng.2008.12.004.

[155] C. Maurer, C. Cappel, and T. E. Kuhn, “Progress in building-integrated solar thermal systems,” Solar Energy, vol. 154, pp. 158–186, 2017, doi: 10.1016/j.solener.2017.05.065.

[156] D. Lader, S. Short, and J. Gershuny, “The Time Use Survey, 2005 How we spend our time A report on research using the ONS Omnibus Survey produced on behalf of the Economic and Social Research Council (ESRC), Department of Culture, Media and Sport (DCMS), Department for Education and Skills,” 2006. Accessed: November 1, 2023. [Online]. Available: www.opsi.gov.uk/click-use/system/online/pLogin.asp

[157] N. E. Klepeis et al., “The National Human Activity Pattern Survey (NHAPS): a resource for assessing exposure to environmental pollutants.” Accessed: November 1, 2023. [Online]. Available: www.nature.com/jea

[158] M. Herrera, “A review of current and future weather data for building simulation,” Building Services Engineering Research and Technology, vol. 38, no. 5. SAGE Publications Ltd, pp. 602–627, Sep. 01, 2017. doi: 10.1177/0143624417705937.

[159] A. J. McMichael, R. E. Woodruff, and S. Hales, “Climate change and human health- present and future risks”. The Lancet, vol. 367, no. 9513, pp. 859-869, 2006, doi.org/10.1016/S0140-6736(06)68079-3.

[160] P. de Wilde and D. Coley, “The implications of a changing climate for buildings,” Building and Environment, vol. 55. pp. 1–7, Sep. 2012. doi: 10.1016/j.buildenv.2012.03.014.

[161] CIBSE, “CIBSE Guide A: Environmental Design,” 7th ed. London: Chartered Institution of Building Services Engineers, 2006, pp. 1-100.

[162] J. F. Kreider, P. S. Curtiss, and A. Rabl, “HEATING AND COOLING OF BUILDINGS, Design for Efficiency.” 2nd ed. CRC Press, 2010, pp. 1-863.

[163] T. Kusuda, “Fundamentals of Building Heat Transfer.” JOURNAL OF RESEARCH of the National Bureau of Standards, vol. 82, No.2, 1977. https://nvlpubs.nist.gov/nistpubs/jres/82/jresv82n2p97_a1b.pdf

[164] Hens Hugo S. L., “Building Physics - Heat, Air and Moisture : Fundamentals and Engineering Methods with Examples and Exercises”, 2nd ed. Wilhelm Ernst & Sohn Verlag fur Architektur und Technische, 2012.

[165] Z. Afroz, G. M. Shafiullah, T. Urmee, and G. Higgins, “Modeling techniques used in building HVAC control systems: A review,” Renewable and Sustainable Energy Reviews, vol. 83. Elsevier Ltd, pp. 64–84, Mar. 01, 2018. doi: 10.1016/j.rser.2017.10.044.

[166] C. Ghiaus, A. Chicinas, and C. Inard, “Grey-box identification of air-handling unit elements,” Control Eng Pract, vol. 15, no. 4, pp. 421–433, Mar. 2007, doi: 10.1016/j.conengprac.2006.08.005.

[167] R. Z. Homod, “Review on the HVAC System Modeling Types and the Shortcomings of Their Application,” Journal of Energy, vol. 2013, pp. 1–10, 2013, doi: 10.1155/2013/768632.

[168] T. P. Mcdowell, D. E. Bradley, J. W. Thornton, and M. Kummert, “Simulation Synergy: Expanding Trnsys Capabilities And Usability,” SimBuild 2004, IBPSA-USA National Conference Boulder, CO, August 4-6, 2004.

[169] M. J. Duffy, M. Hiller, D. E. Bradley, W. Keilholz, and J. W. Thornton, “Trnsys – Features And Functionality For Building Simulation 2009 Conference.” Eleventh International IBPSA Conference, Glasgow, Scotland, July 27-30, 2009.

[170] C. N. Antoniadis and G. Martinopoulos, “Optimization of a building integrated solar thermal system with seasonal storage using TRNSYS,” Renew Energy, pp. 56–66, Jul. 2019, doi: 10.1016/j.renene.2018.03.074.

[171] S. A. et al Klein, “TRNSYS 18: A Transient System Simulation Program.” University of Wisconsin, Madison, USA, 2017. [Online]. Available: http://sel.me.wisc.edu/trnsys

[172] M. Villa-Arrieta and A. Sumper, “A model for an economic evaluation of energy systems using TRNSYS,” Appl Energy, vol. 215, pp. 765–777, Apr. 2018, doi:10.1016/j.apenergy.2018.02.045.

[173] O. Asa’d, V. I. Ugursal, and N. Ben-Abdallah, “Investigation of the energetic performance of an attached solar greenhouse through monitoring and simulation,” Energy for Sustainable Development, vol. 53. Elsevier B.V., pp. 15–29, Dec. 01, 2019. doi: 10.1016/j.esd.2019.09.001.

[174] R. L. Shrivastava, V. Kumar, and S. P. Untawale, “Modeling and simulation of solar water heater: A TRNSYS perspective,” Renewable and Sustainable Energy Reviews, vol. 67. Elsevier Ltd, pp. 126–143, Jan. 01, 2017. doi: 10.1016/j.rser.2016.09.005.

[175] M. J. R. Abdunnabia, K. M. A . Alakderb, N. A. Alkishriwic and S. M. Abughresc, “Experimental Validation of Forced Circulation of Solar Water Heating Systems in TRNSYS.” Energy Procedia, vol. 57, pp. 2477 – 2486, 2014.

[176] R. L. Shrivastava, V. Kumar, and S. P. Untawale, “Modeling and simulation of solar water heater: A TRNSYS perspective,” Renewable and Sustainable Energy Reviews, vol. 67. Elsevier Ltd, pp. 126–143, Jan. 01, 2017. doi: 10.1016/j.rser.2016.09.005.

[177] R. Chargui and H. Sammouda, “Modeling of a residential house coupled with a dual source heat pump using TRNSYS software,” Energy Convers Manag, vol. 81, pp. 384–399, 2014, doi: 10.1016/j.enconman.2014.02.040.

[178] P. Riederer, W. Keilholz, and V. Ducreux, “Coupling Of Trnsys With Simulink-A Method To Automatically Export And Use Trnsys Models Within Simulink And Vice Versa.” Eleventh International IBPSA Conference, Glasgow, Scotland, July 27-30, 2009.

[179] A. M. Baniyounes, G. Liu, M. G. Rasul, and M. M. K. Khan, “Analysis of solar desiccant cooling system for an institutional building in subtropical Queensland, Australia,” Renewable and Sustainable Energy Reviews, vol. 16, no. 8. pp. 6423–6431, Oct. 2012. doi: 10.1016/j.rser.2012.07.021.

[180] M. S. Ahamed, H. Guo, and K. Tanino, “Modeling heating demands in a Chinese-style solar greenhouse using the transient building energy simulation model TRNSYS,” Journal of Building Engineering, vol. 29, May 2020, doi: 10.1016/j.jobe.2019.101114.

[181] S. N. Al-Saadi and Z. Zhai, “A new validated TRNSYS module for simulating latent heat storage walls,” Energy Build, vol. 109, pp. 274–290, Dec. 2015, doi: 10.1016/j.enbuild.2015.10.013.

[182] M. Liu, W. Saman, and F. Bruno, “Computer simulation with TRNSYS for a mobile refrigeration system incorporating a phase change thermal storage unit,” Appl Energy, vol. 132, pp. 226–235, Nov. 2014, doi: 10.1016/j.apenergy.2014.06.066.

[183] G. Hou, H. Taherian, and L. Li, “A predictive TRNSYS model for long-term operation of a hybrid ground source heat pump system with innovative horizontal buried pipe type,” Renew Energy, vol. 151, pp. 1046–1054, May 2020, doi: 10.1016/j.renene.2019.11.113.

[184] S. Bordignon, G. Emmi, A. Zarrella, and M. De Carli, “Energy analysis of different configurations for a reversible ground source heat pump using a new flexible TRNSYS Type,” Appl Therm Eng, vol. 197, Oct. 2021, doi: 10.1016/j.applthermaleng.2021.117413.

[185] M. Asim, J. Dewsbury, and S. Kanan, “TRNSYS Simulation of a Solar Cooling System for the Hot Climate of Pakistan,” in Energy Procedia, Elsevier Ltd, 2016, pp. 702–706. doi: 10.1016/j.egypro.2016.06.233.

[186] J. T. McLeskey, L. T. Terziotti, and M. L. Sweet, “Modeling seasonal solar thermal energy storage in a large urban residential building using TRNSYS 16,” Energy Build, vol. 45, pp. 28–31, Feb. 2012, doi: 10.1016/j.enbuild.2011.10.023.

[187] M. C. Lekhal, R. Belarbi, A. M. Mokhtari, M. H. Benzaama, and R. Bennacer, “Thermal performance of a residential house equipped with a combined system: A direct solar floor and an earth–air heat exchanger,” Sustainable Cities and Society, vol. 40. Elsevier Ltd, pp. 534–545, Jul. 01, 2018. doi: 10.1016/j.scs.2018.05.012.

[188] M. S. A. Khan, A. W. Badar, T. Talha, M. W. Khan, and F. S. Butt, “Configuration based modeling and performance analysis of single effect solar absorption cooling system in TRNSYS,” Energy Convers Manag, vol. 157, pp. 351–363, Feb. 2018, doi: 10.1016/j.enconman.2017.12.024.

[189] A. F. Altun and M. Kilic, “Economic feasibility analysis with the parametric dynamic simulation of a single effect solar absorption cooling system for various climatic regions in Turkey,” Renew Energy, vol. 152, pp. 75–93, Jun. 2020, doi: 10.1016/j.renene.2020.01.055.

[190] EnergyPlus, “EnergyPlus software.” 2020. Accessed: November 1, 2023, [Online]. Available: https://energyplus.net/sites/all/modules/custom/nrel_custom/pdfs/pdfs_v9.2.0/GettingStarted.pdf

[191] D. B. Crawley, J. W. Hand, M. Kummert, and B. T. Griffith, “Contrasting the capabilities of building energy performance simulation programs,” Build Environ, vol. 43, no. 4, pp. 661–673, Apr. 2008, doi: 10.1016/j.buildenv.2006.10.027.

[192] B. Shen, J. New, and V. Baxter, “Air source integrated heat pump simulation model for EnergyPlus,” Energy Build, vol. 156, pp. 197–206, Dec. 2017, doi: 10.1016/j.enbuild.2017.09.064.

[193] A. Boyano, P. Hernandez, and O. Wolf, “Energy demands and potential savings in European office buildings: Case studies based on EnergyPlus simulations,” Energy Build, vol. 65, pp. 19–28, 2013, doi: 10.1016/j.enbuild.2013.05.039.

[194] K. S. Cetin, M. H. Fathollahzadeh, N. Kunwar, H. Do, and P. C. Tabares-Velasco, “Development and validation of an HVAC on/off controller in EnergyPlus for energy simulation of residential and small commercial buildings,” Energy Build, vol. 183, pp. 467–483, Jan. 2019, doi: 10.1016/j.enbuild.2018.11.005.

[195] R. Kamal, F. Moloney, C. Wickramaratne, A. Narasimhan, and D. Y. Goswami, “Strategic control and cost optimization of thermal energy storage in buildings using EnergyPlus,” Appl Energy, vol. 246, pp. 77–90, Jul. 2019, doi: 10.1016/j.apenergy.2019.04.017.

[196] H. Gao, C. Koch, and Y. Wu, “Building information modelling based building energy modelling: A review,” Applied Energy, vol. 238. Elsevier Ltd, pp. 320–343, Mar. 15, 2019. doi: 10.1016/j.apenergy.2019.01.032.

[197] N. Fumo, “A review on the basics of building energy estimation,” Renewable and Sustainable Energy Reviews, vol. 31. pp. 53–60, Mar. 2014. doi: 10.1016/j.rser.2013.11.040.

[198] H. Gao, C. Koch, and Y. Wu, “Building information modelling based building energy modelling: A review,” Applied Energy, vol. 238. Elsevier Ltd, pp. 320–343, Mar. 15, 2019. doi: 10.1016/j.apenergy.2019.01.032.

[199] S. A. Klein, “EES – Engineering Equation Solver.” F-Chart Software, 2020. [Online]. Available: http://fchartsoftware.com

[200] B. Tashtoush, A. Alshare, and S. Al-Rifai, “Hourly dynamic simulation of solar ejector cooling system using TRNSYS for Jordanian climate,” Energy Convers Manag, vol. 100, pp. 288–299, Aug. 2015, doi: 10.1016/j.enconman.2015.05.010.

[201] B. Tashtoush, A. Alshare, and S. Al-Rifai, “Performance study of ejector cooling cycle at critical mode under superheated primary flow,” Energy Convers Manag, vol. 94, pp. 300–310, 2015, doi: 10.1016/j.enconman.2015.01.039.

[202] H. Vidal, S. Colle, and G. D. S. Pereira, “Modelling and hourly simulation of a solar ejector cooling system,” Appl Therm Eng, vol. 26, no. 7, pp. 663–672, May 2006, doi: 10.1016/j.applthermaleng.2005.09.012.

[203] The MathWorks Inc., “MATLAB.” The MathWorks Inc., Natick, Massachusetts, 2020. [Online]. Available: https://uk.mathworks.com/?s_tid=gn_logo

[204] N. Alibabaei, A. S. Fung, and K. Raahemifar, “Development of Matlab-TRNSYS co-simulator for applying predictive strategy planning models on residential house HVAC system,” Energy Build, vol. 128, pp. 81–98, Sep. 2016, doi: 10.1016/j.enbuild.2016.05.084.

[205] K. Sudhakar, M. S. Jenkins, S. Mangal, and S. S. Priya, “Modelling of a solar desiccant cooling system using a TRNSYS-MATLAB co-simulator: A review,” Journal of Building Engineering, vol. 24, Jul. 2019, doi: 10.1016/j.jobe.2019.100749.

[206] F. Bava and S. Furbo, “Development and validation of a detailed TRNSYS-Matlab model for large solar collector fields for district heating applications,” Energy, vol. 135, pp. 698–708, 2017, doi: 10.1016/j.energy.2017.06.146.

[207] N. Alibabaei, A. S. Fung, and K. Raahemifar, “Development of Matlab-TRNSYS co-simulator for applying predictive strategy planning models on residential house HVAC system,” Energy Build, vol. 128, pp. 81–98, Sep. 2016, doi: 10.1016/j.enbuild.2016.05.084.

[208] W. Bosschaerts, T. Van Renterghem, O. A. Hasan, and K. Limam, “Development of a Model Based Predictive Control System for Heating Buildings,” in Energy Procedia, Elsevier Ltd, Mar. 2017, pp. 519–528. doi: 10.1016/j.egypro.2017.03.1110.

[209] A. Al-Alili, Y. Hwang, R. Radermacher, and I. Kubo, “Optimization of a solar powered absorption cycle under Abu Dhabi’s weather conditions,” Solar Energy, vol. 84, no. 12, pp. 2034–2040, Dec. 2010, doi: 10.1016/j.solener.2010.09.013.

[210] M. Jones, “Coupling Trnsys And Matlab For Genetic Algorithm Optimization In Sustainable Building Design.” Third German-Austrian IBPSA Conference, Vienna University of Technology. BauSIM, Austria 2020.

[211] A. R. M. Rezk and R. K. Al-Dadah, “Physical and operating conditions effects on silica gel/water adsorption chiller performance,” Appl Energy, vol. 89, no. 1, pp. 142–149, 2012, doi: 10.1016/j.apenergy.2010.11.021.

[212] R. P. Sah, B. Choudhury, R. K. Das, and A. Sur, “An overview of modelling techniques employed for performance simulation of low–grade heat operated adsorption cooling systems,” Renewable and Sustainable Energy Reviews, vol. 74. Elsevier Ltd, pp. 364–376, 2017. doi: 10.1016/j.rser.2017.02.062.

[213] A. S. Rattner and S. Garimella, “Low-source-temperature diffusion absorption refrigeration. Part II: Experiments and model assessment,” International Journal of Refrigeration, vol. 65, pp. 312–329, May 2016, doi: 10.1016/j.ijrefrig.2015.11.016.

[214] A. Koyfman, M. Jelinek, A. Levy, and I. Borde, “An experimental investigation of bubble pump performance for diffusion absorption refrigeration system with organic working fluids,” Appl Therm Eng, vol. 23, no. 15, pp. 1881–1894, Oct. 2003, doi: 10.1016/S1359-4311(03)00162-5.

[215] D. J. Reinemann, J. Y. Parlange, and M. B. Timmons, “Theory of small-diameter airlift pumps,” International Journal of Multiphase Flow, vol. 16, no. 1, pp. 113–122, Jan. 1990, doi: 10.1016/0301-9322(90)90042-H.

[216] S. W. Jo, S. A. Sherif, and W. E. Lear, “Numerical Simulation of Saturated Flow Boiling Heat Transfer of Ammonia/Water Mixture in Bubble Pumps for Absorption–Diffusion Refrigerators,” ASME. J. Thermal Sci. Eng. Appl., vol. 6, no. 1, p. 011007, 2014, doi: https://doi.org/10.1115/1.4025091.

[217] A. Benhmidene, B. Chaouachi, S. Gabsi, and M. Bourouis, “Modelling of heat flux received by a bubble pump of absorption-diffusion refrigeration cycles,” Heat and Mass Transfer/Waerme- und Stoffuebertragung, vol. 47, no. 11, pp. 1341–1347, Nov. 2011, doi: 10.1007/s00231-011-0799-3.

[218] S. Mazouz, R. Mansouri, and A. Bellagi, “Experimental and thermodynamic investigation of an ammonia/water diffusion absorption machine,” International Journal of Refrigeration, vol. 45, pp. 83–91, 2014, doi: 10.1016/j.ijrefrig.2014.06.002.

[219] F. Assilzadeh, S. A. Kalogirou, Y. Ali, and K. Sopian, “Simulation and optimization of a LiBr solar absorption cooling system with evacuated tube collectors,” Renew Energy, vol. 30, no. 8, pp. 1143–1159, 2005, doi: 10.1016/j.renene.2004.09.017.

[220] M. Kottek, J. Grieser, C. Beck, B. Rudolf, and F. Rubel, “World map of the Köppen-Geiger climate classification updated,” Meteorologische Zeitschrift, vol. 15, no. 3, pp. 259–263, Jun. 2006, doi: 10.1127/0941-2948/2006/0130.

[221] Weatherspark, “Climate and Weather: New Delhi, Volgograd, Swansea, Tunis,” Accessed: November 1, 2023. [online]. Available: https://weatherspark.com/compare/y/103581~109174~37763~65683/Comparison-of-the-Average-Weather-in-Volgograd-New-Delhi-Swansea-and-Tunis.

[222] Y. Bhusal, A. Hassanzadeh, L. Jiang, and R. Winston, “Technical and economic analysis of a novel low-cost concentrated medium-temperature solar collector,” Renew Energy, vol. 146, pp. 968–985, Feb. 2020, doi: 10.1016/j.renene.2019.07.032.

[223] Y. S. Kim, K. Balkoski, L. Jiang, and R. Winston, “Efficient stationary solar thermal collector systems operating at a medium-temperature range,” Appl Energy, vol. 111, pp. 1071–1079, 2013, doi: 10.1016/j.apenergy.2013.06.051.

[224] Trimble, “Trimble SketchUp.” Accessed: April 6, 2024. [Online]. Available: https://www.sketchup.com.

[225] LABC Warranty, “Are Britain’s Houses Getting Smaller? (New Data),” Accessed: April 2, 2024. [Online]. https://www.labcwarranty.co.uk/news-blog/are-britain-s-houses-getting-smaller-new-data.

[226] P. W. O’Callaghan and S. D. Probert, “Sol-air temperature,” Appl Energy, vol. 3, no. 4, pp. 307–311, Oct. 1977, doi: 10.1016/0306-2619(77)90017-4.

[227] H. B. Awbi, Parker, K. Butcher, and Chartered Institution of Building Services Engineers, “Building performance modelling,” 2nd ed. The Chartered Institution of Building Services Engineers, London, 2015, pp. 1-213.

[228] D. Neyer, M. Ostheimer, D. Mugnier, and S. White, “10 key principles for successful solar air conditioning design – A compendium of IEA SHC Task 48 experiences,” Solar Energy, vol. 172, pp. 78–89, Sep. 2018, doi: 10.1016/j.solener.2018.03.086.

[229] S. A. Kalogirou, “Solar Economic Analysis,” Solar Energy Engineering, Elsevier, pp. 701–734, 2014, doi: 10.1016/b978-0-12-397270-5.00012-1.

[230] D. Mugnier, D. Neyer, and S. White, The Solar Cooling Design Guide, 1st ed. Wiley, 2017, pp. 1-158.

[231] A. Yildiz and M. A. Ersöz, "Energy and exergy analyses of the diffusion absorption refrigeration system," Energy, vol. 60, pp. 407–415, Oct. 2013, doi: 10.1016/j.energy.2013.07.062.

[232] G. Li, Y. Hwang, R. Radermacher, and H. H. Chun, "Review of cold storage materials for subzero applications," Energy, vol. 51. Elsevier Ltd, pp. 1–17, 2013. doi: 10.1016/j.energy.2012.12.002.

[233] Q. Deng, Z. Yang, L. Zhang, and M. Jia, "The control strategy and economic analysis of a new type of solar cold storage," Energy Storage, vol. 52, Aug. 2022, doi: 10.1016/j.est.2022.104865.

[234] F. Agyenim, I. Knight, and M. Rhodes, "Design and experimental testing of the performance of an outdoor LiBr/H2O solar thermal absorption cooling system with a cold store," Solar Energy, vol. 84, no. 5, pp. 735–744, May 2010, doi: 10.1016/j.solener.2010.01.013.

[235] M. Kapsalaki, V. Leal, and M. Santamouris, "A methodology for economic efficient design of Net Zero Energy Buildings," Energy Build, vol. 55, Dec. 2012, doi: 10.1016/j.enbuild.2012.10.022.

[236] Y. Jiang et al., "Energy, exergy, economic and environmental assessment of the triangular solar collector assisted heat pump," Solar Energy, vol. 236, pp. 280–293, Apr. 2022, doi: 10.1016/j.solener.2022.03.007.

[237] X. Li, A. Lin, C. H. Young, Y. Dai, and C. H. Wang, "Energetic and economic evaluation of hybrid solar energy systems in a residential net-zero energy building," Appl Energy, vol. 254, Nov. 2019, doi: 10.1016/j.apenergy.2019.113709.

[238] D. K. Sharma, D. Sharma, and A. H. H. Ali, "Energy, exergy, environmental impact, and economic analyses of evacuated tube compound parabolic concentrator–powered solar thermal domestic water heating system," Environmental Science and Pollution Research, vol. 29, no. 54, pp. 82390–82410, Nov. 2022, doi: 10.1007/s11356-022-21505-2.

[239] H. M. Henning, "Solar assisted air conditioning of buildings - an overview," Appl Therm Eng, vol. 27, no. 10, pp. 1734–1749, Jul. 2007, doi: 10.1016/j.applthermaleng.2006.07.021.

[240] A. Arsalis and A. N. Alexandrou, "Parametric study and cost analysis of a solar-heating-and-cooling system for detached single-family households in hot climates," Solar Energy, vol. 117, pp. 59–73, Jul. 2015, doi: 10.1016/j.solener.2015.04.024.

[241] A. S. Farooq and P. Zhang, "Technical assessment, economic viability, and environmental impact of a solar-driven integrated space and water heating system in various configurations,"

Energy for Sustainable Development, vol. 71, pp. 330–340, Dec. 2022, doi: 10.1016/j.esd.2022.10.002.

[242] I. Sartori, A. Napolitano, and K. Voss, “Net zero energy buildings: A consistent definition framework,” Energy Build, vol. 48, pp. 220–232, May 2012, doi: 10.1016/j.enbuild.2012.01.032.

[243] A. Mohamed, A. Hasan, and K. Sirén, “Fulfillment of net-zero energy building (NZEB) with four metrics in a single family house with different heating alternatives,” Applied Energy, vol. 114. Elsevier Ltd, pp. 385–399, 2014. doi: 10.1016/j.apenergy.2013.09.065.

[244] W. Wei and H. M. Skye, “Residential net-zero energy buildings: Review and perspective,” Renewable and Sustainable Energy Reviews, vol. 142. Elsevier Ltd, May 01, 2021. doi: 10.1016/j.rser.2021.110859.

[245] A. Ebrahimpour and M. Maerefat, “A method for generation of typical meteorological year,” Energy Convers Manag, vol. 51, no. 3, pp. 410–417, Mar. 2010, doi: 10.1016/j.enconman.2009.10.002.

[246] D. Ciobanu, E. Eftimie, and C. Jaliu, “The influence of measured/simulated weather data on evaluating the energy need in buildings,” in Energy Procedia, Elsevier Ltd, pp. 796–805 2014, doi: 10.1016/j.egypro.2014.02.092.

[247] S. Hatwaambo, P. C. Jain, B. Perers, and B. Karlsson, “Projected beam irradiation at low latitudes using Meteonorm database,” Renew Energy, vol. 34, no. 5, pp. 1394–1398, May 2009, doi: 10.1016/j.renene.2008.09.011.

[248] Y. Boukhris, L. Gharbi, and N. Ghrab-Morcos, “Coupling the building simulation tool ZAER with a sunspot model. Case study in Tunis,” *Energy Build*, vol. 70, pp. 1–14, Feb. 2014, doi: 10.1016/j.enbuild.2013.11.002.

[249] Oanda, “Oanda Currency converter,” Accessed: November 1, 2023. [Online]. Available: https://www.oanda.com/embedded/converter/show/b2FuZGFlY2N1c2VyLy9vYW5kYV9ob21lX3BhZ2U=/0/en/new.

[250] Global Petrol Prices, “Electricity prices,” Accessed: November 1, 2023. [Online]. Available: https://www.globalpetrolprices.com/electricity_prices/.

[251] Global Petrol Prices, “Gas prices,” Accessed: November 1, 2023. [Online]. Available: https://www.globalpetrolprices.com/natural_gas_prices/.

[252] P. Jain, “Gas prices,” Accessed: November 1, 2023. [Online]. Available: https://ieefa.org/resources/flexible-generation-role-indias-stressed-and-stranded-gas-based-power-plants.

[253] United Nations Framework Convention on Climate Change, “Electricity and Natural Gas Grid emission factors,” Accessed: November 1, 2023. [Online]. Available: https://unfccc.int/sites/default/files/resource/Harmonized_Grid_Emission_factor_data_set.xlsx.

[254] A. Divya, T. Adish, P. Kaustubh, and P. S. Zade, “Review on recycling of solar modules/panels,” Solar Energy Materials and Solar Cells, vol. 253, p. 112151, May 2023, doi: 10.1016/j.solmat.2022.112151.

[255] R. R. Rao, S. Priyadarshani, and M. Mani, “Examining the use of End-of-Life (EoL) PV panels in housing and sustainability,” Solar Energy, vol. 257, pp. 210–220, Jun. 2023, doi: 10.1016/j.solener.2023.04.033.

[256] F. Wang and T. You, “Comparative analysis on the life cycle climate performance of ground source heat pump using alternative refrigerants,” Case Studies in Thermal Engineering, vol. 42, Feb. 2023, doi: 10.1016/j.csite.2023.102761.

[257] A. Y. Sulaiman et al., “A solar powered off-grid air conditioning system with natural refrigerant for residential buildings: A theoretical and experimental evaluation,” Cleaner Energy Systems, vol. 5, p. 100077, Aug. 2023, doi: 10.1016/j.cles.2023.100077.

[258] International Energy Agency, “Net Zero by 2050 - A Roadmap for the Global Energy Sector,” 2050. Accessed: November 1, 2023. [Online]. Available: www.iea.org/t&c/

[259] F. D. Chaves, M. F. S. Moreira, R. N. Koury, L. Machado, and M. F. B. Cortez, “Experimental study and modeling within validation of a diffusion absorption refrigerator,” International Journal of Refrigeration, vol. 101, pp. 136–147, May 2019, doi: 10.1016/j.ijrefrig.2019.01.019.

[260] Artic Solar, “Solar thermal Absorption Air Conditioning,” Jacksonville, USA, Accessed: April 4, 2024. [Online]. Available: https://articsolar.com/wp-content/uploads/2017/08/Absorption-Chillers-102816-1.pdf

[261] M. L. Yousfi, M. Saighi, A. Dalibard, D. Schneider, and U. Eicker, “Performance of a 5 kW hot water driven diffusion absorption chiller,” Appl Therm Eng, vol. 127, pp. 789–799, Dec. 2017, doi: 10.1016/j.applthermaleng.2017.08.035.

[262] R. Ben Jemaa, R. Mansouri, and A. Bellagi, “Dynamic testing and modeling of a diffusion absorption refrigeration system,” International Journal of Refrigeration, vol. 67, pp. 249–258, Jul. 2016, doi: 10.1016/j.ijrefrig.2016.03.008.

[263] M. I. S. Adjibade, A. Thiam, C. Awanto, B. A. Ndiogou, and V. Sambou, “Dynamic investigation of the diffusion absorption refrigeration system NH3-H2O-H2,” Case Studies in Thermal Engineering, vol. 10, pp. 468–474, Sep. 2017, doi: 10.1016/j.csite.2017.10.006.

[264] D. Micallef and C. Micallef, “Mathematical model of a vapour absorption refrigeration unit,” International Journal of Simulation Modelling, vol. 9, no. 2, pp. 86–97, Jun. 2010, doi: 10.2507/IJSIMM09(2)3.153.

[265] F. Schmid, B. Bierling, and K. Spindler, “Development of a solar-driven diffusion absorption chiller,” Solar Energy, vol. 177, pp. 483–493, Jan. 2019, doi: 10.1016/j.solener.2018.11.040.

[266] S. Mazouz, R. Mansouri, and A. Bellagi, “Experimental and thermodynamic investigation of an ammonia/water diffusion absorption machine,” International Journal of Refrigeration, vol. 45, pp. 83–91, 2014, doi: 10.1016/j.ijrefrig.2014.06.002.

[267] C. Coquelet, A. Valtz, and P. Théveneau, “Experimental Determination of Thermophysical Properties of Working Fluids for ORC Applications.” IntechOpen, Accessed: April 4, 2024. [Online], Available: doi: 10.5772/intechopen.87113 [Online].

[268] Z. Sayadi, N. Ben Thameur, M. Bourouis, and A. Bellagi, “Performance optimization of solar driven small-cooled absorption-diffusion chiller working with light hydrocarbons,” Energy Convers Manag, vol. 74, pp. 299–307, 2013, doi: 10.1016/j.enconman.2013.05.029.

[269] T. D. Eastop and A. McConkey, Applied Thermodynamics for Engineering Technologists, 5 ed. Longman, 1993, pp. 1-736.

[270] Y. Du, “Cold energy storage: fundamentals and applications”, PhD thesis, University of Leeds, Leeds, United Kingdom, 2014.

[271] M. E. Afshan and A. G. Lucas, “Technology in Design of Heat Exchangers for Thermal Energy Storage”, IntechOpen, Accessed: April 4, 2024. [Online], Available: doi: 10.5772/intechopen.108462

[272] Which, “Air source heat pump costs and savings,” Accessed: April 4, 2024. [online]. Available:https://www.which.co.uk/reviews/ground-and-air-source-heat-pumps/article/ground-and-air-source-heat-pumps/air-source-heat-pump-costs-and-savings-akySY6N5Y6Dd.

[273] N. Park, S.-H. Jung, H.-J. Choi, S. Chin, H.-W. Park, and H. Jung, “Payback Period Estimation of Ground-Source and Air-Source Multi Heat Pumps in Korea Based on Yearly Running Cost Simulation,” International Refrigeration and Air Conditioning Conference, Paper 1146, Purdue, 2010. [Online]. Available: http://docs.lib.purdue.edu/iracc/1146

[274] D. Gibb, J. Rosenow, R. Lowes, and N. J. Hewitt, “Coming in from the cold: Heat pump efficiency at low temperatures,” Joule, vol. 7, no. 9. Cell Press, pp. 1939–1942, Sep. 20, 2023. doi: 10.1016/j.joule.2023.08.005.

[275] The IEA, “Average efficiency of new air conditioners 2000-2020 and in the Net Zero Scenario,” Paris, Nov. 2021. Accessed: November 1, 2023. [Online]. Available: https://www.iea.org/data-and-statistics/charts/average-efficiency-of-new-air-conditioners-2000-2020-and-in-the-net-zero-scenario